Der Mechanismus

des microRNA-vermittelten mRNA-Abbaus

Mechanism of microRNA-mediated mRNA Decay

Dissertation

der Mathematisch-Naturwissenschaftlichen Fakultät

der Eberhard Karls Universität Tübingen

zur Erlangung des Grades eines

Doktors der Naturwissenschaften

(Dr. rer. nat.)

vorgelegt von

Jörg Eberhard Braun

aus Heilbronn-Neckargartach

Tübingen

2012

Tag der mündlichen Qualifikation: 16.05.2012

Dekan: Prof. Dr. Wolfgang Rosenstiel

1. Berichterstatter: Prof. Dr. Hans Bisswanger

2. Berichterstatter: Prof. Dr. Elisa Izaurralde

This thesis describes work carried out in the laboratory of Prof. Dr. Elisa Izaurralde at the Max Planck Institute for Developmental Biology Tübingen, Germany, from July 2008 until February 2012. The work was supervised by Prof. Dr. Hans Bisswanger at the Eberhard Karls University Tübingen, Germany, and was supported by an International PhD program Tübingen fellowship. I declare that this thesis is the product of my own work. Wherever parts of the work have been published, wherever other sources have been used as well as wherever parts of the work were done by colleagues of mine, this has been indicated accordingly.

Table of contents

1A Zusammenfassung

Um sich an ihre spezielle Situation anzupassen, regulieren Zellen in hohem Maße die Proteinproduktion in jedem Schritt der Genexpression. Dazu kontrollieren Zellen die Mengen an Boten-RNA (mRNA) nicht nur während der Transkription, sondern auch posttranskriptional. In den letzten Jahren wurde eine Reihe von posttranskriptionalen Genregulationswegen beschrieben, wobei jedoch in vielen Fällen ein tiefes mechanistisches Verständnis dieser Regulationswege auf molekularer Ebene noch nicht erlangt wurde. Bisherige Studien haben gezeigt, dass diese Regulationswege trotz ihrer Verschiedenheit ein ähnliches Sortiment von generellen Translationsregulatoren und mRNA-Abbaufaktoren als Effektormoleküle einsetzen. Eine Untersuchung dieser generellen mRNA-abbauenden Proteine verspricht daher, unser allgemeines Verständnis der Regulation der Genexpression zu erweitern.

In meiner Doktorarbeit habe ich den mRNA-Abbauweg als einen Mechanismus von posttranskriptionaler Genregulation untersucht. Insbesondere habe ich mich auf die mRNA-Deadenylierung und die Hydrolyse der mRNA-5‘-Kappenstruktur (Decapping), die Schlüsselschritte des mRNA-Abbaus, fokussiert. Trotz ihrer Bedeutung war nur eine eingeschränkte mechanistische Erkenntnis in diese mRNA-Abbauprozesse vorhanden, insbesondere in Vielzellern. Ich habe daher *Drosophila melanogaster (Dm)* und *Homo sapiens (Hs)* als Modellsysteme ausgewählt, um sowohl mRNA-Deadenylierung als auch Decapping zu untersuchen. Des Weiteren habe ich den microRNA (miRNA)-Weg untersucht um eingehend zu verstehen, wie dieser Weg die generellen mRNA-Abbaufaktoren einsetzt.

Im ersten Teil meiner Doktorarbeit habe ich systematisch die mRNA-Decapping-Proteine und ihre Proteinkomplexe, die sie bilden, um den mRNA-Abbau voranzutreiben, an den Beispielen von Decapping protein 1 (DCP1), DDX6/Me31B und Pat untersucht. Ich habe die Verbindungen, Domänen und funktionalen Sequenzen des Decapping-Komplexes in Vielzellern in den Modellsystemen *Dm* und *Hs* bestimmt, sowie deren Bedeutung für den Aufbau von Decapping-Aktivator-Komplexen und mRNA-Abbau *in vitro* und in Zellen. Die Untersuchung zur Rolle von DCP1 hat eine unerwartete Komplexität und Verbindung im Aufbau von Decapping-Aktivator-Komplexen gezeigt. Ein anderes Projekt konzentrierte sich auf den Aufbau der sich gegenseitig ausschließenden Komplexe mit der Helikase DDX6/Me31B als gemeinsamen Partner und bietet auf molekularer Ebene eine Erklärung dafür, wie diese Helikase unterschiedliche Funktionen bei der Regulation von mRNAs

ausüben kann. Zusammen mit einer Untersuchung des Decapping-Aktivators Pat hat diese Arbeit das bis dahin vorherrschende Modell eines statischen Super-Decapping-Aktivatoren-Komplexes in Frage gestellt. Diese beiden Studien weisen eher auf verschiedene Unterkomplexe von Decapping-Aktivatoren hin, die sich durch sich gegenseitig ausschließende Wechselwirkungen dynamisch bilden und auflösen können.

Im zweiten Teil meiner Doktorarbeit habe ich untersucht, wie der miRNA-Weg die generelle mRNA-Abbau-Maschinerie heranzieht, um mRNA-Angriffsziele der miRNAs beschleunigt abzubauen. Eine wachsende Zahl an Belegen in der neueren Literatur legte nahe, dass mRNA-Abbau eine weitverbreitete Folge der Regulation durch miRNAs ist. Jedoch blieb der Mechanismus, wie miRNAs ihre Angriffsziele beschleunigt abbauen, unklar. Hier konnte ich eine direkte Verbindung zwischen der Kernkomponente des miRNA-Weges und zwei Deadenylierungsfaktoren bestimmen. Diese Proteine wiederum bringen ihre jeweiligen Deadenylierungs-Komplexe zu mRNA-Angriffszielen heran, um sie zu deadenylieren. Meine Arbeit liefert eine mechanistische Verbindung zwischen miRNA-geleiteter Angriffszielerkennung und Angriffszielabbau und zeigt, wie zelluläre Wege, die bisher als voneinander unabhängig betrachtet wurden, tatsächlich stark miteinander vernetzt sind.

1B Summary

Cells highly regulate protein production at any step of gene expression in order to adapt to the specific situation they are in. To this end, cells not only control mRNA levels transcriptionally, but also post-transcriptionally. In the last years a multitude of post-transcriptional gene regulation pathways have been described, but a deep mechanistic understanding at the molecular level of these pathways has not been achieved yet in many cases. However, a common outcome that emerged from previous studies was that despite their diversity, these pathways employ a similar set of general translation regulators and mRNA decay factors at the effector steps. Therefore, studying these general mRNA effector proteins promises to increase our general understanding of regulated gene expression.

During my PhD thesis I studied the mRNA decay pathway as a mechanism of post-transcriptional gene regulation. In particular, I focused on mRNA deadenylation and decapping, the key steps of mRNA decay. Despite their importance the mechanistic insight into these mRNA degradation processes had been limited, especially in metazoa. Therefore, I chose *Drosophila melanogaster (Dm)* and *Homo sapiens (Hs)* as model systems to study both mRNA deadenylation and decapping. Furthermore, I studied the microRNA (miRNA) pathway to understand in detail how this pathway employs the general mRNA degradation factors.

In the first part of my thesis, I systematically dissected the proteins involved in mRNA decapping and the protein complexes they form to promote mRNA decay taking as examples the Decapping protein 1 (DCP1), DDX6/Me31B and Pat. I mapped the connectivity, domains and functional sequences of the metazoan decapping complex in the model systems *Dm* and *Hs* as well as their relevance for assembly of decapping activator complexes and mRNA degradation *in vitro* and in cells. A study on the role of the DCP1 revealed an unexpected complexity and connectivity of decapping activator complexes. Another project focused on the assembly of mutually exclusive complexes with the helicase DDX6/Me31B as common partner and provided an explanation at the molecular level of how this helicase can exert diverse functions in mRNA regulation. Together with a study on the decapping activator Pat, this work challenged the so far prevailing concept of a static super-decapping activator complex. These two studies rather suggest that distinct sub-complexes of decapping activators are formed and disassemble dynamically due to mutually exclusive interactions between the decapping factors.

In the second part of my PhD project, I studied how the miRNA pathway recruits the general mRNA decay machinery to promote degradation of miRNA targets. Growing evidence from recent literature suggested that mRNA degradation is a widespread consequence of miRNA regulation. However, the mechanism of how miRNAs promote target degradation remained elusive. Here, I could identify a direct link between the core silencing machinery and two deadenylation factors. These proteins in turn recruit their respective deadenylation complexes to the mRNA targets to promote deadenylation. My work provides a mechanistic connection between miRNA guided target recognition and target degradation and shows how cellular pathways that have been previously seen as distinct are actually highly interconnected.

2 Introduction

2.1 mRNA synthesis and processing in metazoa

Messenger RNAs (mRNAs) mediate the flow of information from genes to ribosomes, which synthesize the proteins. The basic mechanisms of mRNA synthesis and processing as well as mRNA degradation are conserved in metazoa. Therefore the following description applies to metazoa in general, however regarding protein names and paralogs this description focuses on the two model organisms *Homo sapiens (Hs)* and *Drosophila melanogaster (Dm)*, since I worked with *Hs* and *Dm* cells in my PhD.

During transcription mRNAs are capped at the 5' end with a cap-structure (Figure 1), that protects the mRNA from rapid degradation, while the 3' end is processed and polyadenylated. Splicing of the pre-mRNA starts co-transcriptionally resulting in the mature mRNA that is subsequently exported from the nucleus into the cytoplasm.

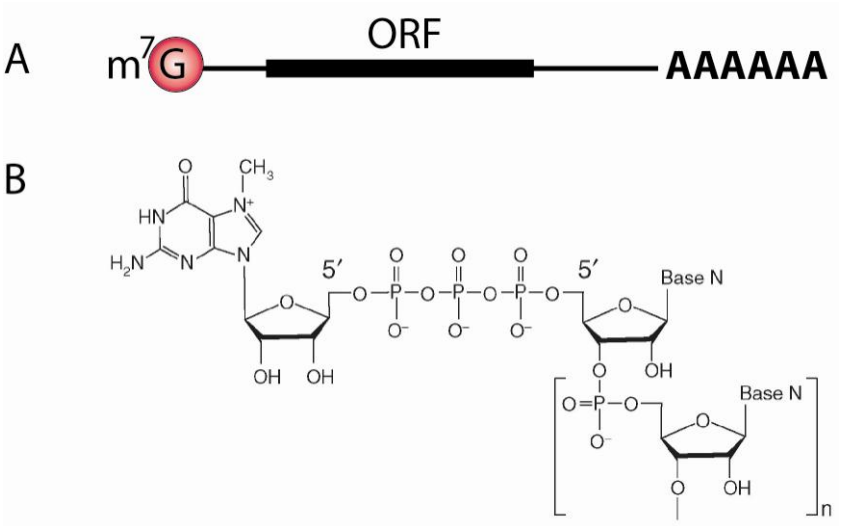

Figure 1: A) Scheme of an mRNA; m^7G, 7-methyl-guanosine; ORF, open reading frame **B)** The mRNA cap structure in eukaryotes: The cap consists of m^7G linked by an inverted 5'-to-5' triphosphate bridge to the first nucleoside of the mRNA chain (adopted from Gu and Lima, 2005).

In the cytoplasm mRNAs are bound by a number of general as well as mRNA-specific proteins to form a dynamic messenger ribonucleoprotein (mRNP) complex. The cap is bound by the eukaryotic translation initiation factor 4E (eIF4E) and the poly(A) tail is bound by

cytoplasmic poly(A)-binding proteins (PABPCs) (Figure 2). Several paralogs of PABPC have been identified, but most studies on PABPC focused on the prototypcical PABPC1 or did not discriminate between the different paralogs. Therefore PABP, PABPC and PABPC1 are used in a synonymous way in the literature (Smith and Gray, 2010). Both eIF4E and PABPC interact with eIF4G, so the mRNA is circularized promoting efficient translation (Sonenberg and Hinnebusch, 2009).

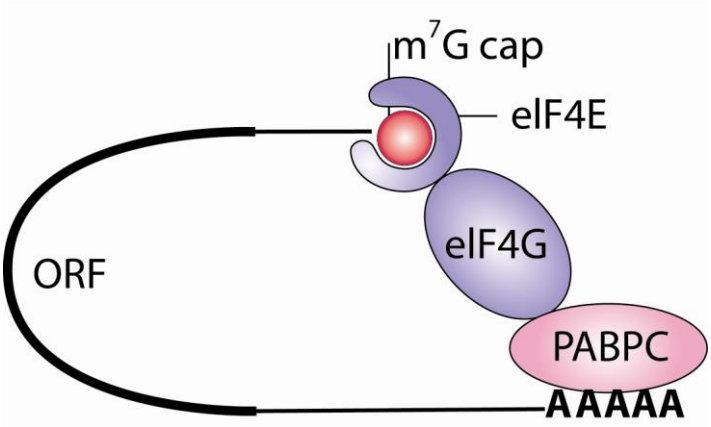

Figure 2: The mRNA cap structure binds to eIF4E and the mRNA poly(A) tail binds to PABPC. Both eIF4E and PABPC interact with eIF4G allowing the mRNA to adopt a closed loop conformation.

2.2 mRNA degradation in metazoa

Cytoplasmic mRNA degradation in metazoa is generally initiated by deadenylation of the mRNA, i.e. shortening of the poly(A) tail (Figure 3). Deadenylation followed by a loss of PABPC interferes with the closed-loop conformation of the mRNA, reduces translation efficiency, and increases the accessibility of the mRNA ends to exonucleases. The translation initiation factors eIF4E and eIF4G are displaced upon deadenylation during the transition to a decapping competent mRNA, but details of this process are currently unclear (Franks and Lykke-Andersen, 2008; Goldstrohm and Wickens, 2008).

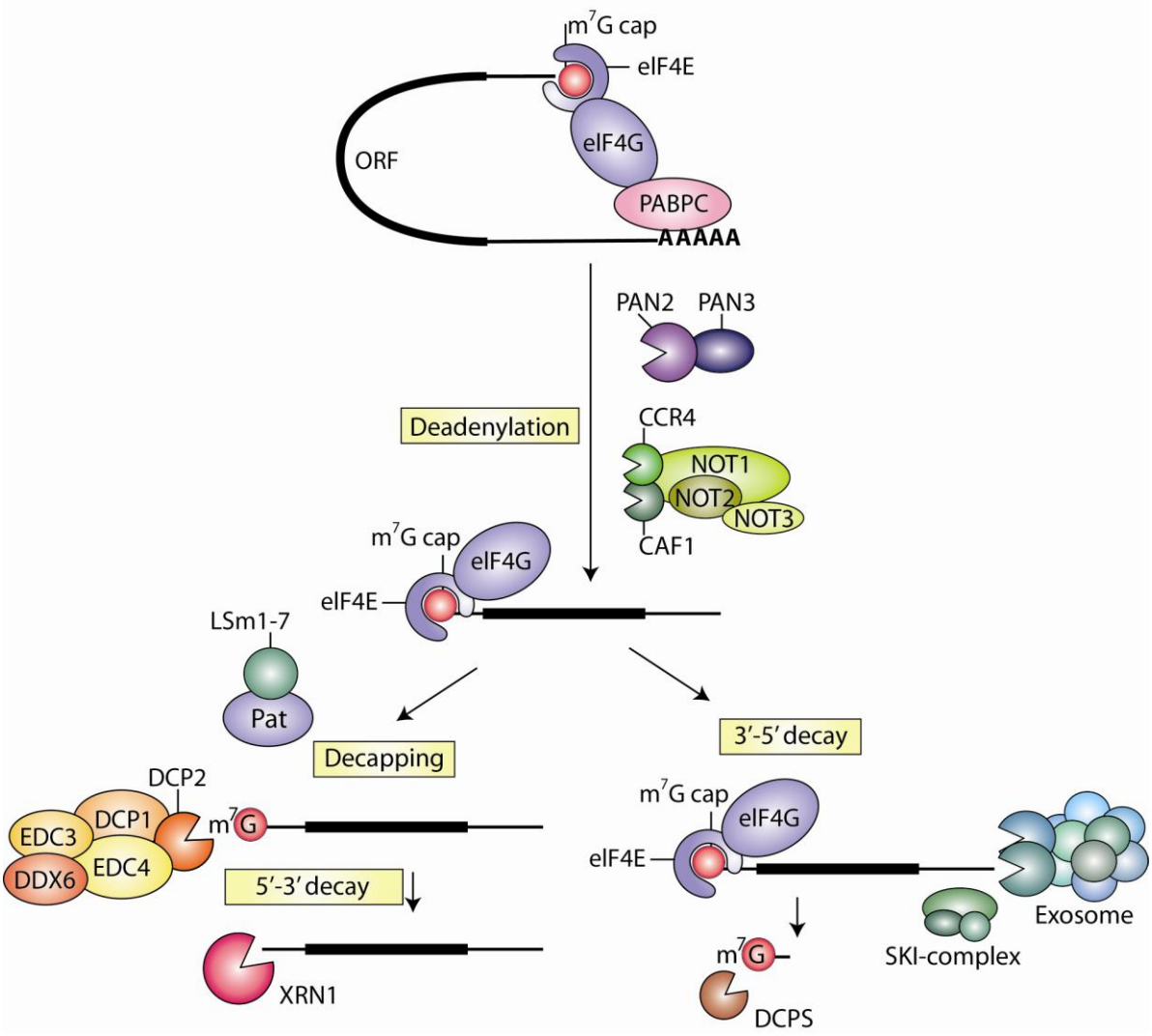

Figure 3: The general mRNA decay pathways in metazoa. mRNA degradation is initiated by shortening of the poly(A) tail by the two major cytoplasmic deadenylases: the PAN2-PAN3 complex with the components poly(A) specific ribonucleases PAN2 and PAN3 and the CCR4-NOT complex with the components Negative regulators of transcription (NOT1-3), Carbon catabolite repressor protein 4 (CCR4) and CCR4-associated factor 1 (CAF1). During deadenylation the mRNA loses PABPC and can no longer adopt the mRNA protecting closed loop conformation. The deadenylated mRNA can be either decapped and degraded 5' to 3' or degraded 3' to 5' by the exosome. Pat together with the LSm1-7 ring acts s scaffold important for the transition to decapping. The Decapping protein 2 (DCP2) has the catalytic activity, which is regulated by a set of decapping activators: the Decapping protein 1 (DCP1), the Enhancer of decapping 3 (EDC3), the Enhancer of decapping 4 (EDC4) and the DEAD box helicase DDX6/Me31B. The exonuclease XRN1 degrades mRNAs that are no longer protected by the cap structure. Alternatively to the degradation from the 5' to 3' end, the deadenylated mRNA can be degraded via the 3' to 5' pathway by the exosome assisted by the SKI-complex. The resulting 5' fragment is degraded by the scavenger decapping protein (DCPS).

Two major deadenylation complexes have been identified in the cytoplasm of eukaryotic cells: the poly(A) specific ribonuclease (PAN2-PAN3) complex and the Carbon catabolite

repressor protein 4 - Negative regulator of transcription (CCR4-NOT) complex (Goldstrohm and Wickens, 2008). Deadenylation is started in a distributive manner by the PAN2-PAN3 complex with PAN2 as the catalytic subunit (Figure 3). PAN3 interacts with PABPC and is important for the recruitment of PAN2 to the mRNA (Yamashita et al., 2005). At a certain length of the poly(A) tail, that depends on the organism, the CCR4-NOT continues deadenylation in a processive manner. However, the first phase of deadenylation catalyzed by the PAN2-PAN3 complex is not essential to deadenylate mRNAs, since the CCR4-NOT complex is sufficient for deadenylation in cells depleted from the PAN2-PAN3 deadenylation activity (Tucker et al., 2001; Yamashita et al., 2005). The CCR4-NOT complex has two catalytic subunits: the CCR4 protein (there are two paralogs CCR4a and CCR4b in human cells, but only one ortholog CCR4 in *Dm*) and the CAF1 or the related POP2 protein (in human cells there are two proteins CAF1 and POP2, but in *Dm* there is only one protein POP2/CAF1). The CCR4-NOT complex contains also several NOT proteins, that are important for the activity of the complex in cells (Collart and Panasenko, 2011). An additional cellular deadenylase, the PARN protein, has also been identified. The PARN dedeadenylase has been shown to be important for *X.laevis* development, but no homolog has been identified in *D. melanogaster* suggesting, that PARN activity is not generally required in metazoa (Goldstrohm and Wickens, 2008).

Upon deadenylation the mRNA is either degraded by the 5' to 3' pathway or the 3' to 5' pathway (Figure 3). In the 5' to 3' pathway, the mRNA is decapped by the decapping protein 2 (DCP2), which is activated and regulated by several decapping activators, i.e. the decapping protein 1 (DCP1), the metazoa-specific enhancer of decapping 4 (EDC4), the DEAD box helicase DDX6 and the enhancer of decapping 3 (EDC3). In yeast, DCP1 directly interacts with DCP2 and stimulates decapping activity *in vitro* and *in vivo*, but in metazoa an additional protein EDC4 is necessary to stabilize this interaction (Fenger-Grøn et al., 2005). The Pat protein in complex with the LSm1-7 ring associates with deadenylated mRNAs and is a scaffold protein important for the transition of a translationally active mRNA to an mRNA subjected to degradation (Tharun et al., 2000; Tharun and Parker, 2001). During the decapping reaction the cap-structure (Figure 1B) is hydrolyzed by DCP2 and m^7GDP and 5' monophosphorylated mRNA are released.

In specific situations deadenylation as a prerequisite for decapping can be bypassed, as shown for the degradation of the mRNA coding for ribosomal protein Rps28b. Here the decapping machinery is directly recruited to the mRNA (Badis et al., 2004). mRNA decappping can even

occur co-translationally (Hu et al., 2009). Recently, an additional decapping protein, Nudt16, has been identified in mammals, suggesting redundancy and/or target-specificity also at the step of mRNA decapping (Song et al, 2010).

When the mRNA is no longer protected by the cap-structure, the mRNA body is rapidly degraded from the 5' end by the exoribonuclease 1 (XRN1) (Figure 3). Since there is strong evidence that the step of decapping irreversibly commits an mRNA to degradation, the step of decapping has to be tightly controlled (Franks and Lykke-Andersen, 2008).

Alternatively, following deadenylation mRNAs can be degraded from the 3' end by the cytoplasmic exosome assisted by the SKI-complex. The resulting 5' fragment is hydrolyzed by the scavenger decapping protein DCPS (Parker and Song, 2004; Figure 3).

In addition to the general mRNA decay pathways initiated by deadenylation, there are also specific pathways involving an initial cleavage within the mRNA by an endonuclease such as in the nonsense-mediated mRNA decay (NMD) or the small interfering RNA (siRNA) pathway, and the resulting fragments are further degraded by XRN1 and the exosome (Tomecki and Dziembowski, 2010). Replication dependent histone mRNAs do not have a poly(A) tail, but a histone stem-loop structure in the 3' UTR. Histone mRNAs is degraded after completion of DNA replication dependent on the stem-loop binding protein (SLBP) (Marzluff et al., 2008).

Interestingly, the proteins involved in mRNA degradation colocalize into so-called processing bodies (P bodies), but the function of these RNA granules is currently not completely understood (Eulalio et al., 2007).

2.3 Post-transcriptional regulation of gene expression

2.3.1 Importance of post-transcriptional regulation of gene expression

The steady-state levels of mRNAs are determined both by the rates of synthesis and degradation. For a rapid adjustment of the mRNA levels a short mRNA half-life is critical, but longer mRNA half-lives allow for efficient protein synthesis of gene products over a longer period of time. Indeed, mRNA half-lives vary from minutes to days, as determined in mouse cells (Sharova et al., 2009). Because mRNA abundance and efficiency of translation both

define the amount of protein produced by the cell, the step of translation is also regulated by multiple mechanisms. Translational activation or repression can be reversible and allow for a very rapid adaptation of gene expression to the needs of the cells.

2.3.2 Regulated translation of mRNAs

A well-studied example of regulated translation of mRNAs involves eIF4E-binding proteins (4E-BPs) that regulate the step of translation initiation. 4E-BPs compete with eIF4G for binding to eIF4E and thereby inhibit translation initiation since eIF4E-eIF4G interaction is important for efficient translation initiation (Figure 2). The kinase mTOR controls the status of 4E-BP phosphorylation, which in turn regulates binding to eIF4E. Phosphorylated 4E-BPs interact weaker with eIF4E than hypophosphorylated 4E-PBs. Therefore phosphorylation of 4E-BPs allows cells to adjust translation efficiency to extra- and intracellular stimuli (Sonenberg and Hinnebusch, 2009).

2.3.3 Regulated mRNA degradation

Regulation of mRNA degradation is well-understood for a certain class of short lived mRNAs, that are characterized by AU-rich elements (AREs) in their 3' UTR, such as the mRNAs coding for the cytokines IL-2 or TNF-α. AREs are recognized by the RNA-binding protein Tristetraprolin that mediates rapid degradation of mRNA targets. Tristetraprolin activity depends on its phosphorylation status, which allows regulation of mRNA stability by kinases and phosphatases as e.g. in macrophages during inflammation (Sandler and Stoecklin, 2008). Recently, Tristetraprolin has been shown to interact with NOT1 which in turn recruits the deadenylase CAF1 providing a mechanistic basis for how Tristetraprolin mediates CCR4-NOT complex-dependent degradation of its mRNA target (Sandler et al., 2011).

For a certain set of mRNAs during development in *Dm* it has been shown that the CCR4-NOT complex is recruited by RNA-binding proteins such as Smaug or the Pumilio-Nanos complex (Goldstrohm and Wickens, 2008).

2.4 microRNA-pathway

2.4.1 Biological impact of the microRNA-pathway

microRNAs (miRNAs) are a class of small RNAs that are endogenously transcribed. In mammals several hundreds of miRNAs have been identified. Each animal miRNA is predicted to regulate hundreds of targets, so approximately half of the human transcriptome is estimated to be fine-tuned by miRNAs. Thus, it is not surprising that miRNAs are implicated in a broad range of biological processes, such as growth, development and metabolism (Bartel, 2009).

2.4.2 microRNA biogenesis and function

Animal miRNAs are transcribed as long primary transcripts and processed subsequently by the RNases Drosha and Dicer to the mature miRNA duplex. The two strands of the duplex each have a length of approximately 21 nucleotides and a phosphate at the 5' end. One of the two strands, the guide strand, is loaded into an Argonaute (AGO) protein, the central component of the miRNA-induced silencing complex (miRISC). The guide strand guides the miRISC to the mRNA target by partial sequence complementarity (Krol et al., 2010).

The miRISC causes translational repression and/or mRNA degradation of the mRNA target (Huntzinger and Izaurralde, 2011). Initially, animal miRNAs were thought to mainly repress translation as shown for the example of lin-4 miRNA (Olsen and Ambros, 1999). Subsequently several studies provided evidence, that miRNAs can promote target degradation (Bagga et al., 2005; Krützfeldt et al., 2005; Lim et al., 2005; Wu and Belasco, 2005). Recent transcriptome-wide studies showed that decreased mRNA levels of miRNA targets explain in most of the cases the decreased protein production, so mRNA degradation is a predominant effect of miRNA regulation (Baek et al., 2008; Selbach et al., 2008; Hendrickson et al., 2009; Guo et al., 2010; Huntzinger and Izaurralde, 2011).

2.4.3 Mechanism of microRNA-mediated gene silencing

In contrast to the related siRNA-pathway, in the miRNA-pathway AGO proteins generally do not cleave their targets endonucleolytically, but recruit a protein of the GW182 protein family. Indeed, GW182 proteins are essential for silencing in animal cells and are considered together with the miRNA loaded AGO proteins as the core miRISC (Eulalio et al., 2009a). Only one ortholog of GW182 is present in *Dm*, but in human cells there are three paralogs of GW182: the Trinucleotide repeat-containing gene 6 proteins TNRC6A, TNRC6B and TNRC6C, which seem to be redundant. The domain organization of GW182 proteins is conserved from human to flies (Figure 4).

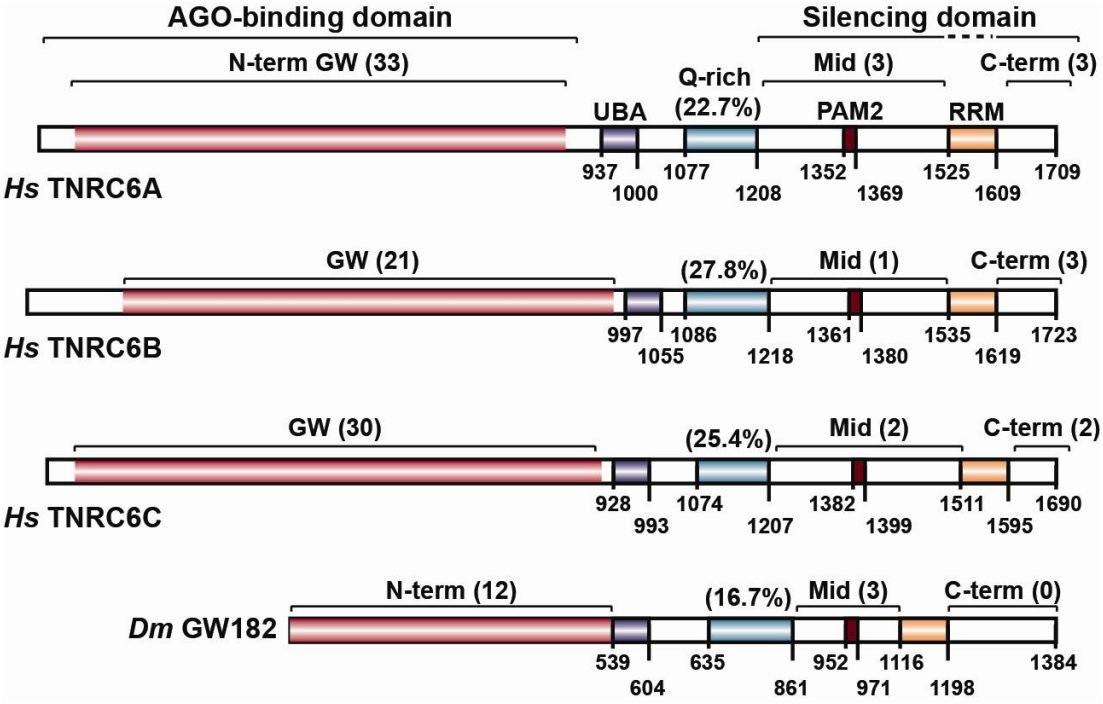

Figure 4: Domain organization of GW182 proteins: *Hs*, *Homo sapiens*; *Dm*, *Drosophila melanogaster*. N-term, Mid and C-term: N-terminal, middle and C-terminal GW-repeat-containing regions, respectively (the number of GW-repeats in each region is indicated in brackets). UBA: ubiquitin associated-like domain; Q-rich: region rich in glutamine; PAM2: PABPC-interacting motif 2; RRM: RNA recognition motif. Numbers underneath the protein schematic represent amino acid positions at the fragment boundaries for each protein. The AGO-binding and silencing domains are indicated (adopted from Eulalio et al., 2009a).

GW182 proteins have multiple Gly-Trp (GW)-repeats in their N-terminal region, which mediate direct binding to the AGO proteins. Single GW-repeats have only low affinity for AGOs, but together they contribute to efficient AGO-binding. The relative contribution of a

GW-repeat to AGO-binding depends on its specific sequence context in the GW182 protein. The N-terminal region therefore has been termed AGO-binding domain. The AGO-binding domain is followed by a conserved ubiquitin associated-like domain (UBA), a region rich in glutamine (Q-rich) and the silencing domain. The silencing domain has been shown to be necessary and sufficient for silencing activity in human cells and contains a middle region (Mid) and a C-terminal region (C-term). GW182 proteins also contain a conserved RNA recognition motif (RRM), but its functional importance is currently not well understood (Eulalio et al., 2009a).

GW182 proteins are the effector proteins of the miRNA pathway and cause translational repression and/or mRNA degradation of their targets. Degradation of mRNA targets requires the activities of the CCR4-NOT complex and the decapping complex, but also the PAN2-PAN3 complex has been implicated in the miRNA pathway. The molecular mechanism of translational repression by miRNAs is not well understood and several models have been proposed: Translational repression could occur at the step of initiation or at the step of elongation and even cotranslational degradation of the nascent peptide has been proposed, but only the first two models are strongly supported by experimental evidence (Fabian et al., 2010; Huntzinger and Izaurralde, 2011).

Recently, GW182 proteins were shown to interact directly with PABPC via a conserved PABP-interacting motif-2 (PAM2), and this interaction is important for silencing *in vitro* and in cells (Fabian et al., 2009; Zekri et al., 2009). The interaction of GW182 with PABPC was proposed to compete with PABPC-eIF4G-binding and/or to interfere with the protection of the poly(A) tail by PABPC and/or to promote deadenylation. In Figure 5 the working model from 2010 of the mechanism of miRNA-mediated gene silencing is shown (Fabian et al., 2010; Huntzinger and Izaurralde, 2011).

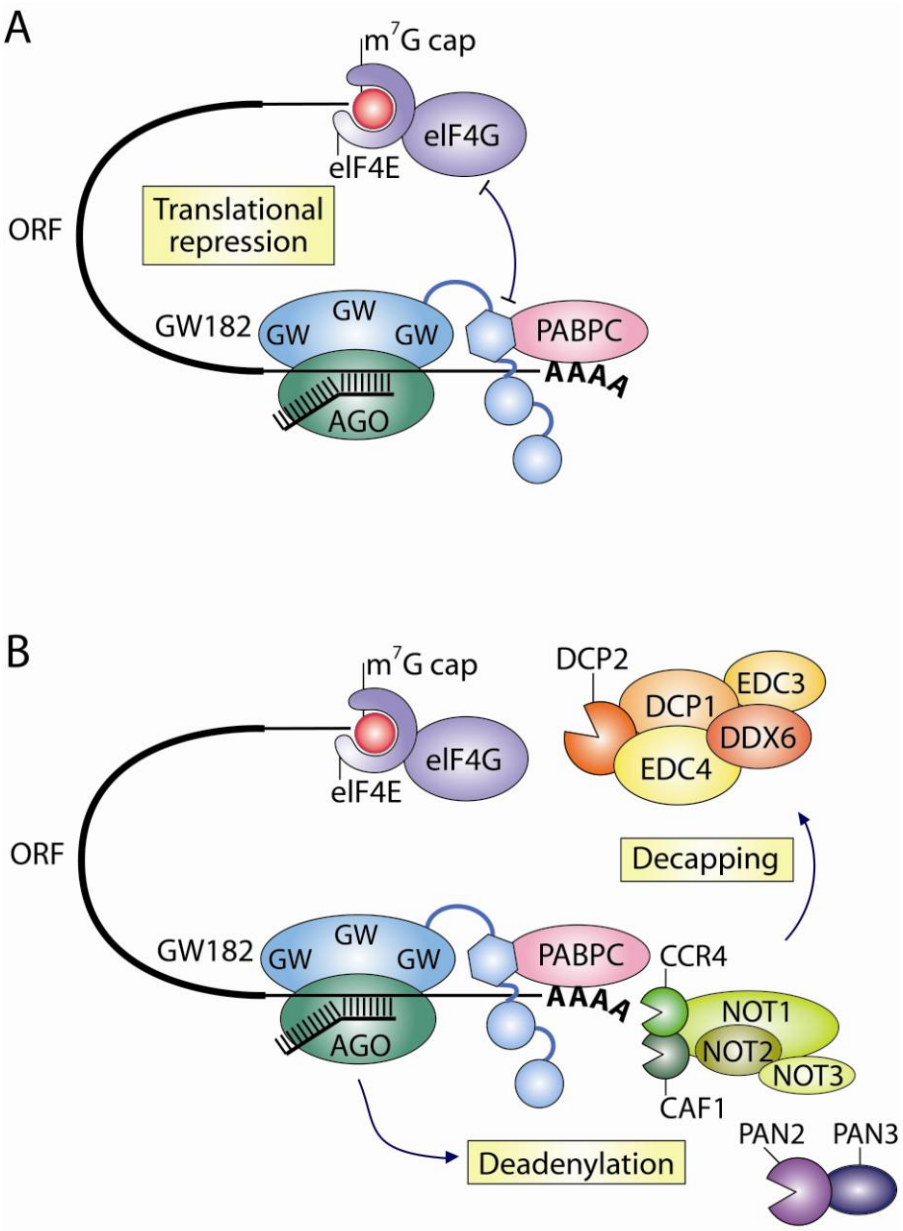

Figure 5: Mechanism of miRNA-mediated gene silencing: silencing is effected by an Argonaute (AGO) protein recruiting a GW182 protein. GW182 proteins in turn interact with PABPC and promote translational repression **(A)** and/or mRNA degradation **(B)**. **A)** GW182 has been shown to compete with the eukaryotic initiation factor 4G (eIF4G) for binding to PABPC to repress translation. **B)** mRNA degradation is initiated by deadenylation dependent on the PAN2-PAN3 and CCR4-NOT complexes. The deadenylated mRNA can be stored or degraded by the 5' to 3' decay pathway (adopted from Tritschler et al., 2010).

3 Motivation and aims

3.1 How do decapping activators assemble to promote mRNA decapping in metazoa?

When I started my PhD in July 2008, proteins involved in the 5' to 3' mRNA degradation pathway had been identified in genetic screens and biochemical purifications. However, functional and mechanistic studies on the 5' to 3' mRNA degradation pathway were mainly limited to yeast, despite its importance for general mRNA degradation and target specific pathways such as the miRNA-pathway. In particular how the decapping activators contribute to mRNA decapping was unclear (Franks and Lykke-Andersen, 2008). Furthermore, even for proteins that are conserved in yeast, the metazoan homologs contain additional domains and extensions adding another layer of complexity to the metazoan mRNA degradation machinery (Figure 6).

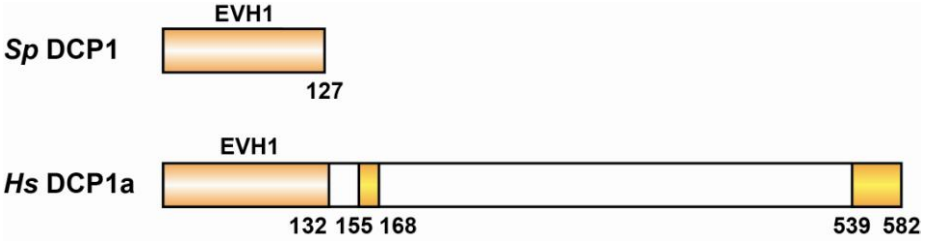

Figure 6: Domain organization of DCP1 proteins: *Sp, Schizosaccharomyces pombe* and *Hs, Homo sapiens*. The conserved Ena-VASP homology 1 (EVH1) domain and metazoan specific conserved sequences are colored. Numbers underneath the protein schematic represent amino acid positions at the fragment boundaries for each protein (adopted from Tritschler et al., 2009b).

For most of the mRNA decay factors the specific function during mRNA degradation as well as their interaction with other decay factors was not precisely characterized. In the decapping field the model of a super-decapping activator complex was favored. According to this hypothesis decapping activators bind to the mRNA committed to decay simultaneously or subsequently until ultimately a static decapping activator complex comprising the full set of protein factors important for decapping is assembled (Parker and Sheth, 2007). Specifically, my work addressed 4 main questions:

3.1.1 What is the role of metazoan DCP1 and how does it promote mRNA decapping?

To improve the mechanistic understanding of how decapping activators promote mRNA decapping and to test the model of a super-decapping complex I studied how mRNA decapping factors assemble precisely and how this is relevant for mRNA decapping. I chose to study the role of DCP1 in decapping activator complexes based on the prominent role of DCP1 among the decapping activators. Indeed, DCP1 was the first protein identified as being required for mRNA decapping even before DCP2 itself (Beelman et al., 1996). Studying the role of DCP1 in decapping complexes therefore was expected to yield insights into fundamental aspects of mRNA decapping. I focused on metazoan DCP1, since in addition to a lack of mechanistic understanding of the process of mRNA decapping itself, it was unclear how mRNA decay is integrated by target specific decay pathways involved in post-transcriptional gene regulation in metazoa. In Figure 6 the domain organization of yeast and human DCP1 proteins is shown. Both orthologs have an N-terminal conserved Ena-VASP homology 1 (EVH1) domain, but metazoan DCP1 has a long C-terminal extension with additional motifs conserved in metazoa. This illustrates the increased complexity of metazoan DCP1 and the rationale of studying metazoan DCP1.

3.1.2 How can Pat act as a scaffold to promote mRNA decapping?

According to the established "super-decapping activator complex model" decapping activators assemble during the commitment of an mRNA to decapping. The Pat protein has been shown to be important for the transition of a translationally active mRNA to an mRNA committed to decapping (Tharun and Parker, 2001; Coller and Parker, 2005). Mapping the interactions of Pat with other decapping activators was the next step towards mechanistic insights into the scaffold function of Pat. Previously, the yeast ortholog Pat1 had been studied, but the mechanistic insights were limited, so there was still much to learn (Pilkington and Parker, 2008). Studying this protein also promised to be the key to investigate if decapping factors indeed assemble sucessively to a super-decapping complex or if they rather form dynamically linked distinct decapping activator complexes. This competing model could not be excluded or proven by experimental evidence at that time.

3.1.3 How does the DEAD box helicase DDX6/Me31B assemble into distinct complexes in translational repression and mRNA decapping?

Previous data from our lab suggested that DDX6/Me31B assembles into distinct decapping activator complexes (Tritschler et al., 2007; Tritschler et al., 2008). Indeed, it had been shown that DDX6 associates either into a complex containing DCP1 and the translational repressors Trailer Hitch (Tral) and Cup or into another complex containing EDC3, DCP1 and DCP2. However insights into the molecular details und functional importance of these interactions was only limited (Tritschler et al., 2008). In addition, DDX6/Me31B had been shown to interact with Pat (Coller et al., 2001), which raised the question how the complex of DDX6/Me31B with Pat was related to these two previously described complexes. Using the crystal structure of DDX6/Me31B, which was solved by another PhD student (Felix Tritschler) in the lab, I designed and tested mutants to dissect how DDX6/Me31B is recruited into distinct functional complexes and to test the relevance of these assemblies for DDX6/Me31B function.

3.2 How are general mRNA decay factors recruited to miRNA targets?

Pathways of post-transcriptional gene regulation had been described to employ general mRNA decay factors, but it remained unclear how these factors are integrated. As an example for this, it was of outstanding interest to study the miRNA pathway in detail to understand how mRNA degradation is promoted by miRISCs. Several lines of evidence suggested that mRNA degradation is a widespread consequence of miRNA regulation (Eulalio et al., 2009b). However the mechanism of how miRNAs promote target degradation remained elusive. Even the idea that miRNAs promote mRNA target degradation was under debate. The elucidation of how the miRNA pathway recruits the general mRNA decay machinery to promote degradation of miRNA targets was therefore expected to provide mechanistic insights into the mechanism of miRNA-mediated gene silencing in particular, but also how general mRNA decay factors are integrated into specialized post-transcriptional gene regulation pathways.

4 Results and discussion

4.1 Decapping activators assemble into distinct mRNA decapping complexes in metazoan to promote mRNA decapping.

To dissect the interaction network of decapping activators, I systematically investigated the connectivity, domains and functional sequences of the metazoan decapping activators in the model systems *Dm* and *Hs* and tested their relevance for decapping and mRNA degradation *in vitro* and in cells.

Analysis of metazoan DCP1 showed an unexpected complexity and connectivity of the metazoan decapping complex (4.1.1), which is important to mechanistically understand the process of decapping itself in metazoan and also sheds light on how in metazoa specific pathways integrate the general mRNA decay factors at the effector steps.

Studying how Pat (4.1.2) and DDX6/Me31B (4.1.3) assemble into distinct decapping complexes provided a molecular explanation for their functions and challenged the prevailing model of a super-decapping complex.

4.1.1 DCP1 self-interacts to assemble into active mRNA decapping complexes in metazoa.

The work described in this chapter has been published in Tritschler et al., 2009b. Experimental data and detailed description of experimental procedures are available in the attached manuscript.

In this study, I investigated the role of metazoan DCP1 in the assembly of mRNA decapping complexes. The composition of the metazoan decapping complex had been described by Fenger-Grøn and colleges in 2005, but it was not clear how this complex assembles and which role DCP1 plays in this complex. Structural and functional analysis of DCP1 was limited to its EVH1 domain (She et al., 2008). Yeast DCP1 consists only of the EVH1 domain, but metazoan DCP1 has a C-terminal extension (Figure 6).

Analyzing this metazoan specific C-terminal extension of DCP1 I could identify two novel conserved motifs, motif I and the so called trimerization domain. The trimerization domain

was subsequently shown by another PhD student (Felix Tritschler) in the lab to mediate homotrimerization, therefore referred to as trimerization domain. In human cells, there are two paralogs of DCP1 (DCP1a and DCP1b), and in this study I focused on DCP1a. As the first step, I generated expression constructs for wild-type DCP1a and deletion mutants, that either lacked motif I (DCP1a-ΔMI) or the trimerization domain (DCP1a-ΔTD). I tested these mutants in an *in vitro* decapping assay (Lykke-Andersen, 2002). To this end, I expressed GFP-tagged wild-type or mutant DCP1a in human HEK293 cells and immunoprecipitated the respective DCP1a protein and copurifying interaction partners. I incubated the immunoprecipitate with a capped RNA substrate. Since I labeled the cap-structure of this RNA substrate radioactively, I could detect by autoradiography non converted still capped RNA substrate and m^7GDP, the product of the decapping reaction. After stopping the *in vitro* decapping reaction with EDTA, I spotted an aliquot on a polyethylenimine-modified cellulose plate and separated the reaction mix by thin-layer chromatography. Decapping activity copurifies with wild-type DCP1a and DCP1a-ΔMI, but not with DCP1a-ΔTD. The absence of *in vitro* decapping activity in DCP1a-ΔTD immunoprecipitate could be either due to an impaired ability of DCP1a-ΔTD to stimulate DCP2 activity or DCP1a-ΔTD could no longer be incorporated into active decapping complexes.

To discriminate between these two possibilities and to answer the question why the trimerization domain is essential for DCP1a to immunoprecipate decapping activity, I tested wild-type DCP1a, DCP1a-ΔMI and DCP1a-ΔTD in coimmunoprecipitation experiments for interactions with decapping activators and for self-interaction. I showed that motif I is critical for DCP1a to interact with EDC3 and DDX6/Me31B, but not for the interaction with EDC4 or DCP2. In contrast the trimerization domain mediates self-interaction. Furthermore, this domain also confers binding to DCP2 and EDC4. However it is not important for binding of DCP1a to EDC3 or DDX6/Me31B.

My results suggested that DCP1a has central role in the assembly of two decapping complexes (DCP1a-EDC3-DDX6/Me31B and DCP1a-DCP2-EDC4). Together with the self-interaction of DCP1a, these two decapping activator complexes could interact suggesting the existence of larger decapping complexes formed from these building blocks.

To study the role of DCP1 *in vivo* I established a complementation assay for DCP1 in *Dm* S2 cells (Figure 7). In such a complementation assay the cellular function of a certain protein – here DCP1 – is monitored. The cells are depleted of endogenous DCP1 by RNA interference

(RNAi). These knockdowns are typically achieved in *Dm* S2 cells by siRNAs targeting the open reading frame of DCP1 mRNA or long double-stranded RNAs (dsRNAs) targeting its untranslated regions. However using these approaches the knockdown efficiency was not sufficient. I therefore established a new approach in which long dsRNAs targeting the open reading frame of DCP1 were used. A version of DCP1, that I made resistant to the long dsRNAs by silent mutations in the several hundred nucleotides long targeted sequence, is then added back to the cells. In this way I could test whether DCP1 mutants can complement the loss of endogenous DCP1 as efficient as wild-type DCP1 or if the mutations affect the protein function. I established this complementation strategy successfully for DCP1 in *Dm* S2 cells and meanwhile this complementation strategy has been frequently used also in other studies in S2 cells. When I tested DCP1 lacking the trimerization domain in this complementation assay, I observed clearly reduced decapping activity, showing that the trimerization domain is important for efficient decapping *in vivo*.

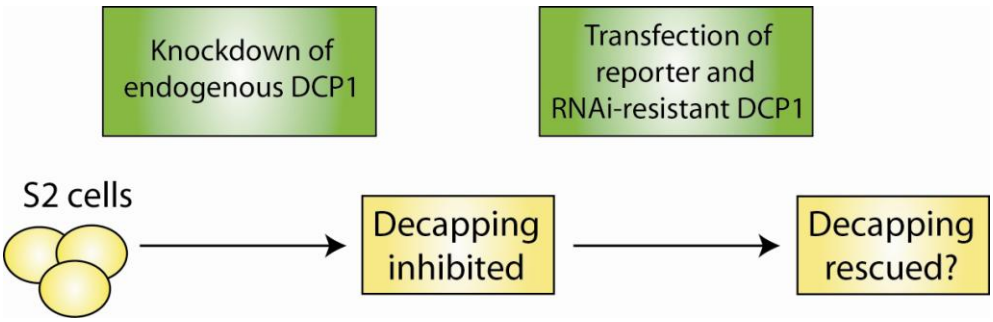

Figure 7: Complementation assay in *Dm* S2 cells. S2 cells are depleted from endogenous DCP1 by RNA interference (RNAi) and decapping is inhibited. An RNAi-resistant version of DCP1 wild-type or mutant is transfected together with a reporter to monitor decapping. This allows for testing if the mutant DCP1 rescues decapping in cells comparable to wild-type or if the mutation affects its function in cells.

Summarizing this study on DCP1, I found that metazoan DCP1 – in contrast to yeast DCP1 – self-interacts and establishes an interaction network via motif I and the trimerization domain (Figure 8). This results in an unexpected connectivity and complexity of the metazoan decapping complex and explains the central role of DCP1 in decapping activator assembly and activation of decapping.

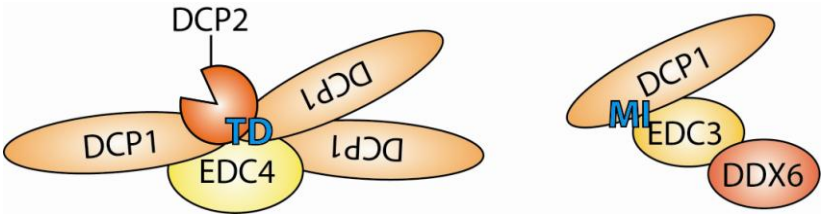

Figure 8: Metazoan DCP1 assembles via the trimerization domain (TD) and motif I (MI) into two decapping activator complexes. TD mediates DCP1 self-interaction and binding to DCP2 and EDC4 and M1 confers binding to EDC3 and DDX6.

4.1.2 Pat assembles into distinct mRNA decapping complexes.

The work described in this chapter has been published in Braun et al., 2010. Experimental data and detailed description of experimental procedures are available in the attached manuscript.

As mentioned above, the Pat protein plays an important role in the transition of translationally active mRNAs to mRNAs that are repressed and committed to degradation. However the molecular details of how the Pat protein serves as a scaffold in this transition was unclear, in particular for the human Pat protein (Coller and Parker, 2005; Scheller et al., 2007; Pilkington and Parker, 2008). In this study I dissected the human Pat protein and determined how it assembles into distinct decapping activator complexes. In human there are two paralogs of the Pat protein, however only PatL1 and not PatL2 is a functional ortholog of the yeast Pat1 protein, which is why I studied the human PatL1 protein.

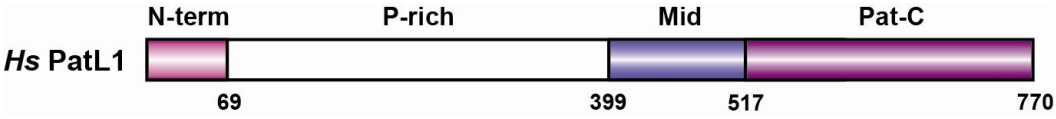

Figure 9: Domain organization of *Hs* PatL1: PatL1 consists of a conserved N-terminal sequence (N-term), a proline-rich region (P-rich), a conserved Middle domain (Mid) and a conserved C-terminal domain (Pat-C). Numbers underneath the protein schematic represent amino acid positions at the fragment boundaries (adopted from Braun et al., 2010).

First, I examined the interaction of PatL1 with decapping activators in coimmunoprecipitation experiments in human HEK293 cells. I could detect interactions of PatL1 with

DDX6/Me31B, DCP2, EDC4 and the LSm1-7 ring. Analysis of the domain organization of PatL1 revealed a conserved N-terminal sequence (N-term), a proline-rich region (P-rich), a conserved Middle domain (Mid) and a conserved C-terminal domain (Pat-C) (Figure 9). To map which part of the PatL1 protein is important for these interactions, I generated a series of expression constructs to express fragments of PatL1. I showed that DDX6/Me31B interacts with the N-term of PatL1. Using deletion constructs I found Pat-C is essential for PatL1 to interact with DCP2, EDC4 and the LSm1-7 ring. The P-rich cooperates with Pat-C to bind DCP2 and EDC4, whereas Mid and Pat-C form a bipartite binding site for the LSm1-7 ring. Interestingly, a construct of PatL1 comprising the P-rich in addition to the Mid and the Pat-C interacts less efficient with the LSm1-7 ring than Mid and Pat-C alone, therefore the P-rich interferes with LSm1-7 ring binding. This might be due to the induction of a different conformation of PatL1 with lower affinity for the LSm1-7 ring in consequence of DCP2/EDC4-binding. Alternatively binding of an as yet unknown factor X to the P-rich could block the accessibility of the Mid domain to the LSm1-7 ring.

In summary, I could describe several distinct PatL1 complexes (Figure 10). DDX6-binding to PatL1 is independent of the binding of DCP2, EDC4 and the LSm1-7 ring, however I could observe a negative correlation of DCP2/EDC4- and LSm1-7-binding to PatL1. Therefore, either the Mid and Pat-C domains cooperate to bind the LSm1-7 ring (Figure 10A) or the P-rich binds together with Pat-C to DCP2 and EDC4 (Figure 10B). An additional complex with an as yet unknown protein (factor X) binding to the P-rich region and blocking the accessibility of the Mid domain to the LSm1-7 ring cannot be excluded (Figure 10C).

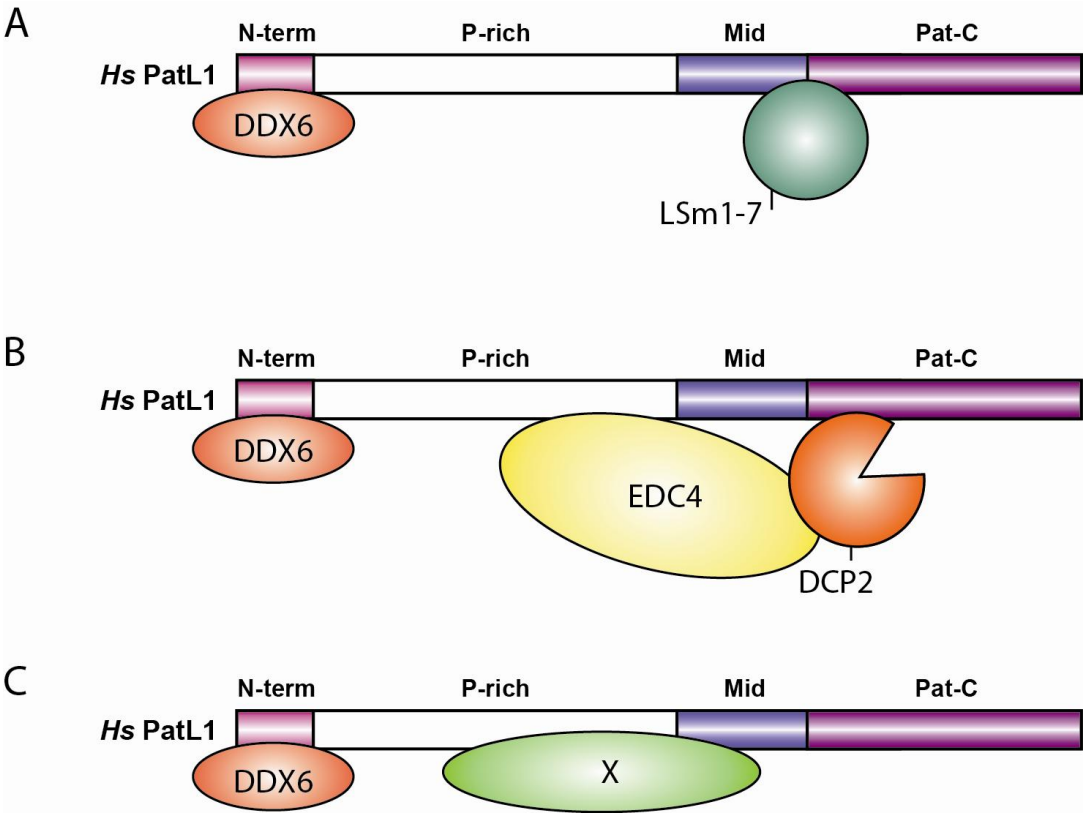

Figure 10: *Hs* PatL assembles into distinct mRNA decapping complexes and may adopt different conformations: **A)** one with the ability to interact with the LSm1-7 ring and the other **B)** interacting either with EDC4 and DCP2. A third complex **C)** with an as yet unknown protein factor (X) binding to the P-rich region and blocking the accessibility of the Mid domain to the LSm1-7 ring cannot be excluded.

Since PatL1 interacts with DCP2 I asked whether decapping activity can be copurified with PatL1. To address this question I performed an *in vitro* decapping assay as described in 4.1.1 and showed that PatL1coimmunoprecipitates decapping activity. I mapped using deletion constructs which part of PatL1 is important to incorporate PatL1 into active decapping complexes. Consistently with the interaction data described above Pat-C is essential for PatL1 incorporation into active decapping complexes.

In conclusion, the mapping of interactions revealed distinct complexes of PatL1 with potentially specific function or representing sequential steps of mRNA decay challenging the prevailing model of a static super-decapping complex. Further this indicates a central role for the Pat-C domain in PatL1, which has been described to be dispensable in the yeast Pat1 ortholog (Pilkington and Parker, 2008).

4.1.3 The DEAD box helicase DDX6/Me31B interacts with EDC3, Tral and Pat to form distinct complexes with roles in translational repression and mRNA decapping.

The work described in this chapter has been published in Tritschler et al., 2009a and Haas et al., 2010. Experimental data and detailed description of experimental procedures are available in the attached manuscripts.

The DEAD box helicase DDX6/Me31B has been implicated in translational repression and mRNA decapping (Weston and Sommerville, 2006). Consistently, DDX6/Me31B interacts with the decapping factors EDC3, DCP1, DCP2, Pat and the LSm1-7 ring and with Tral and Cup, which are involved in translational repression. The resulting protein complexes might explain the functional diversity of DDX6/Me31B. Previous work from our lab identified two complexes in *Dm*, one complex contains minimally DCP1, Tral and Cup and another complex EDC3, DCP1 and DCP2 (Tritschler et al., 2007; Tritschler et al., 2008). Taking advantage of the structural information on the interaction interface of DDX6/Me31B with EDC3 (3.1.3) I tested a set of mutants of DDX6/Me31B and EDC3 predicted to be defective in DDX6/Me31B-EDC3 interaction in coimmunoprecipitation experiments in *Dm* S2 cells.

I identified amino acids in DDX6/Me31B important for EDC3-binding. These mutants allowed me to test in coimmunoprecipitation experiments, if Tral uses a mode of interaction similar to EDC3 to interact with DDX6/Me31B. Indeed, Tral binds to the same protein surface of DDX6/Me31B as EDC3. I also generated mutants of EDC3 deficient in DDX6/Me31B-binding and defined the amino acids of EDC3 critical for the interaction with DDX6/Me31B. Sequence similarities between EDC3 and Tral suggested that a related Phe-Asp-Phe motif (FDF) in Tral is important for binding to DDX6/Me31B. I confirmed this prediction in coimmunoprecipitation experiments. These interaction mutants of DDX6/Me31B and EDC3 also allowed me to test the functional importance of the interaction of DDX6/Me31B with EDC3 and Tral to repress the expression of bound mRNAs in tethering assays. Wild-type DDX6/Me31B or EDC3 repress translation of bound mRNAs. In contrast, DDX6/Me31B or EDC3 mutants that no longer interact were also unable to repress the expression of the mRNA target.

Interestingly, DDX6/Me31B not only interacts with EDC3 and Tral, but also with HPat. Testing a mutant of DDX6/Me31B that is deficient in EDC3 and Tral binding in coimmunoprecipation experiments I could show that different amino acids of DDX6/Me31B are important for the interaction with HPat than with EDC3 and Tral. Nevertheless, the

binding of DDX6/Me31B to HPat and EDC3 or Tral is mutually exclusive, as I observed in competition experiments.

Summarizing this data, I could provide evidence for three mutually exclusive complexes containing DDX6/Me31B as common factor (Figure 11). These distinct complexes containing translational repressors and decapping activators suggest how at the molecular level different function of DDX6/Me31B dependent on the respective interaction partners could be achieved.

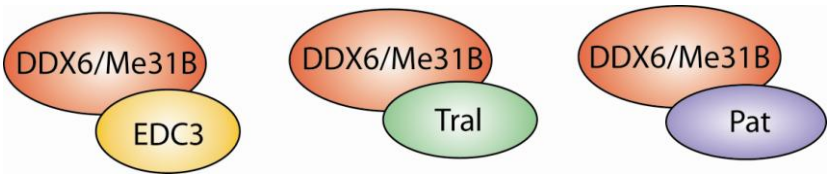

Figure 11: DDX6/Me31B establishes mutually exclusive interactions with EDC3, Tral and Pat.

4.2 GW182 proteins directly recruit cytoplasmic deadenylase complexes to miRNA targets.

The work described in this chapter has been published in Braun et al., 2011 and Huntzinger et al., 2010. Experimental data and detailed description of experimental procedures are available in the attached manuscripts.

miRISCs cause translational repression and/or mRNA degradation of miRNA targets. miRNA-mediated mRNA degradation is initiated by deadenylation. But despite strong evidence that miRISCs can promote deadenylation the mechanism of how they accelerate deadenylation has remained controversial and two models can be envisioned: 1) miRISCs could directly promote deadenylation of miRNA targets, 2) the observed accelerated deadenylation could be only an indirect consequence of miRISC activity. In the latter case the translational block or the interaction of GW182 proteins with PABPC could indirectly promote deadenylation of miRNA targets.

To discriminate between these possibilities I systematically screened for interactions between the miRISC and subunits of the two cytoplasmic deadenylation complexes in human and *Dm* cells.

I started with a systematic screen between the AGO/GW182 proteins as the core components of the miRISC and the components of the two major cytoplasmic deadenylases, the CCR4-NOT complex and the PAN2-PAN3 complex in human HEK293 cells and *Dm* S2 cells by coimmunoprecipitation experiments. I observed that human and *Dm* GW182 proteins interact with subunits of the CCR4-NOT and the PAN2-PAN3 complexes. When I compared the three human GW182 proteins I could not observe a significant difference in their interaction profile consistent with the functional data so far available on these proteins suggesting a redundant function in the miRNA pathway. I detected only much weaker interactions between the AGO proteins and the deadenylase factors, so I focused on the GW182 proteins.

In human cells I could observe interactions between the GW182 proteins and PAN3, NOT1, NOT2, CCR4a, CCR4b, CAF1 and POP2. Since this screen for interactions was done with transiently overexpressed proteins, it was important to validate these interactions with endogenous proteins, what I did for PAN3 and NOT1, for which suitable antibodies were available.

Since these interaction studies were done in cell lysates, the discussed interactions could be direct or mediated by another protein present in the cell lysate. To address this question, I tested the positive hits of the interaction screen as candidates for direct interactions in GST-pulldown experiments, where I incubated GST-tagged GW182 purified from *E. coli* with the respective *in vitro* translated deadenylation factor. Only PAN3 and NOT1 interacted with GW182 under these conditions.

However neither PAN3 nor NOT1 have deadenylase activity themselves, so to test if PAN3 and NOT1 indeed recruit the PAN2-PAN3 and the CCR4-NOT complex to the GW182 proteins to promote deadenylation, I performed a combination of overexpression and depletion experiments. These experiments provided evidence, that PAN3 can recruit PAN2 and NOT1 can recruit the CCR4-NOT complex to miRNA targets (Figure 12).

Further these experiments showed also that NOT1 and PAN3 mediate at least in part indirect binding of GW182 to PABP that I recently observed in human cells (Huntzinger et al., 2010).

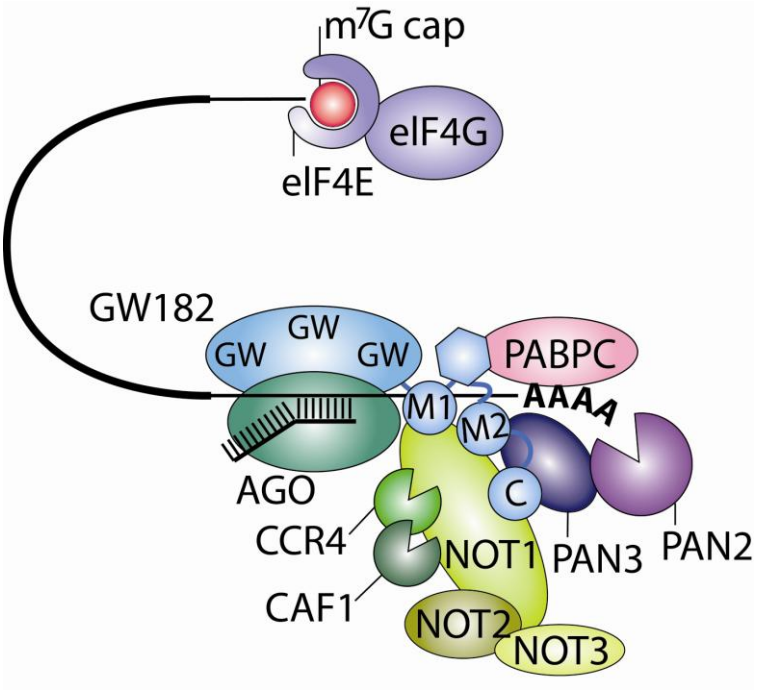

Figure 12: GW182 is recruited by the AGO-protein to the miRNA target and interacts with PABPC. GW182 directly recruits the CCR4-NOT and PAN2-PAN3 complexes to promote deadenylation of the miRNA target. Mid1 (M1), Mid2 (M2) and the C-term (C) of the silencing domain are important for the direct interactions with PAN3 and NOT1 as depicted.

To define which part of the GW182 proteins confers binding to the deadenylation factors, I tested not only full-length GW182 proteins, but also a fragment lacking the silencing domain or only the silencing domain alone. I found the silencing domain was necessary and sufficient for these interactions, which is consistent with the observation that the silencing confers the silencing activity.

Thus, the silencing domain of GW182 proteins provides a binding platform for PABPC (Fabian et al., 2009; Zekri et al., 2009; Huntzinger et al., 2010) and deadenylase complexes to promote silencing. Further these results indicate that deadenylation is a direct effect of miRNA regulation.

5 Conclusions

In the first part of my PhD thesis I studied how decapping activators assemble into distinct mRNA decapping complexes in metazoa to promote mRNA decapping. Studying the examples of DCP1, Pat and DDX6/Me31B provided detailed insights into the decapping activator network and revealed an unexpected complexity and connectivity. The results also confirmed the prediction, that studying mRNA decapping in metazoa was relevant to obtain new insights into principles of activation and regulation of mRNA decapping.

The observed interactions could also provide the molecular basis for RNA granules/P body formation. Previous models that suggested P body formation by prion-like aggregation (Decker et al., 2007; Reijns et al., 2007) were questioned by an investigation of the physical properties of such RNA granules, which show rather the behavior of liquid droplets (Brangwynne et al., 2009). Detailed information about the interactions of decay factors will be essential to model the physical properties of such decay ensembles and compare them with the observed physical properties of RNA granules in cells.

My results challenge also the prevailing model of a super-decapping activator complex, since distinct, and at least partially mutual exclusive, decapping activator complexes seem to be a common characteristic of decapping activators assemblies. In future it will be of great interest to determine if these distinct complexes represent different pathways or sequential events of a single pathway.

Motif I of metazoan DCP1 as well as the FDF motif of EDC3 and Tral represent short linear motifs. Linear motifs are short protein sequences with a specific function, such as localization signals, phosphorylation sites or mediation of protein-protein interactions (Neduva and Russell, 2005; Davey et al., 2012). Due to their shortness linear motifs can evolve rapidly and are difficult to predict from protein sequence. Therefore, experimental identification and characterization of linear motifs in decapping factors was important to dissect the assembly of decapping complexes. It is interesting to note in this context that in later studies linear motifs similar to the motif I of DCP1 were identified in yeast DCP2 that interact with EDC3 in a similar way (Harigaya et al., 2010; Fromm et al., 2011).

In the second part of my PhD thesis, I studied how general mRNA decay factors can be recruited by specialized pathways to degrade the mRNA target. In particular, I focused on the miRNA pathway. Despite that several previous studies (Meister et al., 2005; Landthaler et al., 2008; Chen et al., 2009; Zekri et al., 2009; Piao et al., 2010) failed to detect any significant interaction of the miRISC with components of deadenylase complexes, I could identify two deadenylation factors as new direct binding partners using a systematic coimmunoprecipitation screening approach. This experimental approach could also be applied to other target specific decay pathways.

Future challenges in the field are now to study how the intricate network of AGO proteins, GW182 proteins, PABPC, the PAN2-PAN3 complex and the CCR4-NOT complex cooperate to promote translational repression and mRNA degradation of miRNA targets. It will be of great interest to dissect how translational repression and mRNA degradation or miRNA targets are interconnected. Specific interaction mutants of the proteins mentioned above would greatly contribute to this task. In order to get time-resolved information about mRNA decay it will be also important to further develop time-course experiments in cells to study miRISC function, since *in vitro* systems currently seem to insufficiently recapitulate the full aspect of miRNA mediated gene silencing.

Exciting progress in observing single events in RNA metabolism has recently been made in the field of splicing (Hoskins et al., 2011). Using a combination of genetic engineering, chemical biology, and multi-wavelength fluorescence microscopy the authors were able to follow the assembly of single spliceosomes in real time in yeast whole-cell extracts. The authors reasonably suggest that this experimental setup is expected to prove widely useful for mechanistic analysis of macromolecular enzymes in environments approaching the complexity of living cells. The application of this approach to the field of mRNA decay or miRNA-mediated gene silencing promises deep mechanistic insights into these fundamental processes of post-transcriptional gene regulation.

6 References

Badis, G., Saveanu, C., Fromont-Racine, M. and Jacquier, A. (2004). "Targeted mRNA degradation by deadenylation-independent decapping." *Mol. Cell* **15**(1): 5-15.

Baek, D., Villén, J., Shin, C., Camargo, F. D., Gygi, S. P. and Bartel, D. P. (2008). "The impact of microRNAs on protein output." *Nature* **455**(7209): 64-71.

Bagga, S., Bracht, J., Hunter, S., Massirer, K., Holtz, J., Eachus, R. and Pasquinelli, A. E. (2005). "Regulation by let-7 and lin-4 miRNAs results in target mRNA degradation." *Cell* **122**(4): 553-63.

Bartel, D. P. (2009). "MicroRNAs: target recognition and regulatory functions." *Cell* **136**(2): 215-33.

Beelman, C. A., Stevens, A., Caponigro, G., LaGrandeur, T. E., Hatfield, L., Fortner, D. M. and Parker, R. (1996). "An essential component of the decapping enzyme required for normal rates of mRNA turnover." *Nature* **382**(6592): 642-646.

Brangwynne, C. P., Eckmann, C. R., Courson, D. S., Rybarska, A., Hoege, C., Gharakhani, J., Jülicher, F. and Hyman, A. A. (2009). "Germline P granules are liquid droplets that localize by controlled dissolution/condensation." *Science* **324**(5935): 1729-32.

Braun, J. E., Tritschler, F., Haas, G., Igreja, C., Truffault, V., Weichenrieder, O. and Izaurralde, E. (2010). "The C-terminal alpha-alpha superhelix of Pat is required for mRNA decapping in metazoa." *EMBO J.* **29**(14): 2368-80.

Braun, J. E., Huntzinger, E., Fauser, M. and Izaurralde, E. (2011). "GW182 proteins directly recruit cytoplasmic deadenylase complexes to miRNA targets." *Mol. Cell* **44**(1): 120-33.

Chekulaeva, M., Mathys, H., Zipprich, J. T., Attig, J., Colic, M., Parker, R. and Filipowicz, W. (2011). "miRNA repression involves GW182-mediated recruitment of CCR4-NOT through conserved W-containing motifs." *Nat. Struct. Mol. Biol.* **18**(11):1218-26.

Chen, C. Y., Zheng, D., Xia, Z. and Shyu, A. B. (2009). " Ago-TNRC6 triggers microRNA-mediated decay by promoting two deadenylation steps." *Nat. Struct. Mol. Biol.* **16**(11): 1160-6.

Coller, J. M., Tucker, M., Sheth, U., Valencia-Sanchez, M. A. and Parker, R. (2001). "The DEAD box helicase, Dhh1p, functions in mRNA decapping and interacts with both the decapping and deadenylase complexes." *RNA* **7**(12): 1717-1727.

Coller, J. and Parker, R. (2005). "General translational repression by activators of mRNA decapping." *Cell* **122**(6): 875-886.

Collart, M. A. and Panasenko, O. O. (2012). "The Ccr4-Not complex." *Gene* **492**(1): 42-53.

Davey, N. E., Van Roey, K., Weatheritt, R. J., Toedt, G., Uyar, B., Altenberg, B., Budd, A., Diella, F., Dinkel, H. and Gibson, T. J. (2012). "Attributes of short linear motifs." *Mol. Biosyst.* **8**(1):268-81.

Decker, C. J., Teixeira, D. and Parker, R. (2007). "Edc3p and a glutamine/asparagine-rich domain of Lsm4p function in processing body assembly in *Saccharomyces cerevisiae*." *J. Cell. Biol.* 2007 **179**(3): 437-49.

Eulalio, A., Behm-Ansmant, I. and Izaurralde, E. (2007). "P bodies: at the crossroads of post-transcriptional pathways." *Nat. Rev. Mol. Cell. Biol.* **8**(1): 9-22.

Eulalio, A., Tritschler, F. and Izaurralde, E. (2009a). "The GW182 protein family in animal cells: new insights into domains required for miRNA-mediated gene silencing." *RNA* **15**(8): 1433-42.

Eulalio, A., Huntzinger, E., Nishihara, T., Rehwinkel, J., Fauser, M., Izaurralde, E. (2009b). "Deadenylation is a widespread effect of miRNA regulation." *RNA* **15**(1):21-32.

Fabian, M. R., Mathonnet, G., Sundermeier, T., Mathys, H., Zipprich, J. T., Svitkin, Y. V., Rivas, F., Jinek, M., Wohlschlegel, J., Doudna, J. A., Chen, C. Y., Shyu, A. B., Yates, J. R. 3rd, Hannon, G. J., Filipowicz, W., Duchaine, T. F. and Sonenberg, N. (2009). "Mammalian miRNA RISC recruits CAF1 and PABP to affect PABP-dependent deadenylation." *Mol. Cell* ***35***(6): 868-80.

Fabian, M. R., Sonenberg, N. and Filipowicz, W. (2010). "Regulation of mRNA translation and stability by microRNAs." *Annu. Rev. Biochem.* **79**: 351-79.

Fabian, M. R., Cieplak, M. K., Frank, F., Morita, M., Green, J., Srikumar, T., Nagar, B., Yamamoto, T., Raught, B., Duchaine, T. F. and Sonenberg, N. (2011). "miRNA-mediated deadenylation is orchestrated by GW182 through two conserved motifs that interact with CCR4-NOT." *Nat. Struct. Mol. Biol.* **18**(11):1211-7.

Fenger-Grøn, M., Fillman, C., Norrild, B. and Lykke-Andersen, J. (2005). "Multiple processing body factors and the ARE binding protein TTP activate mRNA decapping." *Mol. Cell* **20**(6): 905-915.

Franks, T. M. and Lykke-Andersen, J. (2008). "The control of mRNA decapping and P-body formation." *Mol. Cell* **32**(5): 605-615.

Fromm, S. A., Truffault, V., Kamenz, J., Braun, J. E., Hoffmann, N. A., Izaurralde, E. and Sprangers, R. (2011). "The structural basis of Edc3- and Scd6-mediated activation of the Dcp1:Dcp2 mRNA decapping complex." *EMBO J.* **31**(2): 279-90.

Goldstrohm, A. C. and Wickens, M. (2008). "Multifunctional deadenylase complexes diversify mRNA control." *Nat. Rev. Mol. Cell. Biol.* **9**(4): 337-44.

Guo, H., Ingolia, N. T., Weissman, J. S. and Bartel, D. P. (2010). "Mammalian microRNAs predominantly act to decrease target mRNA levels." *Nature* **466**(7308): 835-40.

Gu, M. and Lima, C. D. (2005). "Processing the message: structural insights into capping and decapping mRNA." *Curr. Opin. Struct. Biol.* **15**(1): 99-106.

Haas, G., Braun, J. E., Igreja, C., Tritschler, F., Nishihara, T. and Izaurralde, E. (2010). "HPat provides a link between deadenylation and decapping in metazoa." *J. Cell. Biol.* **189**(2): 289-302.

Harigaya, Y., Jones, B. N., Muhlrad, D., Gross, J. D., Parker, R. (2010). " Identification and analysis of the interaction between Edc3 and Dcp2 in *Saccharomyces cerevisiae*." *Mol. Cell. Biol.* **30**(6): 1446-56.

Hendrickson, D. G., Hogan, D. J., McCullough, H. L., Myers, J. W., Herschlag, D., Ferrell, J. E. and Brown, P. O. (2009). "Concordant regulation of translation and mRNA abundance for hundreds of targets of a human microRNA." *PLoS Biol.* **7**(11): e1000238.

Hoskins, A. A., Friedman, L. J., Gallagher, S. S., Crawford, D. J., Anderson, E. G., Wombacher, R., Ramirez, N., Cornish, V. W., Gelles, J. and Moore, M. J. (2011). "Ordered and dynamic assembly of single spliceosomes." *Science* **331**(6022): 1289-95.

Hu, W., Sweet, T. J., Chamnongpol, S., Baker, K. E. and Coller, J. (2009). "Co-translational mRNA decay in *Saccharomyces cerevisiae*." *Nature* **461**(7261): 225-229.

Huntzinger, E., Braun, J. E., Heimstädt, S., Zekri, L. and Izaurralde, E. (2010). "Two PABPC1- binding sites in GW182 proteins promote miRNA-mediated gene silencing." *EMBO J.* **29**(24): 4146-60.

Huntzinger, E. and Izaurralde, E. (2011). "Gene silencing by microRNAs: contributions of translational repression and mRNA decay." *Nat. Rev. Genet.* **12**(2): 99-110.

Krol, J., Loedige, I. and Filipowicz, W. (2010). "The widespread regulation of microRNA biogenesis, function and decay." *Nat. Rev. Genet.* **11**(9): 597-610.

Lim, L. P., Lau, N. C., Garrett-Engele, P., Grimson, A., Schelter, J. M., Castle, J., Bartel, D. P., Linsley, P. S. and Johnson, J. M. (2005). "Microarray analysis shows that some microRNAs downregulate large numbers of target mRNAs." *Nature* **433**(7027): 769-73.

Krützfeldt, J., Rajewsky, N., Braich, R., Rajeev, K. G., Tuschl, T., Manoharan, M. and Stoffel, M. (2005). "Silencing of microRNAs in vivo with 'antagomirs'." *Nature* **438**(7068): 685-9.

Landthaler, M., Gaidatzis, D., Rothballer, A., Chen, P. Y., Soll, S. J., Dinic, L., Ojo, T., Hafner, M., Zavolan, M. and Tuschl, T. (2008). "Molecular characterization of human Argonaute-containing ribonucleoprotein complexes and their bound target mRNAs." *RNA* **14**(12): 2580-96.

Lykke-Andersen, J. (2002) "Identification of a human decapping complex associated with hUpf proteins in nonsense-mediated decay." *Mol. Cell. Biol.* **22**(23):8114-21.

Marzluff, W. F., Wagner, E. J. and Duronio, R. J. (2008). "Metabolism and regulation of canonical histone mRNAs: life without a poly(A) tail." *Nat. Rev. Genet.* **9**(11): 843-54.

Meister, G., Landthaler, M., Peters, L., Chen, P. Y., Urlaub, H., Lührmann, R. and Tuschl, T. (2005). "Identification of novel argonaute-associated proteins." *Curr. Biol.* **15**(23): 2149-55.

Neduva, V. and Russell, R. B. (2005). "Linear motifs: evolutionary interaction switches." *FEBS Lett.* **579**(15): 3342-5.

Olsen, P. H. and Ambros, V. (1999). "The lin-4 regulatory RNA controls developmental timing in *Caenorhabditis elegans* by blocking LIN-14 protein synthesis after the initiation of translation." *Dev. Biol.* **216**(2): 671-80.

Parker, R. and Sheth, U. (2007). "P bodies and the control of mRNA translation and degradation." *Mol. Cell* **25**(5): 635-646.

Parker, R. and Song, H. (2004). "The enzymes and control of eukaryotic mRNA turnover." *Nat. Struct. Mol. Biol.* **11**(2): 121-127.

Piao, X., Zhang, X., Wu, L. and Belasco, J. G. (2010). " CCR4-NOT deadenylates mRNA associated with RNA-induced silencing complexes in human cells." *Mol. Cell. Biol.* **30**(6):1486-94.

Pilkington, G. R. and Parker, R. (2008). "Pat1 contains distinct functional domains that promote P-body assembly and activation of decapping." *Mol. Cell. Biol.* **28**(4): 1298-1312.

Reijns, M. A., Alexander, R. D., Spiller, M. P. and Beggs, J. D. (2008) "A role for Q/N-rich aggregation-prone regions in P-body localization." *J. Cell. Sci.* **121**(Pt 15):2463-72.

Sandler, H. and Stoecklin, G. (2008). "Control of mRNA decay by phosphorylation of tristetraprolin." *Biochem. Soc. Trans.* **36**(Pt 3): 491-496.

Sandler, H., Kreth, J., Timmers, H. T. and Stoecklin, G. (2011). "Not1 mediates recruitment of the deadenylase Caf1 to mRNAs targeted for degradation by tristetraprolin." *Nucleic Acids Res.* **39**(10): 4373-86.

Scheller, N., Resa-Infante, P., de la Luna, S., Galao, R. P., Albrecht, M., Kaestner, L., Lipp, P., Lengauer, T., Meyerhans, A. and Díez, J. (2007). "Identification of PatL1, a human homolog to yeast P body component Pat1." *Biochimica Et Biophysica Acta-Molecular Cell Research* **1773**(12): 1786-1792.

Selbach, M., Schwanhäusser, B., Thierfelder, N., Fang, Z., Khanin, R. and Rajewsky, N. (2008). "Widespread changes in protein synthesis induced by microRNAs." *Nature* **455**(7209): 58-63.

Sharova, L. V., Sharov, A. A., Nedorezov, T., Piao, Y., Shaik, N. and Ko, M. S. (2009). "Database for mRNA half-life of 19 977 genes obtained by DNA microarray analysis of pluripotent and differentiating mouse embryonic stem cells." *DNA Res.* **16**(1): 45-58.

She, M., Decker, C. J., Svergun, D. I., Round, A., Chen, N., Muhlrad, D., Parker, R. and Song, H. (2008). "Structural basis of dcp2 recognition and activation by dcp1." *Mol. Cell* **29**(3): 337-349.

Smith, R. W. and Gray, N. K. (2010). "Poly(A)-binding protein (PABP): a common viral target." *Biochem. J.* **426**(1): 1-12.

Sonenberg, N. and Hinnebusch, A. G. (2009). "Regulation of translation initiation in eukaryotes: mechanisms and biological targets." *Cell* **136**(4): 731-45.

Song, M. G., Li, Y. and Kiledjian, M. (2010). "Multiple mRNA decapping enzymes in mammalian cells." *Mol. Cell* **40**(3): 423-32.

Tharun, S., He, W., Mayes, A. E., Lennertz, P., Beggs, J. D. and Parker, R. (2000). "Yeast Sm-like proteins function in mRNA decapping and decay." *Nature* **404**(6777): 515-518.

Tharun, S. and Parker, R. (2001). "Targeting an mRNA for decapping: displacement of translation factors and association of the Lsm1p-7p complex on deadenylated yeast mRNAs." *Mol. Cell* **8**(5): 1075-1083.

Tomecki, R. and Dziembowski, A. (2010). "Novel endoribonucleases as central players in various pathways of eukaryotic RNA metabolism." *RNA* **16**(9): 1692-724.

Tritschler, F., Eulalio, A., Truffault, V., Hartmann, M. D., Helms, S., Schmidt, S., Coles, M., Izaurralde, E. and Weichenrieder, O. (2007). "A divergent Sm fold in EDC3 proteins mediates DCP1 binding and P-body targeting." *Mol. Cell. Biol.* **27**(24): 8600-8611.

Tritschler, F., Eulalio, A., Helms, S., Schmidt, S., Coles, M., Weichenrieder, O., Izaurralde, E. and Truffault, V. (2008). "Similar modes of interaction enable Trailer Hitch and EDC3 to associate with DCP1 and Me31B in distinct protein complexes." *Mol. Cell. Biol.* **28**(21): 6695-6708.

Tritschler, F., Braun, J. E., Eulalio, A., Truffault, V., Izaurralde, E. and Weichenrieder, O. (2009a). "Structural basis for the mutually exclusive anchoring of P body components EDC3 and Tral to the DEAD box protein DDX6/Me31B." *Mol. Cell* **33**(5): 661-668.

Tritschler, F., Braun, J. E., Motz, C., Igreja, C., Haas, G., Truffault, V., Izaurralde, E. and Weichenrieder, O. (2009b). "DCP1 forms asymmetric trimers to assemble into active mRNA decapping complexes in metazoa." *Proc. Natl. Acad. Sci. USA* **106**(51): 21591-21596.

Tritschler, F., Huntzinger, E. and Izaurralde, E. (2010). "Role of GW182 proteins and PABPC1 in the miRNA pathway: a sense of déjà vu." *Nat. Rev. Mol. Cell. Biol.* **11**(5): 379-384.

Tucker, M., Valencia-Sanchez, M. A., Staples, R. R., Chen, J., Denis, C. L. and Parker, R. (2001). "The transcription factor associated Ccr4 and Caf1 proteins are components of the major cytoplasmic mRNA deadenylase in *Saccharomyces cerevisiae*." *Cell* **104**(3): 377-86.

Weston, A. and Sommerville, J. (2006). "Xp54 and related (DDX6-like) RNA helicases: roles in messenger RNP assembly, translation regulation and RNA degradation." *Nucleic Acids Res.* **34**(10): 3082-3094.

Wu, L. and Belasco, J. G. (2005). "Micro-RNA regulation of the mammalian lin-28 gene during neuronal differentiation of embryonal carcinoma cells." *Mol. Cell. Biol.* **25**(21): 9198-208.

Yamashita, A., Chang, T. C., Yamashita, Y., Zhu, W., Zhong, Z., Chen, C. Y. and Shyu, A. B. (2005). "Concerted action of poly(A) nucleases and decapping enzyme in mammalian mRNA turnover." *Nat. Struct. Mol. Biol.* **12**(12): 1054-63.

Zekri, L., Huntzinger, E., Heimstädt, S. and Izaurralde, E. (2009). "The silencing domain of GW182 interacts with PABPC1 to promote translational repression and degradation of microRNA targets and is required for target release." *Mol. Cell. Biol.* **29**(23): 6220-31.

7 Abbreviations

AGO	Argonaute
ARE	AU-rich elements
CAF1	CCR4-associated factor 1
CCR4	Carbon catabolite repressor protein 4
C-term	C-terminal
Dm	*Drosophila melanogaster*
DCP1	decapping protein 1
DCP2	decapping protein 2
DCPS	scavenger decapping protein
DDX6	DEAD (Asp-Glu-Ala-Asp) box polypeptide 6
DEAD box	Asp-Glu-Ala-Asp box
DNA	deoxyribonucleic acid
dsRNAs	double-stranded RNAs
E. coli	*Escherichia coli*
EDC3	enhancer of decapping 3
EDC4	enhancer of decapping 4
eIF	eukaryotic translation initiation factor
eIF4E-BP	eIF4E binding protein
EVH1	Ena-VASP homology 1 domain
F-Luc	firefly luciferase
FDF	Phe-Asp-Phe
GDP	guanosine diphosphate
GMP	guanosine monophosphate
GST	glutathione-S-transferase

GTP	guanosine triphosphate
GW-repeat	Gly-Trp-repeat
GW182	Gly-Trp repeat containing protein of 182 kDa
Hs	*Homo sapiens*
HA	hemagglutinin
Hedls	human enhancer of decapping large subunit
HEK293 cells	human embryonic kidney 293 cells
HeLa cells	cancer cell line derived from from the patient Henrietta Lacks
HPat	homolog of Pat1
LSm	Sm-like
m^7G	7-methyl-guanosine
MBP	maltose binding protein
Me31B	maternal expression at 31B
Mid	Middle
miRISC	miRNA induced silencing complex
miRNA	microRNA
mRNA	messenger ribonucleic acid
mRNP	messenger ribonucleoprotein
Mut	mutant
NMD	nonsense-mediated mRNA decay
N-term	N-terminal
NOT	Negative regulator of transcription homolog
nt	nucleotide(s)
ORF	open reading frame
P body	mRNA processing body
PABPC	cytoplasmic poly(A) binding protein

PAM2	PABPC-interacting motif 2
PAN	poly(A) specific ribonuclease subunit homolog
Pat-C	C-terminal domain of Pat proteins
Pat1	protein associated with topoisomerase II
PatL1	Pat1-like
poly(A) tail	poly adenine tail
POP2	Poly(A) ribonuclease POP2
pre-mRNA	precursor mRNA
Q-rich	region rich in glutamine
R-Luc	*Renilla* luciferase
RNA	ribonucleic acid
RNAi	RNA interference
RNP	ribonucleoprotein
RRM	RNA recognition motif
SD	silencing domain of GW182
Sp	*Schizosaccharomyces pombe*
S2 cells	*Dm* Schneider 2 cells
siRNA	small interfering RNA
TD	trimerization domain of DCP1
TNRC6	Trinucleotide repeat-containing gene 6 protein
Tral	Trailer Hitch
UBA	ubiquitin associated-like domain
UTR	untranslated region
XRN1	exoribonuclease 1

8 Appendix

8.1 List of publications

8.1.1 Discussed publications

Braun, J. E., Huntzinger, E., Fauser, M. and Izaurralde, E. (2011). "GW182 proteins directly recruit cytoplasmic deadenylase complexes to miRNA targets." *Mol. Cell* **44**(1): 120-33.

Huntzinger, E., **Braun, J. E.**, Heimstädt, S., Zekri, L. and Izaurralde, E. (2010). "Two PABPC1- binding sites in GW182 proteins promote miRNA-mediated gene silencing." *EMBO J.* **29**(24): 4146-60.

Braun, J. E. *, Tritschler, F. *, Haas, G., Igreja, C., Truffault, V., Weichenrieder, O. and Izaurralde, E. (2010). "The C-terminal alpha-alpha superhelix of Pat is required for mRNA decapping in metazoa." *EMBO J.* **29**(14): 2368-80.

* shared first authorship

Haas, G., **Braun, J. E.**, Igreja, C., Tritschler, F., Nishihara, T. and Izaurralde, E. (2010). "HPat provides a link between deadenylation and decapping in metazoa." *J. Cell. Biol.* **189**(2): 289-302.

Tritschler, F. *, **Braun, J. E.** *, Motz, C., Igreja, C., Haas, G., Truffault, V., Izaurralde, E. and Weichenrieder, O. (2009b). "DCP1 forms asymmetric trimers to assemble into active mRNA decapping complexes in metazoa." *Proc. Natl. Acad. Sci. USA* **106**(51): 21591-21596.

* shared first authorship

Tritschler, F., **Braun, J. E.**, Eulalio, A., Truffault, V., Izaurralde, E. and Weichenrieder, O. (2009a). "Structural basis for the mutually exclusive anchoring of P body components EDC3 and Tral to the DEAD box protein DDX6/Me31B." *Mol. Cell* **33**(5): 661-668.

8.1.2 Further publications

Braun, J. E., Huntzinger, E. and Izaurralde, E. (2012) "A molecular link between miRISCs and deadenylases provides new insight into the mechanism of gene silencing by microRNAs." *"Translational Control" Cold Spring Harbour Monograph Series*, in press.

Fromm, S. A., Truffault, V., Kamenz, J., **Braun, J. E.**, Hoffmann, N. A., Izaurralde, E. and Sprangers, R. (2011). "The structural basis of Edc3- and Scd6-mediated activation of the Dcp1:Dcp2 mRNA decapping complex." *EMBO J.* **31**(2): 279-90.

8.2 Acknowledgements

I would like to thank Prof. Dr. Elisa Izaurralde for being an excellent supervisor and for giving me the opportunity to work in her laboratory on very exciting research projects. I really had a great time!

I also would like to thank Dr. Felix Tritschler and Dr. Eric Huntzinger for great collaborations over many projects.

Further I would like to thank all past and present lab members for the nice working atmosphere, especially Dr. Ana Eulalio, Andreas Boland, Anna Schneider, Birgit Schuster, Dr. Gabrielle Haas, Dr. Heike Budde, Dr. Isao Kashima, Maria Fauser, Marie Palaj, Regina Büttner, Dr. Stefanie Jonas, Dr. Steffen Schmidt, Dr. Susanne Heimstädt, Dr. Tadashi Nishihara, Dr. Vincent Truffault and Dr. Oliver Weichenrieder for their support and inspiring discussions.

I am very grateful to Prof. Dr. Hans Bisswanger for the supervision of this thesis at the Eberhard Karls University Tübingen.

Molecular Cell
Article

GW182 Proteins Directly Recruit Cytoplasmic Deadenylase Complexes to miRNA Targets

Joerg E. Braun,[1] Eric Huntzinger,[1] Maria Fauser,[1] and Elisa Izaurralde[1,*]
[1]Department of Biochemistry, Max Planck Institute for Developmental Biology, Spemannstrasse 35, D-72076 Tübingen, Germany
*Correspondence: elisa.izaurralde@tuebingen.mpg.de
DOI 10.1016/j.molcel.2011.09.007

SUMMARY

miRNAs are posttranscriptional regulators of gene expression that associate with Argonaute and GW182 proteins to repress translation and/or promote mRNA degradation. miRNA-mediated mRNA degradation is initiated by deadenylation, although it is not known whether deadenylases are recruited to the mRNA target directly or by default, as a consequence of a translational block. To answer this question, we performed a screen for potential interactions between the Argonaute and GW182 proteins and subunits of the two cytoplasmic deadenylase complexes. We found that human GW182 proteins recruit the PAN2-PAN3 and CCR4-CAF1-NOT deadenylase complexes through direct interactions with PAN3 and NOT1, respectively. These interactions are critical for silencing and are conserved in *D. melanogaster*. Our findings reveal that GW182 proteins provide a docking platform through which deadenylase complexes gain access to the poly(A) tail of miRNA targets to promote their deadenylation, and they further indicate that deadenylation is a direct effect of miRNA regulation.

INTRODUCTION

MicroRNAs (miRNAs) are key regulators of gene expression that posttranscriptionally silence mRNA targets containing complementary sequences (Huntzinger and Izaurralde, 2011). To do so, they associate with Argonaute and GW182 family proteins into effector complexes known as miRNA-induced silencing complexes (miRISCs), which repress translation and promote target mRNA degradation. Recent studies have indicated that target degradation is a widespread effect of miRNA-based regulation that accounts for an important fraction of the repression mediated by miRNAs (reviewed by Huntzinger and Izaurralde, 2011).

Although miRNAs can induce the degradation of fully complementary targets via endonucleolytic cleavage catalyzed by Argonaute proteins, they rarely do so in animal cells, in which the vast majority of targets are partially complementary (reviewed by Huntzinger and Izaurralde, 2011). In such cases, the mRNA target is degraded by the enzymes involved in the cellular 5′-to-3′ mRNA decay pathway (Behm-Ansmant et al., 2006; Chen et al., 2009; Eulalio et al., 2007, 2009; Giraldez et al., 2006; Piao et al., 2010; Wu et al., 2006). In this pathway, after being deadenylated, mRNAs are decapped by the decapping enzyme DCP2. Decapped mRNAs are ultimately degraded by the major cytoplasmic 5′-to-3′ exonuclease XRN1.

In eukaryotes, the mRNA poly(A) tail is removed by the consecutive action of two cytoplasmic deadenylase complexes (Yamashita et al., 2005). The PAN2-PAN3 complex is involved in an early phase of deadenylation in which long poly(A) tails are shortened to approximately 50–110 nucleotides, depending on the organism (Yamashita et al., 2005). The PAN2-PAN3 complex is stimulated by the cytoplasmic poly(A)-binding protein PABPC1 (Boeck et al., 1996; Brown et al., 1996; Uchida et al., 2004). Accordingly, PAN3 interacts with PABPC1 and recruits PAN2, the catalytic subunit, to mRNA targets (Brown et al., 1996; Mangus et al., 2004; Siddiqui et al., 2007; Uchida et al., 2004). The second, more rapid phase of deadenylation is catalyzed by the CCR4-CAF1-NOT complex (Tucker et al., 2001; Yamashita et al., 2005), which is sufficient for mRNA deadenylation in the absence of PAN2 (Brown et al., 1996; Tucker et al., 2001; Yamashita et al., 2005).

Several lines of evidence support a role for the two cytoplasmic deadenylase complexes in miRNA-mediated gene silencing. First, depletion of components of the CCR4-CAF1-NOT complex partially suppresses silencing by inhibiting miRNA target deadenylation and their subsequent decay (Behm-Ansmant et al., 2006; Eulalio et al., 2007; Piao et al., 2010). Second, transcriptome analysis of cells depleted of CCR4-CAF1-NOT complex components showed that the majority of miRNA targets (both predicted and validated) are upregulated, indicating that deadenylation is indeed important for global miRNA regulation (Eulalio et al., 2009). Third, overexpression of catalytically inactive CCR4a, CAF1, or POP2 (a CAF1 paralog) mutants also suppresses silencing in a dominant negative manner (Chen et al., 2009; Piao et al., 2010). Although PAN2 depletion does not suppress silencing (Behm-Ansmant et al., 2006; Piao et al., 2010), overexpression of a catalytically inactive PAN2 mutant slows down the initial phase of target deadenylation (Chen et al., 2009), indicating that the PAN2-PAN3 complex is involved in but is not essential for degradation of miRNA targets.

Although the role of the PAN2-PAN3 and the CCR4-CAF1-NOT deadenylase complexes in the miRNA pathway is well

established, the molecular mechanism underlying their recruitment has remained a controversial question, and three distinct models have been proposed. One model suggests that miRISC components (e.g., AGO and/or GW182 proteins) recruit (directly or indirectly) deadenylases to miRNA targets (Behm-Ansmant et al., 2006; Eulalio et al., 2007; 2009; Fabian et al., 2009; Huntzinger et al., 2010; Huntzinger and Izaurralde, 2011; Zekri et al., 2009). An alternative model proposes that miRISCs indirectly increase the efficacy of deadenylation, for example, by making the mRNA poly(A) more susceptible to deadenylases without increasing their local concentration. The observation that GW182 proteins contain a PAM2 motif, which confers direct binding to PABPC1 supports this model (Fabian et al., 2009; Huntzinger et al., 2010; Jinek et al., 2010; Kozlov et al., 2010; Zekri et al., 2009). Indeed, GW182 proteins could facilitate PABPC1 dissociation from the mRNA poly(A) tail, thereby exposing it to deadenylases (Fabian et al., 2009; Huntzinger et al., 2010; Zekri et al., 2009). A third model suggests that deadenylases are recruited to miRNA targets by default as an indirect consequence of a primary inhibitory effect of miRISCs on translation (reviewed by Djuranovic et al., 2011).

To investigate whether deadenylases are recruited directly to miRNA targets, we systematically screened for potential interactions between AGO and GW182 and each subunit of the PAN2-PAN3 and CCR4-CAF1-NOT complexes in both human and *D. melanogaster* cells. We found that the three human GW182 paralogs (known as TNRC6A-C) associate with the PAN2-PAN3 and CCR4-CAF1-NOT complexes through direct interactions with PAN3 and NOT1, respectively. These interactions are independent of each other and are conserved in *D. melanogaster*. Our findings indicate that the TNRC6 proteins provide a binding platform for deadenylation factors to cause rapid deadenylation of mRNA targets and further suggest that deadenylation is a direct effect of miRNA regulation.

RESULTS

TNRC6 Proteins Interact with Subunits of Cytoplasmic Deadenylase Complexes

To systematically screen for potential interactions between miRISCs and components of the two major cytoplasmic deadenylase complexes (the PAN2-PAN3 and CCR4-CAF1-NOT complexes), we coexpressed either GFP-tagged AGO2 or TNRC6C with HA-tagged subunits of these complexes in human HEK293 cells and performed coimmunoprecipitation assays using anti-GFP antibodies.

The conserved core of the CCR4-CAF1-NOT complex in metazoan consists of 5 subunits: NOT1, NOT2, NOT3 (also known as NOT3/5), and two catalytically active subunits, CCR4a or its paralog CCR4b and CAF1 or its paralog POP2 (Table S1) (Lau et al., 2009; Temme et al., 2004). Of these, TNRC6C coimmunoprecipitated NOT1, NOT2, CCR4a/b, CAF1, and POP2 (Figures 1B, 1C, and 1E–1H). TNRC6C showed weak but reproducible interactions with NOT3 and NOT10, but no significant interaction with the human-specific subunits TAB182 and C2ORF29 (Figures 1D and S1) (Lau et al., 2009).

Additionally, TNRC6C interacted with PAN3, a subunit of the dimeric PAN2-PAN3 complex, but not with PAN2, which is the catalytically active subunit (Figures 1I and 1J). Interactions with deadenylation factors were observed in cell lysates treated with either RNase A or micrococcal nuclease, suggesting that they are not mediated by RNA. Importantly, the deadenylation factors did not discriminate between TNRC6 paralogs because similar binding profiles were observed for TNRC6A and TNRC6B (see Figures 3 [below], S2, and S3).

In contrast to TNRC6s, human AGO2 exhibited weak interactions with CCR4a/b and POP2, as previously reported (Fabian et al., 2009), and it associated weakly with NOT1 and NOT2 (Figure S4). These interactions, however, are not mediated by TNRC6s because an AGO2 mutant that no longer binds TNRC6s (the F2V2 mutant [Eulalio et al., 2008]) interacted with deadenylation factors as well as wild-type (Figure S4). In summary, TNRC6s (and to a lesser extent AGO2) coimmunoprecipitate components of both of the major cytoplasmic deadenylase complexes, suggesting that miRISCs have the ability to recruit these complexes to mRNA targets. Here, we limit our analysis to the more prominent interactions mediated by GW182 proteins.

The Interactions with Deadenylation Factors Are Conserved

Next, we investigated whether the interactions observed in human cells are conserved in *Drosophila melanogaster* (*Dm*). We found that *Dm* GW182 coimmunoprecipitated NOT1, NOT2, PAN3, and to a much lesser extent PAN2 (Figures 2A, 2B, 2G, and 2H). The interaction of GW182 with PAN2 was strongly enhanced in cells in which PAN3 was coexpressed (Figure 2I, lane 8 versus 6), suggesting that PAN3 bridges the GW182-PAN2 interaction. This observation prompted us to test whether PAN3 also bridges TNRC6-PAN2 interaction in human cells. We observed that TNRC6C did indeed coimmunopecipitate PAN2 in HEK293 cells in which PAN3 was also coexpressed (Figure 2J, lane 8 versus 6).

Additionally, in agreement with the results obtained in human cells, *D. melanogaster* GW182 exhibited weak but reproducible interactions with CCR4, POP2, and NOT3/5 (Figures 2C, 2E, and 2F), suggesting that these interactions may be bridged by the other components of the CCR4-CAF1-NOT complex. Finally, NOT4 did not associate with *Dm* GW182 (Figure 2D), consistent with the observation that NOT4 is not an integral subunit of the complex in human or *D. melanogaster* cells (Lau et al., 2009; Temme et al., 2004).

Our findings indicate that the interactions of GW182 proteins with components of the two major cytoplasmic deadenylase complexes are conserved. In particular, PAN3, NOT2, and NOT1 coimmunoprecipitated with TNRC6s and *Dm* GW182 to an extent similar to that observed with endogenous PABPC1 (Figure 1H), which interacts with GW182 proteins directly (Fabian et al., 2009; Huntzinger et al., 2010; Jinek et al., 2010; Kozlov et al., 2010).

Validation of the Interaction Screen

Because the interaction screen was performed with transiently expressed proteins, it was important to validate the newly identified TNRC6s partners using alternative approaches. First, we confirmed the interactions with PAN3 and NOT1 in reciprocal

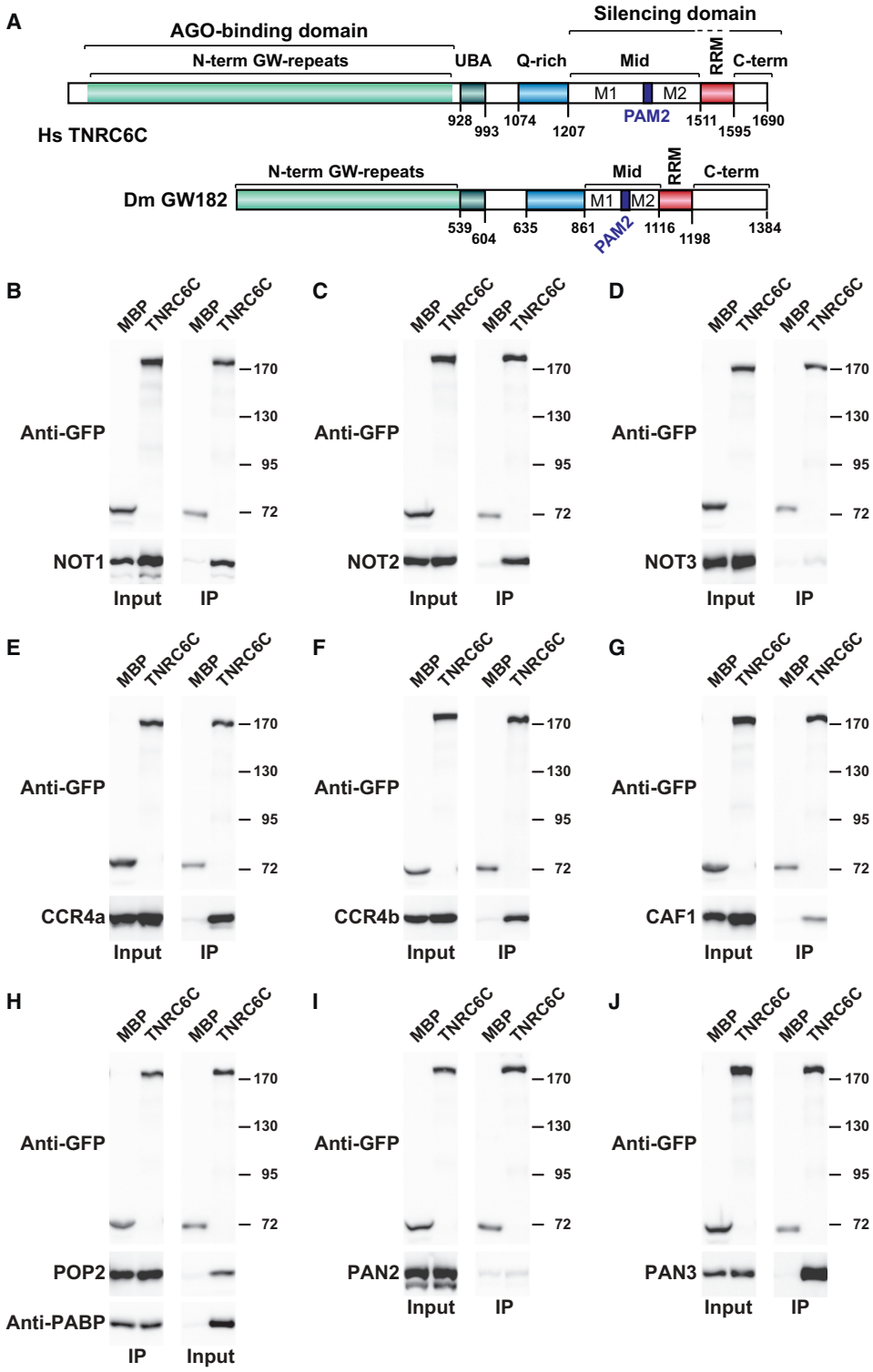

Figure 1. TNRC6C Interacts with Deadenylation Factors

(A) The domain organization of *Hs* TNRC6C and *Dm* GW182. Human TNRC6C and *Dm* GW182 consist of an N-terminal AGO-binding domain, which contains multiple GW-repeats (light green), and a bipartite silencing domain (SD), which includes the middle (Mid) and C-terminal (C-term) regions. UBA: ubiquitin associated domain; Q-rich: region rich in glutamine; PAM2: PABP-interacting motif 2; RRM: RNA recognition motif; M1 and M2: regions within the Mid region. (B–J) Human HEK293 cells were cotransfected with plasmids expressing GFP-tagged TNRC6C and HA-tagged deadenylase subunits as indicated. GFP-tagged maltose-binding protein (MBP) served as a negative control. Cell lysates were immunoprecipitated with a polyclonal anti-GFP antibody. Inputs and

immunoprecipitations in which bait and prey proteins were exchanged. We found that GFP-tagged PAN3 and NOT1 coimmunoprecipitated HA-TNRC6C (Figures S5A and S5B). Second, we immunoprecipitated GFP-TNRC6C and identified endogenous PAN3, NOT1, and NOT2 in the immunoprecipitates using specific antibodies (Figure S5C). Remarkably, endogenous proteins coimmunoprecipitated with GFP-TNRC6C more efficiently than the transiently expressed counterparts (compare Input and IP ratios in Figure 1 versus Figure S5C), most likely because the transiently expressed subunits may not be quantitatively incorporated into endogenous complexes.

Finally, we confirmed the interactions described above using endogenous proteins. We observed that endogenous TNRC6 proteins coimmunoprecipitated endogenous PAN3 and NOT1 (Figure 3A), which are the two directly interacting subunits of the endogenous deadenylase complexes (see below). Furthermore, we performed a similar experiment in *Drosophila* cells and showed that endogenous Dm GW182 coimunoprecipitated with endogenous NOT1 (Figure 3B). In summary, our results indicate that the TNRC6 proteins associate with subunits of the two major cytoplasmic deadenylase complexes.

The Silencing Domains of TNRC6s Confer Binding to Deadenylation Factors

To define domains within TNRC6s that are important for their interaction with deadenylase complex subunits, we performed coimmunoprecipitations with a series of TNRC6B deletion mutants. We observed that deleting the TNRC6B silencing domain (SD, amino acids 1218–1723) abolished its interaction with NOT1, NOT2, CCR4a/b, CAF1, POP2 and PAN3 (Figure 3C–I, lane 7). Conversely, the silencing domain was sufficient to interact with NOT1, NOT2, CCR4a/b, CAF1 and POP2 as efficiently as full-length TNRC6B (Figure 3C–3H, lanes 8 versus 6), but was slightly impaired for PAN3 binding (Figure 3I, lane 8 versus 6). Similar results were obtained with the silencing domains of TNRC6A and C (Figures S2 and S3). Thus, the silencing domains are both necessary and sufficient for TNRC6s to interact with deadenylase subunits.

Notably, although the interaction with PAN3 and NOT1 are conserved in *D. melanogaster*, deletion of the GW182 SD did not abolish NOT1 and PAN3 binding (Figures 3J and 3K, lanes 8 versus 6), suggesting that, in contrast to the human proteins, additional regions in *Dm* GW182 also contribute to these interactions.

TNRC6 Silencing Domains Bind PAN3 and NOT1 Directly

To investigate whether the interaction of TNRC6 proteins with deadenylation factors is direct, we performed GST (glutathione S-transferase) pull-down assays with recombinant proteins expressed in *E. coli*. In particular, we focused on the conserved interactions with PAN3, NOT1, and NOT2. We also tested the interaction of recombinant TNRC6s with CCR4a because CCR4a/b were efficiently coimmunoprecipitated with TNRC6s from human cell lysates (Figures 1E and 1F).

The results showed that a GST fusion of the TNRC6B-silencing domain (GST-6B-SD) pulled down full-length PAN3 (Figure 4A, lane 10). This interaction was specific because PAN3 did not bind to beads coated with GST (Figure 4A, lane 7). In contrast to PAN3, neither NOT2 nor CCR4a bound to GST-6B-SD in vitro (Figure 4A, lanes 11 and 12), indicating that the interaction of these proteins with TNRC6s in cell lysates is indirect.

NOT1 was expressed at low levels in *E. coli* (NOT1 contains 2371 amino acids), and in addition to the full-length protein we obtained shorter polypeptides that may have arose from degradation, premature translation termination, or internal initiation due to the length of NOT1 ORF. Nevertheless, the higher molecular weight polypeptides were pulled down with the TNRC6B silencing domain (Figure 4B, lane 4). To confirm these results, we performed GST pull-down assays with in vitro translated NOT1 in wheat germ extracts (Figures 4C and 4D). As shown in Figure 4C, in wheat germ extracts, we also obtained full-length NOT1 and additional shorter polypeptides. Again, the higher molecular weight polypeptides were pulled down with GST-6B-SD (Figure 4C, lane 3). In vitro translated PAN3 and PABPC1, which interact directly with TNRC6s and therefore served as positive controls, were also pulled down under these conditions, as expected (Figure 4C, lane 3). In contrast, in vitro translated NOT2 and CCR4a did not interact with TNRC6B-SD above background levels (Figure 4C), which is in agreement with the results shown in Figure 4A using recombinant proteins expressed in *E. coli*. Finally, in vitro translated POP2 also failed to interact with the silencing domain (Figure 4C). These results suggest that we observed only direct interactions in wheat germ extracts. Taken together, our observations indicate that the silencing domain of the TNRC6 proteins interact directly with PAN3 and NOT1.

NOT1 Mediates the Interaction of TNRC6s with the CCR4-CAF1-NOT Complex

To investigate the interdependence of TNRC6 interactions with PAN3, the CCR4-CAF1-NOT1 complex, and PABPC1, we performed immunoprecipitation assays in cells in which either PAN3 or NOT1 proteins were depleted using pooled siRNAs. We observed that PAN3 depletion did not affect the interaction of TNRC6C with NOT1, NOT2, or CCR4a (Figures 5A–5C, lanes 8 versus 4), although PAN3 levels were reduced down to ~25% (Figure S6A). In contrast, PAN3 depletion slightly reduced the interaction of TNRC6 with endogenous PABPC1 (Figure 5D, lane 8 versus 4), indicating that PAN3, although not essential, could facilitate PABPC1 binding.

When we reduced the levels of NOT1 (by 50%), we observed that the interaction of TNRC6C with NOT2, CCR4a, and POP2 was also strongly reduced (Figures 5E–5G and S6B). In contrast, NOT1 depletion did not affect TNRC6 binding to PAN3 but slightly decreased PABPC1 binding (Figure 5G and 5H, lanes 8 versus 4).

Three conclusions can be drawn from these experiments. First, NOT1 and PAN3 interact with TNRC6s independently of each other. Second, NOT1 mediates the interactions between TNRC6s and the additional subunits of the CCR4-CAF1-NOT

immunoprecipitates were subjected to Western blotting using anti-GFP and anti-HA antibodies. For the GFP-tagged proteins, 1% of the input and 5% of the immunoprecipitate was loaded, whereas for the HA-tagged proteins, 1% of the input and 30% of the immunoprecipitate was analyzed. In each panel, cell lysates were treated with RNase A prior to immunoprecipitation. See also Figures S1–S4 and Table S1.

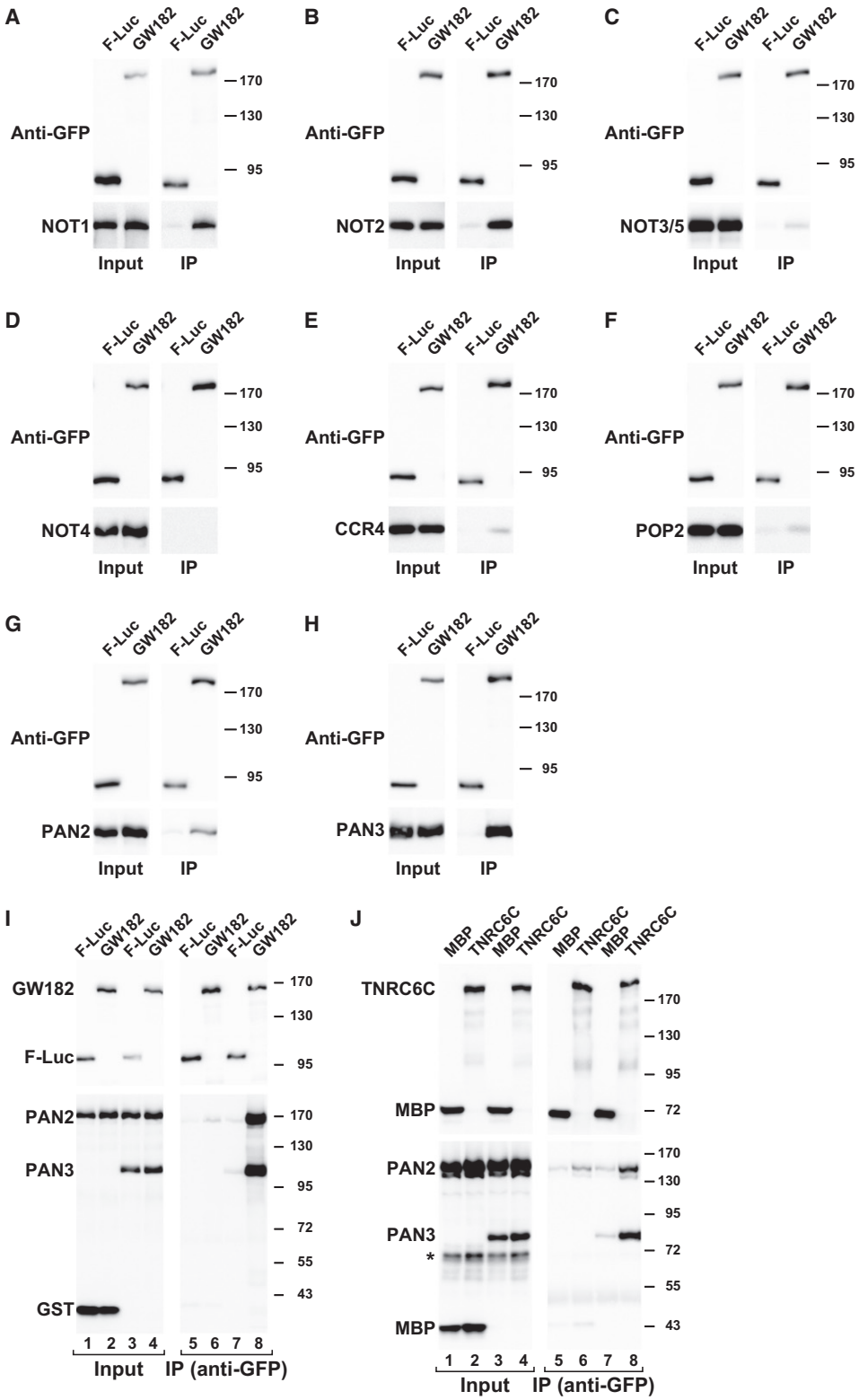

Figure 2. The Interactions of GW182 Proteins with Deadenylation Factors Are Conserved in *D. melanogaster*

(A–H) Lysates from S2 cells cotransfected with plasmids expressing GFP-tagged *Dm* GW182 and HA-tagged deadenylase subunits were immunoprecipitated using a polyclonal anti-GFP antibody. GFP-tagged firefly luciferase served as a negative control. Inputs and immunoprecipitates were analyzed by western blotting as described in Figure 1, with the exception that 1% of the input and 40% of the immunoprecipitates were loaded for the HA-tagged proteins.

complex because these interactions are abolished in NOT1-depleted cells. Finally, PAN3 and NOT1 may facilitate TNRC6-PABPC1 interaction, in agreement with the fact that PAN3 also contains a PAM2 motif (Mangus et al., 2004; Siddiqui et al., 2007).

PAN3 and NOT1 Bind to the Mid and C-Term Regions of the Silencing Domains

The silencing domain of TNRC6 proteins consists of four regions: M1, PAM2 motif, M2, and C term (Figure 1A) (Huntzinger et al., 2010; Zekri et al., 2009; Huntzinger and Izaurralde, 2011). The RRM domain connecting the M2 and C-term regions is not required for silencing. To further delineate regions within the silencing domain that contribute to interaction with PAN3 and NOT1 we deleted each region alone or in combination and performed GST pull-down assays.

We observed that GST-6B-SD mutants lacking either the M1 region or the PAM2 motif interacted with PAN3 to the same extent as full-length GST-6B-SD (Figure 6A, lanes 11–13). In contrast, deleting the M2 or C-term regions individually reduced the interaction of GST-6B-SD with PAN3 (Figure 6A, lanes 14 and 15). The interaction was abolished when both regions were deleted (Figure 6A, lane 18), suggesting that the M2 and C-term regions contribute to PAN3 binding in an additive manner. Accordingly, the M2 and C-term regions (with or without the connecting RRM domain) were sufficient for binding to PAN3 in vitro (Figure S6C, lanes 11 and 12).

When the same series of GST-6B-SD deletion mutants was tested for interactions with in vitro translated NOT1, we observed that the M1, M2, and C-term regions all contributed to binding because deleting each one of these regions individually slightly reduced, but did not abolish, NOT1 binding (Figures 6B [lanes 4, 6, and 7] and S6D). Binding was strongly reduced when any two of these three regions were deleted simultaneously (Figures 6B [lanes 8–10] and S6D). In contrast, deletion of the PAM2 motif did not affect binding to NOT1 (Figure 6B, lane 5). Additionally, we observed that NOT1 binding to GST-6B-SD was not affected (i.e., neither stimulated nor inhibited) in the presence of a large excess of recombinant human PAN3 (data not shown), suggesting that, although the PAN3 and NOT1-binding sites on TNRC6s overlap, their binding is neither interdependent nor mutually exclusive. Combined, these experiments demonstrate that the interactions of the TNRC6 proteins with PAN3 and NOT1 are mediated by the Mid and C-term regions of the silencing domain. These interactions are independent of each other and are also compatible, suggesting that TNRC6s could bind PAN3 and NOT1 simultaneously.

TNRC6 Proteins Interact with the PAN3 C-Terminal Domain

PAN3 proteins are characterized by an N-terminal region (amino acids 1–290) and a C-terminal domain (amino acids 291–687). The N-terminal region contains a canonical PAM2 motif and interacts with PABPC1, whereas the C-terminal domain is required for PAN3 association with PAN2 (Mangus et al., 2004; Siddiqui et al., 2007; Uchida et al., 2004). In GST pull-down assays, we observed that the PAN3 C-terminal domain (PAN3 C term) was sufficient for binding to GST-6B-SD (Figure S6C, lane 14). The PAN3 C term was also pulled down by TNRC6B protein fragments containing the M2 and C-term regions (Figure S6C, lanes 15 and 16). We conclude that the TNRC6B M2 and C-term regions bind directly to the PAN3 C-terminal domain, which itself interacts with PAN2 but not with PABPC1, reinforcing the conclusion that PAN3 interacts with GW182 independently of PABPC1.

The M2 and C-Term Regions of TNRC6s Are Critical for Silencing

To evaluate how the interactions between TNRC6 proteins and deadenylase subunits contribute to silencing, we tested whether a TNRC6 mutant lacking the M2 and C-term regions, which cannot bind PAN3 and has reduced NOT1 binding, could rescue silencing in cells lacking endogenous TNRC6s. In this complementation assay, endogenous TNRC6A and TNRC6B were depleted from HeLa cells using specific siRNAs targeting the corresponding mRNAs. Cells were then transfected with plasmids expressing siRNA-resistant versions of either wild-type or mutant TNRC6A together with a miRNA reporter. Control cells were treated with a siRNA against β-Gal (β-Gal-siRNA).

Codepletion of TNRC6A and TNRC6B efficiently suppresses silencing of a *Renilla* luciferase reporter containing three let-7 binding sites in its 3′UTR (Figure 6C, R-Luc-3xlet-7 [Huntzinger et al., 2010]). Silencing is restored when these cells are transfected with a plasmid expressing a siRNA-resistant wild-type TNRC6A (Huntzinger et al., 2010) (Figure 6C).

Remarkably, deleting both the M2 and C-term regions strongly impaired TNRC6A silencing activity, indicating that these regions are critical for silencing (Figure 6C). As previously reported, a TNRC6A mutant that does not interact with PABPC1 (i.e., lacking the PAM2 motif) was also largely unable to rescue silencing of the let-7 reporter (Figure 6C) (Huntzinger et al., 2010), although this mutant was still able to interact with deadenylation factors (Figures 6A and 6B). TNRC6A silencing activity was abolished when the entire silencing domain was deleted, which is consistent with previously published work (Figure 6C) (Huntzinger et al., 2010). Each protein was expressed to a similar level (Figure 6D).

Two important conclusions can be drawn from these results. First, there is a correlation between the deadenylation factor binding and the silencing activity of TNRC6A. Second, a TNRC6A mutant that does not bind PABPC1 (ΔPAM2) has impaired silencing activity even though this mutant is able to interact

(I) S2 cells were cotransfected with a mixture of two plasmids: one expressing HA-PAN2 and one expressing either GFP-GW182 or GFP-F-Luc (negative control). In addition, the transfection mixtures contained a third plasmid expressing either HA-GST (lanes 1, 2, 5, and 6) or HA-PAN3 (lanes 3, 4, 7 and 8). Cell lysates were immunoprecipitated and analyzed by western blotting as described above.

(J) Human HEK293 cells were co-transfected with plasmids expressing HA-PAN2 and either GFP-TNRC6C or GFP-MBP (negative control). In lanes 1, 2, 5 and 6, the transfection mixtures also contained a plasmid expressing HA-MBP, whereas in lanes 3, 4, 7, and 8, the transfection mixtures contained a plasmid expressing HA-PAN3. Cell lysates were immunoprecipitated and analyzed as described in Figure 1. The asterisk indicates cross-reactivity of the anti-HA antibody.

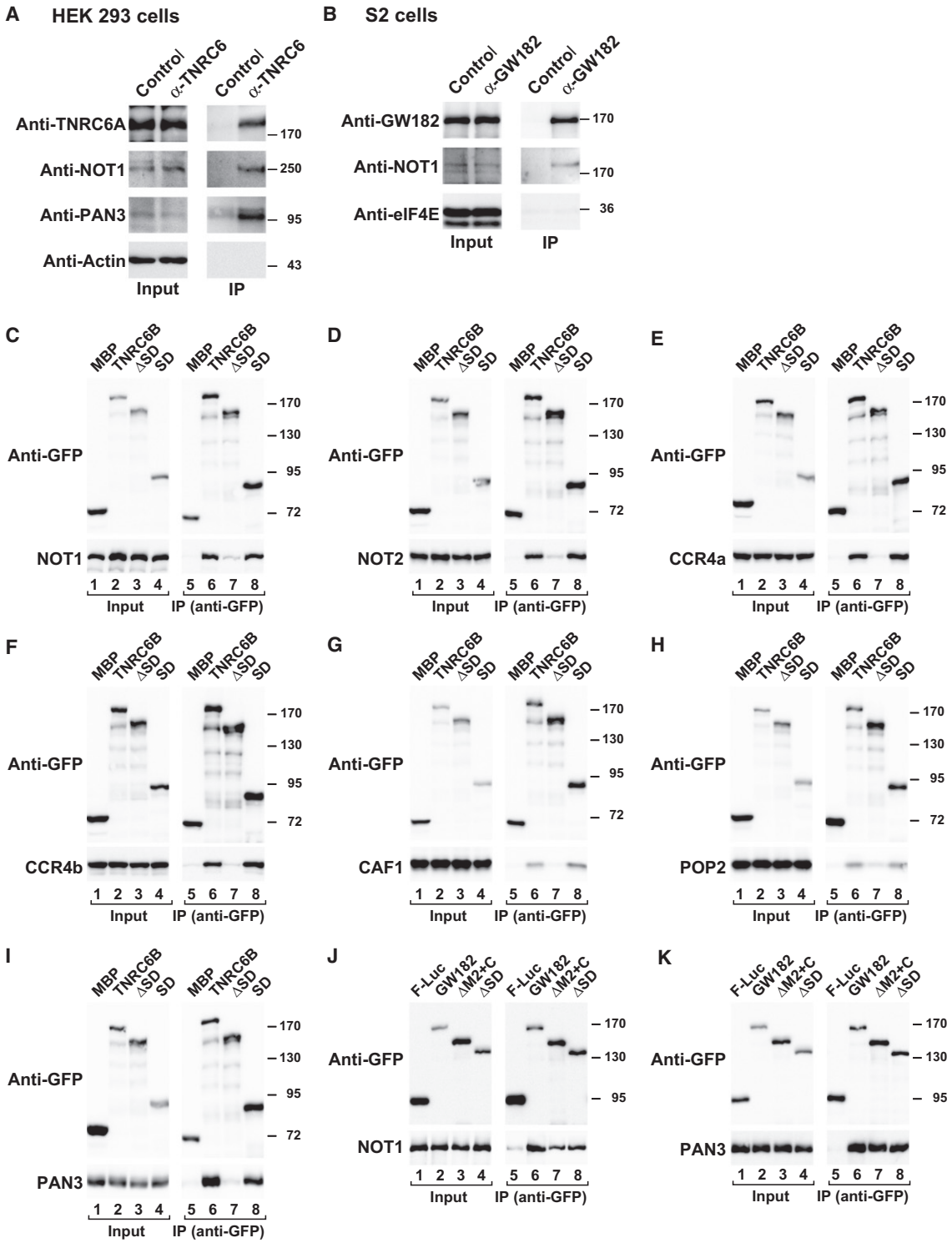

Figure 3. Endogenous TNRC6 Proteins Coimmunoprecipitate Subunits of the Endogenous Deadenylase Complexes

(A) Lysates from human HEK293 cells were immunoprecipitated with a control antibody (anti-GFP antibody) or an antibody recognizing TNRC6s. Inputs and immunoprecipitates were analyzed by western blotting using antibodies recognizing endogenous NOT1 or PAN3. An antibody to endogenous Actin served as a control to determine the specificity of the immunoprecipitations.

(B) S2 cell lysates were immunoprecipitated with a control antibody (anti-GFP antibody) or an antibody recognizing Dm GW182. Inputs and immunoprecipitates were analyzed by western blotting using an antibody specific for NOT1. An antibody to endogenous eIF4E served as a negative control.

with deadenylation factors (Figures 6A and 6B), indicating that the mere recruitment of deadenylases is not sufficient for full silencing activity. Conversely, PABPC1 binding is not sufficient for silencing. Thus, TNRC6 proteins may require interaction with both deadenylation factors and PABPC1 for full silencing activity. Nevertheless, because both the M2 and C-term regions must be deleted to inhibit binding to deadenylase complexes, we cannot rule out that these regions are also required for additional interactions.

The CCR4-CAF1-NOT Complex Provides a Major Contribution to miRNA-Mediated mRNA Degradation

It has been shown that knockdown of the components of the CCR4-CAF1-NOT1 complex strongly reduces miRNA-mediated mRNA deadenylation and decay both in *Drosophila* and human cells (Behm-Ansmant et al., 2006; Chen et al., 2009; Eulalio et al., 2009; Piao et al., 2010), whereas inactivation of the PAN2-PAN3 complex slows down the initial deadenylation rate of miRNA targets in human cells, but deadenylation and decay still occur (Chen et al., 2009), providing one explanation for the observation that PAN2-PAN3 complex inactivation minimally affects miRNA target levels at steady state (Behm-Ansmant et al., 2006; Chen et al., 2009; Piao et al., 2010). Furthermore, these results are consistent with previous observations indicating that the CCR4-CAF1-NOT complex takes over cytoplasmic deadenylation in the absence of the PAN2-PAN3 complex (Tucker et al., 2001; Yamashita et al., 2005) and that deadenylation mediated by the CCR4-CAF1-NOT complex leads to decay of the mRNA body, whereas PAN2-PAN3-mediated deadenylation results in an initial shortening of the poly(A) tail without further mRNA decay (Yamashita et al., 2005).

The data presented above indicate that both deadenylase complexes can be recruited to miRNA targets independently of each other and may independently contribute to miRNA target degradation. Therefore, we re-examined the contribution of these complexes to the degradation of miRNA targets in *Drosophila* cells, in which the effect of depleting the PAN2-PAN3 complex on miRNA target half-life has not been analyzed. The decay rate of miRNA targets was analyzed in cells depleted of PAN3 and NOT1 either individually or in combination. For this assay, we used the F-Luc-Nerfin reporter that was previously shown to be deadenylated in the presence of miR-9b in S2 cells (Behm-Ansmant et al., 2006; Eulalio et al., 2007). We exposed transfected cells to actinomycin D to inhibit transcription and compared F-Luc-Nerfin mRNA levels over time with the long-lived rp49 mRNA, which has a half-life >8 hr.

In the absence of miR-9b, the half-life of F-Luc-Nerfin mRNA was 35 ± 4 min, whereas its half-life was 14 ± 2 min in cells expressing miR-9b (Figures 7A–7C). In PAN3-depleted cells, the F-Luc-Nerfin reporter exhibited a half-life of 18 ± 1 min (Figures 7A and 7D), which is in agreement with previous studies showing that depletion of the PAN2-PAN3 complex does not significantly prevent miRNA-mediated mRNA decay (Behm-Ansmant et al., 2006). In contrast, NOT1 depletion brought miR-9b-mediated decay of the F-Luc-Nerfin mRNA almost to a halt, resulting in an mRNA half-life of 39 ± 6 min, which is similar to the mRNA half-life in the absence of miR-9b (Figures 7A and 7E). Codepleting PAN3 and NOT1 resulted in only a slight increase in the mRNA half-life relative to the single NOT1 knockdown (Figures 7A and 7F). These results confirm previous studies showing that the CCR4-CAF1-NOT complex provides the major contribution to miRNA target degradation (Behm-Ansmant et al., 2006; Chen et al., 2009; Eulalio et al., 2009; Piao et al., 2010). Importantly, firefly luciferase activity was not fully restored in NOT1-depleted cells even though mRNA degradation was prevented, suggesting that the F-Luc-Nerfin mRNA was still translationally repressed (Figure 7G), as previously reported (Behm-Ansmant et al., 2006). Similar results were obtained with a F-Luc-Par-6 reporter, which is silenced by miR-1 (Figures S7A and S7B), except that for this reporter, the increase on mRNA abundance correlated with a corresponding increase in firefly luciferase activity, indicating that this reporter is silenced predominantly at the mRNA level.

To further confirm these results, we analyzed the decay rate of endogenous Vha-68 mRNA, which is a validated target of miR-9b (Behm-Ansmant et al., 2006). In control cells, this mRNA is rapidly degraded through the miRNA pathway (Behm-Ansmant et al., 2006) and exhibits a half-life of 28 ± 1 min (Figures 7H and S7C–S7F). In PAN3-depleted cells, the transcript was slightly stabilized and exhibited a half-life of 38 ± 3 min (Figure 7H). Again, NOT1 depletion strongly stabilized the mRNA, resulting in a half-life >360 min (Figure 7H). The half-life was slightly increased both PAN3 and NOT1 were codepleted (Figures 7H and S7F).

The role of the PAN2-PAN3 complex in silencing was also analyzed by determining the effects of PAN3 and NOT1 depletion on silencing that was mediated directly by tethering the GW182 protein. In this assay, GW182 was fused to a peptide derived from the N protein of the bacteriophage λ (λN tag) to enable tethering to a firefly luciferase (F-Luc) reporter containing five Box B hairpins (5BoxB) inserted in the 3′UTR. It has been shown that tethered GW182 promotes deadenylation of the mRNA reporter, which is followed by decay of the mRNA body (Behm-Ansmant et al., 2006; Eulalio et al., 2007). Codepleting PAN3 and NOT1 suppressed silencing of the R-Luc-5BoxB reporter slightly more efficiently than the depletion of NOT1 alone, whereas PAN3 depletion had only a minor effect (Figure 7I). As observed for the F-Luc-Par-6 reporter, the increase in F-Luc-5BoxB mRNA abundance correlated with a corresponding increase in F-Luc activity.

These results together with previous studies indicate that the CCR4-CAF1-NOT complex is a major contributor to miRNA target decay, with the PAN2-PAN3 complex playing only a

(C–I) Lysates from human HEK293 cells coexpressing GFP-TNRC6B wild-type or mutants together with HA-tagged deadenylation factors were immunoprecipitated and analyzed as described in Figure 1. Similar immunoprecipitation assays were performed with TNRC6A and TNRC6C (Figures S2 and S3).
(J and K) Lysates from S2 cells coexpressing GFP- tagged wild-type Dm GW182 or the indicated mutants together with HA-tagged deadenylation factors were immunoprecipitated and analyzed as described in Figure 2.

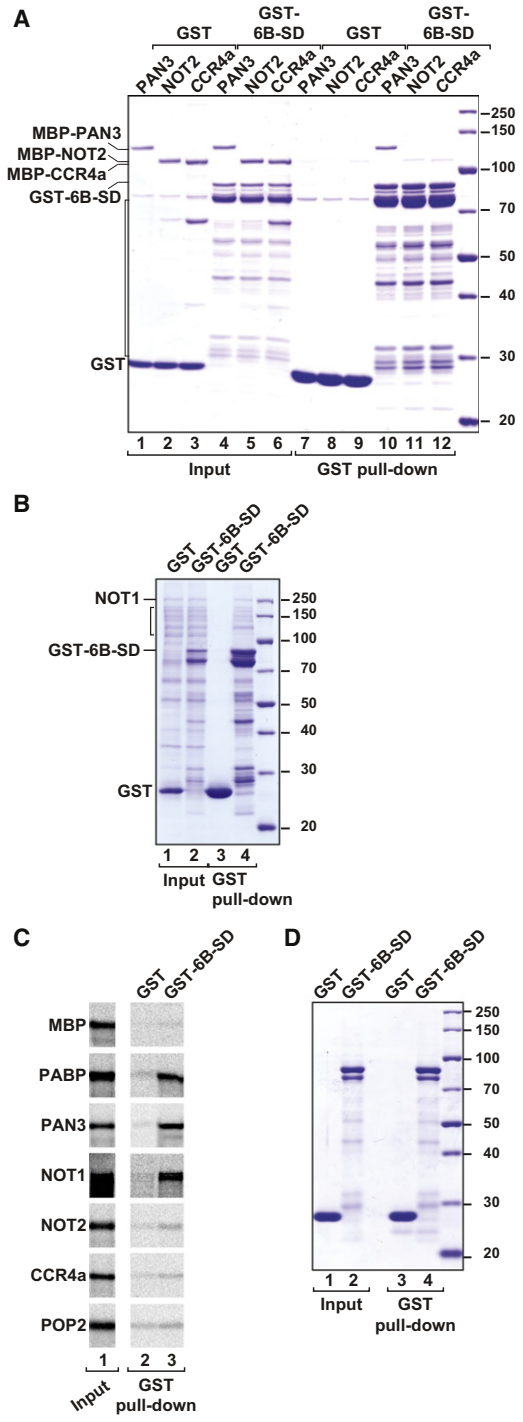

Figure 4. The Silencing Domain of TNRC6B Directly Binds PAN3 and NOT1

(A) Interaction of recombinant MBP-tagged PAN3, NOT2, or CCR4a with GST-tagged TNRC6B-SD (GST-6B-SD). GST served as a negative control. Inputs (1%) and bound fractions (10%) were analyzed by 10% SDS-PAGE (note that NOT2 and CCR4a have similar molecular weights). GST-6B-SD shows multiple degradation fragments (indicate in brackets). See also Figure S6C.

(B) Recombinant 6xHis-tagged NOT1 was pulled down using GST or GST-6B-SD coated beads. NOT1 shows multiple degradation fragments.

(C and D) GST-tagged TNRC6B-SD (GST-6B-SD) or GST was used to pull down [^{35}S]-methionine-labeled in vitro translated PABPC1 or the indicated deadenylation factors. Inputs (1%) and bound fractions (16%) were analyzed by 10% SDS-PAGE followed by fluorography (C). The corresponding Coomassie-stained gel is shown in (D).

minor role. However, it is still possible that the PAN2-PAN3 complex may be important for the silencing of a subset of miRNA targets.

Deadenylases Are Also Required for Silencing Unadenylated Targets

Thus far, our data indicate that GW182 proteins recruit deadenylase complexes to miRNA targets via direct protein-protein interactions, suggesting that deadenylases could also be recruited to mRNAs lacking a poly(A) tail and could eventually promote silencing in the absence of deadenylation. This possibility has been suggested by a recent report showing that a catalytically inactive CAF1 mutant can repress the translation of an mRNA reporter to which it is tethered without promoting deadenylation (Cooke et al., 2010). To investigate this possibility, we used a F-Luc-5BoxB reporter whose 3′ end is generated by a self-cleaving hammerhead ribozyme (F-Luc-5BoxB-HhR) and thus lacks a poly(A) tail. In agreement with previous studies, expression of λN-GW182 reduced luciferase activity without affecting mRNA abundance (Figure 7J) (Eulalio et al., 2008). Remarkably, for this reporter, codepleting PAN3 and NOT1 also suppressed silencing slightly more efficiently than depletion of NOT1 alone, suggesting that the two deadenylase complexes cooperate to repress the expression of the unadenylated reporter.

DISCUSSION

Emerging evidence suggests that mRNA deadenylation is part of the mechanism used by miRNAs to silence gene expression. Indeed, deadenylation of miRNA targets has now been reported in zebrafish and *C. elegans* embryos, human and *D. melanogaster* cells, and in various cell-free extracts that recapitulate silencing (reviewed by Huntzinger and Izaurralde, 2011). However, whether miRISCs directly recruit deadenylases to miRNA targets has remained unclear.

This study provides compelling evidence that the silencing domains (SDs) of TNRC6 proteins contain binding sites for PAN3 and NOT1, which are subunits of each of the two major cytoplasmic deadenylase complexes. These findings provide strong support for the hypothesis that GW182 proteins enhance poly(A) tail removal by directly recruiting deadenylases to associated mRNA targets. More broadly, our results have implications for the understanding of miRNA-based regulation because they show that target deadenylation is not merely a consequence of a translational block.

GW182 Proteins Interact with Two Cytoplasmic Deadenylase Complexes

Previous studies have reported conflicting evidence regarding the interaction of deadenylation factors with the two major

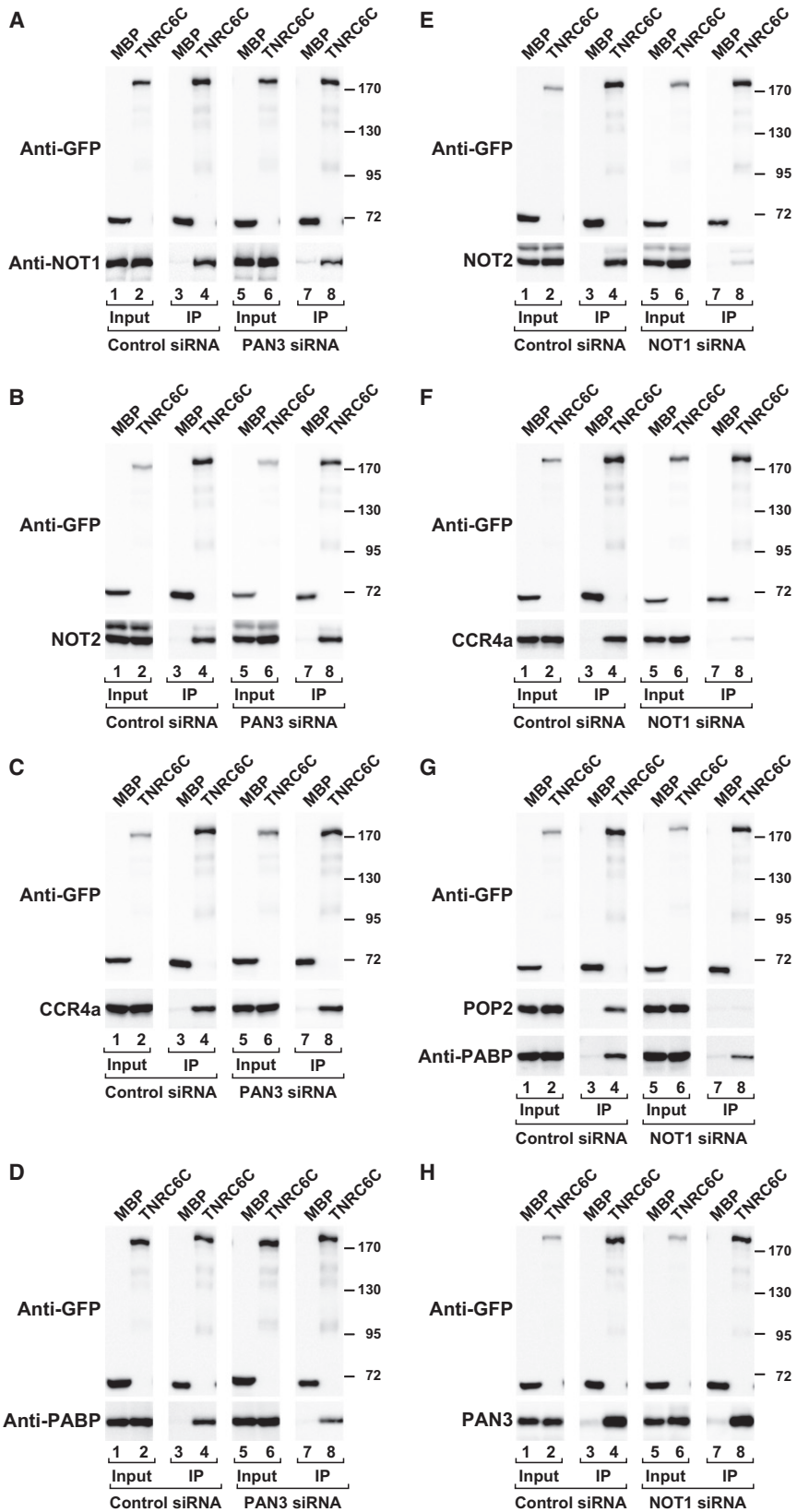

Figure 5. NOT1 and PAN3 Interact with TNRC6 Independently of Each Other

(A–D) Human HEK293 cells were treated with a control siRNA (targeting β-Gal) or a siRNA pool targeting PAN3. In panels A–C, cells were then co-transfected with plasmids expressing GFP-TNRC6C or GFP-MBP (negative control) and HA-tagged deadenylase subunits, as indicated. Cell lysates were immunoprecipitated and analyzed as described in Figure 1. The presence of endogenous PABPC1 in the immunoprecipitates was determined in (D). The efficiency of PAN3 depletion is shown in Figure S6A.

(E–H) A similar experiment was performed in HEK293 cells treated with control siRNA or a siRNA pool targeting NOT1. The presence of endogenous PABPC1 in the immunoprecipitates was analyzed in (G). The efficiency of NOT1 depletion is shown in Figure S6B.

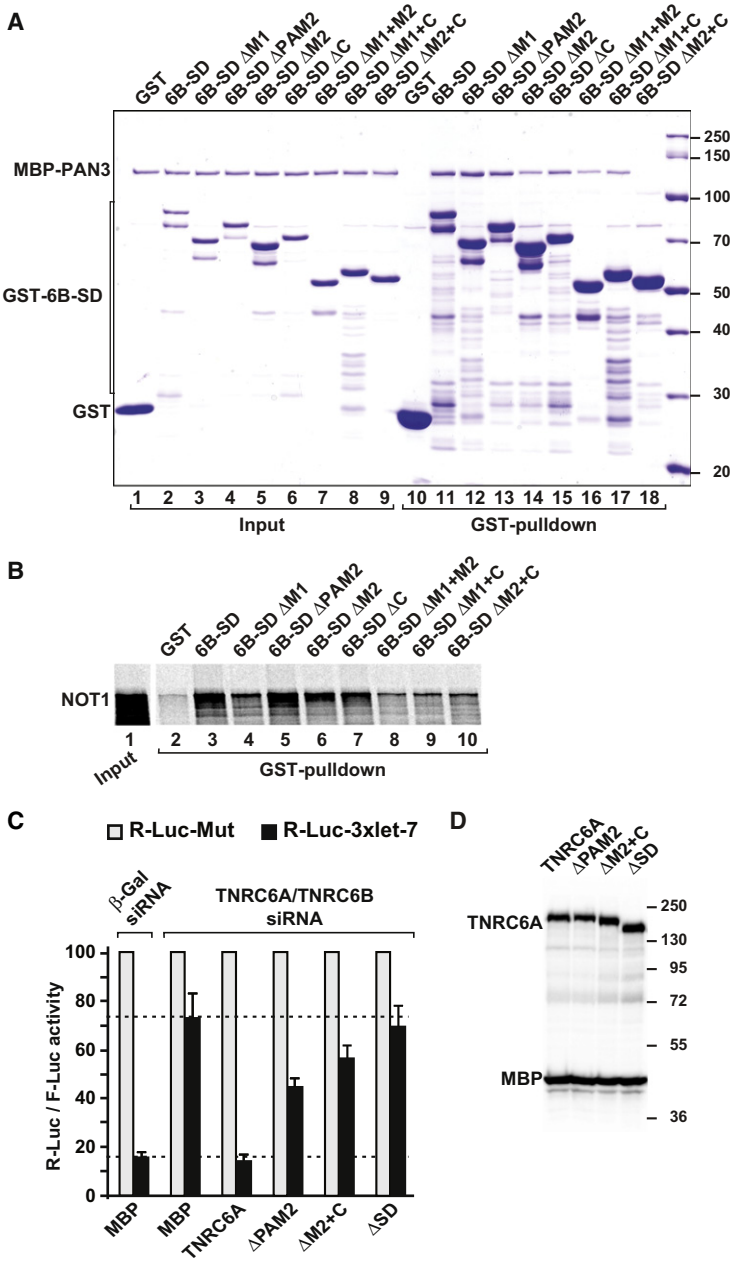

Figure 6. The M2 and C-term Regions of the Silencing Domains Interact with PAN3 and NOT1 and Are Required for Silencing

(A) Interaction of recombinant MBP-PAN3 with either wild-type or mutant GST-6B-SD.

(B) GST pull-down assays were performed with [^{35}S]-methionine labeled full-length NOT1 and either wild-type or mutant GST-6B-SD. GST served as a negative control. Samples were analyzed as described in Figure 4C. The corresponding Coomassie-stained gel is shown in Figure S6D.

(C and D) HeLa cells were transfected with a control β-Gal siRNA or a mixture of siRNAs targeting TNRC6A and TNRC6B. Two days later, the cells were retransfected with the same siRNAs and a mixture of three plasmids: R-Luc-3xlet-7 or a corresponding reporter lacking the let-7-binding sites (R-Luc-Mut), a plasmid expressing F-Luc as a transfection control, and a plasmid expressing either MBP or siRNA-resistant HA-TNRC6A (wild-type or mutant). *Renilla* luciferase activity was measured and normalized to that of F-Luc, setting the value to 100 in cells expressing the reporter lacking the let-7-binding sites for each condition (gray bars). The mean values ± standard deviations from three independent experiments are shown. (D) shows protein expression level.

components of miRISCs (AGO and GW182). Indeed, several studies failed to detect a significant interaction between human AGO or TNRC6 proteins and components of deadenylase complexes, including POP2, CAF1, CCR4a, CCR4b, and PAN2 (Chen et al., 2009; Landthaler et al., 2008; Meister et al., 2005; Piao et al., 2010; Zekri et al., 2009). In contrast, Fabian et al. (2009) observed an interaction of miRISCs with CAF1 and CCR4.

Using coimunoprecipitation and in vitro pull-down assays, we determined that PAN3 and NOT1 interact directly with TNRC6-SDs, whereas the interaction with PAN2 and the additional components of the CCR4-CAF1-NOT complex is indirect and bridged by PAN3 and NOT1, respectively. These observations provide one explanation for the negative results reported in previous studies (Chen et al., 2009; Piao et al., 2010; Zekri et al., 2009). Indeed, these studies focused on the interaction of AGO and GW182 with subunits of the deadenylase complexes that interact indirectly (e.g., the catalytic subunits and NOT3). These indirect interactions are likely to be affected by the efficiency of the immunoprecipitation and the expression of the tagged proteins relative to the expression of the endogenous bridging factors. In agreement with this interpretation, we showed that human TNRC6C did not coimmunoprecipitate PAN2, as reported by Chen et al. (2009) and Piao et al. (2010); nevertheless, an interaction with PAN2 was observed when PAN3 (the bridging factor) was overexpressed (Figure 2J).

A Network of Protein-Protein Interactions Recruits PABPC1 and Deadenylation Factors to the TNRC6-Silencing Domains

Previous studies have shown that the silencing domain of GW182 proteins contains two binding sites for PABPC1: one in the PAM2 motif and one in the M2 and C-terminal regions (Figure 1A) (reviewed by Huntzinger and Izaurralde, 2011). The PAM2 motif interacts directly with the C-terminal MLLE domain of PABPC1 (Fabian et al., 2009; Huntzinger et al., 2010; Jinek et al., 2010; Kozlov et al., 2010). The M2 and C-terminal regions mediate indirect binding to PABPC1, which is only observed in cell lysates (Huntzinger et al., 2010). Here, we show that the TNRC6 M2 and C-term regions mediate direct binding to PAN3. PAN3, in turn, binds to PABPC1 and PAN2 and may act as a bridging factor. We also show that the M1, M2, and C-term regions of the silencing domain confer direct binding to NOT1, which, in turn, mediates

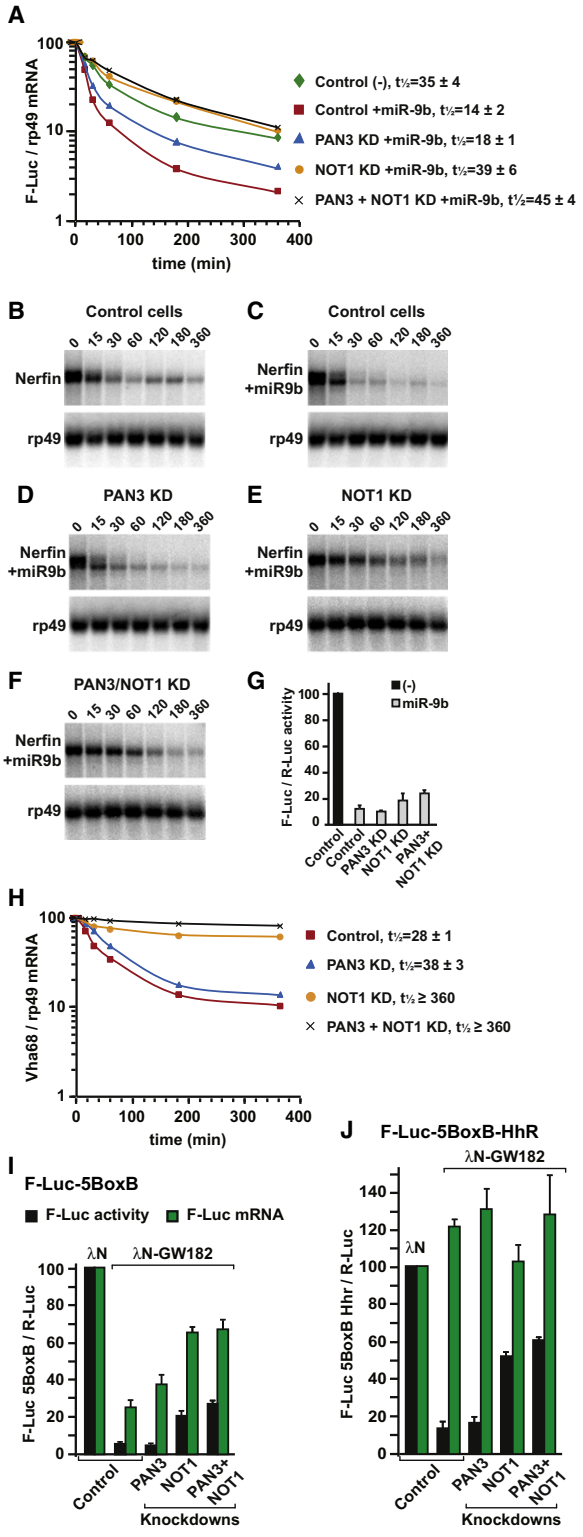

Figure 7. The CCR4-CAF1-NOT Complex Provides a Major Contribution to miRNA-Mediated Target Degradation

(A–G) Control S2 cells or cells depleted PAN3, NOT1, or PAN3 and NOT1 were transfected with a mixture of three plasmids: one expressing the F-Luc-Nerfin reporter, one expressing miR-9b primary transcripts or the corresponding empty vector (–), and a plasmid expressing *Renilla* luciferase (R-Luc). The decay of F-Luc-Nerfin mRNA was monitored following inhibition of transcription by actinomycin D. F-Luc-Nerfin mRNA levels were normalized to rp49 mRNA and plotted against time. mRNA half-lives ($t_{1/2}$) ± standard deviations calculated from the decay curves are indicated on the right of (A). In (G), samples were collected before actinomycin D treatment, and firefly luciferase activity was measured and normalized to that of the *Renilla* luciferase. For each knockdown, normalized F-Luc values were set to 100 in cells transfected with the empty vector (i.e., in the absence of miR-9b, black bar shown only for control cells). The mean values ± standard deviations from three independent experiments are shown. KD, knockdown. Similar results were obtained for the F-Luc-Par6 reporter (Figures S7A and S7B).

(H) The decay of the endogenous Vha-68 mRNA was monitored in control and knockdown cells as described in (A). Northern blots corresponding to the decay curves are shown in Figures S7C–S7F.

(I) S2 cells treated with dsRNAs targeting GFP, PAN2 or NOT1 or a mixture of PAN2 and NOT1 dsRNAs. These cells were transfected with a mixture of three plasmids: one expressing the F-Luc-5BoxB reporter, one expressing *Renilla* luciferase (R-Luc) as a transfection control and a plasmid expressing λN or λN-GW82, as indicated. For each knockdown, firefly luciferase activity and mRNA levels were normalized to those of *Renilla* luciferase and set to 100 in cells expressing λN. The mean values ± standard deviations from three independent experiments are shown.

(J) An experiment similar to that described above was performed using an F-Luc-5BoxB reporter in which the cleavage and polyadenylation signal had been substituted with a self-cleaving hammerhead ribozyme (F-Luc-5BoxB-HhR).

interaction with the additional subunits of the CCR4-CAF1-NOT complex.

Figure S8 represents a model that summarizes the interactions uncovered in our work as well as those from previous studies. TNRC6 proteins are recruited to miRNA targets through their interaction with AGOs, and they contact PABPC1 directly through their PAM2 motifs (Figures S8A and S8B) (Fabian et al., 2009; Huntzinger et al., 2010; Jinek et al., 2010; Kozlov et al., 2010). TNRC6 proteins also bind PAN3 and NOT1 via their Mid and C-term regions, as shown in our study. These interactions may occur consecutively, simultaneously, or alternatively (for clarity in Figure S8, they are shown as alternative). PAN3 interacts with the catalytic subunit PAN2 (Mangus et al., 2004). Additionally, PAN3 contains an N-terminal PAM2 motif that could bind to the MLLE domain of a second PABPC1 molecule (Figures S8C and S8D) (Siddiqui et al., 2007). Finally, NOT1 recruits the additional subunits of the CCR4-CAF1-NOT complex (Figure S8E). Although the detailed molecular interactions between the deadenylases, PABPC1 and TNRC6s need to be further elucidated, an important conclusion emerging from our studies is that TNRC6 proteins engage in multiple interactions with deadenylases and PABPC1 to promote target mRNA degradation. Moreover, the observation that depletion of PAN3 and NOT1 suppresses silencing of an unadenylated reporter, suggests that deadenylase complexes could also contribute to translational repression in addition to promoting deadenylation and decay. Thus, it is possible that translational repression and deadenylation are two distinct outcomes triggered by the recruitment of deadenylase complexes to the 3′UTR of miRNA targets. Further studies will determine how deadenylase complexes interact with TNRC6 proteins at the molecular level, and the role they may play in translational repression.

EXPERIMENTAL PROCEDURES

Coimmunoprecipitation Assays and Western Blot Analysis

Subunits of the deadenylase complexes were cloned as indicated in Table S1. Plasmids for the expression of GFP-GW182, full-length AGO2 or the corresponding F2V2 mutant were described by Eulalio et al. (2008). Plasmids for the expression of full-length TNRC6A-C or the corresponding silencing domains were generated by inserting the corresponding cDNAs into the pEGFP-C1 vector (Clontech) using the following restriction sites: XhoI-PstI (TNRC6A), HindIII-BamHI (TNRC6B) and XhoI-SalI (TNRC6C). Coimmunoprecipiation assays in human HEK293 and *Drosophila* S2 cells were performed as described by Huntzinger et al. (2010). Detailed protocols for the immunoprecipitations, Western blotting, and knockdowns in human cells are given in the Supplemental Experimental Procedures.

GST Pull-Down Assays

To express the silencing domain of TNRC6B (amino acids 1218–1723) in *E. coli*, the corresponding cDNA was cloned into the pGEX6P1 vector (GE Healthcare), resulting in an N-terminal GST fusion protein. Deletions and mutations were introduced using the QuikChange Mutagenesis Kit (Stratagene) and appropriate oligos. Human PAN3, NOT2, and CCR4a cDNAs were cloned into the pETM41 vector, resulting in N-terminal MBP fusion proteins. Human NOT1 cDNA was cloned into the pET-Duet vector, resulting in N-terminal 6xHistidine fusion protein. GST pull-down assays were performed as described by Huntzinger et al. (2010). See additional information in the Supplemental Experimental Procedures.

Complementation Assay in Human Cells and Knockdowns in S2 Cells

Complementation assays in human HeLa cells and RNA interference in S2 cells were performed as described by Huntzinger et al. (2010). Knockdowns in S2 cells and plasmids expressing miRNA primary transcripts, F-Luc mRNA reporters, and λN-HA-tagged proteins have been described by Behm-Ansmant et al. (2006). siRNA sequences and detailed protocols are given in the Supplemental Experimental Procedures.

SUPPLEMENTAL INFORMATION

Supplemental Information includes eight figures, one table, and Supplemental Experimental Procedures and can be found with this article online at doi:10.1016/j.molcel.2011.09.007.

ACKNOWLEDGMENTS

We are grateful to E. Wahle for the kind gift of anti-NOT1 antibodies, S. Helms for providing purified NOT1, B. Singer-Krueger for generating a plasmid expressing GFP-TNRC6C, and C. Fetzer and L. Wohlbold for providing expression vectors for subunits of the human and *D. melanogaster* deadenylase complexes. This study was supported by the Max Planck Society, by grants from the Deutsche Forschungsgemeinschaft (DFG, FOR855 and the Gottfried Wilhelm Leibniz Program awarded to E.I.) and by the Sixth Framework Programme of the European Commission through the SIROCCO Integrated Project LSHG-CT-2006-037900.

Received: March 17, 2011
Revised: June 20, 2011
Accepted: September 16, 2011
Published: October 6, 2011

REFERENCES

Behm-Ansmant, I., Rehwinkel, J., Doerks, T., Stark, A., Bork, P., and Izaurralde, E. (2006). mRNA degradation by miRNAs and GW182 requires both CCR4:NOT deadenylase and DCP1:DCP2 decapping complexes. Genes Dev. *20*, 1885–1898.

Boeck, R., Tarun, S., Jr., Rieger, M., Deardorff, J.A., Müller-Auer, S., and Sachs, A.B. (1996). The yeast Pan2 protein is required for poly(A)-binding protein-stimulated poly(A)-nuclease activity. J. Biol. Chem. *271*, 432–438.

Brown, C.E., Tarun, S.Z., Jr., Boeck, R., and Sachs, A.B. (1996). PAN3 encodes a subunit of the Pab1p-dependent poly(A) nuclease in Saccharomyces cerevisiae. Mol. Cell. Biol. *16*, 5744–5753.

Chen, C.Y., Zheng, D., Xia, Z., and Shyu, A.B. (2009). Ago-TNRC6 triggers microRNA-mediated decay by promoting two deadenylation steps. Nat. Struct. Mol. Biol. *16*, 1160–1166.

Cooke, A., Prigge, A., and Wickens, M. (2010). Translational repression by deadenylases. J. Biol. Chem. *285*, 28506–28513.

Djuranovic, S., Nahvi, A., and Green, R. (2011). A parsimonious model for gene regulation by miRNAs. Science *331*, 550–553.

Eulalio, A., Rehwinkel, J., Stricker, M., Huntzinger, E., Yang, S.F., Doerks, T., Dorner, S., Bork, P., Boutros, M., and Izaurralde, E. (2007). Target-specific requirements for enhancers of decapping in miRNA-mediated gene silencing. Genes Dev. *21*, 2558–2570.

Eulalio, A., Huntzinger, E., and Izaurralde, E. (2008). GW182 interaction with Argonaute is essential for miRNA-mediated translational repression and mRNA decay. Nat. Struct. Mol. Biol. *15*, 346–353.

Eulalio, A., Huntzinger, E., Nishihara, T., Rehwinkel, J., Fauser, M., and Izaurralde, E. (2009). Deadenylation is a widespread effect of miRNA regulation. RNA *15*, 21–32.

Fabian, M.R., Mathonnet, G., Sundermeier, T., Mathys, H., Zipprich, J.T., Svitkin, Y.V., Rivas, F., Jinek, M., Wohlschlegel, J., Doudna, J.A., et al. (2009). Mammalian miRNA RISC recruits CAF1 and PABP to affect PABP-dependent deadenylation. Mol. Cell *35*, 868–880.

Giraldez, A.J., Mishima, Y., Rihel, J., Grocock, R.J., Van Dongen, S., Inoue, K., Enright, A.J., and Schier, A.F. (2006). Zebrafish MiR-430 promotes deadenylation and clearance of maternal mRNAs. Science *312*, 75–79.

Huntzinger, E., Braun, J.E., Heimstädt, S., Zekri, L., and Izaurralde, E. (2010). Two PABPC1-binding sites in GW182 proteins promote miRNA-mediated gene silencing. EMBO J. *29*, 4146–4160.

Huntzinger, E., and Izaurralde, E. (2011). Gene silencing by microRNAs: contributions of translational repression and mRNA decay. Nat. Rev. Genet. *12*, 99–110.

Jinek, M., Fabian, M.R., Coyle, S.M., Sonenberg, N., and Doudna, J.A. (2010). Structural insights into the human GW182-PABC interaction in microRNA-mediated deadenylation. Nat. Struct. Mol. Biol. *17*, 238–240.

Kozlov, G., Safaee, N., Rosenauer, A., and Gehring, K. (2010). Structural basis of binding of P-body-associated proteins GW182 and ataxin-2 by the MIle domain of poly(A)-binding protein. J. Biol. Chem. *285*, 13599–13606.

Landthaler, M., Gaidatzis, D., Rothballer, A., Chen, P.Y., Soll, S.J., Dinic, L., Ojo, T., Hafner, M., Zavolan, M., and Tuschl, T. (2008). Molecular characterization of human Argonaute-containing ribonucleoprotein complexes and their bound target mRNAs. RNA *14*, 2580–2596.

Lau, N.C., Kolkman, A., van Schaik, F.M., Mulder, K.W., Pijnappel, W.W., Heck, A.J., and Timmers, H.T. (2009). Human Ccr4-Not complexes contain variable deadenylase subunits. Biochem. J. *422*, 443–453.

Mangus, D.A., Evans, M.C., Agrin, N.S., Smith, M., Gongidi, P., and Jacobson, A. (2004). Positive and negative regulation of poly(A) nuclease. Mol. Cell. Biol. *24*, 5521–5533.

Meister, G., Landthaler, M., Peters, L., Chen, P.Y., Urlaub, H., Lührmann, R., and Tuschl, T. (2005). Identification of novel argonaute-associated proteins. Curr. Biol. *15*, 2149–2155.

Piao, X., Zhang, X., Wu, L., and Belasco, J.G. (2010). CCR4-NOT deadenylates mRNA associated with RNA-induced silencing complexes in human cells. Mol. Cell. Biol. *30*, 1486–1494.

Siddiqui, N., Mangus, D.A., Chang, T.C., Palermino, J.M., Shyu, A.B., and Gehring, K. (2007). Poly(A) nuclease interacts with the C-terminal domain of polyadenylate-binding protein domain from poly(A)-binding protein. J. Biol. Chem. *282*, 25067–25075.

Temme, C., Zaessinger, S., Meyer, S., Simonelig, M., and Wahle, E. (2004). A complex containing the CCR4 and CAF1 proteins is involved in mRNA deadenylation in Drosophila. EMBO J. *23*, 2862–2871.

Tucker, M., Valencia-Sanchez, M.A., Staples, R.R., Chen, J., Denis, C.L., and Parker, R. (2001). The transcription factor associated Ccr4 and Caf1 proteins are components of the major cytoplasmic mRNA deadenylase in Saccharomyces cerevisiae. Cell *104*, 377–386.

Uchida, N., Hoshino, S., and Katada, T. (2004). Identification of a human cytoplasmic poly(A) nuclease complex stimulated by poly(A)-binding protein. J. Biol. Chem. *279*, 1383–1391.

Wu, L., Fan, J., and Belasco, J.G. (2006). MicroRNAs direct rapid deadenylation of mRNA. Proc. Natl. Acad. Sci. USA *103*, 4034–4039.

Yamashita, A., Chang, T.C., Yamashita, Y., Zhu, W., Zhong, Z., Chen, C.Y., and Shyu, A.B. (2005). Concerted action of poly(A) nucleases and decapping enzyme in mammalian mRNA turnover. Nat. Struct. Mol. Biol. *12*, 1054–1063.

Zekri, L., Huntzinger, E., Heimstädt, S., and Izaurralde, E. (2009). The silencing domain of GW182 interacts with PABPC1 to promote translational repression and degradation of microRNA targets and is required for target release. Mol. Cell. Biol. *29*, 6220–6231.

Note Added in Proof

Two other studies are simultaneously reporting the interaction of the CCR4-NOT complex with TNRC6 proteins in Nat. Struct. Mol. Biol. (Chekulaeva, M., Mathys, H., Zipprich, J.T., Attig, J., Colic, M., Parker, R., and FilipowiczW. [2011]. miRNA repression involves GW182-mediated recruitment of CCR4-NOT through conserved W-containing motifs. Nat. Struct. Mol. Biol., in press. Published online October 7, 2011. 10.1038/nsmb.2166; Fabian, M.R., Cieplak, M.K., Frank, F., Morita, M., Green, J., Srikumar, T., Nagar, B., Yamamoto, T., Raught, B., Duchaine, T.F., and Sonenberg, N. [2011]. miRNA-mediated deadenylation is orchestrated by GW182 through two conserved motifs that interact with CCR4–NOT. Nat. Struct. Mol. Biol., in press. Published online October 7, 2011. 10.1038/nsmb.2149).

Molecular Cell, Volume *44*

Supplemental Information

GW182 Proteins Directly Recruit Cytoplasmic Deadenylase Complexes to miRNA Targets

Joerg E. Braun, Eric Huntzinger, Maria Fauser, and Elisa Izaurralde

Figure S1

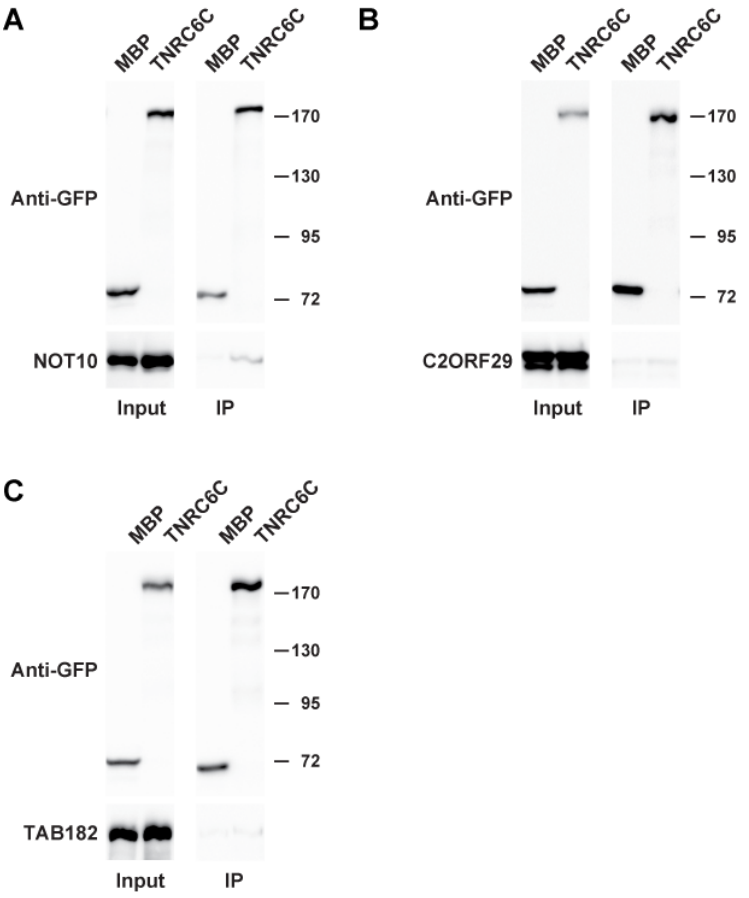

Figure S1. TNRC6C interacts with deadenylation factors.

(A–C) Human HEK293 cells were transfected with a plasmid expressing GFP-tagged TNRC6C together with plasmids expressing HA-tagged deadenylase subunits as indicated. GFP-tagged Maltose Binding Protein (MBP) served as a negative control. Two days after transfection, the cells were lysed and proteins were immunoprecipitated as described in Figure 1. Related to main Figure 1.

Figure S2

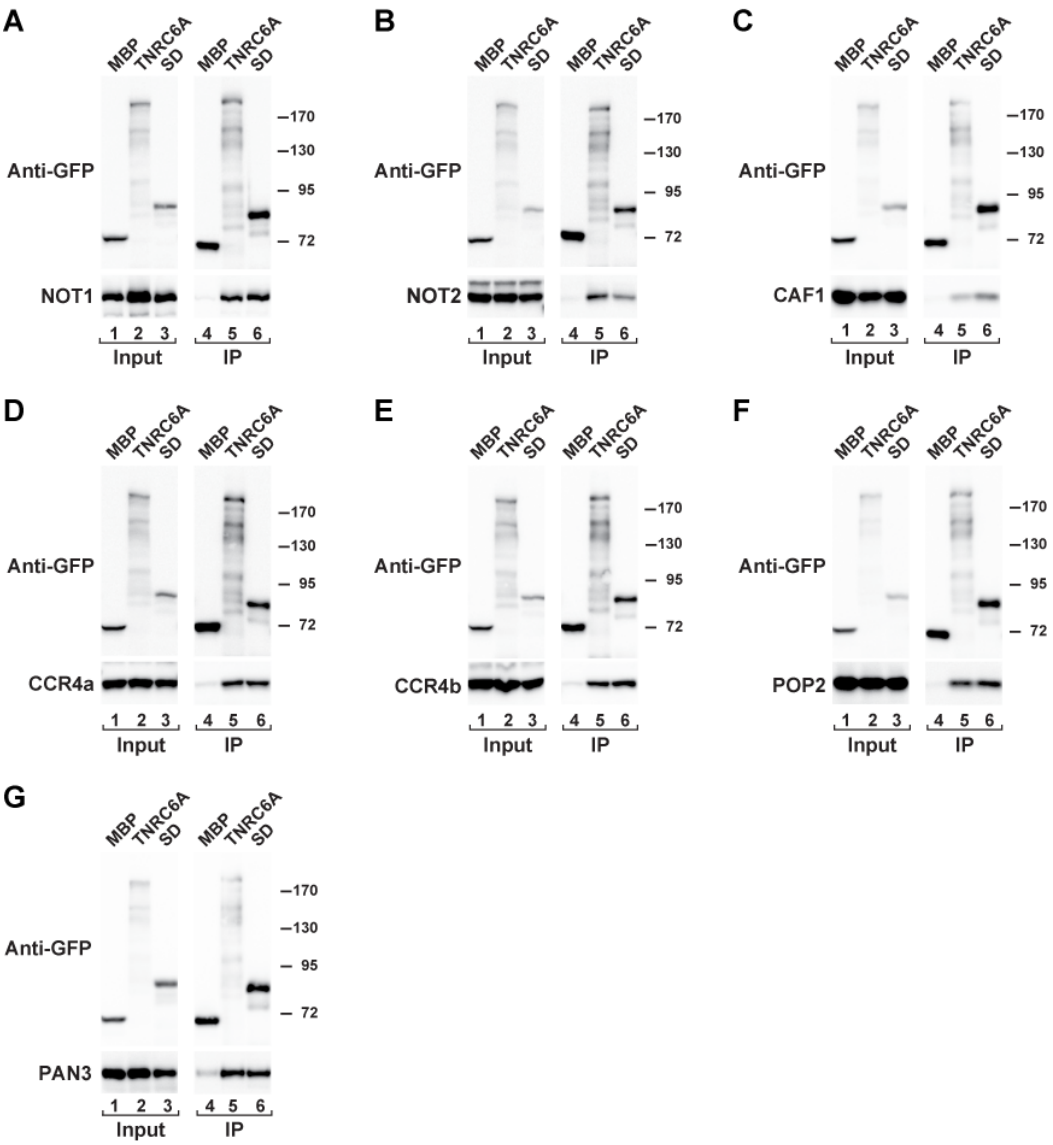

Figure S2. The silencing domain of TNRC6A is sufficient for binding to deadenylation factors.

(A–G) Human HEK293 cells expressing GFP-tagged TNRC6A or the TNRC6A silencing domain together with HA-tagged deadenylation factors were lysed two days after transfection. Proteins were immunoprecipitated from the cell lysates using a polyclonal anti-GFP antibody and analyzed by Western blotting as described in Figure 1. TNRC6A is subject to extensive proteolytic degradation in cell lysates even in the presence of protease inhibitors. Related to main Figures 1 and 3.

Figure S3

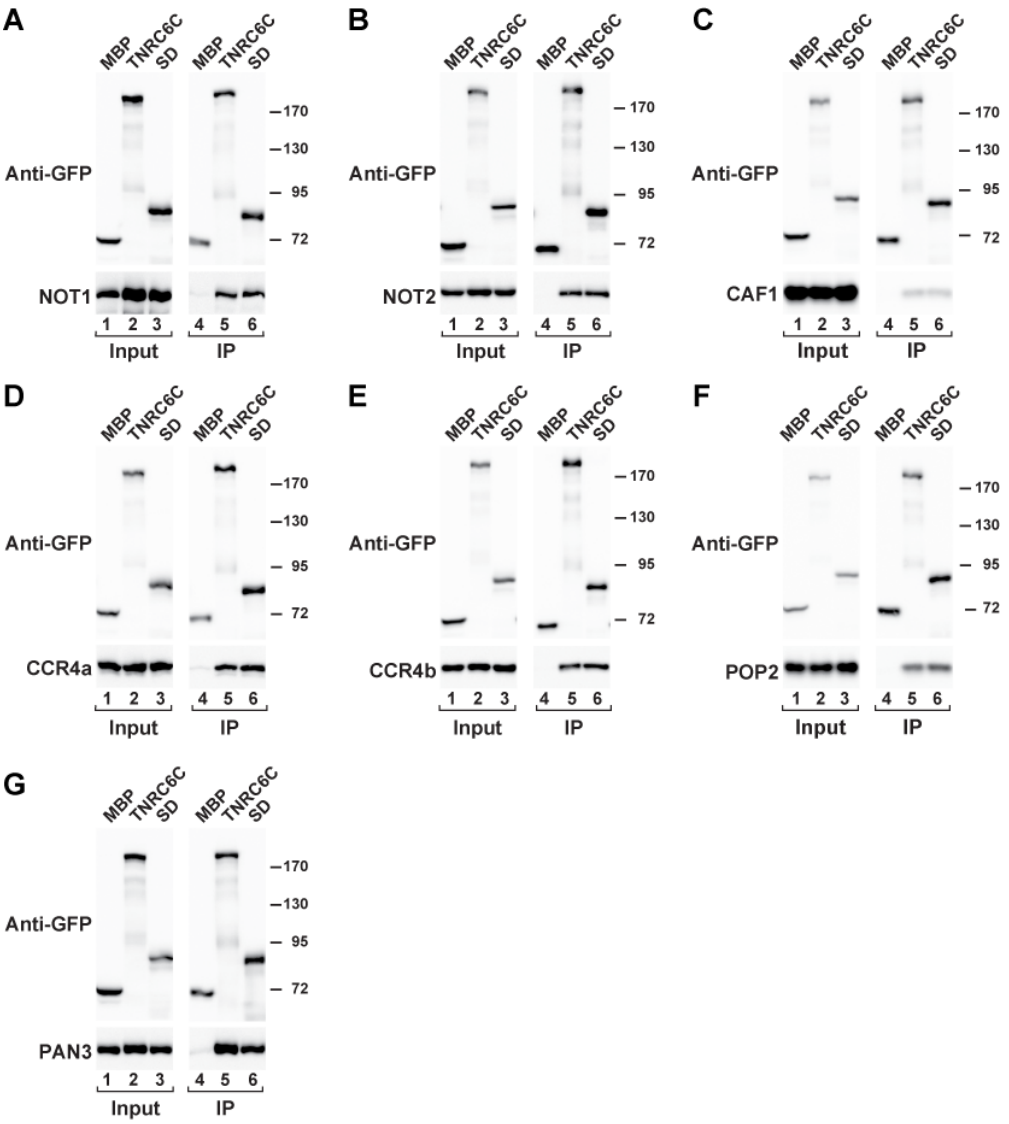

Figure S3. The silencing domain of TNRC6C is sufficient for binding to deadenylation factors.

(A–G) Human HEK293 cells expressing GFP-tagged TNRC6C or the TNRC6C silencing domain together with HA-tagged deadenylation factors were lysed two days after transfection. The cell lysates were immunoprecipitated with a polyclonal anti-GFP antibody and analyzed by Western blotting as described in Figure 1. Related to main Figures 1 and 3.

Figure S4

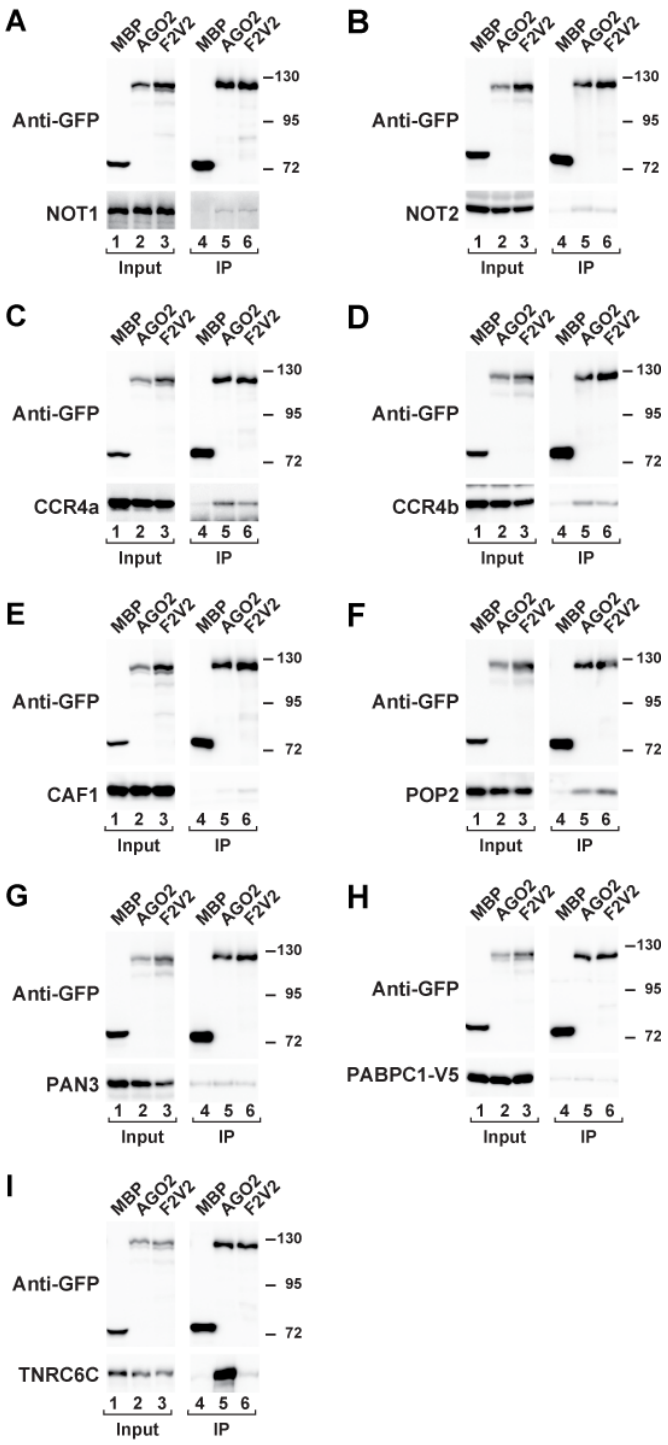

Figure S4. AGO2 interacts with subunits of the CCR4-CAF1-NOT complex.

(A–G) Human HEK293 cells were transfected with plasmids expressing GFP-AGO2 (either wild-type or F2V2 mutant) together with HA-tagged deadenylase subunits as indicated. GFP-tagged Maltose Binding Protein (MBP) served as a negative control. Two days after transfection, the cells were lysed and proteins were immunoprecipitated with a polyclonal anti-GFP antibody. Inputs and immunoprecipitates were subjected to Western blotting using anti-GFP and anti-HA

antibodies. In all panels, the cell lysates were treated with RNase A prior to immunoprecipitation.

(H) Coimmunoprecipitation of V5-tagged PABPC1 with wild-type GFP-AGO2 or the F2V2 mutant.

(I) Interaction of AGO2 or the AGO2 F2V2 mutant with HA-TNRC6C.Related to main Figure 1.

Figure S5

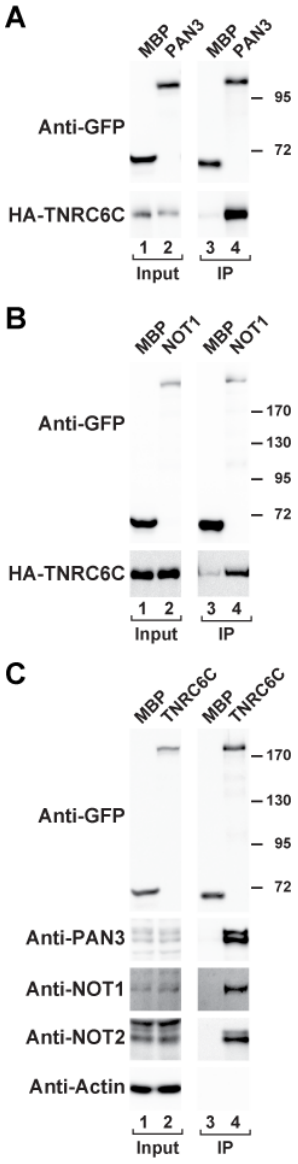

Figure S5. Validation of the interaction screen.

(A, B) Human HEK293 cells were co-transfected with a plasmid expressing HA-TNRC6C and plasmids expressing either GFP-PAN3 or GFP-NOT1. GFP-MBP served as a negative control. Cell lysates were immunoprecipitated using a polyclonal anti-GFP antibody and were analyzed as described in Figure 1. Related to main Figure 3.

(C) Human HEK293 cells were transfected with a plasmid expressing GFP-TNRC6C or GFP-MBP (negative control). Cell lysates were immunoprecipitated using a polyclonal anti-GFP antibody. Inputs and immunoprecipitates were analyzed by western blotting using anti-GFP antibodies or antibodies recognizing endogenous NOT1, PAN3, or NOT2, as indicated. An antibody to endogenous actin served as a control to determine the specificity of the immunoprecipitations. For endogenous proteins, 1% of the input and 30% of the immunoprecipitates were loaded.

Figure S6

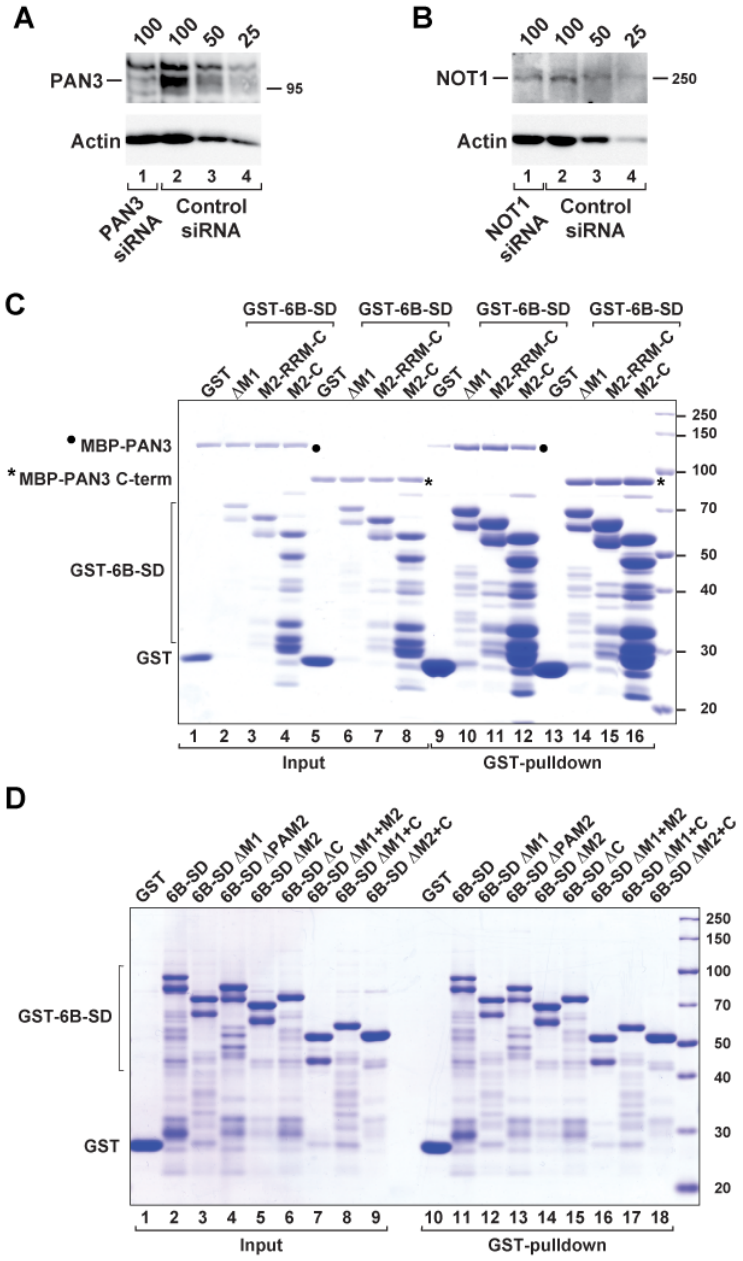

Figure S6. TNRC6B interacts with the PAN3 C-terminal domain.

(A, B) The efficiency of PAN3 and NOT1 depletion was determined by western blot analysis using specific antibodies. Actin served as a loading control. In lanes 2–4,

dilutions of lysates from control cells were loaded to estimate the efficacy of the depletion.

(C) The interaction of GST-6B-SD deletion mutants with recombinant MBP-tagged PAN3 (filled circle) or the PAN3 C-terminal domain (asterisk) was analyzed as describe in Figure 5A. The GST-6B-SD ΔM1 mutant was used instead of GST-6B-SD because the later co-migrates with MBP-PAN3 C-term.

(D) Coomassie stained gel corresponding to the GST pull down shown in Figure 6B.

Related to main Figures 5 and 6.

Figure S7

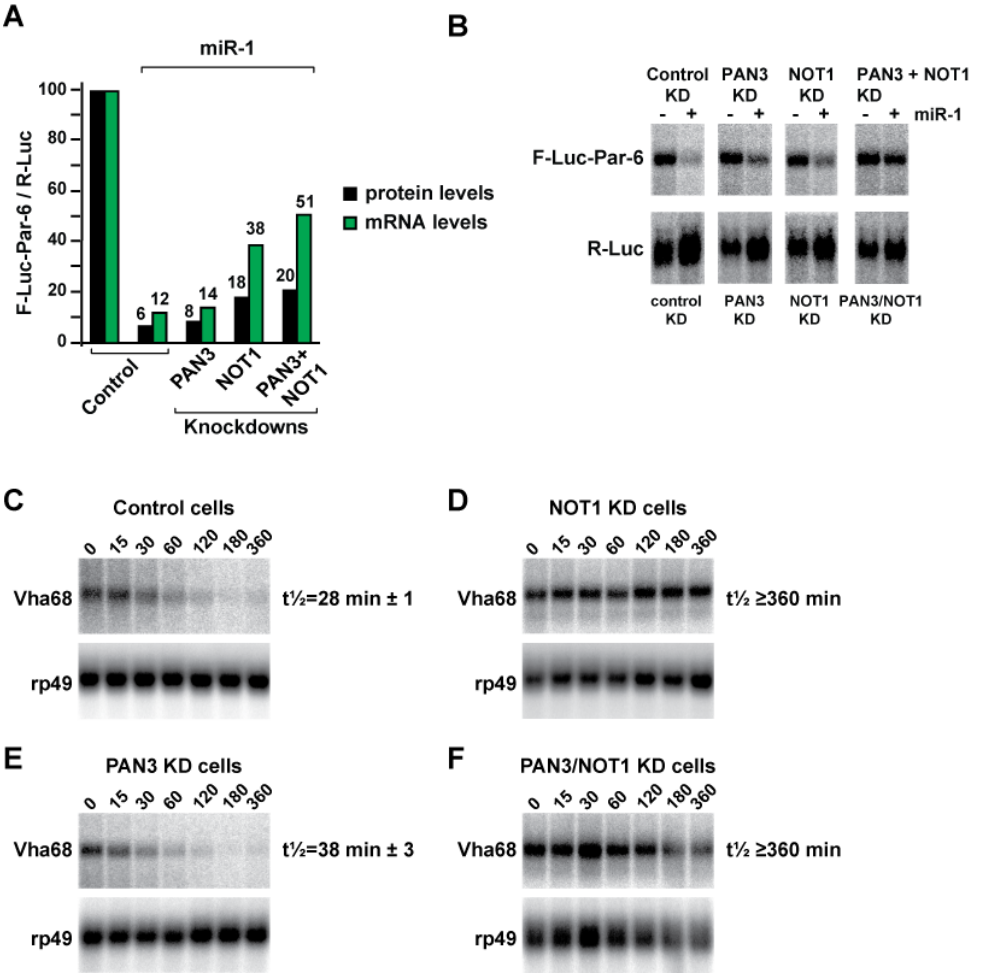

Figure S7. The CCR4-CAF1-NOT complex provides a major contribution to miRNA-mediated target degradation.

(A,B) Control S2 cells or cells depleted PAN3, NOT1 or PAN3 and NOT1 were transfected with a mixture of three plasmids: one expressing the F-Luc-Par-6 reporter, one expressing miR-1 primary transcripts or the corresponding empty vector (-) and a plasmid expressing *Renilla* luciferase (R-Luc). For each knockdown, firefly luciferase activity and mRNA levels were normalized to those of the *Renilla* luciferase

transfection control and set to 100 in cells transfected with the empty vector (*i.e.* in the absence of miR-1, shown only for control cells).

(C–F) The decay of the endogenous Vha-68 mRNA was monitored in control and knockdown cells following inhibition of transcription by actinomycin D and analyzed by northern blot. The corresponding decay curves are shown in Figure 7H. mRNA half-lives ($t_{1/2}$) ± standard deviations calculated from the decay curves are indicated on the right. Related to main Figure 7.

Figure S8

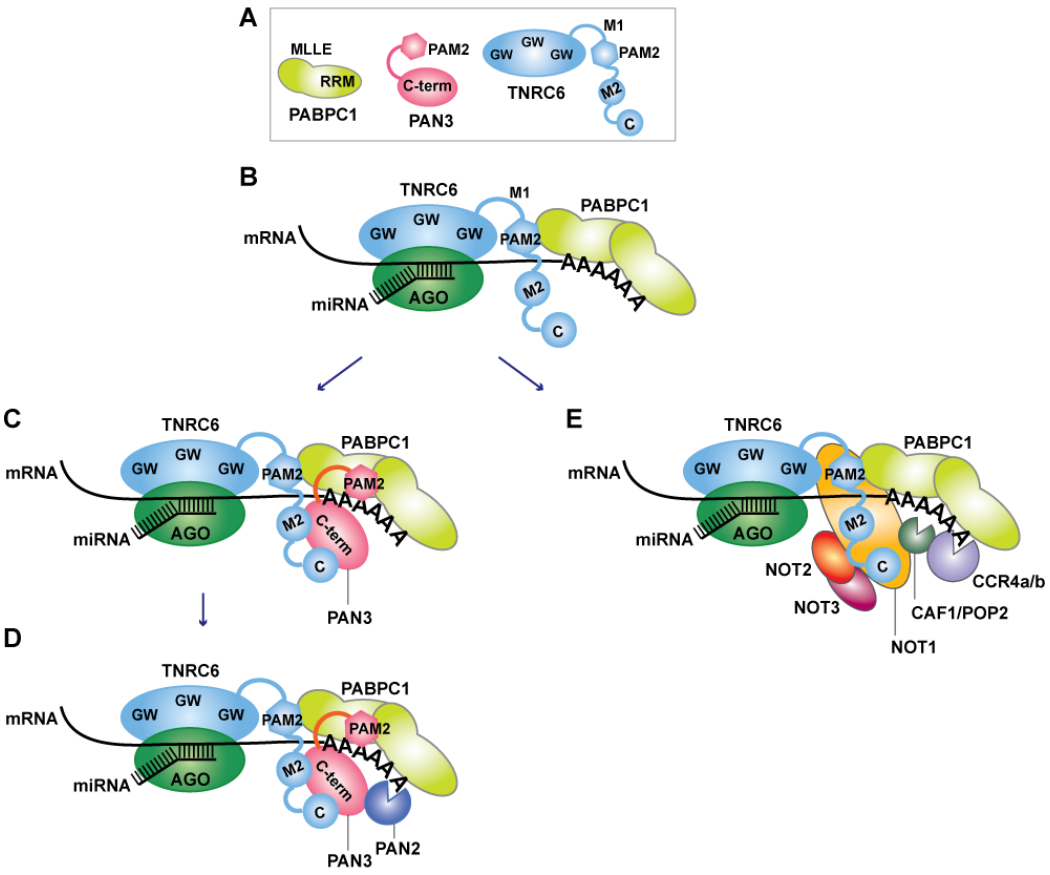

Figure S8. A model for the recruitment of deadenylases to miRNA targets.

(A) The TNRC6 domains are as described in Figure 1A. PABPC1 consist of an N-terminal domain (containing four RRMs), a linker region and a C-terminal domain termed MLLE. PAN3 consist of N-terminal and C-terminal domain. The N-terminal domain contains a PAM2 motif and directly interacts with the PABPC1 MLLE domain (Siddiqui et al., 2007). The C-terminal domain interacts simultaneously with PAN2 and the M2 and C-term regions of the TNRC6-SD (Mangus et al., 2004; this study).

(B) Animal miRNAs in complex with AGO and TNRC6 proteins recognize their mRNA targets by base-pairing to partially complementary binding sites

predominantly located in the 3' UTR. TNRC6 proteins interact directly with PABPC through their PAM2 motifs.

(C, D) PAN3 directly binds to the M2 and C-term regions of TNRC6 and recruits PAN2. PAN3 can also contact a second PABPC1 protein through its PAM2 motif (note that one PABPC1 protein cannot interact with the PAM2 motifs of PAN3 and TNRC6 simultaneously).

(E) Consecutively (or simultaneously) the M1, M2 and C-term regions of the TNRC6 silencing domain interact with the CCR4-CAF1-NOT complex trough NOT1. It is important to note that it is not clear whether the interactions between TNRC6 proteins interactions and PAN3 or NOT1 occur simultaneously or consecutively.

Table S1. Subunits of the CCR4-CAF1-NOT and PAN2-PAN3 deadenylase complexes

Human (alternative names) /ORF length in amino acids / accession and cloning sites	***D. melanogaster* (alternative names) / ORF length in amino acids / accession and cloning sites**
Human CAF1-CCR4-NOT complex	***Dm* CAF1-CCR4-NOT complex**
CAF1 (CNOT7) *[1] / 285 / NM_013354.5 / cloned XhoI–NotI into pCIneo-λN-HA	
POP2 (CNOT8) *[1] / 292 / NM_004779.4 / cloned SacII–BamHI into pλN-HA-C1	POP2 (CG5684) / 297 / NM_140281.2 / cloned EcoRV–NotI into pAc5.1B-λN-HA
CCR4a (CNOT6) / 557 / NM_015455.3 / cloned XhoI–KpnI into pλN-HA-C1	CCR4 (CG31137, Twin) / 552 / NM_170129.2 / cloned EcoRI–NotI into pAc5.1B-λN-HA
CCR4b (CNOT6L) / 555 / NM_144571.2 / cloned Xho–EcoRI into pλN-HA-C1	
CNOT1 / 2371 / EF553522.1 / cloned XhoI–SacII into pλN-HA-C1	NOT1 (CG34407) / 2505 / NM_001103772.2 / cloned PacI–XbaI into pAc5.1B-λN-HA
CNOT2 / 540 / NM_014515.4 / cloned HindIII–SacII into pλN-HA-C1	NOT2 (CG2161, Rga) / 585 / NM_169080.1 / cloned HindIII–XbaI into pAc5.1B-λN-HA
CNOT3 / 753 / NM_014516.2 / cloned SacII–BamHI into pλN-HA-C1	NOT3/5 *[2] (CG8426) / 844 / NM_136332.2 / cloned HindIII–NotI into pAc5.1B-λN-HA
CNOT4	NOT4 (CG31716) /1048 / NM_164919.1 / cloned XhoI–BstBI into pAc5.1B-λN-HA
CNOT9 (RQCD1, RCD-1)	CAF40 (CG14213)
CNOT10 / 744 / NM_015442.1 / cloned XhoI–BamHI into pλN-HA-C1	CG18616
C2ORF29 (C40) / 510 / NM_017546.4 cloned KpnI–BamHI into pλN-HA-C1	CG13567
TAB182 (TNKS1BP1) / 1729 / NM_033396.2 cloned SalI–XbaI into pλN-HA-C1	
Human PAN2-PAN3 complex	***Dm* PAN2-PAN3 complex**
PAN2 / 1202 / BC094885.1 / cloned XhoI–EcoRI into pλN-HA-C1	PAN2 (CG8232) / 1241 / LP04771 / cloned EcoRV–SacII into pAc5.1B-λN-HA
PAN3 / 687 / BC128180.1 / cloned XhoI–KpnI into pλN-HA-C1	PAN3 (CG11486) / 790 / LD14901 / cloned EcoRI–NotI into pAc5.1B-λN-HA

Subunits in blue are considered core components of the CCR4-CAF1-NOT complex. NOT4 and CAF40 are not integral core components (Temme et al., 2004; 2010; Lau et al; 2009) and it is unclear whether the *D. melanogaster* homologs of CNOT10, C2ORF29 and TAB182 are part of the complex in *D. melanogaster*.

*[1] CAF1 and POP2 are related proteins.

*[2] In yeast there are two similar proteins NOT3 and NOT5, but humans *and D. melanogaster* contain only one orthologous protein termed NOT3 or NOT3/5.

Supplemental Experimental Procedures

Co-immunoprecipitation assays and western blot analysis of human cells

For co-immunoprecipitation assays, HEK293 cells were grown in 10-cm dishes and transfected using Lipofectamine 2000 (Invitrogen). The transfection mixtures contained 8 μg of plasmid expressing GFP-tagged AGO2, TNRC6A–C or the corresponding mutants and 7 μg of HA-tagged deadenylation factor. In reciprocal immunoprecipitations in which bait and prey proteins were exchanged, transfection mixtures contained 8 μg of plasmid expressing GFP-tagged deadenylation subunits, and 7 μg of HA-tagged TNRC6C. Knockdowns in human HeLa and HEK293 cells were performed as described by Huntzinger et al. (2010) using β-Gal siRNA as a negative control (5'-CUACACAAAUCAGCGAUUUUU-3'; Dharmacon) and PAN3 or NOT1 SMARTpool siRNA (Dharmacon).

Cells were harvested two days after transfection and lysed for 15 min on ice in NET buffer (50 mM Tris (pH 7.4), 150 mM NaCl, 1 mM EDTA, and 0.1% Triton X-100) supplemented with protease inhibitors and 10% glycerol (1 ml NET buffer/ plate). Cell lysates were treated with RNase A for 30 min and spun at 18,000 g for 15 min at 4°C. Alternatively, cell lysates were supplemented with 2.5 mM $CaCl_2$ and treated with micrococcal nuclease for 30 min. Immunoprecipitation was performed as described by Huntzinger et al. (2010). Endogenous proteins were detected with the following antibodies: TNRC6A (Bethyl Laboratories A302-329A; 1:10,000), PABPC1 (Abcam ab21060; 1:10,000), PAN3 (Abcam ab96325; 1:1,000), and NOT2 (Abcam ab90703; 1:1,000). An anti-NOT1 antibody was kindly provided by Elmar Wahle. β-Actin was detected using a monoclonal antibody (SIGMA, A5441, clone AC-15). HA-tagged and GFP-tagged proteins were detected using HRP-conjugated monoclonal anti-HA (Roche 3F10; 1:5,000) and anti-GFP antibodies (Roche 11814460001; 1:2,000), respectively. V5-tagged proteins were detected with anti-V5 antibodies (Invitrogen, 1:5,000). All western blots were developed with the ECL

western blotting detection system (GE Healthcare) as recommended by the manufacturer.

Co-immunoprecipitation assays and western blot analysis of *D. melanogaster* S2 cells

For co-immunoprecipitation assays, S2 cells (10–12 x 10^6 cells) were collected 3 days after transfection, washed with PBS, and lysed in 0.5 ml of NET buffer supplemented with protease inhibitors. Cell lysates were treated with RNase A for 30 min and spun at 18,000 g for 15 min at 4°C. Immunoprecipitations were performed as described by Huntzinger et al. (2010). NOT1 and tagged proteins were detected as described above. Endogenous GW182 and eIF4E were detected with polyclonal antibodies raised in rabbits against the N-terminal domain of GW182 (amino acids 1–539) and full-length eIF4E.

GST pull-down assays

In vitro transcription/translation reactions were performed using the TNT T7-coupled Wheat Germ Extract System (Promega, L4140) and [^{35}S]-methionine (EasyTag, Perkin Elmer, NEG709A) according to the manufacturer's instructions.

For the GST pull-down assays shown in Figure 4A, 12 µg of purified GST or GST-TNRC6B silencing domain was mixed with purified MBP-tagged PAN3, NOT2 or CCR4a in 1 ml of binding buffer (10 mM Hepes (pH 7.5), 150 mM NaCl, 1 mM DTT and 1% [v/v] Triton X-100). The samples were incubated with 20 µL of Protino Glutathione Agarose 4B beads (Macherey Nagel) for 1 hr at 4°C. The beads were washed three times with 1 ml of binding buffer. The proteins were then eluted with 40 µL of SDS-PAGE loading buffer and analyzed by 10% SDS-PAGE.

For all other GST pull down assays, lysate from *E. coli* cells expressing GST, GST-TNRC6B-SD, or the indicated deletion mutant were incubated with 20 µL of Protino

Glutathione Agarose 4B beads in lysis buffer (10 mM Hepes (pH 7.5), 300 mM NaCl, 5 mM $MgCl_2$ and 1 mM DTT) for 1 hr at 4°C. The beads were washed three times with 1 ml of lysis buffer. The pre-coated beads were then incubated with approximately 25 µg of recombinant MBP-PAN3, MBP-PAN3-C-term or 6xHis-NOT1 in 1 ml of binding buffer for 1 hr at 4°C. Alternatively, pre-coated beads were incubated with *in vitro* translated proteins in 150 µl of NET buffer (see above) supplemented with 1mM DTT and 0.1 g/l BSA. The beads were washed four times with 1 ml of binding buffer and eluted as indicated above. The proteins were eluted with 40 µL of SDS-PAGE loading buffer and analyzed by 10% SDS-PAGE. [^{35}S]-methionine-labeled proteins were detected by fluorography using Amplify (NAMP100, GE Healthcare) according to the instructions of the manufacturer.

Complementation assay in human cells

The *Renilla* and firefly luciferase reporters have been described before (Huntzinger et al., 2010; Pillai et al., 2005). Complementation assays in human HeLa cells were performed as described by Huntzinger et al. (2010). The following siRNAs were used: TNRC6A 5'-GCCUAAUCUCCGUGCUCAATT-3', TNRC6B 5'-GGCCUUGUAUUGCCAGCAATT-3', and β-Gal 5'-CUACACAAAUCAGCGAUUUUU-3'; Dharmacon). R-Luc and F-Luc activities were measured using the Dual-Luciferase Reporter Assay System (Promega).

Knockdowns in S2 cells, RNA analysis and luciferase assays

Transfection of S2 cells was performed in 6-well or 24-well dishes using Effectene transfection reagent (Qiagen). For the λN-tethering assay, the following plasmids were cotransfected: 0.1µg reporter plasmid (F-Luc-5BoxB), 0.4µg pAc5.1-R-Luc as transfection control and 10ng of pAc5.1λN-HA construct for the expression of λN-

HA-fusion proteins. For the miRNA reporter experiments, the following plasmids were cotransfected: 0.1μg of F-Luc-Nerfin (or F-Luc-Par-6) reporter plasmid, 0.4μg pAc5.1-R-Luc (as transfection control), and 0.1μg of pAc5.1 plasmid without insert (empty vector) or expressing miRNA primary transcripts.

For the measurement of mRNA half-life, transfected cells were treated with actinomycin D (5μg/ml final concentration) 3 days after transfection and harvested at the indicated time points. Firefly and *Renilla* luciferase activity was measured using the Dual-Luciferase reporter assay system (Promega), and total RNA was isolated using TriFast (peqlab biotechnologies). RNA samples were analyzed as described by Behm-Ansmant et al. (2006).

The EMBO Journal (2010) 29, 4146–4160 | © 2010 European Molecular Biology Organization | Some Rights Reserved 0261-4189/10
www.embojournal.org

THE EMBO JOURNAL

EMBO open

Two PABPC1-binding sites in GW182 proteins promote miRNA-mediated gene silencing

Eric Huntzinger, Joerg E Braun, Susanne Heimstädt, Latifa Zekri and Elisa Izaurralde*

Department of Biochemistry, Max Planck Institute for Developmental Biology, Tübingen, Germany

miRNA-mediated gene silencing requires the GW182 proteins, which are characterized by an N-terminal domain that interacts with Argonaute proteins (AGOs), and a C-terminal silencing domain (SD). In *Drosophila melanogaster* (Dm) GW182 and a human (Hs) orthologue, TNRC6C, the SD was previously shown to interact with the cytoplasmic poly(A)-binding protein (PABPC1). Here, we show that two regions of GW182 proteins interact with PABPC1: the first contains a PABP-interacting motif 2 (PAM2; as shown before for TNRC6C) and the second contains the M2 and C-terminal sequences in the SD. The latter mediates indirect binding to the PABPC1 N-terminal domain. In *D. melanogaster* cells, the second binding site dominates; however, in HsTNRC6A–C the PAM2 motif is essential for binding to both Hs and DmPABPC1. Accordingly, a single amino acid substitution in the TNRC6A–C PAM2 motif abolishes the interaction with PABPC1. This mutation also impairs TNRC6s silencing activity. Our findings reveal that despite species-specific differences in the relative strength of the PABPC1-binding sites, the interaction between GW182 proteins and PABPC1 is critical for miRNA-mediated silencing in animal cells.

The EMBO Journal (2010) **29,** 4146–4160. doi:10.1038/emboj.2010.274; Published online 9 November 2010
Subject Categories: RNA
Keywords: argonaute; miRNAs; mRNA decay; silencing; TNRC6

Introduction

GW182-family proteins are essential in animal cells for miRNA-mediated silencing (reviewed by Ding and Han, 2007; Eulalio *et al*, 2009a). Analysis of GW182 domains in *Drosophila melanogaster* (Dm) and human cells identified two domains that are required for silencing. The first is the N-terminal domain, which contains multiple glycine-tryptophan repeats (GW repeats) and confers binding to Argonaute proteins (AGOs; Behm-Ansmant *et al*, 2006; Till *et al*, 2007; Eulalio *et al*, 2008; Lazzaretti *et al*, 2009; Takimoto *et al*, 2009). The second is a bipartite silencing domain (SD), consisting of the Mid and C-terminal regions, which elicits translational repression and degradation of miRNA targets (Figure 1A; Eulalio *et al*, 2009b; Lazzaretti *et al*, 2009; Zipprich *et al*, 2009).

Exactly how the bipartite SD of GW182 proteins interferes with translation and accelerates mRNA degradation is not completely understood, but recent studies provide important insight by showing that these domains interact with the cytoplasmic poly(A)-binding protein PABPC1, both in *D. melanogaster* and human cells (Fabian *et al*, 2009; Zekri *et al*, 2009).

PABPC1 is a highly conserved eukaryotic protein that binds the poly(A) tail of mRNAs and stimulates translation through multiple interactions with translation factors (reviewed by Kahvejian *et al*, 2001; Derry *et al*, 2006). PABPC1 contains four N-terminal RNA recognition motifs (RRM1–4), a proline-rich unstructured linker and a C-terminal domain (termed PABC or MLLE, because of a conserved KITGMLLE signature motif in this domain; Figure 1A; Kozlov *et al*, 2010a). The MLLE domain recognizes a conserved motif termed PABP-interacting motif 2 (PAM2), which was first identified in the translational regulators Paip1 and Paip2 (PABP-interacting proteins 1 and 2) and is also present in multiple proteins involved in translation or mRNA decay (Khaleghpour *et al*, 2001; Roy *et al*, 2002; Albrecht and Lengauer, 2004; Kozlov *et al*, 2004, 2010a).

Interestingly, the SD of TNRC6C contains a PAM2 motif (previously termed conserved motif III or DUF; Figure 1A). This PAM2 motif in TNRC6C interacts directly with the PABPC1 MLLE domain in a way similar of those found in Paip1 and Paip2 (Fabian *et al*, 2009; Jínek *et al*, 2010; Kozlov *et al*, 2010b). In particular, when both TNRC6C and Paip2 bind to the MLLE domain, the invariant glutamate, phenylalanine and proline residues of the PAM2 motifs occupy structurally equivalent positions (Jínek *et al*, 2010; Kozlov *et al*, 2010b). Moreover, when the phenylalanine residue is substituted with alanine, the interaction of TNRC6C with the MLLE domain is abolished as shown before for Paip2 (Kozlov *et al*, 2004, 2010a, b).

The PAM2 motif is also conserved in DmGW182. Surprisingly, however, our previous studies showed that this motif is dispensable for PABPC1 binding in cell lysates (Zekri *et al*, 2009). DmGW182 instead binds PABPC1 via sequences downstream of the PAM2 motif (termed M2), plus sequences in the very C-terminal (C-term) region (Figure 1A). Nevertheless, the affinity of these regions for PABPC1 in-

*Corresponding author. Department of Biochemistry, Max Planck Institute for Developmental Biology, Spemannstrasse 35, 72076 Tübingen, Germany. Tel.: +49 7071 601 1350; Fax: +49 7071 601 1353; E-mail: elisa.izaurralde@tuebingen.mpg.de

Received: 5 June 2010; accepted: 12 October 2010; published online: 9 November 2010

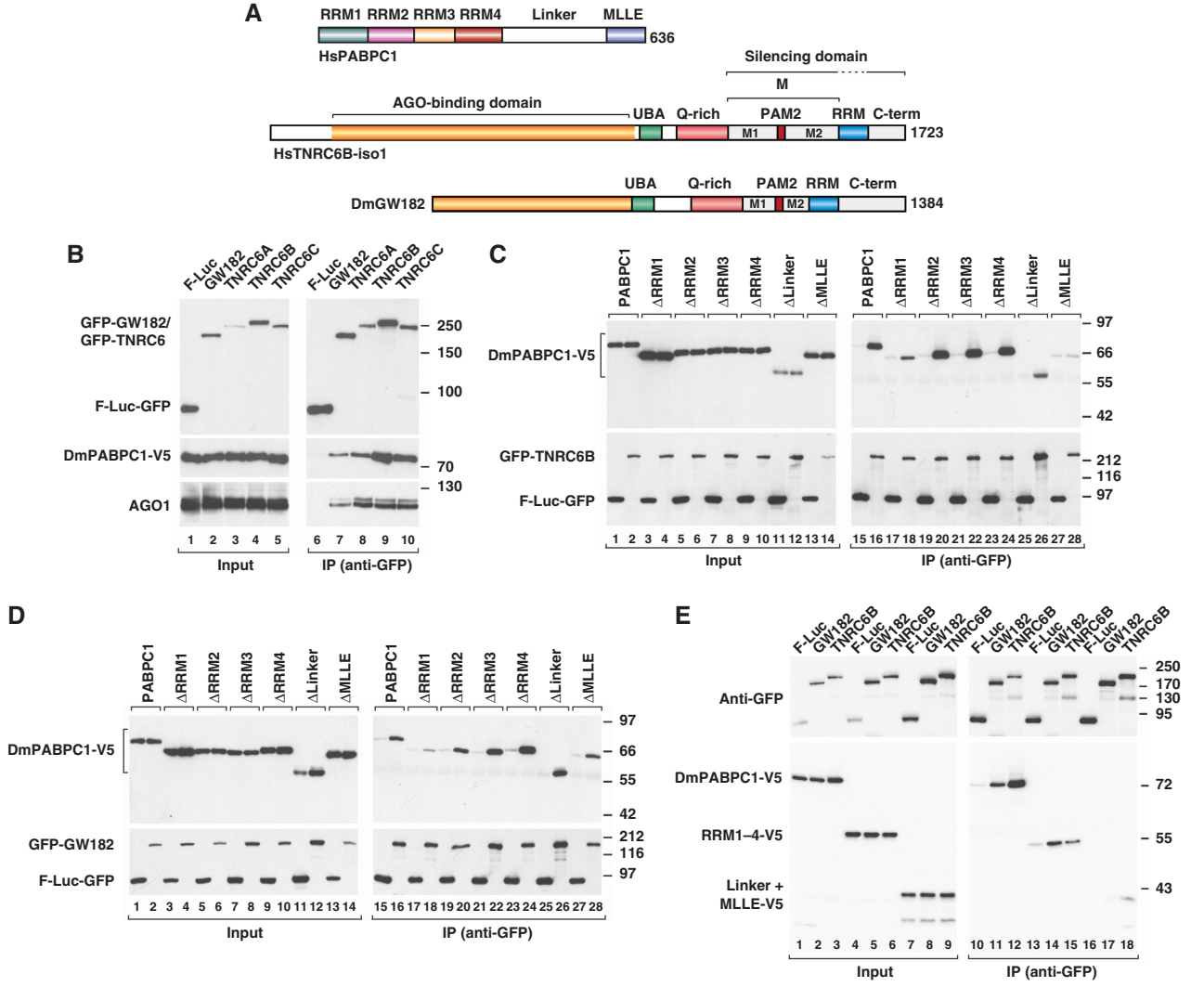

Figure 1 PABPC1 provides two binding sites for GW182 proteins. (**A**) Domain organization of HsPABPC1, HsTNRC6B isoform 1 and DmGW182. PABPC consists of four N-terminal RRM domains, a proline-rich unstructured linker, and a conserved C-terminal domain, termed MLLE. HsTNRC6B and DmGW182 consist of an N-terminal AGO-binding domain, which contains multiple GW-repeats (yellow); and a bipartite silencing domain (SD) which includes the Mid (M) and C-terminal regions but not the RRM. UBA, ubiquitin-associated domain; Q-rich, region rich in glutamine; PAM2, PABP-interacting motif 2; RRM, RNA recognition motif; M1 and M2, regions within the Mid (M) domain; C-term, C-terminal region. (**B**) S2 cells were transfected with a plasmid expressing V5-tagged DmPABPC1 together with plasmids for expression of GFP-tagged proteins (DmGW182, human TNRC6A–C, or firefly luciferase (F-Luc, which served as a negative control)). Three days after transfection, cells were lysed and proteins were immunoprecipitated using a polyclonal anti-GFP antibody. Inputs and immunoprecipitates were analysed by western blotting using anti-GFP and anti-V5 antibodies. The presence of endogenous AGO1 in the immunoprecipitates was analysed using a specific anti-AGO1 antibody. (**C**–**E**) The interaction of GFP-TNRC6B or GFP-GW182 with full-length DmPABPC1-V5 or the indicated PABPC1 deletion mutants (V5 tagged) was analysed as described in panel (**B**). Note that in panel (**E**), cell lysates were treated with micrococcal nuclease prior to immunoprecipitation.

creases when the PAM2 motif is included (Zekri *et al*, 2009); however, deleting the PAM2 motif does not affect the DmGW182 silencing activity *in vivo* (Eulalio *et al*, 2009b). The M2 and C-term regions of DmGW182 do not interact with the MLLE domain of DmPABPC1 but rather interact with the N-terminal PABPC1 RRM domains (Zekri *et al*, 2009). These observations raise a key question: Do the differences in human TNRC6C and DmGW182 reflect differences in the mechanisms of silencing between these distant species?

Another important question that remains open is to what extent the interaction between GW182 proteins and PABPC1 contributes to silencing *in vivo*. Currently, two lines of evidence support a role for PABPC1 in silencing. First, overexpressing PABPC1 in both *D. melanogaster* and human cells suppresses silencing (Zekri *et al*, 2009; Walters *et al*, 2010). Second, depleting PABPC1 from cell-free extracts abolishes miRNA-mediated deadenylation (Fabian *et al*, 2009). It has been difficult to obtain more direct evidence of a role for PABPC1 in the miRNA pathway (i.e. using RNAi knockdowns) because depleting PABPC1 causes rapid cell death and general mRNA destabilization (Behm-Ansmant *et al*, 2007).

In this study, we investigate further the interaction of DmGW182 and human TNRC6A–C proteins with PABPC1. We show that PABPC1 provides two binding sites for GW182 proteins: one on the MLLE domain and another on the RRM domains. Conversely, GW182 proteins contain two PABPC1-binding sites: the PAM2 motif, which confers direct binding to the MLLE domain (as shown before for TNRC6C; Fabian *et al*,

2009; Jínek *et al*, 2010; Kozlov *et al*, 2010b), and a less-defined sequence comprising the M2 and C-term regions, which interacts indirectly with the PABPC1 RRMs (as shown before for DmGW182; Zekri *et al*, 2009). Both sites contribute to PABPC1-binding *in vivo*, but for the human proteins, the dominant interaction is between PABPC1 MLLE and PAM2, whereas for DmGW182, the critical interaction is with PABPC1 RRMs. These results reconcile the apparent discrepancy between earlier studies in human and *D. melanogaster* cells (Fabian *et al*, 2009; Zekri *et al*, 2009).

We also show that in *D. melanogaster* cells depleted of endogenous GW182, human TNRC6B can rescue silencing. Remarkably, this ability to restore silencing is abrogated by a single amino acid substitution in the PAM2 motif of TNRC6B. This mutation also abolishes TNRC6s binding to both Dm and HsPABPC1. Moreover, a chimeric DmGW182 construct containing the PAM2 motif, plus the M2 and C-term regions of human TNRC6B, requires the PAM2 motif to interact with PABPC1. Importantly, a phenylalanine to alanine substitution within the PAM2 motif abrogated both PABPC1 binding and the silencing activity of the chimeric protein. Finally, we show that a TNRC6A protein lacking the PAM2 motif or carrying a single amino acid substitution in this motif does not interact with HsPABPC1 and is strongly impaired in restoring silencing in human cells depleted of endogenous TNRC6A and TNRC6B. Together, our results definitively establish a crucial role for GW182–PABPC1 interaction in the miRNA pathway.

Results

PABPC1 provides two binding sites for GW182 proteins

Previous studies reported that DmGW182 and TNRC6C interact with different PABPC1 domains (see Introduction). Therefore, we wished to determine whether, the species-specific binding differences reside in the GW182 proteins, in PABPC1 or both. To do this, we examined the interaction of human TNRC6s with DmPABPC1 in *D. melanogaster* Schneider-2 cells (S2 cells). In S2 cells, the expression level of TNRC6B was comparable to that of DmGW182, whereas human TNRC6A and TNRC6C were expressed at lower levels (Figure 1B, lanes 2–5). Nevertheless, considering the amount of proteins detected in the immunoprecipitates, the three human proteins coimmunoprecipitated DmPABPC1 and endogenous DmAGO1 more efficiently than DmGW182 (Figure 1B, lanes 7–10).

To define the domains in DmPABPC1 that are important for the interaction with either DmGW182 or human TNRC6B, we tested each with a series of DmPABPC1 deletion mutants. PABPC1 contains four RRMs connected to the C-terminal MLLE domain by a flexible linker (Figure 1A; Derry *et al*, 2006). Deleting RRM1 reduced the PABPC1 interaction with both DmGW182 and TNRC6B (Figure 1C and D, lane 18 versus lane 16). In contrast, deleting the MLLE domain inhibited PABPC1 from binding to TNRC6B but not to DmGW182 (Figure 1C and D, lane 28). Deleting RRM2, RRM3, RRM4 or the linker region had no effect in any of these interactions (Figure 1C and D, lanes 19–26). Together, these results indicate that PABPC1 has two binding sites for GW182 proteins: one that is contributed by the RRM1 domain and another by the MLLE domain.

We next asked whether PABPC1 RRMs or the MLLE domain were sufficient for binding to DmGW182 and TNRC6B, respectively. We observed that TNRC6B interacted with PABPC1 fragments comprising either the RRMs or the MLLE domain (Figure 1E, lanes 15 and 18). However, these interactions were less efficient than those observed with full-length PABPC1 (Figure 1E, lane 12), suggesting that the RRM and the MLLE domains contribute (additively or synergistically) to the interaction with TNRC6B. Furthermore, we confirmed that, in cell lysates, DmGW182 interacts with the PABPC1 RRMs but not the MLLE domain as shown before (Figure 1E, lanes 14 and 17; Zekri *et al*, 2009). Importantly, the interactions shown in Figure 1E were observed in cell lysates treated with micrococcal nuclease, suggesting that they are not mediated by RNA.

GW182 proteins interact with PABPC1 through two distinct binding sites

We next tested how the various sequences within the SDs of DmGW182 and TNRC6B contribute to PABPC1 binding. Both SDs consist of four segments: M1, PAM2 motif, M2 and C-term (Figures 1A and 2A). Deleting the TNRC6B PAM2 motif abolished the interaction with PABPC1, whereas no effect was observed when the M2 and C-term regions were deleted individually (Figure 2B, lanes 10–12). When, however, the M2 and C-term regions were both deleted, then PABPC1 binding was reduced, suggesting that these regions work in concert to bind PABPC1 (Figure 2B, lane 13). Thus, for TNRC6B, although the PAM2 motif is the high-affinity PABPC1-binding site, the M2 and C-term regions also contribute.

In the case of DmGW182, we previously reported that the same three regions (PAM2 motif and the M2 and C-term regions) contribute to PABPC1 binding (Zekri *et al*, 2009). However, the contribution of the PAM2 motif and the M2 region was apparent only when binding to PABPC1 was impaired, for example by deleting the C-term region (Zekri *et al*, 2009). The results shown in Figure 2C confirm and extend these previous observations. Indeed, we confirmed that the interaction of GW182 with PABPC1 is not affected when the M2 region or the PAM2 motif are deleted individually (Figure 2C, lanes 13 and 14; Zekri *et al*, 2009). In contrast, deleting the C-term region reduced PABPC1 binding (Figure 2C, lane 15). PABPC1 binding was further decreased when the C-term region was deleted in combination with the M2 region or the PAM2 motif (Figure 2C, lanes 16 and 17; Zekri *et al*, 2009). PABPC1 binding was abolished when all three regions were deleted (i.e. PAM2, M2 and C-term; Figure 2C, lane 19; Zekri *et al*, 2009). Similar results were obtained when cell lysates were treated with micrococcal nuclease (Supplementary Figure S1).

An important implication of the results shown in Figure 2C is that the GW182 C-term region provides a major PABPC1-binding sites in cell lysates, however, the M2 region and the PAM2 motif also contribute, although on their own they are not sufficient. This conclusion is further supported by experiments aimed at defining the minimal PABPC1-binding domain in DmGW182. We observed that a protein fragment containing the PAM2 motif and the M2 and C-ter regions was sufficient for PABPC1 binding (Supplementary Figure S2A, lane 17 versus lane 13; Zekri *et al*, 2009), whereas fragments containing one or two of these sequences exhibited reduced

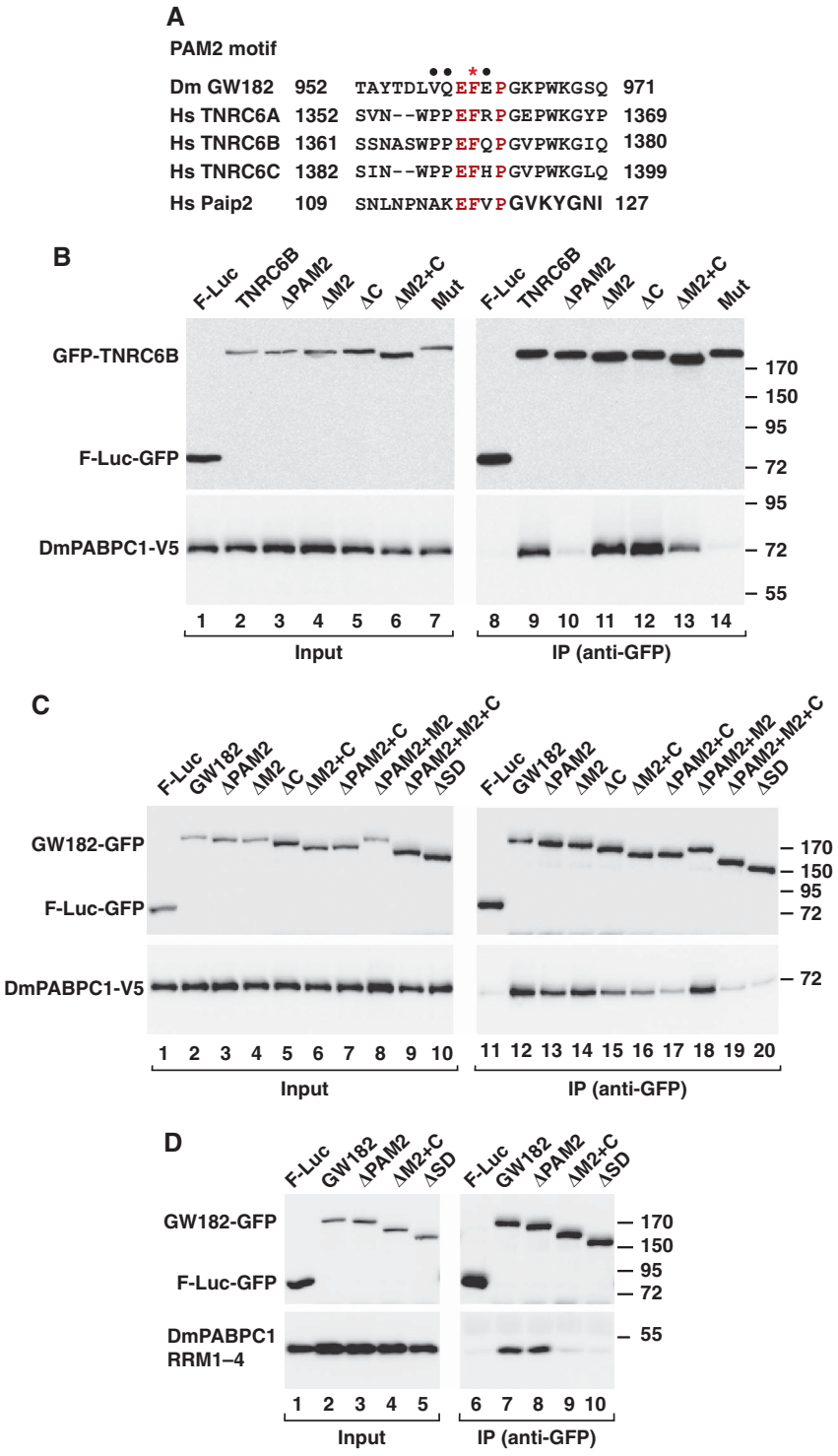

Figure 2 GW182 proteins contain two PABPC1-binding sites. (**A**) Sequence alignment of PAM2 motifs of human TNRC6A–C, Paip2 and DmGW182. Invariant residues are shown in red. The asterisk indicates the phenylalanine residue that is substituted with alanine in our mutants (Mut). Dots indicate the residues in the PAM2 motif of GW182 that were substituted in the experiment shown in Figure 3B. (**B**, **C**) S2 cells expressing GFP-TNRC6B, GFP-DmGW182 or the corresponding protein mutants together with DmPABPC1-V5 were lysed 3 days after transfection. Proteins were immunoprecipitated from cell lysates using a polyclonal anti-GFP antibody and analysed by western blotting as described in Figure 1. (**D**) Interaction of GFP-DmGW182 or the indicated mutants with a V5-tagged DmPABPC1 fragment containing RRM1–4.

or no affinity for PABPC1 in cell lysates (Supplementary Figure S2A, lanes 15, 16 and 18–22). These results remained unchanged in the presence of micrococcal nuclease (Supplementary Figure S2B).

The results described above, together with the observation that DmGW182 interacts with the RRM domains as efficiently with full-length PABPC1, suggest that the role of the M2 and C-term regions is to confer binding to PABPC1 RRMs.

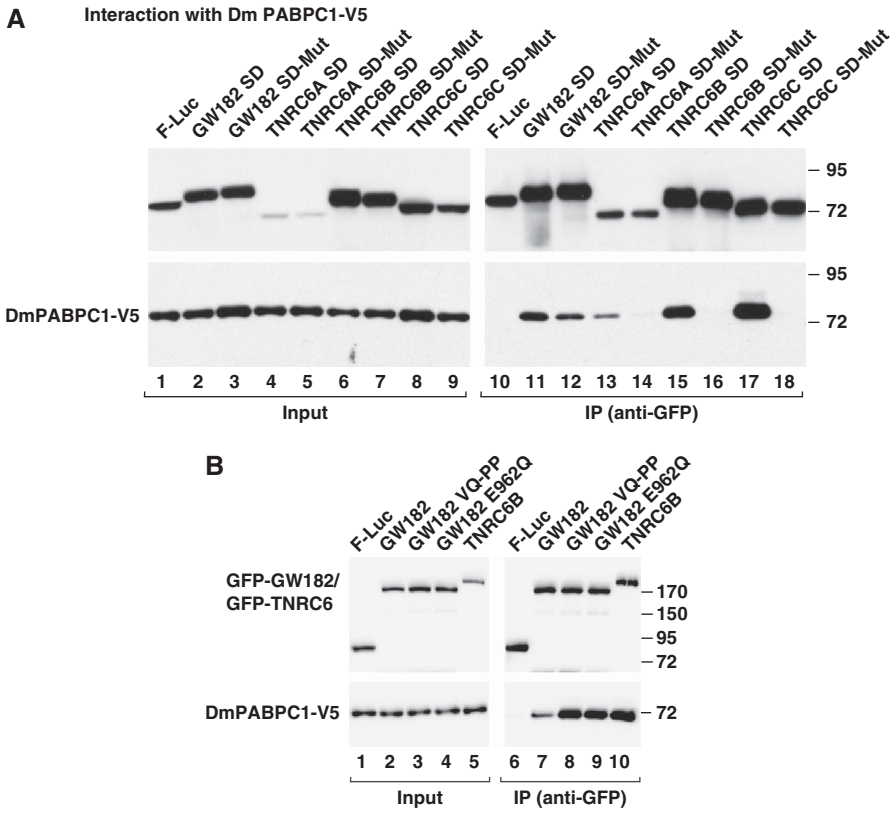

Figure 3 The invariant phenylalanine residue in human PAM2 motifs is essential for binding to DmPABPC1. (**A**) The interaction of DmPABPC1-V5 with GFP-tagged DmGW182 or human TNRC6A–C silencing domains was analysed by coimmunoprecipitation assays as described in Figure 1B. Protein mutants (Mut) contain an alanine to phenylalanine substitution in the PAM2 motif (see Figure 2A, asterisk). (**B**) S2 cells transiently expressing DmPABPC1-V5 together with GFP-GW182 wild type or the indicated GW182 mutants were lysed 3 days after transfection. Proteins were immunoprecipitated from cell lysates using anti-GFP antibodies and analysed as described in Figure 1B. GW182 mutants carry substitutions of the amino acids that are indicated with dots in Figure 2A.

Therefore, we constructed a PABPC1 mutant containing only the RRM1–4 domains and tested how well it interacts with various GW182 deletion mutants. We observed that deleting the M2 and C-term regions inhibited DmGW182 from interacting with the PABPC1 RRMs as efficiently as deleting the entire SD (which includes the PAM2 motif); in contrast, deleting the PAM2 motif alone had no effect (Figure 2D, lanes 8–10). Collectively, these results clearly demonstrate that the M2 and C-term regions interact with DmPABPC1 RRM domains in cell lysates.

A single amino acid substitution in the PAM2 motif of human TNRC6s abolishes binding to DmPABPC1

The PAM2 motifs from diverse proteins contain three invariant residues EF(X)P that occupy equivalent structural positions when bound to an MLLE domain (Figure 2A; Jínek *et al*, 2010; Kozlov *et al*, 2010a, b). In particular, the invariant phenylalanine residue is critical for this interaction: if this phenylalanine is substituted with alanine then the Paip2 and TNRC6C PAM2 motifs cannot bind PABPC1 (Kozlov *et al*, 2004, 2010a, b). Similarly, this substitution abolishes the TNRC6B interaction with DmPABPC1 as efficiently as deleting the entire PAM2 motif (Figure 2B, lane 14; Figure 3A, lane 16). The critical role of the invariant phenylalanine residue in the interaction with DmPABPC1 was confirmed for TNRC6A and TNRC6C SDs (Figure 3A, lanes 14 and 18). The equivalent substitution in the PAM2 motif of DmGW182 had only a minor effect on DmPABPC1 binding, as expected (Figure 3A, lane 12).

The coimmunoprecipitation assays suggest that the *D. melanogaster* PAM2 motif has a relatively lower affinity for the DmPABPC1 MLLE domain. This might be because the motif lies in a suboptimal sequence context. However, we consider this possibility unlikely because the human PAM2 motif is functional in the context of DmGW182 (i.e. it enhances DmGW182 binding to PABPC1; see below Figure 8A). An alternative explanation is that the affinity may be lower because a negatively charged residue sits at the core of the PAM2 motif (between the invariant phenylalanine and proline residues, Figure 2A). Indeed, negatively charged residues are extremely rare at the equivalent position in PAM2 motifs from diverse proteins and are absent in all PAM2 motifs validated experimentally (Albrecht and Lengauer, 2004; Kozlov *et al*, 2010a). Additionally, in the human TNRC6A–C, the invariant residues of the PAM2 motifs are preceded by proline residues that establish hydrophobic interactions with the MLLE domain (Kozlov *et al*, 2010b), these residues are substituted with valine and glutamine in DmGW182 (Figure 2A).

We therefore tested whether substituting residues in the PAM2 motif of GW182 with the residues present in the human proteins could enhance PABPC1 binding. Substituting the GW182 PAM2-motif amino acids V958 and Q959 with prolines enhanced GW182 binding to DmPABPC1

(Figure 3B, lane 8 versus lane 7). Similar results were obtained when the negatively charged residue E962 was substituted with glutamine as in TNRC6B (Figure 3B, lane 9). The two GW182 mutants interacted with DmPABPC1 as efficiently as TNRC6B (Figure 3B, lane 10). Thus, the differences in the amino acid sequences of these PAM2 motifs can account for the different affinities for the DmPABPC1 MLLE domain.

The PAM2 motifs of human TNRC6s are essential for binding to HsPABPC1

We next analysed whether the human proteins interact in a similar way with HsPABPC1. We transfected human HEK-293 cells with plasmids expressing either wild-type TNRC6A–C SDs or the corresponding mutants carrying the phenylalanine to alanine substitution in the PAM2 motifs. We observed that the single amino acid substitution in the PAM2 motifs was sufficient to abolish the interaction with endogenous PABPC1 (Figure 4A–C). Thus, the PAM2 motifs of TNRC6A–C are essential in mediating binding to both Hs and DmPABPC1.

We also tested whether the M2 and C-term regions of human TNRC6s contribute to PABPC1 binding in human cell lysates. Remarkably, deleting either the M2 or C-terminal regions in the TNRC6C SD reduced the interaction with PABPC1, whereas deleting the RRM from TNRC6C had no effect (Figure 4D, lanes 12–14). As a control, we confirmed that deleting the PAM2 motif (or the entire Mid domain) abrogated PABPC1 binding (Figure 4D, lanes 10 and 11). Similar results were obtained when cell lysates were treated with micrococcal nuclease (data not shown). These findings demonstrate that TNRC6s contain two PABPC1-binding sites: the PAM2 motif and the M2 plus C-term regions.

To investigate whether the interaction mediated by the M2 and C-term regions of GW182 proteins is direct, we performed glutathione S-transferase (GST) pull-down assays with recombinant proteins expressed in *Escherichia coli*. These experiments revealed the following observations:

First, we observed that a GST-tagged C-terminal fragment of TNRC6B containing the PAM2 motif and the downstream protein sequences (i.e. M2, RRM and C-term) interacted with both human and DmPABPC1, but did not interact with the corresponding PABPC1 mutants lacking the MLLE domain (Figure 4E, lanes 11 versus 14, and 27 versus 30, respectively). Second, deleting the PAM2 motif abolished the interaction of TNRC6B SD with both Hs and DmPABPC1 (Figure 4E, lanes 12 and 28, respectively; Figure 5A, lane 10), in agreement with the coimmunoprecipitation assays. In contrast, deleting the M2 and C-terminal regions did not affect PABPC1-binding *in vitro* (Figure 5A, lane 13). Surprisingly, *in vitro*, the interaction of DmGW182 SD with DmPABPC1 was mediated by the PAM2 motif (Figure 5B, lane 10 versus lane 9). Accordingly, a GW182 SD mutant lacking the M2 and C-terminal regions pulled down DmPABPC1 (Figure 5B, lane 13). Together, these results indicate that the PAM2 motifs of GW182 proteins mediate direct binding to PABPC1, whereas the M2 and C-term regions interact with PABPC1 indirectly, most likely through additional proteins present in cell lysates. Alternatively, the interaction of the M2 and C-term regions with PABPC1 may require post-translational modifications that do not occur in bacteria. Importantly, the observation that the DmGW182 PAM2 motif directly interacts with DmPABPC1 *in vitro*, but is neither sufficient nor necessary for binding to DmPABPC1 in cell lysates, suggest that the DmPAM2 motif might not be able to efficiently compete with additional PAM2-containing proteins for binding to PABPC1 in *D. melanogaster* cells.

GW182 silencing activity correlates with PABPC1 binding

To evaluate how the interaction between GW182 and PABPC1 contributes to silencing, we tested whether DmGW182 mutants that are impaired in PABPC1 binding in cell lysates could complement silencing in cells lacking endogenous GW182. To this end, we used a complementation assay described before (Eulalio *et al*, 2009b). In this assay, endogenous GW182 is depleted using a dsRNA that targets the coding sequence of the *GW182* mRNA. This depletion inhibits miRNA-mediated silencing (Figure 6A–G). GW182 mutants were then tested for the ability to restore silencing in GW182-depleted cells. Transcripts encoding the recombinant proteins were made resistant to the dsRNA by introducing mutations that disrupt basepair interactions with the dsRNA without altering the protein sequence.

We monitored miRNA activity using two different reporters: the F-Luc-Par-6 reporter which is degraded in the presence of miR-1 and the F-Luc-Nerfin reporter which is silenced by miR-9b or miR-279 mainly at the translational level (Behm-Ansmant *et al*, 2006; Eulalio *et al*, 2007). We observed that, independently of the reporter, a DmGW182 mutant lacking the PAM2 motif fully rescued silencing (Figure 6A–F). Deleting the M2 region had a slight inhibitory effect (particularly for the F-Luc-Par-6 reporter), whereas deleting the C-term region impaired silencing for all reporters as shown before (Figure 6A–F; Eulalio *et al*, 2009b). When in addition to the C-term region, the PAM2 motif and the M2 region were deleted, the silencing activity of the protein decreased further and was comparable to that of the protein lacking the entire SD (Figure 6A–F). Note that these deletion mutants did not rescue silencing even though they were expressed at higher levels than the wild type (Figure 6H). Moreover, the activity of wild-type GW182 and mutants remained unchanged when the amounts of transfect plasmid were increased up to 10-fold (Supplementary Figure S3). We conclude that the silencing activity of GW182 mutants strongly correlates with the ability to bind to PABPC1. Nevertheless, because several regions of DmGW182 must be deleted to abolish PABPC1-binding *in vivo*, we cannot rule out that these regions are also required for additional functions.

Human TNRC6s complement silencing in D. melanogaster cells

Next, we investigated whether the human proteins could restore silencing in S2 cells depleted of endogenous DmGW182. As shown above, depleting endogenous GW182 suppresses silencing of the F-Luc-Par-6 reporter, leading to a five- to nine-fold increase in firefly luciferase expression (Figure 6A and B; Supplementary Figure S4). Expressing a dsRNA-resistant form of GW182 fully restored silencing, over a broad range of transfected expression plasmid (from 10 to 200 ng; Supplementary Figures S3 and S4). Similarly, expressing TNRC6B restored silencing almost as efficiently as GW182 (Supplementary Figure S4). In contrast, TNRC6A and TNRC6C rescued silencing significantly only when the

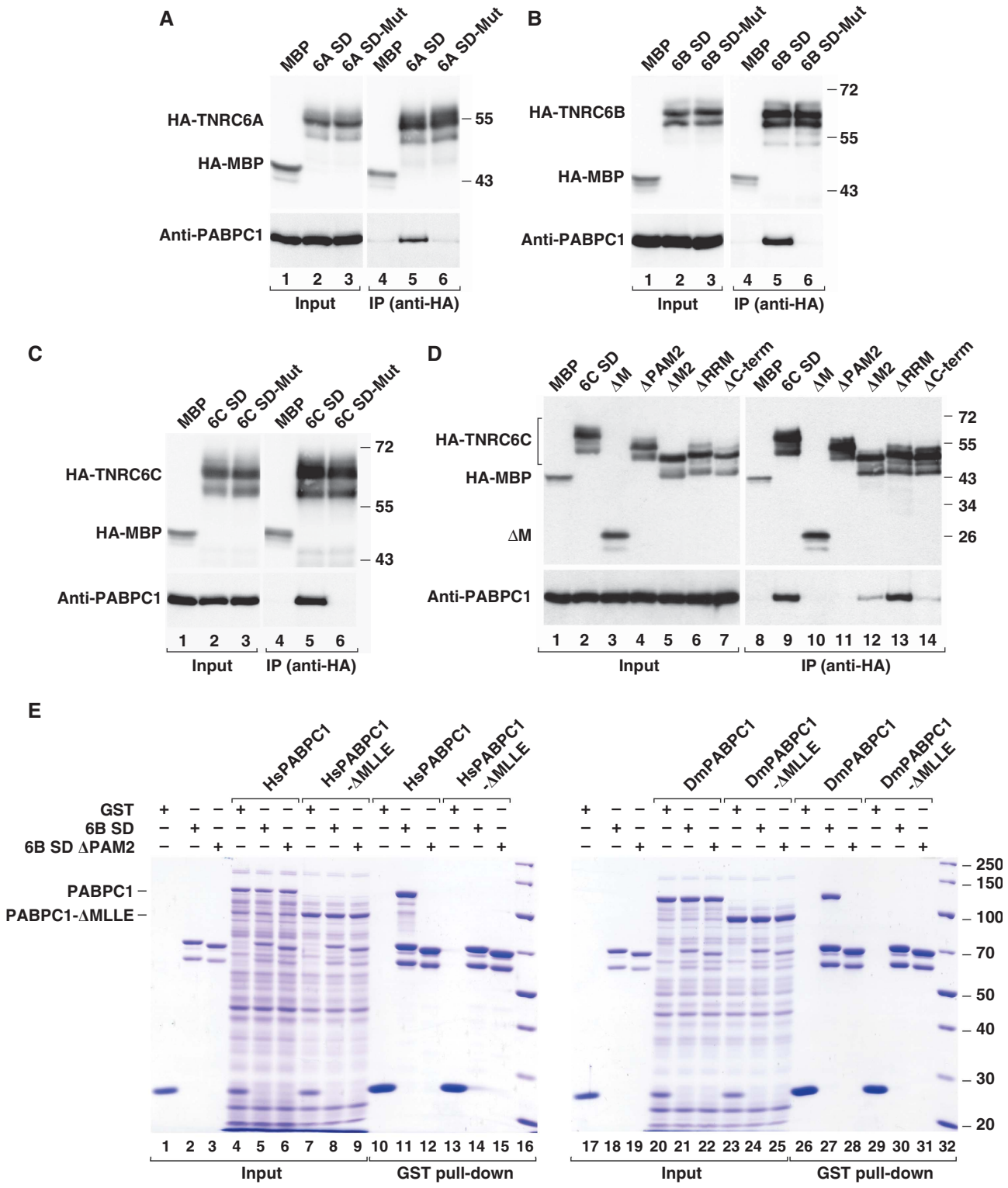

Figure 4 The PAM2 motifs of TNRC6A–C are essential for binding to HsPABPC1. (**A**–**C**) Human HEK-293 cells transiently expressing HA-tagged silencing domains of TNRC6A–C or the indicated mutants were lysed 2 days after transfection. Proteins were immunoprecipitated from RNaseA-treated cell lysates using anti-HA antibodies. HA-tagged maltose-binding protein (MBP) served as a negative control. Inputs and immunoprecipitates were analysed by western blotting using anti-HA antibodies. The presence of endogenous PABPC1 in the immunoprecipitates was analysed using an anti-PABPC1 antibody. (**D**) Interaction of HA-TNRC6C silencing domain or the indicated deletion mutants with endogenous PABPC1, in human cells. Immunoprecipitations were performed as described in panels (**A**–**C**). Note that TNRC6A–C silencing domains are unstable in human cells and show several degradation products (panels **A**–**D**). (**E**) Interaction of recombinant MBP-tagged HsPABPC1 (lanes 1–16), DmPABPC1 (lanes 17–32) or the corresponding mutants lacking the MLLE domain with GST-TNRC6B-SD (6B-SD) or a mutant lacking the PAM2 motif. Inputs (5%) and bound fractions (50%) were analysed on a 10% SDS–PAGE. GST served as a negative control.

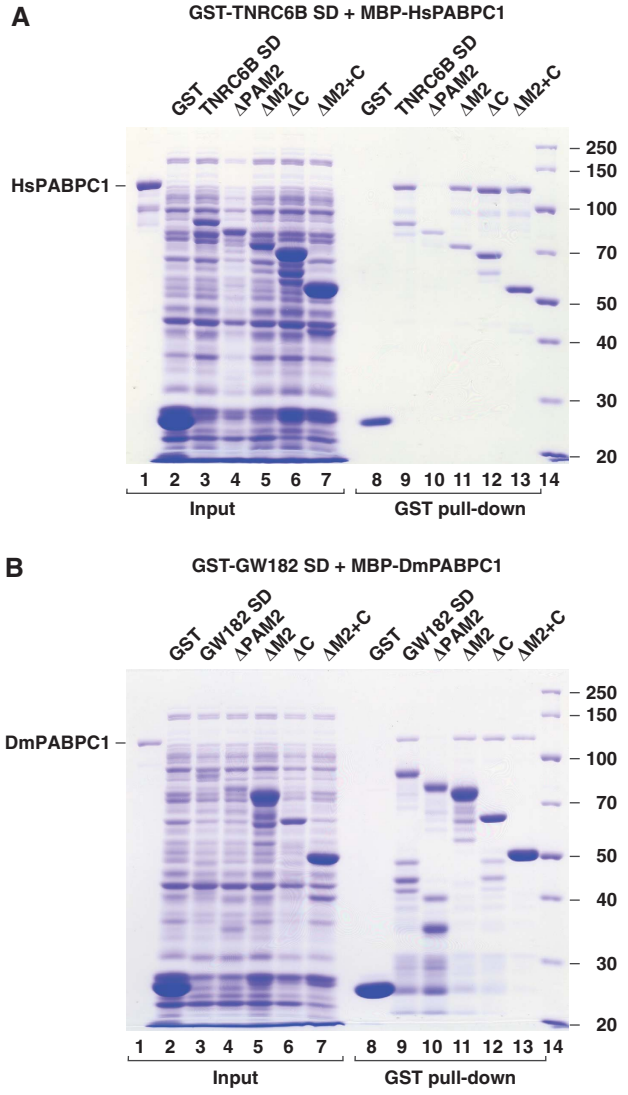

Figure 5 The PAM2 motifs of GW182 proteins confer direct binding to PABPC1 *in vitro*. (**A**) Interaction of recombinant MBP-HsPABPC1 with GST-TNRC6B-SD or the indicated deletion mutants. (**B**) Interaction of recombinant MBP-DmPABPC1 with GST-GW182-SD or the indicated deletion mutants. Inputs (20%) and bound fractions (50%) were analysed on a 10% SDS–PAGE. GST served as a negative control.

highest amount of expression plasmid was transfected (Supplementary Figure S4). The differences in silencing activity between TNRC6s could be due to differences in protein expression levels (see Figure 1B) and not to incompatibility with the *D. melanogaster* silencing machinery, as all three human proteins interact with DmAGO1 and PABPC1 (Figure 1B). However, it is possible that TNRC6A and

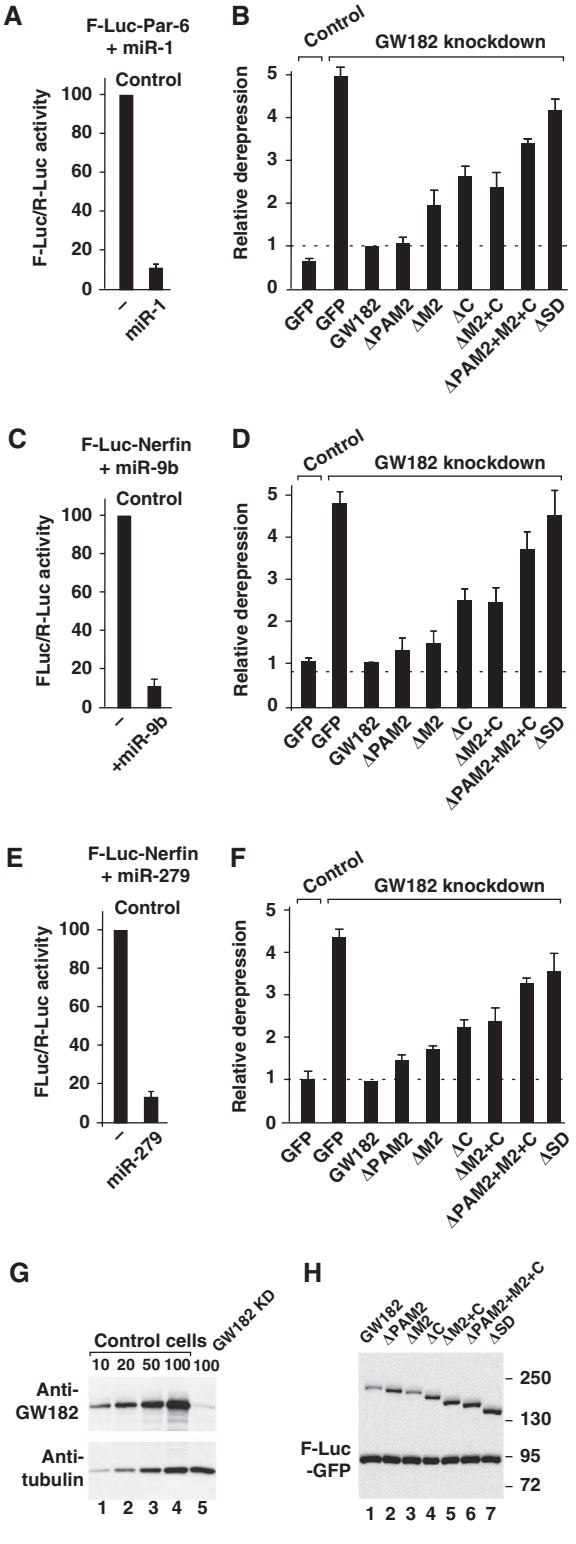

Figure 6 DmGW182 silencing activity correlates with the ability to bind PABPC1 in cell lysates. (**A**–**F**) S2 cells were treated with dsRNA targeting the coding sequence of *GW182* mRNA. Control cells were treated with GST dsRNA. These cells were subsequently transfected with a mixture of three plasmids: one expressing the indicated F–Luc miRNA reporters; another expressing miRNA primary transcripts or the corresponding empty vector (–); and a third expressing *Renilla* luciferase (R–Luc). Plasmids (10 ng) encoding wild-type GFP-GW182 or various deletion mutants were included in the transfection mixtures, as indicated. Firefly luciferase activities were normalized to those of the *Renilla* luciferase transfection control and set to 100 in cells transfected with the empty vector (i.e. in the absence of miRNAs). (**A**, **C**, **E**) Normalized firefly luciferase activities in the absence or presence of miRNAs in control cells (i.e. cells treated with GST dsRNA and expressing GFP). (**B**, **D**, **F**) The relative fold derepression for each condition. Mean values ± s.d. from three independent experiments are shown. (**G**) The effectiveness of the GW182 depletion was analysed by western blotting using anti-GW182 antibodies. In lanes 1–4, dilutions of untreated cells (control) are loaded. Blots were probed with anti-tubulin antibodies to test for equal loading. (**H**) Expression levels of full-length GW182 and mutants. F-Luc-GFP served as a transfection control.

TNRC6C are impaired for interaction with other factors required for silencing.

The TNRC6s–PABPC1 interaction is required for silencing

As TNRC6B can complement silencing in S2 cells and a single point mutation in TNRC6B is sufficient to prevent binding to PABPC1 both *in vivo* and *in vitro*, we had the opportunity to test whether the TNRC6B–PABPC1 interaction is relevant for silencing in a cellular context. In complementation assays in S2 cells, we observed that a TNRC6B mutant lacking the PAM2 motif was strongly impaired (Figure 7A–F). More importantly, a protein carrying the phenylalanine to alanine substitution in the PAM2 motif (Mut, F1370A) also failed to rescue silencing (Figure 7A–F). The equivalent mutation in GW182 (Mut, F961A) had no effect (Figure 7A–F). Deleting the TNRC6B M2 and C-term regions also affected silencing (Figure 7A–F); however, whether this effect reflects that these regions indirectly contribute to PABPC1 binding or that they have additional functions in silencing is unknown.

For the F-Luc-Par-6 reporter that is directed to degradation by miR-1, we analysed transcript levels by Northern blotting. In control cells expressing miR-1, F-Luc-Par-6 mRNA levels were strongly reduced (Figure 7G, lane 2 versus lane 1). Depleting GW182 inhibited miR-1-mediated mRNA degradation as reported before (Figure 7G, lane 4; Eulalio *et al*, 2008). Transfecting GW182-depleted cells with a plasmid expressing either wild-type GW182 or TNRC6B, restored mRNA degradation (Figure 7G, lanes 6 and 12). The GW182 mutant lacking the PAM2 motif also mediated mRNA degradation (Figure 7G, lane 8). In contrast, the TNRC6B mutant lacking the PAM2 motif could not trigger reporter degradation (Figure 7G, lane 14). The control, a GW182 lacking the M2 and C-term regions, failed to restore mRNA degradation (Figure 7G, lane 10). The mutant proteins were expressed at comparable or slightly higher levels than wild type (Figure 7H). We conclude that the TNRC6B–PABPC1 interaction is required for silencing of miRNA targets, regardless of whether the target is degraded (F-Luc-Par-6) or translationally repressed (F-Luc-Nerfin).

A chimeric GW182 protein requires the interaction with PABPC1 to elicit silencing

To further investigate how the GW182–PABPC1 interaction is relevant in silencing, we sought to engineer a DmGW182 protein that requires the PAM2 motif to bind to PABPC1. Initially, we generated a DmGW182 variant in which the PAM2 motif was substituted with the TNRC6B PAM2 motif (GW182-PAM2^{6B}). This chimeric protein interacted with Dm PABPC1 more efficiently than wild-type GW182 (Figure 8A, lane 13 versus lane 11); however, if the F1370A substitution in the PAM2 motif was introduced, binding to PABPC1 was comparable to that of wild-type GW182 (Figure 8A, lane 14 versus lane 11). Accordingly, in cells depleted of endogenous GW182, the chimeric protein complemented silencing regardless of the F1370A substitution (Figures 8B–G). These results further support the conclusion that in the context of DmGW182, the PAM2 motif is dispensable for both PABPC1 binding and silencing.

Next, in addition to the PAM2 motif, we substituted the M2, RRM and C-term sequences of DmGW182 with those from TNRC6B (GW182-SD^{6B}). This chimeric protein behaved like TNRC6B with respect to PABPC1 binding (Figure 8A). Indeed, relative to wild-type GW182, the PABPC1-binding efficiency increased (Figure 8A, lane 15 versus lane 11). More importantly, the F1370A substitution strongly reduced the interaction with PABPC1 (Figure 8A, lane 16 versus lane 15). Thus, as for TNRC6B, the chimeric protein relies mainly on the PAM2 motif to interact with PABPC1. In complementation assays, the chimeric protein carrying the F1370A substitution was impaired (Figure 8B–G), indicating that the interaction of GW182 proteins with PABPC1 is critical for silencing of miRNA targets.

The interaction of TNRC6A with PABPC1 is critical for silencing in human cells

So far, we demonstrated that the interaction between TNRC6s and PABPC1 has a critical function in silencing in *D. melanogaster* S2 cells. To determine whether this is also true in human cells, we examined whether overexpressing TNRC6C in HeLa cells stimulated silencing of an R-Luc reporter containing three let-7-binding sites in the 3′ UTR (Pillai *et al*, 2005). We found that TNRC6C enhanced silencing, decreasing luciferase activity an additional two-fold relative to control cells (Figure 9A and B). In contrast, the TNRC6C mutant carrying the F1389A substitution failed to stimulate silencing (Figure 9A and B).

Next, we depleted TNRC6 proteins using specific siRNAs and tested whether siRNA-resistant forms of the TNRC6s could complement silencing in depleted cells. We observed that siRNAs targeting TNRC6A and TNRC6B efficiently suppressed silencing of the let-7 reporter in HeLa cells (Figure 9C and D; other combinations of siRNAs and protein expression were less effective, data not shown). In cells codepleted of TNRC6A and TNRC6B, the expression of wild-type TNRC6A partially restored silencing, while the TNRC6A mutant either lacking the PAM2 motif or carrying the F1359A substitution were impaired in restoring silencing, although they were expressed at comparable levels as the wild type (Figure 9C–E). A TNRC6A mutant lacking the entire SD was inactive in the complementation assay, although this mutant was expressed at higher levels (Figure 9C–E). Altogether, these data support the idea that the interaction of TNRC6s with PABPC1 is also critical for silencing miRNA targets in human cells.

Discussion

Proteins of the GW182 family have an essential function in the miRNA pathway in diverse organisms (reviewed by Ding and Han, 2007; Eulalio *et al*, 2009a). The GW182 N-terminal and C-terminal domains interact with AGOs and PABPC1, respectively (reviewed by Tritschler *et al*, 2010). Here, we show that the GW182–PABPC1 interaction plays a crucial role in miRNA-mediated gene silencing.

GW182 proteins are PABP-interacting proteins (Paips)

We found GW182 proteins are similar to Paip1 and Paip2 in that they contain two binding sites for PABPC1: one in the PAM2 motif and another in the M2 and C-terminal regions (Figure 9F). In human TNRC6A–C and DmGW182, the PAM2 motif interacts directly with the C-terminal MLLE domain of PABPC1. Previous structural and functional studies indicated that the PAM2 motifs in TNRC6C, Paip1 and Paip2 are

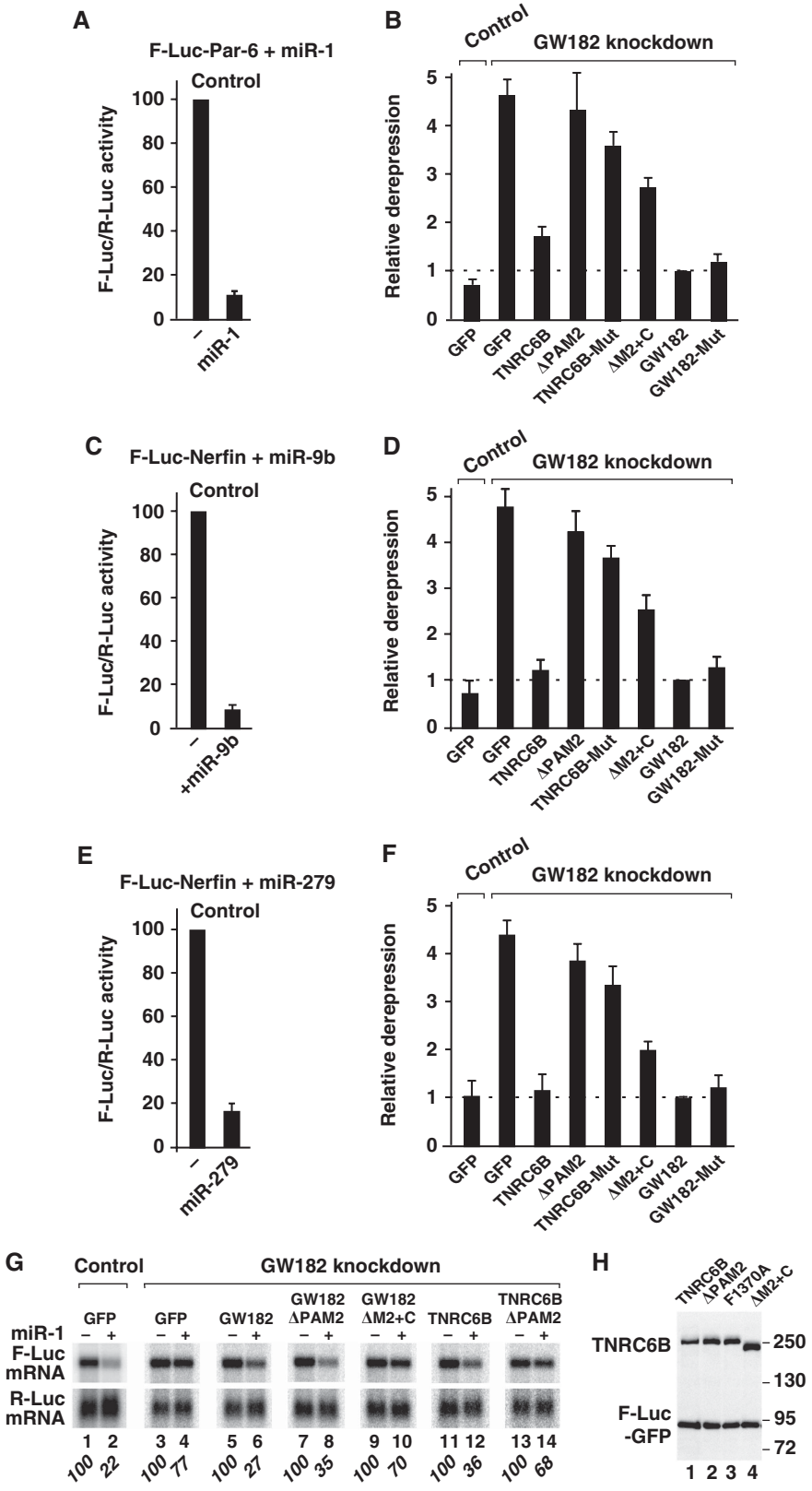

Figure 7 miRNA-mediated gene silencing requires TNRC6B interaction with PABPC1. (**A**–**F**) Complementation assays were performed with wild-type TNRC6B and various TNRC6B mutants (10 ng) and the indicated miRNA reporters, as described in Figure 6. Wild-type GW182 and the corresponding F961A mutant served as controls. (**G**) Northern blot analysis of representative RNA samples are shown in panels (**A**, **B**). Numbers in italics below the panels represent firefly luciferase mRNA levels normalized to those of the *Renilla* and set to 100 in cells transfected with the empty vector (i.e. in the absence of miR-1, (−)) for each condition. (**H**) Western blotting showing the expression levels of recombinant proteins.

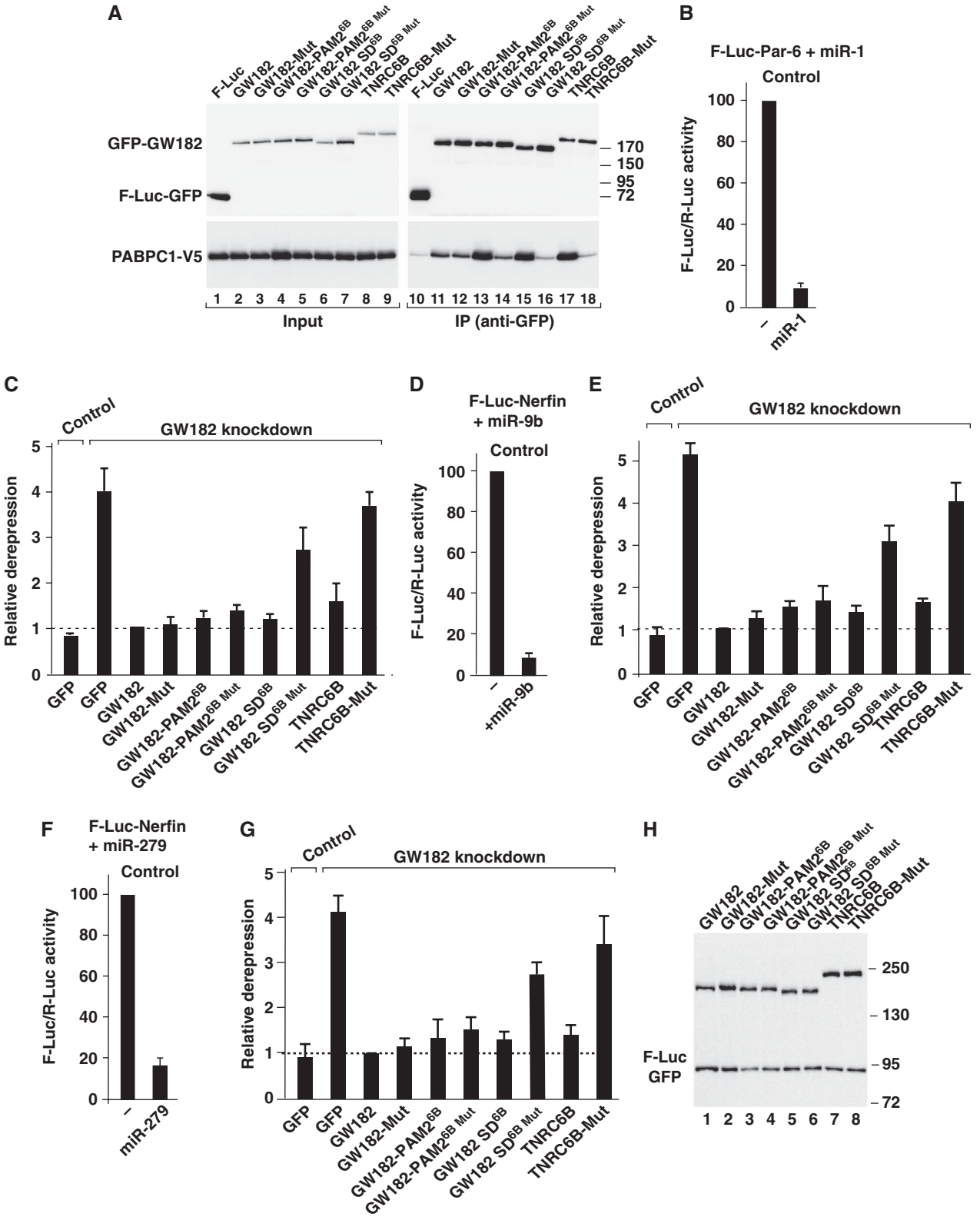

Figure 8 Generation of a chimeric GW182 protein that depends on the PAM2 motif for PABPC1 binding. (**A**) Two DmGW182-TNRC6B chimeric proteins were generated. The protein GW182-PAM2^{6B} consist of DmGW182 protein sequences in which the PAM2 motif was replaced with the PAM2 motif of human TNRC6B. The GW182-SD^{6B} protein contains (in addition to the PAM2 motif), the M2, RRM and C-term regions of TNRC6B. The F1370A substitution was introduced in the two chimeric proteins as indicated (Mut). The ability of the proteins to interact with DmPABPC1 was tested as described in Figure 1B. Wild-type GW182, TNRC6B and the corresponding PAM2 mutants (F961A and F1370A, respectively) were included for comparison. (**B**–**G**) The activity of the chimeric proteins in complementation assays was tested as described in Figure 6. (**H**) Western blotting showing the expression levels of recombinant proteins.

functionally equivalent (Fabian *et al*, 2009; Jínek *et al*, 2010; Kozlov *et al*, 2010b). Our findings extend this conclusion to the PAM2 motifs of TNRC6A and TNRC6B. Indeed, substituting alanine for the invariant phenyalanine in the PAM2 motif abolished binding to Hs or DmPABPC1 for all three human TNRC6 proteins (Figures 2B, 3A and 4). Nevertheless, the M2 and C-term regions also contribute to PABPC1 binding in cell lysates (Figures 2B and 4D). In DmGW182, the M2 and C-terminal site mediates binding to the RRM domains at the PABPC1 N-terminus (Figure 2D); this binding is most likely mediated by additional proteins and not by RNA because it is also observed in cell lysates treated with micrococcal nuclease.

For human TNRC6A–C, PABPC1 binding is mediated predominantly by the PAM2 motifs (Figure 9F). In *D. melanogaster* cell lysates, in contrast, the GW182 PAM2 motif is dispensable for PABPC1 binding. Nevertheless, the *D. melanogaster* PAM2 motif contributes to PABPC1 binding, because when it is deleted from a protein lacking the C-term region, PABPC1-binding efficiency decreases further (Figure 2C). Thus, although the human and *D. melanogaster* PAM2 motifs and M2 and C-term regions differ in their contribution to PABPC1-binding *in vivo* (Figure 9F), it is likely that TNRC6s and GW182 form complexes with PABPC1 that are functionally equivalent. Accordingly, human TNRC6CA–C can complement silencing in S2 cells depleted of endogenous DmGW182 (Figure 7; Supplementary Figure S4), indicating that silencing mechanisms are conserved between these organisms.

How does the GW182–PABPC1 interaction contribute to silencing?

Although both Paip1 and Paip2 contain PAM2 motifs, and interact with PABPC1 in a similar manner, they affect translation in opposite ways: Paip1 stimulates translation whereas Paip2 inhibits translation (Kahvejian *et al*, 2001; Khaleghpour *et al*, 2001; Derry *et al*, 2006). Clearly, GW182 proteins are likely to act like Paip2 and interfere with PABPC1 function in translation and/or mRNA stabilization. So, how do GW182

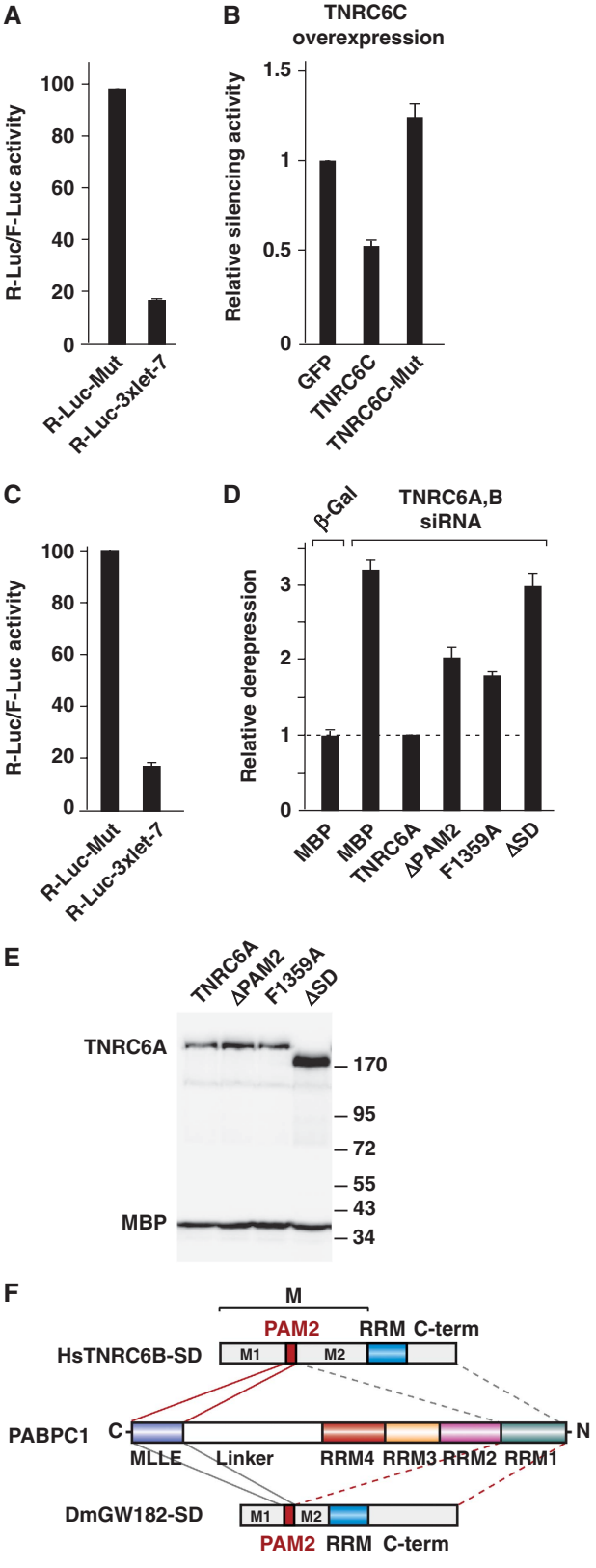

Figure 9 The interaction of TNRC6s with PABPC1 contributes to silencing in human cells. (**A**, **B**) Human HeLa cells were transfected with a mixture of three plasmids: the R-Luc-3xlet-7 or the corresponding reporter lacking let-7-binding sites (R-Luc-Mut), a plasmid expressing firefly luciferase as a transfection control, and plasmids expressing GFP or the indicated GFP-tagged proteins. *Renilla* luciferase activity was normalized to that of the firefly luciferase and set to 100 in cells expressing the reporter lacking the let-7-binding sites for each condition. (**A**) Normalized *Renilla* luciferase activities in control cells (i.e. cells expressing GFP). (**B**) Relative silencing activity for each condition. Mean values ± s.d. are shown. (**C**–**E**) HeLa cells were transfected with a control β-Gal siRNA or a mixture of siRNAs targeting TNRC6A and TNRC6B. Two days later, cells were re-transfected with the same siRNAs and a mixture of three plasmids: the R-Luc-3xlet-7 or the corresponding reporter lacking let-7-binding sites (R-Luc-Mut), a plasmid expressing F-Luc as a transfection control, and plasmids expressing MBP or siRNA-resistant versions of HA-TNRC6A wild type or mutants. Cells were harvested 48 h after the second transfection. *Renilla* luciferase activity was measured and normalized to that of the F-Luc and set to 100 in cells expressing the reporter lacking the let-7-binding sites for each condition. (**C**) Normalized *Renilla* luciferase activities in control cells (i.e. cells treated with β-Gal siRNA and expressing MBP). (**D**) The relative fold derepression for each condition. Mean values ± s.d. are shown. (**E**) Protein expression levels. (**F**) Schematic diagram showing the interaction of HsTNRC6B and DmGW182 silencing domains with the N- and C-terminal domains of PABPC1. Protein domains are as described in Figure 1A. Red lines indicate the dominant interactions observed in cell lysates. Dashed lines indicate interactions observed only in cell lysates but not with recombinant proteins expressed in *E. coli*.

proteins affect PABPC1 function? One possible mechanism is that GW182 proteins prevent mRNA circularization as described previously with Paip2 (Karim *et al*, 2006). This idea is based on the observation that the SD of DmGW182 competes with eukaryotic initiation factor 4G (eIF4G) for binding to PABPC1 in cell lysates (Zekri *et al*, 2009). eIF4G interacts with the N-terminal RRMs of PABPC1; this interaction stimulates translation by enabling the mRNA to adopt a closed-loop conformation (reviewed by Kahvejian *et al*, 2001). Consequently, by interfering with PABPC1–eIF4G interaction, GW182 proteins could inhibit translation. Moreover, when an mRNA is in the open conformation, the 5′ cap and poly(A) tail could be more accessible to the mRNA decay enzymes leading to mRNA degradation.

Another mechanism by which the PABPC1–GW182 interaction could contribute to silencing is by reducing PABPC1 affinity for the poly(A) tail as described for Paip2 (Khaleghpour *et al*, 2001). This could render the poly(A) tail more accessible to deadenylases and thus indirectly interfere with mRNA circularization.

Finally, it is notable that not all proteins containing a PAM2 motif act directly on PABPC1, as shown for Paip1 and Paip2. Other proteins such as human TOB for example, just use PABPC1 as a binding platform that allows them to hook onto mRNAs using a PAM2 motif. TOB also interacts with the CAF1–CCR4–NOT mRNA deadenylase complex, and thus through its interaction with PABPC1, it can promote deadenylation of mRNAs (Ezzeddine *et al*, 2007). Analogously, it is possible that a GW182–PABPC1 complex might provide a binding platform for additional interactions required in silencing; these could include interactions with the CAF1–CCR4–NOT1 deadenylase complex. Indeed, Fabian *et al* (2009) showed that PABPC1 is required for the accelerated deadenylation of miRNA targets observed *in vitro*. Here we show that the role of GW182–PABPC1 interaction is not restricted to promoting deadenylation but rather this interaction is required for silencing independently of whether or not the target is degraded. Thus GW182–PABPC1 interaction may contribute to silencing through multiple mechanisms. Independently of the precise molecular mechanism, our findings indicate that PABPC1 has a crucial function in miRNA-mediated gene silencing in animal cells.

Materials and methods

DNA constructs

Luciferase reporters and plasmids for expression of miRNAs and epitope-tagged proteins were described before (Zekri *et al*, 2009; Eulalio *et al*, 2007, 2008, 2009b). cDNAs encoding human TNRC6A and C were cloned into the *Hin*dIII and *Xho*I site of plasmid pAc5.1-EGFP. Human TNRC6B cDNA was cloned into the *Hin*dIII and *Xba*I sites of plasmid pAc5.1-EGFP. Mutations in DmGW182, DmPABPC1 and human TNRC6A–C were generated by site-directed mutagenesis using the Quick Change mutagenesis kit from Stratagene. The protein GW182-PAM2^{6B} consist of DmGW182 protein sequences in which the PAM2 motif (residues T952–Q971) were replaced with the PAM2 motif of human TNRC6B (residues S1361–Q1380), the corresponding PAM2-motif sequences are shown in Figure 2A). In GW182-SD^{6B} protein sequences downstream of DmGW182 residue N937 were replaced with TNRC6B sequences downstream of residue S1361, which contain the PAM2 motif, the M2 and C-term regions and the RRM.

Complementation and luciferase assays in S2 cells

Complementation assays were performed as described before (Eulalio *et al*, 2008, 2009b). Transfections of S2 cells were performed in 24-well plates, using Effectene transfection reagent (Qiagen). For miRNA-mediated silencing assays, the transfection mixtures contained 0.02 μg of firefly luciferase reporter plasmid, 0.08 μg of the *Renilla* transfection control and 0.04 μg of plasmids expressing miRNA primary transcripts or the corresponding vector without insert. When indicated, 10–200 ng of plasmids expressing recombinant proteins were cotransfected. Firefly and *Renilla* luciferase activities were measured 3 days after transfection using the Dual-Luciferase Reporter Assay System (Promega). Total RNA was isolated using TriFast (Peqlab Biotechnologies) and analysed as described before (Eulalio *et al*, 2007).

Coimmunoprecipitations and western blots in S2 cells

For coimmunoprecipitation assays, S2 cells ($10–12 \times 10^6$ cells) were collected 3 days after transfection, washed with PBS and lysed in 0.5 ml of NET buffer (50 mM Tris at pH 7.4, 150 mM NaCl, 1 mM EDTA, 0.1% Triton) supplemented with protease inhibitors. Immunoprecipitations were performed as described by Zekri *et al* (2009). When indicated, cell lysates were supplemented with 2.5 mM $CaCl_2$, treated with micrococcal nuclease (NEB, M0247S) for 30 min and spun at 18 000 g for 15 min at 4°C prior to immunoprecipitation. Antibodies to AGO1 (dilution 1:1000) were purchased from Abcam (catalogue number ab5070). Endogenous GW182 and GFP-tagged proteins were detected with polyclonal antibodies raised in rabbits. V5-tagged proteins were detected with anti-V5 antibodies (Invitrogen, dilution 1:5000). All western blot experiments were developed with the ECL Western blotting detection system (GE Healthcare) as recommended by the manufacturer.

Coimmunoprecipitations and western blots in human cells

Plasmids driving the expression of full-length TNRC6A–C or the corresponding SDs in human cells were described by Lazzaretti *et al* (2009). For coimmunoprecipitation assays, HEK-293 cells were grown in 10 cm dishes and transfected using the calcium phosphate method. The transfection mixtures contained 25 μg of plasmid for expression of HA-tagged TNRC6A–C SDs. Two days after transfection, cells were washed with PBS and lysed for 15 min on ice in NET buffer supplemented with protease inhibitors and 10% glycerol (1 ml NET buffer/plate). Cell lysates were treated with RNase A for 30 min and spun at 18 000 g for 15 min at 4°C. Alternatively, cell lysates were supplemented with 2.5 mM $CaCl_2$ and treated with micrococcal nuclease for 30 min. Monoclonal anti-HA antibodies (Covance) were added to the supernatants (dilution 1:200). Samples were incubated for 1 h at 4°C. Then, 25 μl of GammaBind G Sepharose (GE Healthcare) were added and the mixtures were rotated for an additional hour at 4°C. Beads were washed three times with NET buffer. Bound proteins were eluted with 100 μl of protein sample buffer and analysed by western blotting. Endogenous PABP was detected with a polyclonal anti-PABPC1 antibody (Abcam ab21060; dilution 1:3000).

Luciferase assays in human cells

Renilla and firefly luciferase reporters were described before (Pillai *et al*, 2005; Lazzaretti *et al*, 2009). For overexpression assays, human HeLa cells were seeded in six-well plates and transfected using the calcium phosphate method. The transfection mixtures contained 0.05 μg of R-Luc-3xlet-7 reporter plasmid or the corresponding reporter carrying mutations in the let-7-binding sites (R-Luc-Mut), 0.5 μg of the pEGFP-N3-F-Luc transfection control and 3 μg of plasmids expressing GFP or GFP-protein fusions. R-Luc and F-Luc activities were measured 48 h after transfection using the Dual-Luciferase Reporter Assay System (Promega).

For complementation assays, human HeLa cells (0.25×10^6) were seeded in six-well plates in DMEM media without antibiotics (day 0). On day 1, cells were transfected with a mixture of two siRNAs targeting TNRC6A and TNRC6B, respectively (75 pmol of each) using Lipofectamine 2000 transfection reagent. Alternatively, cells were transfected with a control siRNA targeting β-Gal. On day 2, cells are reseeded in 12-well plates at 0.25×10^6 cells per well in DMEM without antibiotics. On day 3, cells are retransfected with the same mixture of siRNAs and three plasmids: one expressing the R-Luc-3xlet-7 reporter (20 ng) or the corresponding reporter carrying mutations in the let-7-binding sites (R-Luc-Mut), one expressing the transfection control (120 ng, pEGFP-N3-F-Luc); and a third plasmid (165 ng) expressing HA-tagged TNRC6A wild type or mutants or MBP. Cells were harvested 48 h after the second

transfection. The following siRNAs were used: TNRC6A 5′-GCCUAA UCUCCGUGCUCAATT-3′; TNRC6B 5′-GGCCUUGUAUUGCCAGCAA TT-3′; β-Gal 5′-CUACACAAAUCAGCGAUUUUU-3′; Dharmacon).

GST pull-down assays

To express the SDs of TNRC6B (amino acids 1361–1723) or DmGW182 (amino acids 937–1384) in *E. coli*, the corresponding cDNAs were cloned into the pGEX6P1 vector (GE healthcare), resulting in N-terminal GST fusions. Deletions and mutations were introduced using the QuikChange mutagenesis kit (Stratagene) and the appropriate oligos. For the MBP-tagged HsPABPC1 or DmPABPC1 constructs, the corresponding cDNAs were cloned into the pETM41 vector, resulting in N-terminal fusions with MBP.

For the GST pull-down assays shown in Figure 4E, 12 g of purified GST, GST-TNRC6B SD or the corresponding ΔPAM2 mutant were added to lysates from *E. coli* cells expressing MBP-tagged HsPABPC1, MBP-DmPABPC1 or the corresponding mutants lacking the MLLE domain in a total volume of 1 ml of binding buffer (10 mM Hepes (pH 7.5), 150 mM NaCl, 2 mM $MgCl_2$, 1 mM EDTA and 1% [v/v] Triton-X100). Samples were incubated with 40 μl GST beads (50% slurry) for 1 h at 4°C. The beads were washed three times with 1 ml of binding buffer. The proteins were eluted with 40 μl of sample buffer (50 mM Tris–HCl (pH 6.8), 2% SDS, 10% (v/v) gylcerol, 100 mM DTT and 0.05% bromophenol blue) and analysed on a 10% SDS–PAGE.

For the GST pull-down assays shown in Figure 5, lysates from *E. coli* cells expressing GST, GST-TNRC6B-SD, GST-DmGW182-SD or the indicated deletion mutants, were incubated with 40 μl GST beads (50% slurry) in lysis buffer (10 mM Hepes (pH 7.5), 300 mM NaCl, 5 mM $MgCl_2$ and 1 mM DTT) for 1 h at 4°C. The beads were washed three times with 1 ml of lysis buffer. The pre-coated beads were then incubated with ∼25 μg of recombinant MBP-HsPABPC1 or MBP-DmPABPC1 in a total volume of 1 ml of binding buffer (see above) for 1 h at 4°C. The beads were washed three times with 1 ml of binding buffer. Proteins were eluted with 40 μl of sample buffer and separated on a 10% SDS–PAGE.

Supplementary data

Supplementary data are available at *The EMBO Journal* Online (http://www.embojournal.org).

Acknowledgements

We are grateful to Maria Fauser and Sigrun Helms for excellent technical assistance, and to Carina Motz for providing plasmid for bacterial expression of Hs or DmPABPC1, and TNRC6C or GW182 silencing domains. We thank Witold Filipowicz for providing the R-Luc-3xlet-7 and the corresponding reporter lacking let-7-binding sites, Eduard KL Chan for the kind gift of TNRC6A cDNA, and Gunter Meister for the kind gift of TNRC6B-iso1 cDNA. This study was supported by the Max Planck Society, by grants from the Deutsche Forschungsgemeinschaft (DFG, FOR855 and the Gottfried Wilhelm Leibniz Program awarded to EI), and by the Sixth Framework Programme of the European Commission through the SIROCCO Integrated Project LSHG-CT-2006-037900.

Conflict of interest

The authors declare that they have no conflict of interest.

References

Albrecht M, Lengauer T (2004) Survey on the PABC recognition motif PAM2. *Biochem Biophys Res Commun* **316:** 129–138

Behm-Ansmant I, Rehwinkel J, Doerks T, Stark A, Bork P, Izaurralde E (2006) mRNA degradation by miRNAs and GW182 requires both CCR4:NOT deadenylase and DCP1:DCP2 decapping complexes. *Genes Dev* **20:** 1885–1898

Behm-Ansmant I, Gatfield D, Rehwinkel J, Hilgers V, Izaurralde E (2007) A conserved role for cytoplasmic poly(A)-binding protein 1 (PABPC1) in nonsense-mediated mRNA decay. *EMBO J* **26:** 1591–1601

Derry MC, Yanagiya A, Martineau Y, Sonenberg N (2006) Regulation of poly(A)-binding protein through PABP-interacting proteins. *Cold Spring Harb Symp Quant Biol* **71:** 537–543

Ding L, Han M (2007) GW182 family proteins are crucial for microRNA-mediated gene silencing. *Trends Cell Biol* **17:** 411–416

Eulalio A, Helms S, Fritzsch C, Fauser M, Izaurralde E (2009b) A C-terminal silencing domain in GW182 is essential for miRNA function. *RNA* **15:** 1067–1077

Eulalio A, Huntzinger E, Izaurralde E (2008) GW182 interaction with Argonaute is essential for miRNA-mediated translational repression and mRNA decay. *Nat Struct Mol Biol* **15:** 346–353

Eulalio A, Rehwinkel J, Stricker M, Huntzinger E, Yang SF, Doerks T, Dorner S, Bork P, Boutros M, Izaurralde E (2007) Target-specific requirements for enhancers of decapping in miRNA-mediated gene silencing. *Genes Dev* **21:** 2558–2570

Eulalio A, Tritschler F, Izaurralde E (2009a) The GW182 protein family in animal cells: new insights into domains required for miRNA mediated gene silencing. *RNA* **15:** 1433–1442

Ezzeddine N, Chang TC, Zhu W, Yamashita A, Chen CY, Zhong Z, Yamashita Y, Zheng D, Shyu AB (2007) Human TOB, an antiproliferative transcription factor, is a poly(A)-binding protein-dependent positive regulator of cytoplasmic mRNA deadenylation. *Mol Cell Biol* **27:** 7791–7801

Fabian MR, Mathonnet G, Sundermeier T, Mathys H, Zipprich JT, Svitkin YV, Rivas F, Jinek M, Wohlschlegel J, Doudna JA, Chen CY, Shyu AB, Yates III JR, Hannon GJ, Filipowicz W, Duchaine TF, Sonenberg N (2009) Mammalian miRNA RISC recruits CAF1 and PABP to affect PABP-dependent deadenylation. *Mol Cell* **35:** 868–880

Jínek M, Fabian MR, Coyle SM, Sonenberg N, Doudna JA (2010) Structural insights into the human GW182-PABC interaction in microRNA-mediated deadenylation. *Nat Struct Mol Biol* **17:** 238–240

Kahvejian A, Roy G, Sonenberg N (2001) The mRNA closed-loop model: the function of PABP and PABP-interacting proteins in mRNA translation. *Cold Spring Harb Symp Quant Biol* **66:** 293–300

Karim MM, Svitkin YV, Kahvejian A, De Crescenzo G, Costa-Mattioli M, Sonenberg N (2006) A mechanism of translational repression by competition of Paip2 with eIF4G for poly(A) binding protein (PABP) binding. *Proc Natl Acad Sci USA* **103:** 9494–9499

Khaleghpour K, Kahvejian A, De Crescenzo G, Roy G, Svitkin YV, Imataka H, O'Connor-McCourt M, Sonenberg N (2001) Dual interactions of the translational repressor Paip2 with poly(A) binding protein. *Mol Cell Biol* **21:** 5200–5213

Kozlov G, De Crescenzo G, Lim NS, Siddiqui N, Fantus D, Kahvejian A, Trempe JF, Elias D, Ekiel I, Sonenberg N, O'Connor-McCourt M, Gehring K (2004) Structural basis of ligand recognition by PABC, a highly specific peptide-binding domain found in poly(A)-binding protein and a HECT ubiquitin ligase. *EMBO J* **23:** 272–281

Kozlov G, Ménade M, Rosenauer A, Nguyen L, Gehring K (2010a) Molecular determinants of PAM2 recognition by the MLLE domain of poly(A)-binding protein. *J Mol Biol* **397:** 397–407

Kozlov G, Safaee N, Rosenauer A, Gehring K (2010b) Structural basis of binding of P-body associated protein GW182 and Ataxin-2 by the MLLE domain of poly(A)-binding protein. *J Biol Chem* **285:** 13599–13606

Lazzaretti D, Tournier I, Izaurralde E (2009) The C-terminal domains of human TNRC6A, B and C silence bound transcripts independently of the Argonaute proteins. *RNA* **15:** 1059–1066

Pillai RS, Bhattacharyya SN, Artus CG, Zoller T, Cougot N, Basyuk E, Bertrand E, Filipowicz W (2005) Inhibition of translational initiation by Let-7 MicroRNA in human cells. *Science* **309:** 1573–1576

Roy G, De Crescenzo G, Khaleghpour K, Kahvejian A, O'Connor-McCourt M, Sonenberg N (2002) Paip1 interacts with poly(A) binding protein through two independent binding motifs. *Mol Cell Biol* **22:** 3769–3782

Takimoto K, Wakiyama M, Yokoyama S (2009) Mammalian GW182 contains multiple Argonaute binding sites and functions in microRNA-mediated translational repression. *RNA* **15:** 1078–1089

Till S, Lejeune E, Thermann R, Bortfeld M, Hothorn M, Enderle D, Heinrich C, Hentze MW, Ladurner AG (2007) A conserved motif in Argonaute-interacting proteins mediates functional interactions through the Argonaute PIWI domain. *Nat Struct Mol Biol* **14:** 897–903

Tritschler F, Huntzinger E, Izaurralde E (2010) Role of GW182 proteins and PABPC1 in the miRNA pathway: a sense of déjà vu. *Nat Rev Mol Cell Biol* **11:** 379–384

Walters RW, Bradrick SS, Gromeier M (2010) Poly(A)-binding protein modulates mRNA susceptibility to cap-dependent miRNA-mediated repression. *RNA* **16:** 239–250

Zekri L, Huntzinger E, Heimstädt S, Izaurralde E (2009) The silencing domain of GW182 interacts with PABPC1 to promote translational repression and degradation of miRNA targets and is required for target release. *Mol Cell Biol* **29:** 6220–6231

Zipprich JT, Bhattacharyya S, Mathys H, Filipowicz W (2009) Importance of the C-terminal domain of the human GW182 protein TNRC6C for translational repression. *RNA* **15:** 781–793

Supplementary information

Two PABPC1-binding sites in GW182 proteins promote miRNA-mediated gene silencing

Eric Huntzinger, Joerg E. Braun, Susanne Heimstädt, Latifa Zekri and Elisa Izaurralde

Figure S1

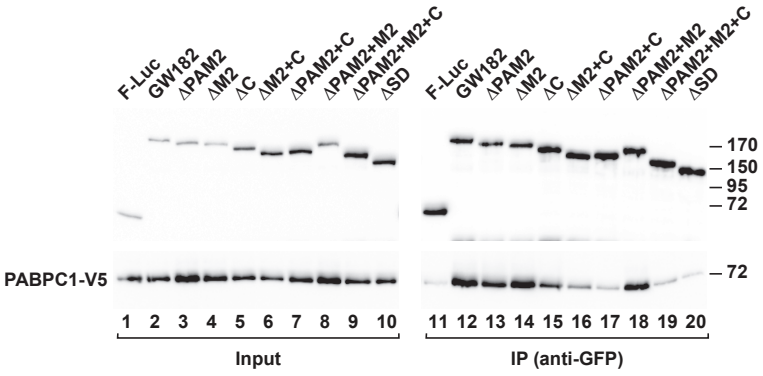

Supplementary Figure S1 GW182-PABPC1 interaction in cell lysates treated with micrococcal nuclease. S2 cells expressing GFP-DmGW182 or the indicated protein mutants together with DmPABPC1-V5 were lysed three days after transfection. Proteins were immunoprecipitated from micrococcal nuclease-treated cell lysates using a polyclonal anti-GFP antibody and analyzed by Western blotting as described in Figure 1.

Huntzinger et al. Figure S2

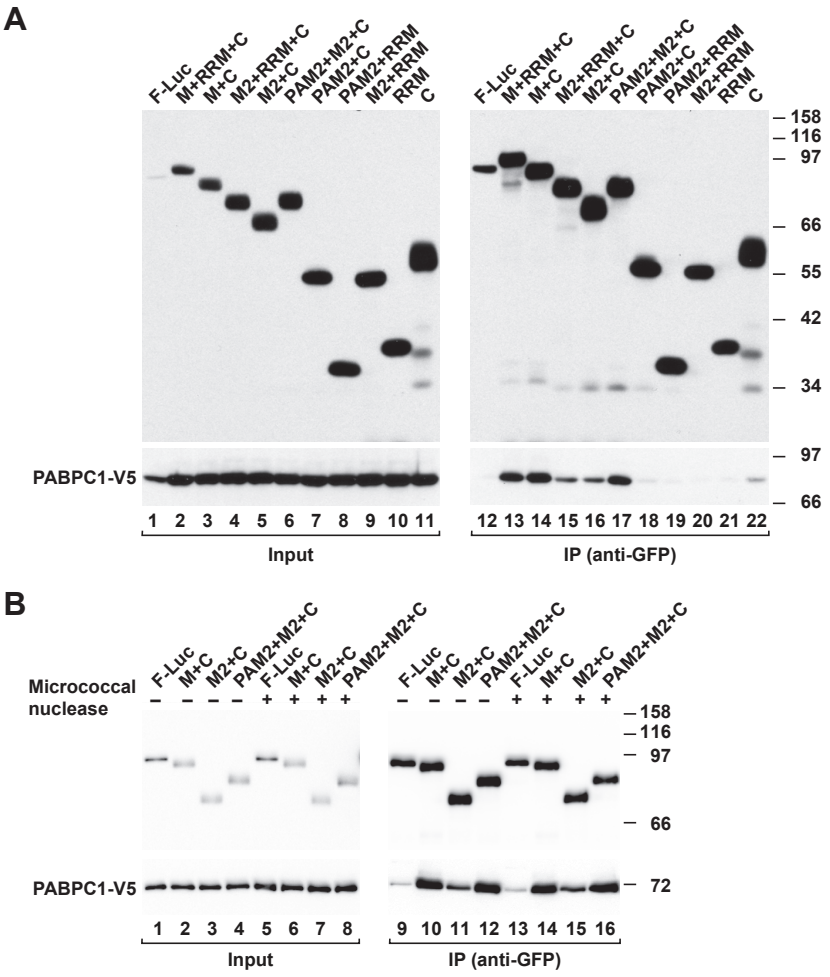

Supplementary Figure 2 The PAM2 motif of DmGW182 together with the M2 and C-term regions are sufficient for DmPABPC1 binding in cell lysates. (*A,B*) S2 cells expressing the indicated GFP-GW182 fragments together with DmPABPC1-V5 were lysed three days after transfection. Proteins were immunoprecipitated from cell lysates using a polyclonal anti-GFP antibody and analyzed by Western blotting as described in Figure 1. In panel (B), the interaction of DmGW182 fragments with DmPABPC1-V5 was analyzed in the absence or presence of micrococcal nuclease as indicated.

Huntzinger et al. Figure S3

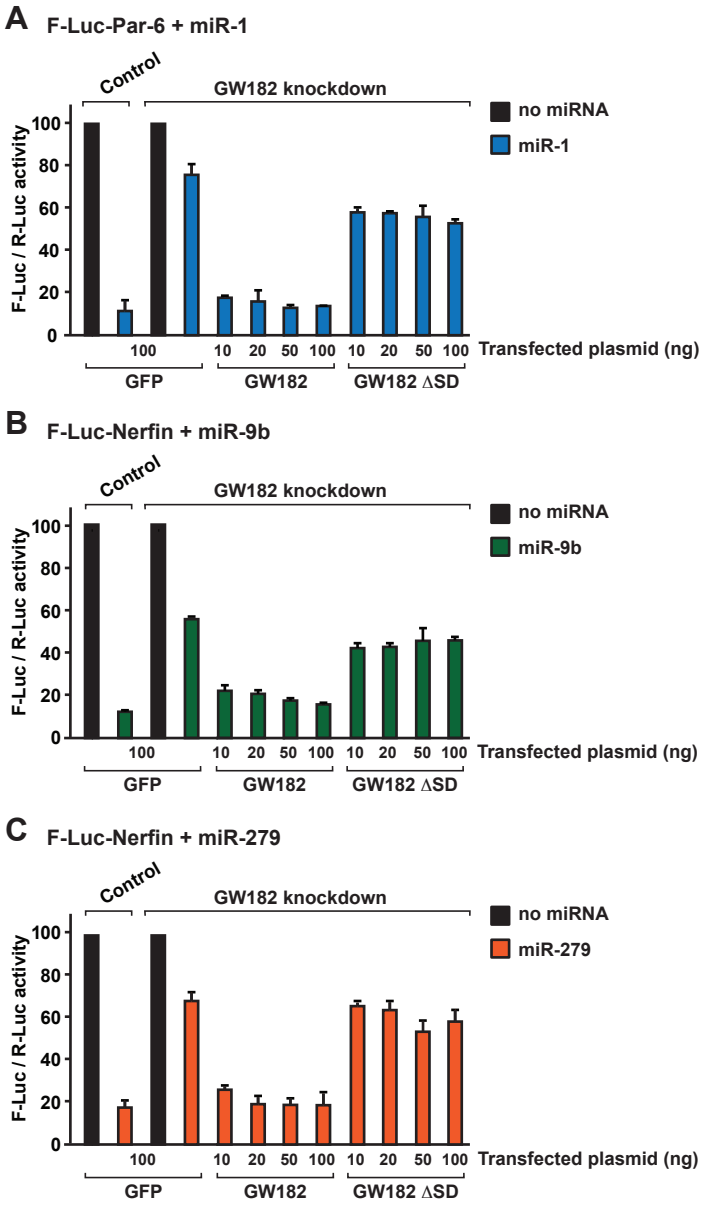

Supplementary Figure 3 Complementation assay in S2 cells. (*A*–*C*) S2 cells were treated with dsRNA targeting the coding sequence of GW182 mRNA. Control cells were treated with GST dsRNA. These cells were subsequently transfected with a mixture of three plasmids: one expressing the indicated miRNA reporters; another expressing miRNA primary transcripts or the corresponding empty vector (-); and a third expressing Renilla luciferase (R Luc). Plasmids (10–100 ng) encoding wild-type GFP-GW182 or GFP-GW182ΔSD were included in the transfection mixtures, as indicated. GFP served as a negative control. Firefly luciferase activities were normalized to those of the Renilla luciferase and set to 100 in cells transfected with the empty vector (i.e. in the absence of miRNA). Mean values ± standard deviations from three independent experiments are shown.

Huntzinger et al. Figure S4

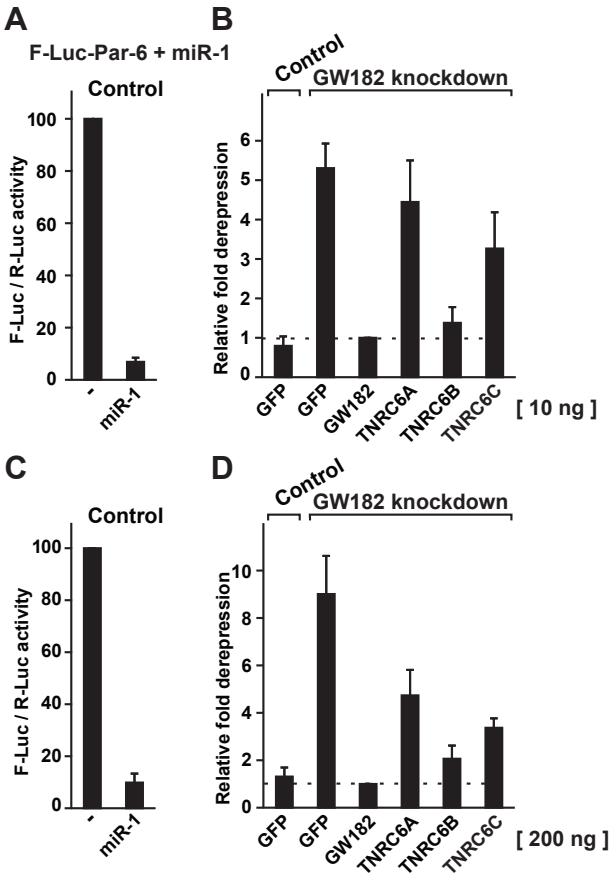

Supplementary Figure 4 Human TNRC6A–C complement silencing in S2 cells. A complementation assay as described in Figure 6 was performed using plasmids encoding wild-type GFP-GW182, GFP-TNRC6A–C or GFP and the F-Luc-Par-6 reporter. In panels (*A*) and (*B*) 10 ng of plasmids were transfected; in panels (*C*) and (*D*) 200 ng. Firefly luciferase activity was analyzed as described in Figure 6. Mean values ± standard deviations from three independent experiments are shown.

The EMBO Journal (2010) 29, 2368–2380 | © 2010 European Molecular Biology Organization | Some Rights Reserved 0261-4189/10
www.embojournal.org

THE EMBO JOURNAL

EMBO open

The C-terminal α–α superhelix of Pat is required for mRNA decapping in metazoa

Joerg E Braun[1], Felix Tritschler[1], Gabrielle Haas, Cátia Igreja, Vincent Truffault, Oliver Weichenrieder* and Elisa Izaurralde*

Department of Biochemistry, Max Planck Institute for Developmental Biology, Tübingen, Germany

Pat proteins regulate the transition of mRNAs from a state that is translationally active to one that is repressed, committing targeted mRNAs to degradation. Pat proteins contain a conserved N-terminal sequence, a proline-rich region, a Mid domain and a C-terminal domain (Pat-C). We show that Pat-C is essential for the interaction with mRNA decapping factors (i.e. DCP2, EDC4 and LSm1–7), whereas the P-rich region and Mid domain have distinct functions in modulating these interactions. DCP2 and EDC4 binding is enhanced by the P-rich region and does not require LSm1–7. LSm1–7 binding is assisted by the Mid domain and is reduced by the P-rich region. Structural analysis revealed that Pat-C folds into an α–α superhelix, exposing conserved and basic residues on one side of the domain. This conserved and basic surface is required for RNA, DCP2, EDC4 and LSm1–7 binding. The multiplicity of interactions mediated by Pat-C suggests that certain of these interactions are mutually exclusive and, therefore, that Pat proteins switch decapping partners allowing transitions between sequential steps in the mRNA decapping pathway.

The EMBO Journal (2010) **29,** 2368–2380. doi:10.1038/emboj.2010.124; Published online 11 June 2010
Subject Categories: RNA
Keywords: DCP1; DCP2; decapping; mRNA decay; P-bodies

Introduction

Decapping of bulk mRNA in eukaryotes occurs after they have been deadenylated. This order of events (deadenylation first, then decapping) ensures that functional, fully polyadenylated mRNAs are not decapped and degraded prematurely (Bail and Kiledjian, 2006; Simon *et al*, 2006; Franks and Lykke-Andersen, 2008). How decapping and deadenylation are coordinated is, however, poorly understood. The yeast protein Pat1 and its orthologs in *Drosophila melanogaster* (HPat) and humans (PatL1) are conserved decapping activators that likely mediate this coordination by interacting both with components of the CAF1-CCR4-NOT1 deadenylase complex and with decapping factors (e.g. the DEAD-box protein Me31B, the decapping enzyme DCP2 and the LSm1–7 ring; Hatfield *et al*, 1996; Bonnerot *et al*, 2000; Bouveret *et al*, 2000; Tharun *et al*, 2000; He and Parker, 2001; Tharun and Parker, 2001; Chowdhury *et al*, 2007; Chowdhury and Tharun, 2008, 2009; Tharun, 2009; Haas *et al*, 2010).

Pat proteins are characterized by a conserved N-terminal sequence of about 50 residues (N-term) followed by a proline-rich region (P-rich), a middle (Mid) domain, and a C-terminal domain termed Pat-C (Figure 1A). Studies in *D. melanogaster* showed that the HPat N-term sequence confers binding to the DEAD-box protein Me31B (*Saccharomyces cerevisiae* Dhh1 and human DDX6/RCK), whereas the Mid domain is necessary and sufficient for LSm1–7 binding (Haas *et al*, 2010). Despite conservation, the N-term sequence is not required to restore decapping in cells depleted of endogenous HPat (Haas *et al*, 2010). In contrast, the P-rich region together with the Mid domain and Pat-C are all required to restore decapping in complementation assays (Haas *et al*, 2010). A somewhat different picture has emerged from studies in *S. cerevisiae* where only the Mid domain was shown to be essential for Pat1 function *in vivo* (Pilkington and Parker, 2008). These differences raise important and unresolved questions: what are the functions of the Pat protein domains in decapping and to what extent are these functions conserved?

In this study, we characterized PatL1, the human ortholog of the Pat protein family. We found that PatL1 interacts with DDX6/RCK, DCP2, EDC4 and the LSm1–7 ring. With the exception of DDX6, these interactions require Pat-C. Moreover, Pat-C is also critical for PatL1 to accumulate in P-bodies and to be incorporated into active decapping complexes. To shed light on the molecular basis for Pat-C functions, we determined the Pat-C three-dimensional structure at 3.1 Å resolution. Pat-C adopts an α–α superhelical fold related to armadillo- and huntigton-elongation-A-subunit-TOR (HEAT)-repeat proteins. Using structure-based mutagenesis, we show that both a basic surface patch and a partially overlapping surface composed of highly conserved residues have a critical function in the interaction with DCP2, EDC4 and the LSm1–7 ring. We further show that the conserved surface of Pat-C is also essential for LSm1–7 binding in *D. melanogaster*. Accordingly, a *D. melanogaster* HPat protein carrying mutations in the conserved Pat-C surface cannot rescue decapping in cells depleted of endogenous HPat. Our results provide structural insight into Pat proteins and show

*Corresponding authors. O Weichenrieder or E Izaurralde, Department of Biochemistry, Max Planck Institute for Developmental Biology, Spemannstrasse 35, 72076 Tübingen, Germany.
Tel.: +49 7071 601 1350; Fax: +49 7071 609 1353
E-mails: oliver.weichenrieder@tuebingen.mpg.de or elisa.izaurralde@tuebingen.mpg.de
[1]These authors contributed equally to this work

Received: 8 April 2010; accepted: 14 May 2010; published online: 11 June 2010

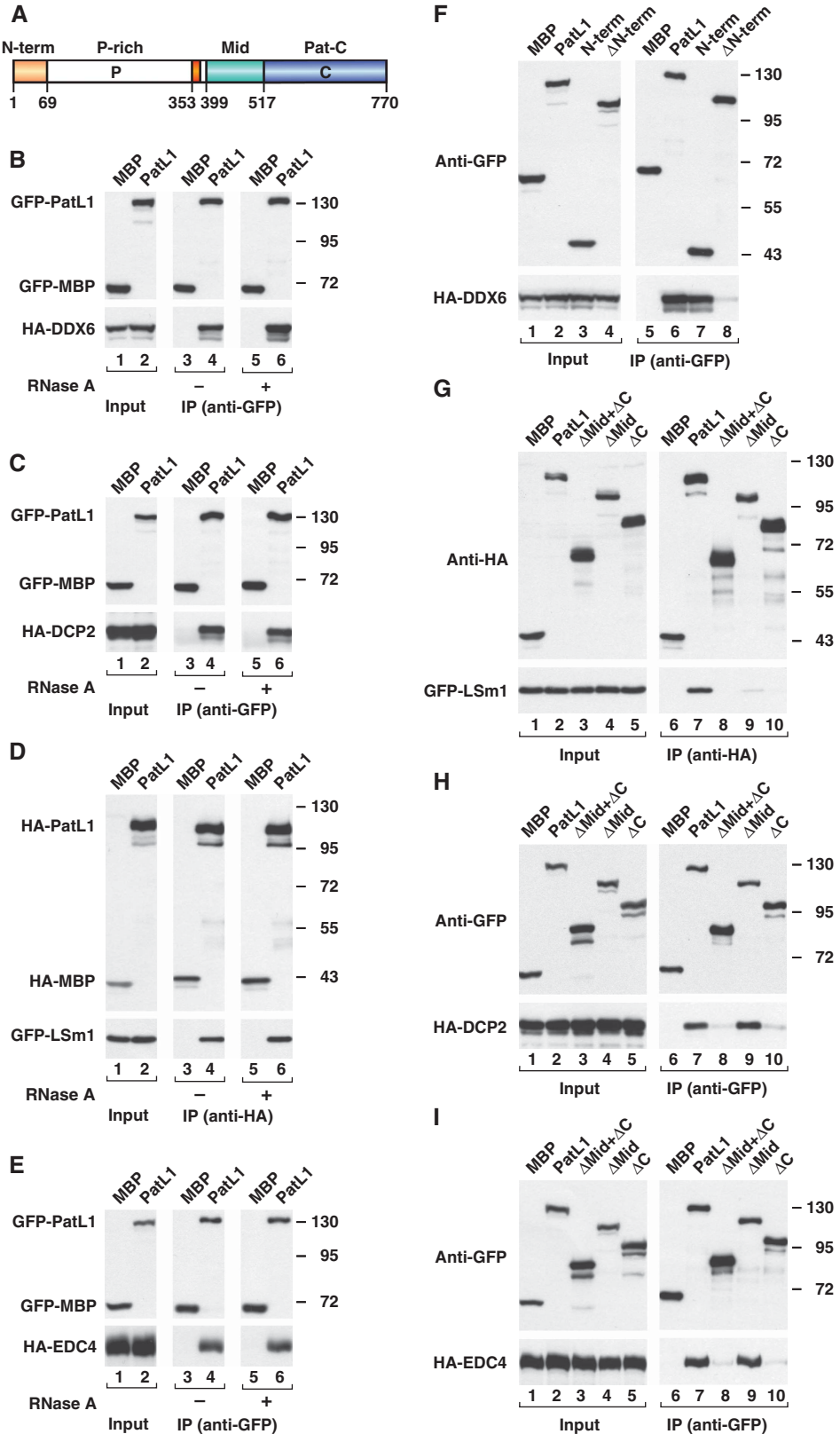

Figure 1 PatL1 coimmunoprecipitates DDX6/RCK, LSm1, DCP2 and EDC4. (**A**) Pat proteins contain a conserved N-term sequence, a P-rich region, a Mid domain and Pat-C. Amino-acid positions at fragment boundaries are indicated for human PatL1. Red box: conserved sequence motif in the P-rich region. (**B–I**) GFP- and HA-tagged proteins were coexpressed in human cells as indicated. Cell lysates were immunoprecipitated using anti-GFP or anti-HA antibodies. GFP- or HA-tagged maltose binding protein (MBP) served as a negative control. In lanes 5–6 of (**B–E**), cell lysates were treated with RNase A before immunoprecipitation. Inputs and immunoprecipitates were analysed by western blotting using anti-GFP and anti-HA antibodies.

that Pat-C has an unprecedented and essential function in mRNA decapping.

Results

PatL1 interacts with DDX6/RCK, DCP2, EDC4 and the LSm1–7 ring

To investigate the function of PatL1 in decapping, we first examined its association with decapping activators in human embryonic kidney 293 cells (HEK293 cells). We observed that epitope-tagged PatL1 coimmunoprecipitated DDX6/RCK, DCP2, LSm1 and EDC4. These interactions were all insensitive to RNase A treatment (Figure 1B–E). Together with earlier studies, these results indicate that Pat proteins establish conserved interactions with DDX6/RCK, DCP2 and the LSm1–7 ring, as these interactions are observed for the orthologous proteins in human, *D. melanogaster*, and *S. cerevisiae* cells (Figure 1B–D; Bonnerot *et al*, 2000; Bouveret *et al*, 2000; Fromont-Racine *et al*, 2000; Tharun *et al*, 2000; Coller *et al*, 2001; Tharun and Parker, 2001; Fischer and Weis, 2002; Haas *et al*, 2010). In contrast, an interaction between Pat proteins and EDC4 has not been reported earlier. This interaction may only occur in metazoa, because there is no EDC4 ortholog in yeast.

Pat-C is the only structured domain in Pat proteins

Pat proteins contain a conserved N-term sequence, the P-rich region, the Mid domain and Pat-C (Figure 1A). Secondary structure predictions suggest that PatL1 residues 1–398 (spanning the N-term sequence and the P-rich region) do not contain a folded protein domain, consistent with the very high content of proline residues (16.4%) and the low level of sequence conservation in the P-rich region.

The two remaining domains (Mid: residues 399–516, and Pat-C: residues 517–770) are well conserved and predicted to be mainly α-helical (Supplementary Figure S1). Using multi-angle static laser-light scattering coupled with size-exclusion chromatography, we found that purified recombinant Pat-C is monomeric in solution (Supplementary Table S1) and elutes as expected for a well behaved, globular protein domain of the respective mass (29 kDa; Supplementary Table S1). A protein fragment containing the Mid domain and Pat-C (residues 399–770) was also monomeric in solution, but eluted much earlier than expected for a globular protein (apparent molecular mass of 75 kDa as opposed to the expected value of 42 kDa (Supplementary Table S1)). These results suggest the Mid domain is unstructured in this context. Accordingly, even if the Mid domain was N-terminally extended to include a conserved motif between residues 353 and 370 (Figure 1A, red box), it did not assume any secondary structure in solution, as determined by NMR analysis (Supplementary Figure S2). Although these results do not rule out the possibility that the Mid domain adopts the predicted secondary structure only when bound to a protein partner, they clearly indicate that Pat-C is the only domain in PatL1 that folds independently as ultimately shown through crystal structure analysis (see below).

PatL1 N-terminal sequence confers binding to DDX6/RCK

In earlier studies, we showed that the N-term sequence of *D. melanogaster* HPat confers binding to Me31B (Haas *et al*, 2010). Accordingly, for human PatL1 the conserved N-term sequence was necessary and sufficient for the interaction with DDX6/RCK (Figure 1F). Two observations support this conclusion: (1) deleting the N-term sequence abolished PatL1 interaction with DDX6/RCK (Figure 1F, lane 8) and (2) when fused to GFP, the N-term sequence alone coimmunoprecipitated DDX6/RCK as efficiently as full-length PatL1 (Figure 1F, lane 7). Thus for PatL1, the ability to bind DDX6/RCK is solely embedded in the conserved N-term sequence.

Pat-C is required for binding to DCP2, EDC4 and the LSm1–7 ring

Next, we investigated which domains of PatL1 are required for the interaction with DCP2, EDC4 and the LSm1–7 ring. We observed that PatL1 interaction with LSm1 required both the Mid domain and Pat-C (Figure 1G). Indeed, deleting these domains either individually or in combination abolished LSm1 binding (Figure 1G, lanes 8–10). In contrast, only Pat-C, but not the Mid domain, was required for PatL1 to interact with DCP2 and EDC4 (Figure 1H and I, lanes 9 and 10). An important implication from these results is that DCP2 and EDC4 interact with PatL1 independently of the LSm1–7 ring. Indeed, a PatL1 mutant lacking the Mid domain (ΔMid) no longer interacts with the LSm1–7 ring but retains the ability to associate with DCP2 and EDC4 (Figure 1G–I, lane 9). Furthermore, PatL1 interaction with LSm1, DCP2 or EDC4 was not affected by deleting the N-term sequence (Supplementary Figure S3A–C), indicating that these proteins associate with PatL1 independently of DDX6/RCK. Of note, DCP2 and EDC4 interact with each other (Fenger-Grøn *et al*, 2005; Jínek *et al*, 2008), and may associate with PatL1 as a complex.

The Pat-C and P-rich regions cooperate to bind DCP2 and EDC4

To gain a precise understanding of the sequences in PatL1 important for DCP2 and EDC4 binding, we performed coimmunoprecipitation assays with several PatL1 fragments. As mentioned above, a PatL1 fragment containing the P-rich region, the Mid domain and Pat-C (PatL1-ΔN-term) behaved similar to wild type in binding DCP2 and EDC4 (Supplementary Figure S3A and B). In contrast, without the P-rich region, the Mid domain and Pat-C showed lower affinity to EDC4 and did not bind DCP2 (Figure 2A and B, lane 10). Thus, in addition to Pat-C, the P-rich region is also required for binding EDC4 and DCP2. Accordingly, a protein fragment containing the P-rich region and Pat-C was sufficient for binding to EDC4 and DCP2 (Figure 2A and B, lane 9). These results provide further evidence that EDC4 and DCP2 binding does not require the Mid domain; and thus, this interaction occurs independently of the LSm1–7 ring.

The Mid domain and Pat-C form a bipartite LSm1-binding site

As shown in Figure 1G, deleting Pat-C abrogates LSm1 binding. This result contrasts with earlier studies showing that the Mid domain is sufficient for LSm1 binding both in *S. cerevisiae* and *D. melanogaster* cells (Pilkington and Parker, 2008; Haas *et al*, 2010). Therefore, we investigated further, for the human protein, the contribution of the Mid domain and Pat-C in LSm1 binding. This analysis revealed two unexpected findings: (1) Pat-C, but not the Mid domain, was sufficient for LSm1 binding; although binding was reduced

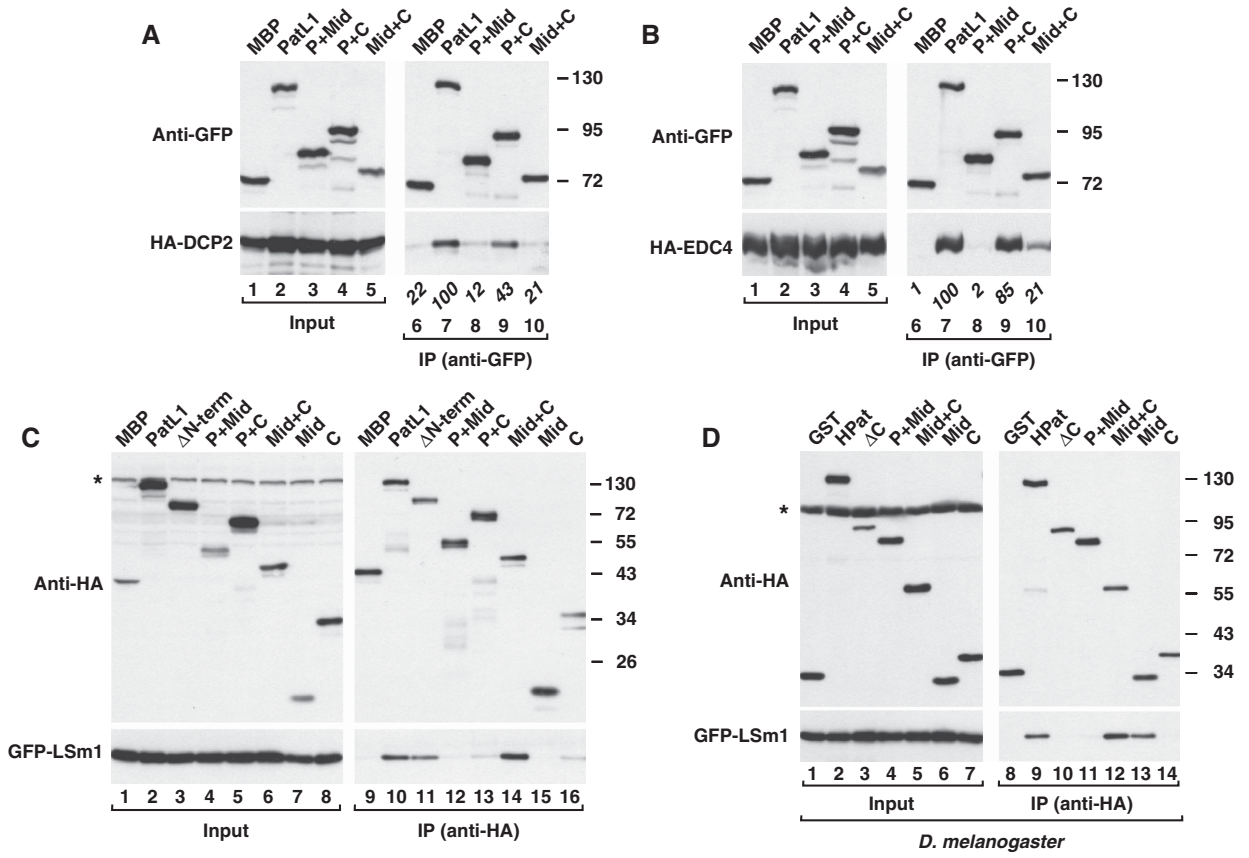

Figure 2 Pat-C is required for binding to DCP2, EDC4 and LSm1–7. (**A–C**) GFP- and HA-tagged proteins were coexpressed in human cells as indicated. Cell lysates were immunoprecipitated using anti-GFP or anti-HA antibodies and analysed as described in Figure 1. Numbers in italics below the lanes in (**A**, **B**) represent coimmunoprecipitation efficiencies relative to wild-type PatL1. Values take into account differences in protein expression levels in the inputs and the relative amount of PatL1 proteins in the immunoprecipitates. (**D**) HA-tagged wild-type HPat and fragments were expressed in *D. melanogaster* S2 cells together with GFP-LSm1. Cell lysates were immunoprecipitated using anti-HA antibodies. Asterisks indicate cross-reactivity of the primary antibodies with an endogenous protein (input panels).

relative to the wild type (Figure 2C, lane 16 versus 10) and (2) in several independent experiments, a fragment containing the Mid domain and Pat-C coimmunoprecipitated LSm1 more efficiently than wild-type PatL1 or PatL1-ΔN-term (Figure 2C, lane 14; Supplementary Figure S3C); these findings suggest that Pat-C and the Mid region cooperate to provide a high-affinity binding site for LSm1. Furthermore, PatL1 must contain sequences that interfere with LSm1 binding because the wild-type protein binds LSm1 less efficiently than a fragment containing the Mid domain and Pat-C. These interfering sequences are located in the P-rich region, because a PatL1 mutant lacking the N-term sequence also showed reduced LSm1 binding (Figure 2C, lane 11). We conclude that the Mid domain and Pat-C provide a bipartite binding site for LSm1–7, and that the P-rich region interferes with this binding.

The P-rich region interferes with LSm1 binding in D. melanogaster

The observations described above prompted us to re-investigate the interaction between HPat and LSm1 in *D. melanogaster*, where we previously showed that the Mid domain was sufficient for LSm1 binding (Haas *et al*, 2010). As reported before (Haas *et al*, 2010), we confirmed that the Mid domain alone, but not Pat-C, was sufficient for LSm1 binding (Figure 2D, lane 13 versus 14). When the Mid domain was fused to Pat-C, the affinity for LSm1 increased slightly, suggesting that Pat-C contributes to the interaction (Figure 2D, lane 12). In contrast, in mutants lacking Pat-C, but containing the Mid domain and the P-rich region, the interaction with LSm1 was abolished (ΔC and P + Mid; Figure 2D, lanes 10 and 11). We conclude that in *D. melanogaster* HPat, the Mid region confers binding to the LSm1–7 ring. This binding is enhanced by Pat-C and inhibited by the P-rich region. The interfering effect of the P-rich region is only observed in the absence of Pat-C, suggesting that Pat-C counteracts the negative effect of the P-rich region. As described above, the negative effect of the P-rich region is less pronounced for human PatL1, most likely because the major LSm1–7-binding site is provided by Pat-C and not by the Mid domain.

Pat-C is required for PatL1 incorporation into active decapping complexes

To investigate which domains of PatL1 are required for the assembly of active decapping complexes, we performed decapping assays *in vitro*. To this end, we immunoprecipitated GFP-PatL1 (wild-type or deletion mutants) from HEK293 cells and, using an m^7G-capped RNA substrate, tested for decapping activity. Immunoprecipitated GFP-PatL1 exhibited decapping activity (Figure 3A, lane 4), whereas a PatL1 mutant lacking the Mid and Pat-C domains did not copurify with decapping activity (Figure 3A, lane 5).

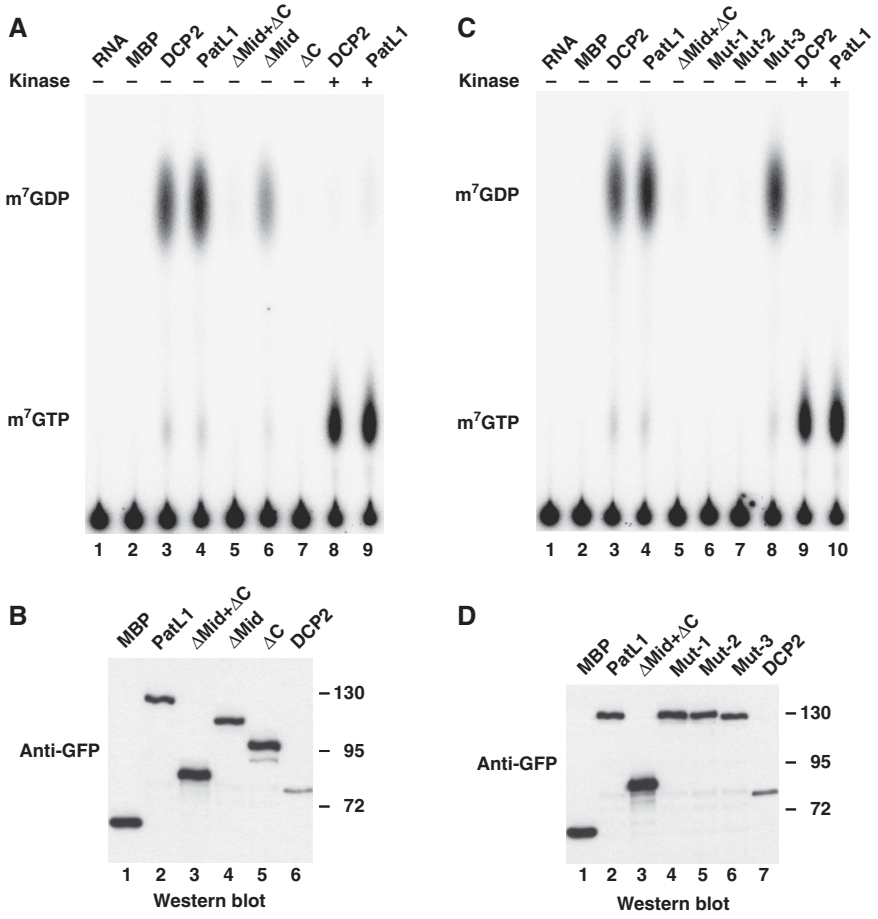

Figure 3 Pat-C is required for PatL1 incorporation into active decapping complexes. (**A**–**D**) GFP-tagged proteins were expressed in human cells. Cell lysates were immunoprecipitated using anti-GFP antibodies. The immunoprecipitates were tested for decapping activity using *in vitro* synthesized ^{32}P-labelled capped mRNA. Samples corresponding to (**A**, **C**) were analysed by western blotting in (**B**, **D**), respectively, to ensure that equivalent amounts of proteins were present in the decapping assay.

Thus, the Mid domain and Pat-C enable PatL1 incorporation into active decapping complexes.

The decapping activity coimmunoprecipitating with PatL1 likely comes from the associated DCP2 (as a positive control, compare an immunoprecipitation of GFP-DCP2; Figure 3A, lane 3). Two observations support this conclusion: (1) if we added nucleotide diphosphate kinase to the decapping reactions containing either PatL1 or DCP2, then the m^{7}GDP product was converted to m^{7}GTP (Figure 3A, lanes 8 and 9; van Dijk *et al*, 2002; Fenger-Grøn *et al*, 2005) and (2) a PatL1 mutant lacking Pat-C, which does not interact with DCP2, did not copurify with decapping activity (Figure 3A, lane 7). In contrast, a mutant carrying a deletion of the Mid domain, which interacts with DCP2 but not with the LSm1–7 ring, was impaired but could still coimmunoprecipitate decapping activity (Figure 3A, lane 6). The amounts of PatL1 mutants in the decapping assay were comparable to those of wild type (Figure 3B). Thus, Pat-C is required for PatL1 association with active decapping complexes.

Pat-C is required for P-body localization

S. cerevisiae Pat1 and its orthologs in metazoa localize to P-bodies and are required for P-body integrity (Scheller *et al*, 2007; Eulalio *et al*, 2007a; Pilkington and Parker, 2008). To define which domains are critical for human PatL1 to localize to P-bodies, we examined the subcellular localization of PatL1 fragments in human cells. GFP-PatL1 localized to endogenous P-bodies (Figure 4A) as judged by the staining with antibodies recognizing EDC4 (Kedersha and Anderson, 2007). A fragment of PatL1 comprising the N-term sequence and P-rich region dispersed throughout the cytoplasm in 96% of cells (Figure 4B). Moreover, 31% of the cells expressing this fragment showed no detectable P-bodies, indicating this protein fragment affects P-body integrity in a dominant-negative manner. In contrast, a protein fragment comprising the Mid domain and Pat-C retained the ability to localize to P-bodies (16% of cells), although much less efficiently than full-length PatL1 (Figure 4C versus 4A).

We next investigated whether the Mid domain or Pat-C are required for PatL1 to localize to P-bodies. A PatL1 mutant lacking the Mid domain was detected in P-bodies in 49% of cells (Figure 4D), suggesting the Mid domain contributes, but is not required for P-body localization. In contrast, a mutant lacking Pat-C spread throughout the cytoplasm in 96% of cells, although EDC4-contaning foci were detectable in 47% of cells (Figure 4E). Together, these results indicate that Pat-C has a critical function in promoting PatL1 accumulation in P-bodies.

Crystal structures of the human Pat-C domain

So far, our data indicate that Pat-C is required for binding to DCP2, EDC4 and LSm1–7 and also enables PatL1 to localize to P-bodies and be incorporated into active decapping complexes. To gain a more detailed understanding of these functions, we determined the crystal structure of Pat-C.

We obtained well-diffracting crystals of Pat-C (residues 517–767) and of Pat-C-Δloop (residues 517–767), where a putative loop (residues 664–673) was replaced by a Gly-Ser linker (Supplementary Figure S1B). Initially, the structure was solved using single anomalous dispersion data (2.2 Å resolution) collected at the absorption peak of a selenomethionine-substituted protein crystal of Pat-C-Δloop. The structure was automatically built starting from an excellent multiple anomalous dispersion electron density map, and was manually refined to an R_{work} of 19.9% (R_{free} = 23.2%), with two molecules per asymmetric unit (crystal form I; Supplementary Table S2; Supplementary Figure S4A).

Subsequently, this model was used in molecular replacement to solve the structure of Pat-C at 3.1 Å resolution, with four molecules per asymmetric unit in a different packing environment (R_{work} = 24.8%, R_{free} = 28.1%, crystal form II; Supplementary Table S2 and Supplementary Figure S4A). Finally, we obtained an unrelated crystal form of Pat-C-Δloop at 2.95 Å resolution (R_{work} = 24.8%, R_{free} = 29.2%, crystal form III; Supplementary Table S2). In this crystal form, two of the three molecules in the asymmetric unit apparently contain a specifically bound sulphate ion from the crystallization condition, coordinated by two arginines (Arg591 and Arg595; Supplementary Figure S4B). Sulphate ions can mimic the phosphate groups of the nucleic acid backbone and therefore indicate potential nucleic acid-binding sites (see below).

Pat-C folds into an α–α superhelix

Pat-C is composed of 13 α-helices, stacked into a superhelix with a right-handed twist. The first two helices are significantly longer than the others and form a hairpin that protrudes ~20 Å from the cylindrical core of the domain, giving Pat-C an overall L-shape (Figure 5A–C).

According to the structural classification of proteins (SCOP; Murzin *et al*, 1995), the α–α superhelix fold (SCOP classification 48370) is a feature of >20 protein superfamilies. Among those, the structure of Pat-C clusters with members of the ARM-repeat superfamily, as revealed by a search using the Dali server (Holm and Sander, 1995). The ARM-repeat superfamily includes families such as the armadillo-, HEAT- and Pumilio-repeat families. The best-scoring structural relatives of Pat-C thus include yeast Cse1 (Matsuura and Stewart, 2004), human Pumilio1 (Wang *et al*, 2002) and interestingly, the C-terminal domain of EDC4 (Jínek *et al*, 2008).

Compared with canonical armadillo-, HEAT- or Pumilio-repeat domains, however, the helical arrangement of Pat-C is

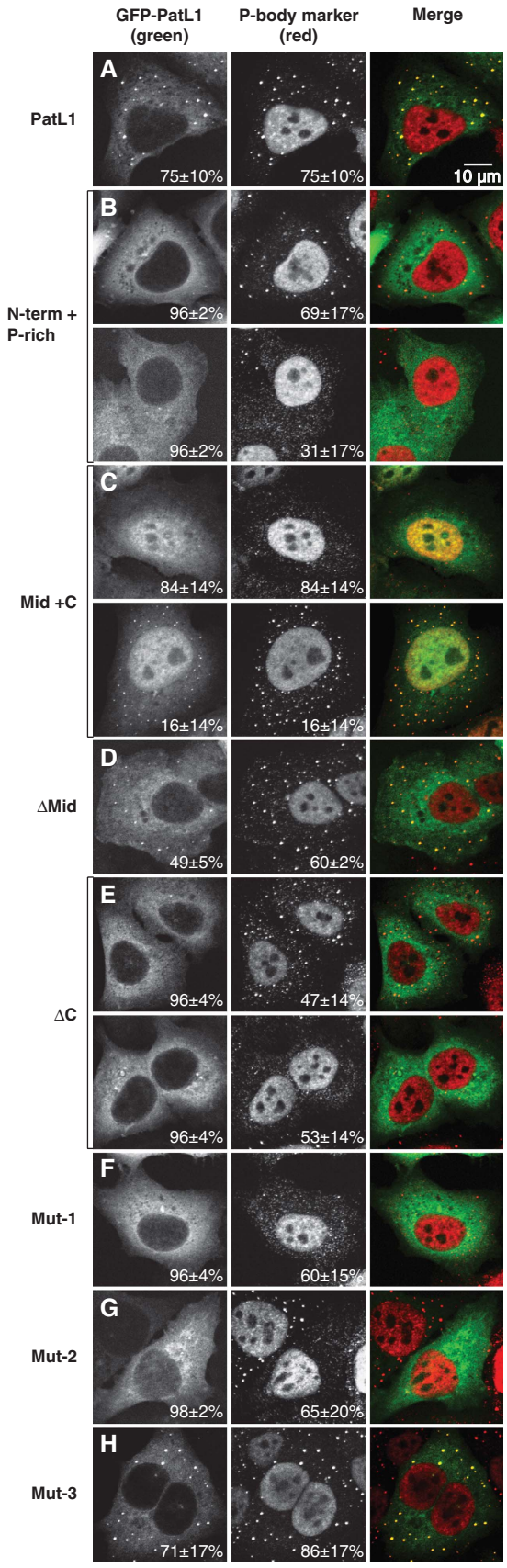

Figure 4 Pat-C is required for PatL1 accumulation in P-bodies. (**A**–**H**) Representative confocal fluorescent micrographs of fixed human HeLa cells expressing wild-type GFP-PatL1 or the mutants indicated on the left. Cells were stained with antibodies cross-reacting with EDC4 and a nuclear human antigen (Kedersha and Anderson, 2007). The merged images show the GFP signal in green and the EDC4 signal in red. The fraction of cells exhibiting a staining identical to that shown in the representative panel was determined by scoring at least 100 cells in each of the three independent transfections performed per protein. Scale bar: 10 μm.

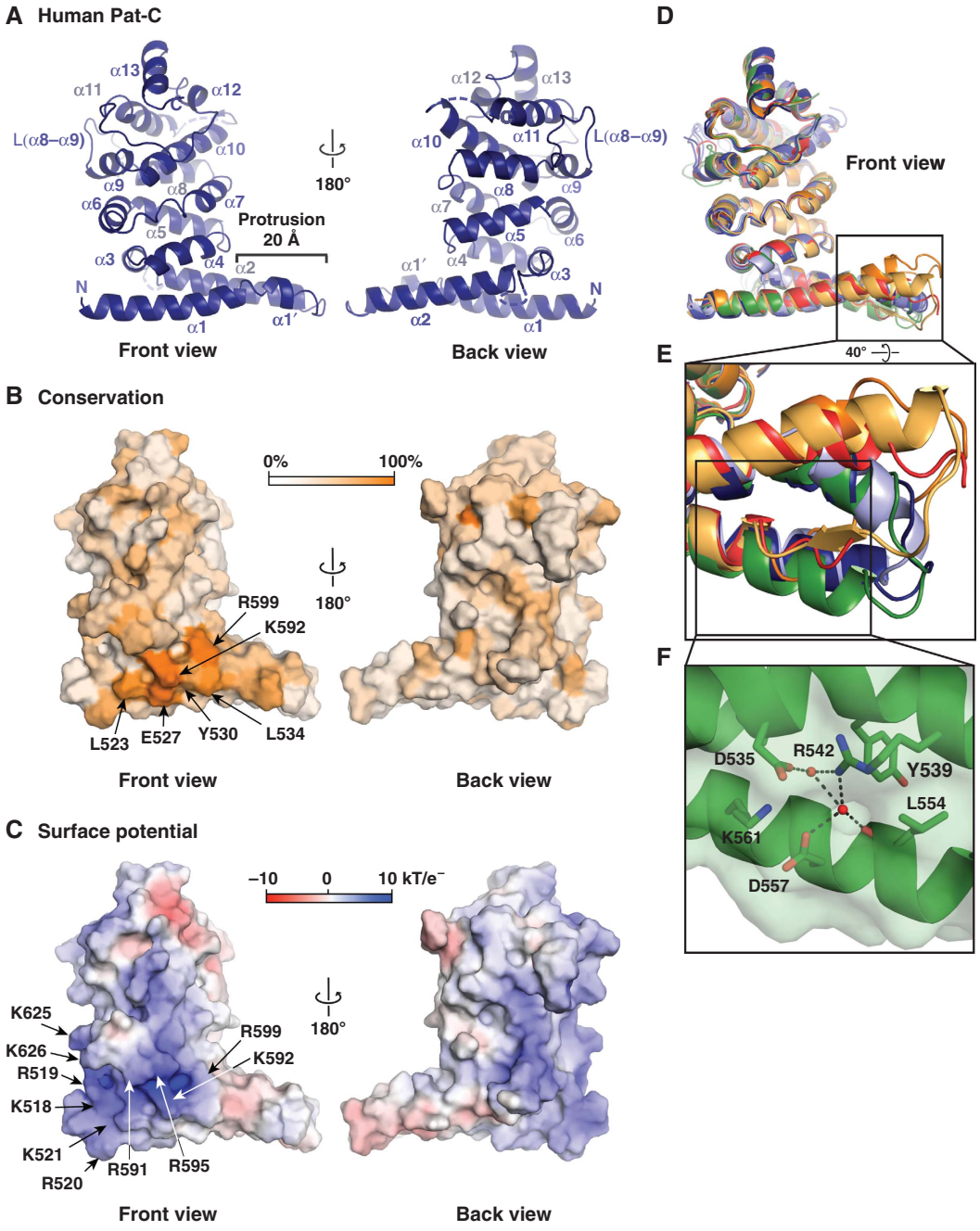

Figure 5 Structure of human Pat-C (Form II, chain A). (**A**) Ribbon diagram in two orientations related by a 180° rotation along a vertical axis. Loop L(α8–α9) is replaced by a Gly-Ser linker in Pat-C-Δ-loop construct. Structural representations were generated using Pymol (http://www.pymol.org). (**B**) Surface representation, coloured by sequence conservation, comparing six species (Supplementary Figure S2B). Colour ramp by identity: orange (100%) to white (0%). Highly conserved solvent exposed residues are labelled. (**C**) Electrostatic potentials are mapped onto the molecular surface of Pat-C and contoured from −10 kT/e$^-$ (red) to 10 kT/e$^-$ (blue). Residues contributing to the positively charged surface patch are labelled. (**D**) Ribbon representation of six Pat-C molecules resulting from the three independent crystal forms. Green (Form I, chain A), dark blue (Form II, chain A), light blue (Form II, chain B), orange (Form III, chain A), red (Form III, chain B), yellow (Form III, chain C). (**E**) Close-up view (40° rotated along a horizontal axis) on the helical protrusion of the six structurally most divergent Pat-C molecules. Colours are as in (**D**). (**F**) Close-up on Form I, chain A, showing two water molecules buried in the helical protrusion. Residues adjacent to the buried water molecules are labelled and shown as sticks with carbons in green, nitrogens in blue and oxygens in red. Hydrogen bonds are shown as dashed lines.

quite irregular and structural alignments of >100 residues consistently yielded C_α root mean square deviations (r.m.s.d.) higher than 2.9 Å. Only the first nine helices (α1–α9) may be classified as ARM-like repeats of three helices each. Furthermore, Pat-C contains three large, partially ordered or disordered loops that cluster on one face of the molecule. These loops are located between helices α2 and α3 (L(α2–α3)), α8 and α9 (L(α8–α9)) and α10 and α11 (L(α10–α11); Figure 5A, back view; and Supplementary Figure S4A).

Aligning the Pat-C sequence across different species shows that key surface and structural residues are highly conserved.

This suggests that Pat-C adopts very similar fold with related functions in all members of the Pat protein family (Supplementary Figure S1B).

The helical protrusion of Pat-C exhibits structural flexibility

The three crystal forms of Pat-C provide nine independent structures, in distinct molecular packing environments. These nine structures superimpose well over the cylindrical core of the domain with an r.m.s.d. of 0.58 Å (excluding loops (L(α2–α3), L(α8–α9) and L(α10–α11); Figure 5D). The helical protrusion, however, displays significant structural variability, especially near the tip of the hairpin (residues 539–557; Figure 5D). The most extreme deviations are found in the structures of crystal form III, with the distal parts of helix α2 (residues 550–558) being melted into an ordered loop (Figure 5E, orange chain), or into an ordered loop with a short β-strand (yellow), or into an entirely disordered loop (red). One reason for this structural variability is likely the hydrophilic nature of residues D535, R542 and D557. Although being exposed to solvent in crystal form III, they are also able to mediate close helix packing in crystal form I, through two deeply buried water molecules (Figure 5F). The structural variability of the helical protrusion suggests a significant flexibility, which might be of functional importance.

A basic surface on Pat-C confers binding to RNA

Proteins with an α–α superhelical fold frequently provide scaffolds for protein or nucleic acid interactions (Huber *et al*, 1997; Edwards *et al*, 2001). In addition to be required for protein–protein interactions, the Pat-C domain of yeast Pat1 shows affinity for RNA (Pilkington and Parker, 2008). We therefore looked for patches of conserved and/or basic residues on the surface of Pat-C that might mediate the observed interactions with decapping factors and/or with RNA. The most highly conserved surface patch on Pat-C is located near the N-terminal end of helix α1, close to the connection to the Mid domain. It shares contributions from Leu523, Glu527, Tyr530 and Leu534 on helix α1 as well as contributions from Lys592 and Arg599 on helix α4 (Figure 5B).

The conserved patch partially overlaps with a region of high positive surface potential (Figure 5C), which coordinates the sulphate ion in crystal form III (Supplementary Figure S4B) and results from a high concentration of positively charged residues (Lys518, Arg519, Arg520, Lys521 on helix α1, Arg591, Lys592, Arg595, Arg599 on helix α4 and Lys625, Lys626 on helix α6). We therefore tested whether Pat-C could bind RNA and found that it directly binds to an U_{30} RNA oligomer in size exclusion chromatography experiments (Supplementary Figure S5A).

In further experiments, we established that Pat-C exhibits RNA-binding properties similar to those reported for the purified yeast Pat1-LSm1–7 complex (Chowdhury *et al*, 2007). For instance, Pat-C interacted with oligo$(rU)_{30}$ but not with oligo$(rA)_{30}$ (Supplementary Figure S5A and F). Similarly, Chowdhury *et al* (2007) showed that yeast Pat1-LSm1–7 complex interacts with oligo(rU) but not with any other homo-oligoribonucleotide. Furthermore, Pat-C interacted with a 30-nucleotide long homo(rU)-oligomer, but failed to interact with oligomers containing 20 and 15 nucleotides (Supplementary Figure S5A–C). Similarly, a requirement that RNA be a minimum length for detectable binding was reported for the purified yeast Pat1-LSm1–7 complex (Chowdhury *et al*, 2007), suggesting that some of the RNA-binding properties of the complex can be attributed to Pat-C. Finally, Pat-C discriminated between ribo- and deoxy-oligoribonucleotides, as it did not interact with 2′-deoxy-oligo$(U)_{30}$ (Supplementary Figure S5F).

To investigate how much the Pat-C conserved and basic patches contribute to RNA and protein binding, we generated three mutants. In mutant 1 (Mut-1), six basic residues in the positively charged patch were substituted with alanines (R519, R520, R591, R595, K625 and K626; Supplementary Figure S1B). In mutant 2 (Mut-2), four residues form the conserved patch were changed into serine or alanine (L523S, E527A, Y530A and L534S; Supplementary Figure S1B). Finally, in mutant 3 (Mut-3), residues 539 to 557 were substituted with a GSGSGSG linker (Supplementary Figure S1B), thus excising the helical protrusion. When expressed, purified and analysed by size exclusion chromatography, all three Pat-C mutants showed the expected elution volumes for folded monomeric proteins of the respective size (Supplementary Table S1), indicating that the mutations do not disrupt the Pat-C fold. Importantly, Mut-1 lost the ability to bind U_{30} RNA, whereas Mut-2 was comparable to the wild-type protein (Supplementary Figure S5D and E). Together, these results indicate that the basic surface on the Pat-C domain confers the ability to bind RNA.

The conserved and basic surfaces on Pat-C are required for binding to DCP2/EDC4 and LSm1–7

We also investigated how the Pat-C conserved and basic patches contribute to the interactions with decapping factors. To this end, we introduced the mutations described above in the context of full-length PatL1 and examined the effect on DCP2, LSm1–7, and EDC4 binding, as well as on decapping and P-body localization. We found that mutations in the basic and conserved patches (Mut-1 and Mut-2) prevented PatL1 from interacting with DCP2, EDC4 and the LSm1–7 ring as efficiently as deleting the Mid and Pat-C domains (Figure 6A–C, lanes 9–11). In contrast, the mutations did not affect the interaction with DDX6/RCK, as expected (Figure 6D). Removing the helical protrusion (Mut-3) did not affect the PatL1 interaction with DCP2 and decapping activators (Figure 6A–C, lane 12).

To assess how the mutations affect PatL1 association with decapping complexes, we tested the activity of the mutants in decapping assays *in vitro*. In accordance with the results of the coimmunoprecipitation assay, Mut-1 and Mut-2 failed to copurify with decapping activity, whereas Mut-3 associated with decapping activity (Figure 3C and D). Taken together, these results show that the Pat-C conserved and basic patches are crucial for the interaction with DCP2, EDC4 and the LSm1–7 ring.

We next tested the ability of PatL1 mutants to localize to P-bodies. We observed that Mut-1 and Mut-2 were dispersed throughout the cytoplasm in about 90% of cells (Figure 4F and G), whereas Mut-3 accumulates in foci (Figure 4H). Furthermore, in about 60% of cells expressing Mut-1 or Mut-2, endogenous P-bodies were dispersed (Figure 4F and G), indicating that these mutants inhibit P-body formation in a dominant-negative manner.

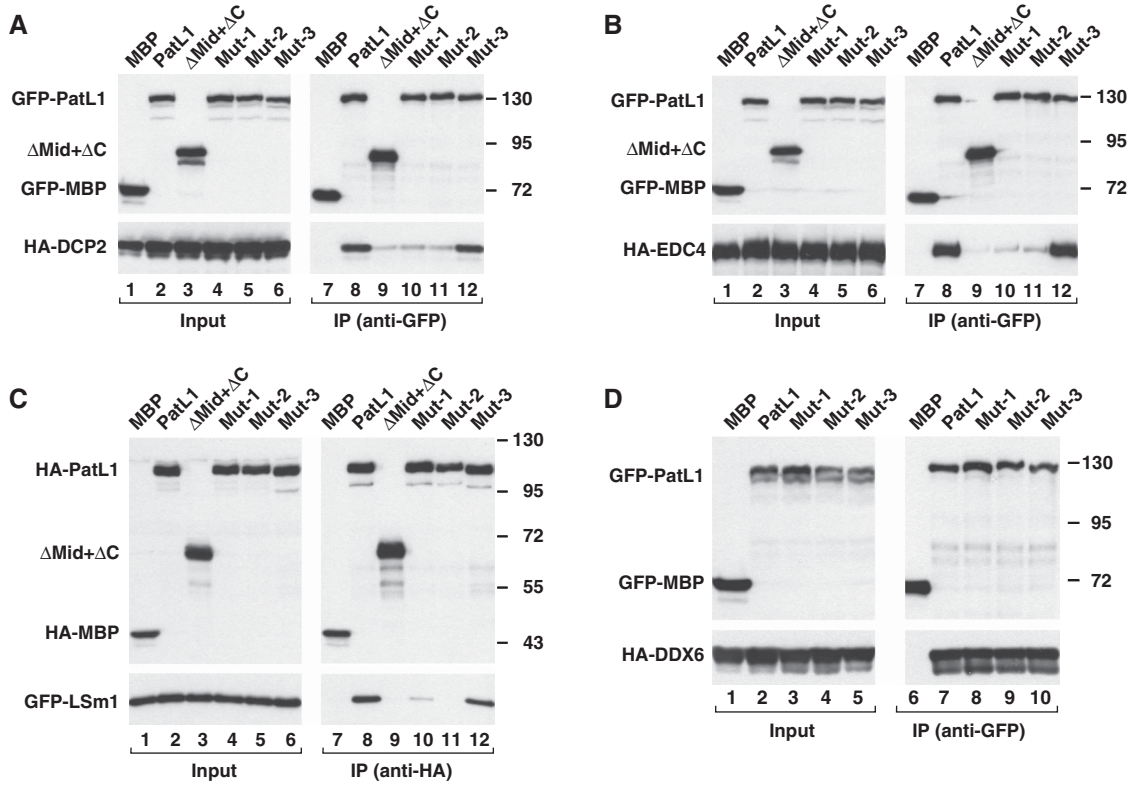

Figure 6 A basic and conserved surface on Pat-C enables PatL1 to interact with DCP2, EDC4 and the LSm1–7 ring. (**A**–**D**) GFP- and HA-tagged proteins were coexpressed in human cells as indicated. Cell lysates were immunoprecipitated using anti-GFP or anti-HA antibodies and analysed as described in Figure 1.

The Pat-C conserved surface is required for mRNA decapping in vivo

To investigate how the Pat-C conserved surface influences decapping *in vivo*, we took advantage of a complementation assay established in *D. melanogaster* S2 cells (Haas *et al*, 2010). First, we mutated conserved residues in *D. melanogaster* HPat corresponding to Mut-2 in human PatL1 (Supplementary Figure S1B) and examined whether the protein could coimmunoprecipitate LSm1 in S2 cells. Similar to results obtained with human PatL1, we found that mutating the conserved residues abrogates the interaction with LSm1 as efficiently as deleting Pat-C entirely (Figure 7A). Thus, the conserved surface on Pat-C is also required for the interaction of *D. melanogaster* HPat with LSm1–7.

Next, we investigated whether HPat Mut-2 could restore decapping and mRNA degradation in cells depleted of endogenous HPat (Haas *et al*, 2010). To monitor decapping, we used the F-Luc-5BoxB reporter, which is rapidly degraded when coexpressed with a λN fusion of the GW182 protein. Indeed, λN-GW182 triggers deadenylation of the F-Luc-5BoxB reporter, after which the mRNA is decapped and then subjected to exonucleolytic digestion (Eulalio *et al*, 2007b). Inhibiting decapping prevents GW182-mediated mRNA degradation and leads to the accumulation of deadenylated mRNA decay intermediates, which exhibit a characteristically higher electrophoretic mobility than polyadenylated transcripts (Figure 7B, lane 4 versus 2; Eulalio *et al*, 2007b). Therefore, monitoring the accumulation of the deadenylated F-Luc-5BoxB mRNA can track a block in decapping.

S2 cells were transiently transfected with three plasmids: the F-Luc-5BoxB reporter; a plasmid expressing λN-GW182 or the λN-peptide; and a transfection control plasmid, encoding *Renilla* luciferase (R-Luc). In the presence of λN-GW182 we observed that, relative to cells expressing the λN-peptide alone, the levels of the F-Luc-5BoxB mRNA were reduced five-fold (Figure 7B, lane 2 versus 1 and Figure 7C). In contrast, codepleting HPat and Me31B inhibited decapping and allowed the deadenylated F-Luc-5BoxB mRNA to accumulate (Figure 7B, lane 4 and Figure 7C).

Expressing HPat wild type in depleted cells restored decapping and degradation of F-Luc-5BoxB mRNA (Figure 7B, lane 6 and Figure 7C). As reported before, the HPat mutant lacking Pat-C was defective in promoting mRNA degradation, indicating that Pat-C is required for decapping *in vivo* (Figure 7B, lane 8; Haas *et al*, 2010). Importantly, HPat Mut-2 was completely defective in restoring decapping and therefore the deadenylated mRNA was still detectable (Figure 7B, lane 10 and Figure 7C). All proteins were expressed at comparable levels (Figure 7D). We conclude that the conserved surface on Pat-C is essential for HPat to promote mRNA decapping *in vivo*.

Discussion

In this study, we determined the structure of PatL1 C-terminal domain (Pat-C), the only domain in Pat proteins that folds independently. Pat-C folds into an α–α superhelix, exposing basic and conserved residues on one side of this domain. Our functional and structural analysis of Pat-C identified several critical and distinct functions for this protein domain: (1) it

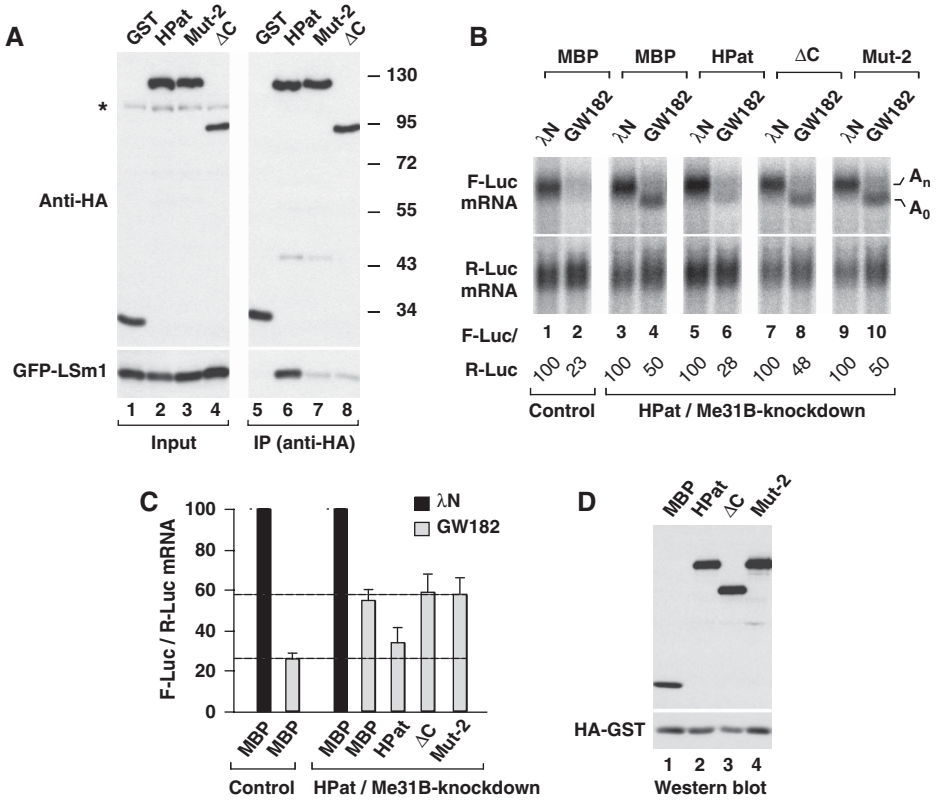

Figure 7 Pat-C is required for decapping *in vivo*. (**A**) Pat-C conserved residues are required for HPat to interact with the LSm1–7 complex. GFP- and HA-tagged proteins were coexpressed in *D. melanogaster* S2 cells as indicated. Cell lysates were immunoprecipitated using a monoclonal anti-HA antibody. HA-GST (Glutathion-S-Transferase) served as negative control. Inputs and immunoprecipitates were analysed as described in Figure 1. (**B**–**D**) Control S2 cells (treated with GFP dsRNA) or cells codepleted of HPat and Me31B were cotransfected with a mixture of three plasmids: one expressing the F-Luc-5BoxB reporter, another expressing λN-HA-GW182 or the λN-HA peptide and a third expressing *Renilla* luciferase (R-Luc). Plasmids (5 ng) expressing HA-MBP, wild-type HA-HPat, HPatΔC or Mut2 were included in the transfection mixtures, as indicated. RNA samples were analysed by northern blot. F-Luc-5BoxB mRNA levels were normalized to those of the *Renilla* luciferase. For each condition, the normalized values of F-Luc mRNA were set to 100 in the presence of the λN-HA peptide. Mean values ± s.d. for three independent experiments are shown in (**C**). (**D**) Full-length HPat and mutants were expressed at comparable levels.

mediates RNA binding through a conserved basic surface; (2) it cooperates with the P-rich region to provide a binding surface for DCP2 and EDC4; (3) it cooperates with the Mid domain to provide a high-affinity interaction with the LSm1–7 ring; (4) it is required for PatL1 to accumulate in P-bodies and (5) it is essential for mRNA decapping *in vivo*. The multiplicity of interactions mediated by Pat-C suggests that these interactions might be synergistic and antagonistic and thus may have a regulatory function as discussed below.

PatL1 interacts with DCP2 and multiple decapping activators

In this article, we show the PatL1 N-term sequence confers binding to DDX6/RCK. This interaction is conserved in *D. melanogaster* where we showed that the HPat N-term sequence also interacts with Me31B (Haas *et al*, 2010). We further show the P-rich region and Pat-C both contribute to the interaction with DCP2 and EDC4, whereas LSm1–7 binding requires the Mid domain and Pat-C (Figures 2 and 8). From our studies, we cannot conclude whether PatL1 interacts with decapping activators and DCP2 directly. Nevertheless, our results allow us to draw several conclusions. First, DCP2, EDC4 and the LSm1–7 ring interact with PatL1 independently of the conserved N-term sequence, and thus independently of DDX6/RCK. Second, EDC4 and DCP2

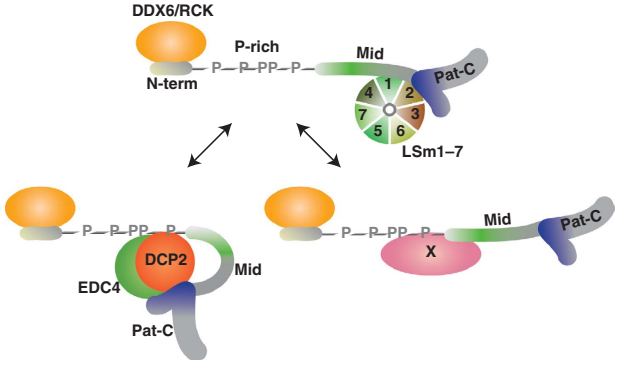

Figure 8 Model summarizing the protein interactions described in this study. PatL1 may adopt two different conformations: one with the ability to interact with LSm1–7 and the other interacting either with EDC4 and DCP2 or with an as yet unknown protein factor (X) binding to the P-rich region and blocking the accessibility of the Mid domain to the LSm1–7 ring.

interact with PatL1 independently of the LSm1–7 ring, because deleting the Mid domain abolishes LSm1–7 binding but not DCP2 or EDC4 binding. Third, LSm1–7 binding anti-correlates with the binding of EDC4/DCP2, because, if the P-rich region is fused to a protein fragment containing the

Mid domain plus Pat-C, then the affinity for LSm1–7 decreases, but binding to DCP2 and EDC4 is stimulated. Finally, binding to DCP2, EDC4 and LSm1–7 is unlikely to be entirely mediated by RNA because mutations in conserved Pat-C surface residues do not affect RNA binding but abolish the interaction with decapping factors. On the other hand, mutations in the positive Pat-C surface abolish the interaction both with RNA and with decapping factors, suggesting that RNA may contribute to the affinity of PatL1 for decapping factors.

The function of Pat-C in mRNA decapping

In this study, we show that Pat-C is required for *D. melanogaster* and human Pat proteins to interact with the LSm1–7 ring. Whether this is also true for yeast has not been directly investigated; however, indirect evidence suggests that Pat-C might also be important for LSm1 binding in yeast. Indeed, Pilkington and Parker (2008) reported that the accumulation of LSm1 in P-bodies depends on Pat1, and that LSm1 interacts with the Pat1 Mid domain. Accordingly, it is intriguing that Pat-C is necessary and sufficient to promote LSm1 accumulation in P-bodies (Pilkington and Parker, 2008). Our results provide an explanation for this, in that although the isolated Mid domain is sufficient for LSm1 binding, Pat-C is also required in the context of full-length Pat proteins and may provide a low-affinity LSm1-binding site.

Nevertheless, studies in *S. cerevisiae* indicated that for Pat1 function *in vivo* Pat-C is dispensable; whereas our studies suggest, in *D. melanogaster* and human cells, this domain is essential (Pilkington and Parker, 2008; Haas *et al*, 2010). One possible explanation for resolving the discrepancy between *S. cerevisiae* and metazoa lies in the realization that the precise composition and stoichiometry of decapping complexes differs significantly between these organisms as for example, yeast lacks an EDC4 ortholog. Thus, it is possible that for metazoa, Pat-C is essential in decapping because it interacts with EDC4 and DCP2. Yeast Pat1 interacts with DCP2 but this interaction is mediated by RNA (Tharun and Parker, 2001). The essential function of Pat-C may therefore reflect additional functions this domain acquired in metazoa.

Does Pat switch decapping partners?

An unexpected observation from our studies is that Pat-C, but not the Mid domain is sufficient for LSm1 binding in human cells, whereas in yeast and *D. melanogaster* cells, the Mid domain but not Pat-C is sufficient (Pilkington and Parker, 2008; Haas *et al*, 2010). Our hypothesis to explain these results is that Pat proteins contain two distinct LSm1-binding sites: one in the Mid domain and one in Pat-C. Human PatL1 interacts with LSm1 predominantly through Pat-C; whereas in *D. melanogaster* and *S. cerevisiae*, the interaction through the Mid domain dominates. However, for LSm1 binding, even when the interaction with the Mid domain dominates, there is a general requirement for Pat-C in the context of full-length Pat. Indeed, in addition to enhance LSm1 binding by the Mid domain, Pat-C is required to counteract a negative effect of the P-rich region. Of note, the N-terminal boundary of the Mid domain is difficult to define and this may contribute to the differences observed between species.

The requirement of Pat-C for LSm1–7 binding raises the question of whether the LSm1–7 ring competes with DCP2/EDC4 for binding to Pat-C. Two lines of evidence support this scenario: (1) as mentioned above, we observed that DCP2/EDC4- and LSm1 binding anti-correlate and (2) it is unlikely that the small conserved patch on Pat-C can bind to DCP2/EDC4 and the LSm1–7 ring simultaneously.

Competition between DCP2/EDC4 and LSm1–7 for Pat binding would also help to explain the negative effects of the P-rich region on the interaction with LSm1–7, because the P-rich region enhances the affinity of DCP2/EDC4 for PatL1. Furthermore, there may be some residual affinity of DCP2/EDC4 for the P-rich region even in the absence of Pat-C. In this case, DCP2/EDC4 could sterically mask the access of the LSm1–7 ring to the Mid domain.

Alternatively, the negative effect of the P-rich region on LSm1–7 binding could be a direct one, for example by occluding the LSm1–7 binding site on the Mid domain. However, it is difficult to conceive how two unstructured protein regions could interact with each other specifically. Consistently, we could not detect an interaction *in trans* between the P-rich region and the Mid domain. A third explanation could be that additional interacting partners bind to the P-rich region and regulate the accessibility of the Mid domain (Figure 8, factor X). Although proteins binding to the P-rich region have not yet been identified, it is likely that this region interacts with additional components of the decay machinery, because in *D. melanogaster* the P-rich region was sufficient to trigger degradation of mRNAs in tethering assays (Haas *et al*, 2010).

Regardless of precisely how the P-rich region inhibits the Mid domain from binding LSm1, our results suggest this binding could be regulated, and that Pat proteins might adopt two different conformations one with and the other without affinity for LSm1–7 (Figure 8). It remains to be established whether these conformations represent distinct complexes with specific functions or sequential steps in the assembly of active decapping complexes on target mRNAs. More generally, our findings challenge the notion that Pat proteins act as simple scaffolds for the simultaneous assembly of decapping factors and rather suggest that certain of the interactions between decapping factors may occur sequentially allowing decapping complexes to assemble in a stepwise manner.

Materials and methods

Protein expression, purification and crystallization

Human PatL1 proteins were expressed with an N-terminal His_6-tag in the *Escherichia coli* strain BL21 (DE3) or BL21 Star (DE3; Invitrogen) at 25°C overnight. After purification by an Ni^{2+}-affinity step (HiTrap Chelating HP column, GE Healthcare), the His_6-tag was cleaved with PreScission protease. The proteins were further purified by ion exchange chromatography and gel filtration (HiTrap SP HP and HiLoad 26/60 Superdex 75 columns, GE Healthcare). A detailed description of the crystallization procedures is provided in the Supplementary data.

Structure determination and refinement

Diffraction data were collected on beamline X10SA of the Swiss Light Source, Villigen, Switzerland. The structure of the human PatL1 fragment, Pat-C-Δloop (Form I), was determined from multiple-wavelength anomalous dispersion data, collected on a crystal of selenomethionine-substituted protein. For Pat-C (Form II) and Pat-C-Δloop with bound sulphate (Form III), the structures were solved by molecular replacement using Pat-C-Δloop (Form I) as search model. Additional information is provided in the Supplementary data.

DNA constructs

Plasmids for expressing DCP2, DDX6/RCK and EDC4 in human cells were described before (Tritschler *et al*, 2009a, b). Plasmids for expressing PatL1 were generated by cloning the corresponding cDNA into the pEGFP-C1 vector (Clontech) or the pλN-HA-C1 vector (Tritschler *et al*, 2009a, b). Human LSm1 was cloned between the XhoI and EcoR1 sites of the pλN-HA-C1 vector. PatL1 mutants were generated by site-directed mutagenesis using the QuickChange mutagenesis kit from Stratagene and the appropriate oligonucleotide sequences.

Coimmunoprecipitation assays, western blotting and fluorescence microscopy

For coimmunoprecipitation assays, HEK-293 cells were grown in 10 cm plates and transfected using Lipofectamine 2000 (Invitrogen). The transfection mixtures contained 7 μg of the GFP and HA constructs. For fluorescence microscopy, human HeLa cells were grown on coverslips in 24-well plates and transfected using Lipofectamine 2000 (Invitrogen). The transfection mixtures contained 0.3 μg of plasmids expressing GFP-protein fusions. Cells were collected 2 days after transfection. Coimmunoprecipitations, western blotting and fluorescence microscopy were performed as described earlier (Tritschler *et al*, 2009b). Additional information is provided in the Supplementary data.

Decapping assays

Decapping assays were performed as described earlier (Lykke-Andersen, 2002; Tritschler *et al*, 2009b), using an *in vitro* synthesized RNA (127 nucleotides). The RNA probe was labelled with [α-^{32}P]GTP using the ScriptCap m^{7}G Capping System and the ScriptCap 2′-O-Methyltransferase kit (EPICENTRE Biotechnologies). Reactions were stopped by adding up to 50 mM EDTA and analysed on PEI cellulose thin-layer chromatography plates (Merck) in 0.75 M LiCl (1 μl/sample). Unlabelled GDP, m^{7}GMP, m^{7}GDP and m^{7}GTP were used as markers.

Immunoprecipitations, RNA interference and complementation assay in D. melanogaster S2 cells

Protein coimmunoprecipitations and complementation in S2 cells were performed as described earlier (Haas *et al*, 2010). Mutants of *D. melanogaster* HPat were generated by site-directed mutagenesis using the plasmid pAc5.1B-HA-HPat (dsRNA resistant) as template, and the QuickChange mutagenesis kit from Stratagene. Transfections of S2 cells were performed in six-well plates, using Effectene transfection reagent (Qiagen). Firefly and *Renilla* luciferase activities were measured 3 days after transfection using the Dual-Luciferase Reporter Assay System (Promega). Total RNA was isolated using TriFast (Peqlab Biotechnologies) and analysed as described earlier (Haas *et al*, 2010).

Coordinate deposition

Coordinates of the human PatL1 C-terminal domain constructs Pat-C-Δloop (Form I), Pat-C (Form II) and Pat-C-Δloop with bound sulphate (Form III) have been deposited in the Protein Data Bank under accession numbers 2xes, 2xeq and 2xer, respectively.

Supplementary data

Supplementary data are available at *The EMBO Journal* Online (http://www.embojournal.org).

Acknowledgements

We are grateful to R Büttner, M Fauser and S Helms for excellent technical assistance. We thank the staff at the PX beamlines of the Swiss Light Source for assistance with data collection. This study was supported by the Max Planck Society, by grants from the Deutsche Forschungsgemeinschaft (DFG, FOR855 and the Gottfried Wilhelm Leibniz Program awarded to EI), and by the Sixth Framework Programme of the European Commission through the SIROCCO Integrated Project LSHG-CT-2006-037900. OW held a personal VIDI fellowship from the Dutch National Science Organization (NWO-VIDI, CW 700.54.427).

Conflict of interest

The authors declare that they have no conflict of interest.

References

Bail S, Kiledjian M (2006) More than 1 + 2 in mRNA decapping. *Nat Struct Mol Biol* **13:** 7–9

Bonnerot C, Boeck R, Lapeyre B (2000) The two proteins Pat1p (Mrt1p) and Spb8p interact *in vivo*, are required for mRNA decay, and are functionally linked to Pab1p. *Mol Cell Biol* **20:** 5939–5946

Bouveret E, Rigaut G, Shevchenko A, Wilm M, Seraphin B (2000) A Sm-like protein complex that participates in mRNA degradation. *EMBO J* **19:** 1661–1671

Chowdhury A, Mukhopadhyay J, Tharun S (2007) The decapping activator Lsm1p-7p-Pat1p complex has the intrinsic ability to distinguish between oligoadenylated and polyadenylated RNAs. *RNA* **13:** 998–1016

Chowdhury A, Tharun S (2008) lsm1 mutations impairing the ability of the Lsm1p-7p-Pat1p complex to preferentially bind to oligoadenylated RNA affect mRNA decay *in vivo*. *RNA* **14:** 2149–2158

Chowdhury A, Tharun S (2009) Activation of decapping involves binding of the mRNA and facilitation of the post-binding steps by the Lsm1-7-Pat1 complex. *RNA* **15:** 1837–1848

Coller JM, Tucker M, Sheth U, Valencia-Sanchez MA, Parker R (2001) The DEAD box helicase, Dhh1p, functions in mRNA decapping and interacts with both the decapping and deadenylase complexes. *RNA* **7:** 1717–1727

Edwards TA, Pyle SE, Wharton RP, Aggarwal AK (2001) Structure of Pumilio reveals similarity between RNA and peptide binding motifs. *Cell* **105:** 281–289

Eulalio A, Behm-Ansmant I, Schweizer D, Izaurralde E (2007a) P-body formation is a consequence, not the cause of RNA-mediated gene silencing. *Mol Cell Biol* **27:** 3970–3981

Eulalio A, Rehwinkel J, Stricker M, Huntzinger E, Yang S-F, Doerks T, Dorner S, Bork P, Boutros M, Izaurralde E (2007b) Target-specific requirements for enhancers of decapping in miRNA-mediated gene silencing. *Genes Dev* **21:** 2558–2570

Fenger-Grøn M, Fillman C, Norrild B, Lykke-Andersen J (2005) Multiple processing body factors and the ARE binding protein TTP activate mRNA decapping. *Mol Cell* **20:** 905–915

Fischer N, Weis K (2002) The DEAD box protein Dhh1 stimulates the decapping enzyme Dcp1. *EMBO J* **21:** 2788–2797

Franks TM, Lykke-Andersen J (2008) The control of mRNA decapping and P-body formation. *Mol Cell* **32:** 605–615

Fromont-Racine M, Mayes AE, Brunet-Simon A, Rain JC, Colley A, Dix I, Decourty L, Joly N, Ricard F, Beggs JD, Legrain P (2000) Genome-wide protein interaction screens reveal functional networks involving Sm-like proteins. *Yeast* **17:** 95–110

Haas G, Braun JE, Igreja C, Tritschler F, Nishihara T, Izaurralde E (2010) HPat provides a link between deadenylation and decapping in metazoa. *J Cell Biol* **189:** 289–302

Hatfield L, Beelman CA, Stevens A, Parker R (1996) Mutations in trans-acting factors affecting mRNA decapping in *Saccharomyces cerevisiae*. *Mol Cell Biol* **16:** 5830–5838

He W, Parker R (2001) The yeast cytoplasmic LsmI/Pat1p complex protects mRNA 3′ termini from partial degradation. *Genetics* **158:** 1445–1455

Holm L, Sander C (1995) Dali: a network tool for protein structure comparison. *Trends Biochem Sci* **20:** 478–480

Huber AH, Nelson WJ, Weis WI (1997) Three-dimensional structure of the armadillo repeat region of beta-catenin. *Cell* **90:** 871–882

Jínek M, Eulalio A, Lingel A, Helms S, Conti E, Izaurralde E (2008) The C-terminal region of Ge-1 presents conserved structural features required for P-body localization. *RNA* **14:** 1991–1998

Kedersha N, Anderson P (2007) Mammalian stress granules and processing bodies. *Methods Enzymol* **431:** 61–81

Lykke-Andersen J (2002) Identification of a human decapping complex associated with hUpf proteins in nonsense-mediated decay. *Mol Cell Biol* **22:** 8114–8121

Matsuura Y, Stewart M (2004) Structural basis for the assembly of a nuclear export complex. *Nature* **432:** 872–877

Murzin AG, Brenner SE, Hubbard T, Chothia C (1995) SCOP: a structural classification of proteins database for the investigation of sequences and structures. *J Mol Biol* **247:** 536–540

Pilkington GR, Parker R (2008) Pat1 contains distinct functional domains that promote P-body assembly and activation of decapping. *Mol Cell Biol* **28:** 1298–1312

Scheller N, Resa-Infante P, de la Luna S, Galao RP, Albrecht M, Kaestner L, Lipp P, Lengauer T, Meyerhans A, Díez J (2007) Identification of PatL1, a human homolog to yeast P body component Pat1. *Biochim Biophys Acta* **1773:** 1786–1792

Simon E, Camier S, Séraphin B (2006) New insights into the control of mRNA decapping. *Trends Biochem Sci* **31:** 241–243

Tharun S (2009) Lsm1-7-Pat1 complex: a link between 3′ and 5′-ends in mRNA decay? *RNA Biol* **6:** 228–232

Tharun S, He W, Mayes AE, Lennertz P, Beggs JD, Parker R (2000) Yeast Sm-like proteins function in mRNA decapping and decay. *Nature* **404:** 515–518

Tharun S, Parker R (2001) Targeting an mRNA for decapping: displacement of translation factors and association of the Lsm1p-7p complex on deadenylated yeast mRNAs. *Mol Cell* **8:** 1075–1083

Tritschler F, Braun JE, Eulalio A, Truffault V, Izaurralde E, Weichenrieder O (2009a) Structural basis for the mutually exclusive anchoring of P-body components EDC3 and Tral to the DEAD-box protein DDX6/Me31B. *Mol Cell* **33:** 661–668

Tritschler F, Braun JE, Motz C, Igreja C, Haas G, Truffault V, Izaurralde E, Weichenrieder O (2009b) DCP1 forms asymmetric trimers to assemble into active mRNA decapping complexes in metazoa. *Proc Natl Acad Sci USA* **106:** 21591–21596

van Dijk E, Cougot N, Meyer S, Babajko S, Wahle E, Séraphin B (2002) Human Dcp2: a catalytically active mRNA decapping enzyme located in specific cytoplasmic structures. *EMBO J* **21:** 6915–6924

Wang X, McLachlan J, Zamore PD, Hall TM (2002) Modular recognition of RNA by a human pumilio-homology domain. *Cell* **110:** 501–512

Supplementary information

The C-terminal α-α superhelix of Pat is required for the assembly of decapping complexes and for mRNA decapping in metazoa

Joerg E. Braun, Felix Tritschler, Gabrielle Haas, Cátia Igreja, Vincent Truffault, Oliver Weichenrieder, and Elisa Izaurralde

Supplementary Methods

Protein expression, purification and crystallization

cDNA sequences encoding the C-terminal domain of human PatL1 (Q86TB9; Asp517 to Arg770) were amplified from oligo$(dT)_{15}$-primed cDNA libraries obtained from human HeLa cells. The amplified cDNA fragments were inserted into a modified pRSFDuet-1 vector (Novagen) downstream of the His_6–tag open reading frame. Constructs for expression of the crystallized proteins Pat-C (517-767) and Pat-C-Δloop (517-767, residues 664-673 replaced by a Gly-Ser linker) were obtained by site directed mutagenesis of the aforementioned expression vector as described in the Materials and Methods. Human PatL1 proteins were expressed with an N-terminal His_6-tag in the E. coli strain BL21 (DE3) or BL21 Star (DE3, Invitrogen) at 25°C overnight. The proteins were purified from cleared cell lysates by a Ni^{2+}-affinity step (HiTrap Chelating HP column, GE Healthcare), the His_6-tag was cleaved with PreScission protease and the proteins were purified to homogeneity by ion exchange chromatography and gel filtration (HiTrap SP HP and HiLoad 26/60 Superdex 75 columns, GE Healthcare).

Diffraction quality crystals were grown by hanging drop vapor diffusion. Highly facetted crystal clusters of Pat-C (Form II, residues 517-767) grew at 19 °C after mixing 1 µl protein solution (16 mg/ml in 10 mM Na-HEPES pH 7.0,

100 mM NaCl and 3 mM DTT) and 1 µl reservoir solution (100 mM Bis-tris propane, pH 7.5, 20% PEG 3350 and 200 mM Na_3-Citrate). Hair-seeding combined with the use of an additive screen (Hampton Research, HR2-428) was necessary to obtain single crystal plates of sufficient size for X-ray diffraction experiments. Briefly, 0.8 µl reservoir solution (100 mM Bis-tris propane, pH 7.8, 10% PEG 3350, 200 mM Na_3-Citrate and 2% glycerol) was mixed with 0.2 µl of a 100 mM urea solution after which 1 µl protein solution (14 mg/ml in 10 mM Na-HEPES pH 7.0, 100 mM NaCl and 3 mM DTT) was added. After one day at 4°C, hair-seeding was done from the supernatant (centrifugation at 2,000 g for 1 min) of crushed crystal clusters. Within ca. one week we obtained diffraction quality crystal plates of ~ 100 x 100 x 10 µm³. Crystals were cryoprotected in 100 mM Bis-tris propane, pH 7.8, 10% PEG 3350, 200 mM Na_3-Citrate and 15% glycerol before flash-cooling in liquid nitrogen.

To obtain crystals of Pat-C-Δloop (Form I), 1 µl protein solution (9 mg/ml in 10 mM Na-HEPES pH 7.0, 100 mM NaCl, 3 mM DTT) was added to 1 µl reservoir solution (12% PEG 3350, 0.2 M KSCN, 5% glycerol) and hair-seeding was done from crushed crystals grown under similar crystallization conditions. Drops were then equilibrated at 4°C over 500 µl of reservoir. Crystal rods grew to a size of 150 x 70 x 70 µm³ within two days. Flash-cooling was done in liquid nitrogen after cryoprotection in 12% PEG 3350, 0.2 M KSCN and 20% glycerol.

Crystals of Pat-C-Δloop with bound sulfate ions (Form III) were obtained in an attempt to co-crystallize Pat-C-Δloop with U_8-RNA. 240 nmol protein was mixed with 360 nmol U_8-RNA in a volume of 400 µl buffer (10 mM Na-

HEPES pH 7.0, 100 mM NaCl, 3 mM DTT), the resulting precipitate was removed by centrifugation and 0.5 µl of the supernatant was added to 0.7 µl reservoir solution (100 mM Tris, pH 8.5, 1.15 M $NH_4(SO_4)_2$, 150 mM Li_2SO_4, 8% glycerol). Drops were incubated at 19°C over 500 µl reservoir solution. Crystal plates were obtained after several days and grew to their full size (ca. 80 x 80 x 20 μm^3) within one month. Flash-cooling was done in liquid nitrogen after cryoprotection with 100 mM Tris, pH 8.5, 1.15 M $NH_4(SO_4)_2$, 150 mM Li_2 SO_4 and 20% glycerol.

Structure determination and refinement

Diffraction data were collected on beamline X10SA of the Swiss Light Source (SLS), Villigen, Switzerland. Data processing and integration was done with XDS (Kabsch 1993). Selenomethionine substituted Pat-C protein crystals diffracted not well enough to obtain suitable phase information. Hence, we first determined the crystal structure of PatL1-C-Δloop using multiple-wavelength anomalous dispersion. Diffraction images of selenomethionine-substituted Pat-C-Δloop protein (Form I, 8 selenomethionines per molecule, 2 molecules per asymmetric unit, Table S2) were collected at the selenium absorption peak and the inflection point and processed with XDS to 2.2 Å resolution. AutoSHARP (Vonrhein at al, 2007) was used to identify (SHELX D) and refine (SHARP) 16 selenium sites. After density modification with PIRATE, as part of the CCP4 suite (Cowtan, 2002) the resulting excellent electron density map was used to automatically build (flex-wARP; Cohen et al, 2008) most of the two Pat-C-Δloop molecules in the asymmetric unit. The model was completed manually with iterative cycles of model building (COOT; Emsley and Cowtan, 2004) and

refinement (PHENIX; Adams et al, 2010) at 2.1 Å against the dataset collected at the selenium absorption peak.

The resulting structure served as search model for molecular replacement (PHASER, McCoy et al, 2007) to solve the structures of Form II using a dataset at 3.1 Å resolution of Pat-C selenomethionine crystals collected at the selenium absorption peak and of Form III using a 2.95 Å native dataset.

Manual model building was done in COOT and refinement was done with PHENIX. Stereochemical properties were analyzed with MOLPROBITY (Davis et al, 2007) and WHATCHECK (Hooft et al, 1996).

Analytical size exclusion chromatography and static light scattering

Proteins were prepared as described for crystallization and analyzed in chromatography buffer (10 mM HEPES pH 7.0, 100 mM NaCl, 3 mM DTT). Proteins or mixtures of protein with RNA or DNA were injected onto a Superdex 75 10/300 GL analytical gel filtration column (GE Healthcare, 12°C, equilibrated in chromatography buffer) as part of an ÄKTA Purifier-10 at a flow rate of 0.5 ml/min. UV absorption was monitored simultaneously at 230 nm, 260 nm and 280 nm. Protein and nucleic acid concentrations were estimated from the theoretical molar extinction coefficients at 280 nm and 260 nm respectively. The relative contributions of protein and nucleic acid to the total absorption at each wavelength were calculated assuming constant ratios of the extinction coefficient at 230 nm to the extinction coefficient at 280 nm for each substance (Müller at al, 2006). Multiangle static laser light scattering was done online with analytical gel filtration chromatography using miniDAWN TREOS and Optilab rEX instruments (Wyatt Technologies) and the associated

software (AstraV) for molecular weight determination.

NMR measurements

^{1}H-NOESY spectra of the extended Mid domain of human PatL1 (353-516) were acquired at 291 K on a Bruker AV III-800 spectrometer, processed and analyzed using the Topspin software (Topspin V. 2.1.3, Bruker, Karlsruhe). The spectrum was recorded with 768 (t_2) × 128 (t_1) complex points using 16 scans per increment, a relaxation delay of 1 s and an NOE mixing time of 70 ms.

Co-immunoprecipitation assays and Western blotting

For co-immunoprecipitation assays, HEK-293 cells were grown in 10 cm plates and transfected using Lipofectamine 2000 (Invitrogen). The transfection mixtures contained 7 µg of the GFP- and HA-constructs. Two days after transfection, cells were washed with PBS and lysed for 15 min on ice, in NET buffer (50 mM Tris at pH 7.5, 150 mM NaCl, 1mM EDTA, 0.1% Triton X-100, 10% glycerol), supplemented with protease inhibitors (1 ml NET buffer/ plate). Cell lysates were spun at 18,000 g for 15 min at 4°C. Polyclonal anti-GFP (dilution 1:1000) or monoclonal anti-HA antibodies (Covance, 1:2000) were added to the supernatants. Samples were incubated for 1h at 4°C. Then, 25 µl of Protein G-agarose were added and the mixtures were rotated for an additional hour at 4°C. Beads were washed three times with NET buffer and once with NET buffer without Triton X-100. Bound proteins were eluted with 100 µl of protein sample buffer and analyzed by Western blotting as described before (Tritschler et al, 2009b)

Fluorescence microscopy

For fluorescence microscopy, human HeLa cells were grown on coverslips in 24-well plates and transfected using Lipofectamine 2000 (Invitrogen). The transfection mixtures contained 0.3 μg of plasmids expressing GFP-protein fusions. Two days after transfection, cells were fixed with 4% paraformaldehyde in PBS for 10 min at room temperature, and permeabilized for 10 min with PBS containing 0.5% Triton-X100. Endogenous P-bodies were detected using a monoclonal antibody (sc-8418, Santa Cruz Biotechnology), which cross-reacts with EDC4 at a 1:1,000 dilution in PBS containing 0.1% Tween-20, and 10% fetal bovine serum (FBS). Alexa Fluor 594-coupled goat-anti-mouse secondary antibody (Molecular probes) was used at a 1:1,000 dilution. Cells were mounted using Fluoromount-G (Southern Biotechnology Associates, Inc.). Images were captured using a confocal fluorescent microscope (TCS SP2, Leica) with a Plan Apo 100x NA 1.40 oil immersion objective equipped with a series of three Hammamatsu Photonics Photomultipliers and Leica confocal software (version 2.61). Images were prepared using Photoshop (Adobe).

Supplementary references

Adams PD, Afonine PV, Bunkóczi G, Chen VB, Davis IW, Echols N, Headd JJ, Hung L-W, Kapral GJ, Grosse-Kunstleve RW, McCoy AJ, Moriarty, NW, Oeffner R, Read RJ, Richardson DC, Richardson JS, Terwilliger TC, Zwart PH (2010) PHENIX: a comprehensive Python-based system for macromolecular structure solution. *Acta Crystallogr D Biol Crystallogr* **66:** 213–221

Cohen SX, Ben Jelloul M, Long F, Vagin A, Knipscheer P, Lebbink J, Sixma TK, Lamzin VS, Murshudov GN, Perrakis A (2008) ARP/wARP and molecular replacement: the next generation. *Acta Crystallogr D Biol Crystallogr* **64:** 49–60

Cowtan K (2002) General quadratic functions in real and reciprocal space and their application to likelihood phasing. *Acta Crystallogr D Biol Crystallogr* **56:** 1612–1621

Davis IW, Leaver-Fay A, Chen VB, Block JN, Kapral GJ, Wang X, Murray LW, Arendall WB 3rd, Snoeyink J, Richardson JS, and Richardson DC (2007) MolProbity: all-atom contacts and structure validation for proteins and nucleic acids. *Nucleic Acids Res* **35:** W375–W383

Emsley P, Cowtan K (2004) Coot: model-building tools for molecular graphics. *Acta Crystallogr D Biol Crystallogr* **60:** 2126–2132

Hooft RW, Vriend G, Sander C, Abola EE (1996) Errors in protein structures. *Nature* **381:** 272

Kabsch W (1993) Automatic processing of rotation diffraction data from crystals of initially unknown symmetry and cell constants. *J Appl Cryst* **26:** 795–800

McCoy AJ, Grosse-Kunstleve RW, Adams PD, Winn MD, Storoni LC, Read RJ (2007) Phaser crystallographic software. *J Appl Cryst* **40:** 658–674

Müller M, Weigand JE, Weichenrieder O, Suess B (2006) Thermodynamic characterization of an engineered tetracycline-binding riboswitch. *Nucleic Acids Res* **34:** 2607–2617

Tritschler F, Braun JE, Motz C, Igreja C, Haas G, Truffault V, Izaurralde E, Weichenrieder O (2009b) DCP1 forms asymmetric trimers to assemble into active mRNA decapping complexes in metazoa. *Proc Natl Acad Sci USA* **106:** 21591–21596

Vonrhein C, Blanc E, Roversi P, Bricogne G (2007) Automated Structure Solution with autoSHARP. *Methods Mol Biol* **364:** 215–230

Supplementary Figure legends

Figure 1 Conservation of the Mid domain and Pat-C. (**A**) Sequence alignment of the extended Mid domain of Pat orthologs from *H. sapiens* (PatL1)*, D. rerio* (Pat1 homolog 1)*, G. gallus* (PatL1), *X. laevis* (PatL1), *D. melanogaster* (HPat), *C. elegans* (Patr-1), *S. cerevisiae* (Pat1) and an *A. thaliana* hypothetical protein. Conserved residues are shaded gray (hydrophobic), red (acidic) and blue (basic). Invariant residues are marked with an asterisk. The black box indicates invariant residues in the Mid extension of vertebrate species. (**B**) Structure-based sequence alignment of Pat-C. Conserved and invariant residues are indicated as in panel A. Triangles indicate residues mutated in this study (red triangles: Mut1; blue triangles: Mut-2). Residues deleted in Mut-3 are indicated by a green bracket. Residues replaced by a Gly-Ser linker in Pat-C-Δloop are indicated by a black bracket. Secondary structure assignment and numbering correspond to human PatL1, Form II, chain A.

Figure 2 ^{1}H-NOESY spectra of the extended PatL1 Mid domain (residues 353–516, unlabelled). As expected for an unfolded protein domain, a negligible chemical shift dispersion is observed in the region of the amide protons (dispersion from 7.75 to 8.35 ppm), thus excluding the possibility for the domain to contain β-strands. Examination of the spectra also shows that the domain does not harbor α-helices, due to the lack of strong sequential H^N – H^N contacts (red, dashed box). Moreover the protein is monomeric at a concentration of 0.1 mM in 300 mM NaCl at pH 7.0, as reflected by a diffusion coefficient of 0.85 (± 0.05) x 10^{-10} m^2/s measured at 291 K.

Figure 3 DCP2, EDC4 and LSm1–7 interact with PatL1 independently of DDX6/RCK. (**A–C**) GFP- and HA-tagged proteins were co-expressed in human cells as indicated. Cell lysates were immunoprecipitated using anti-GFP or anti-HA antibodies and analyzed as described in Figure 1.

Figure 4 Comparison of Pat-C and Pat-C-Δloop structures. (**A**) Structure of Pat-C-Δloop. The crystal form I (Pat-C-Δloop, chain A, green) is superimposed onto the crystal form II (Pat-C, chain A, dark blue) and is shown in two orientations (back view and front view, related by a 180° rotation along a vertical axis, see Figure 5A). Disordered portions of the polypeptide chains are indicated with dashed lines. The loop L(α8- α9), which is replaced by a GlySer-linker in Pat-C-Δ-loop, is shown in magenta. (**B**) Sulfate ion in crystal Form III. Electrostatic potentials were mapped onto the molecular surface of Pat-C (Form III, chain B) and contoured from -10 kT/e^- (red) to 10 kT/e^- (blue), showing a positively charged surface patch. Residues contributing to this surface patch are labeled. A sulfate ion located near residues R591 and R595 is shown as sticks.

Figure 5 Nucleic acid-binding of human Pat-C. Proteins were analyzed by size exclusion chromatography either in the absence (dashed blue lines) or presence (solid blue lines) of nucleic acid substrates (solid red lines). Nucleic acid substrates analyzed in the absence of protein are shown as dashed red lines. Concentrations were calculated from the relative absorption properties of the components.

Figure S1. Braun et al.

A Mid domain

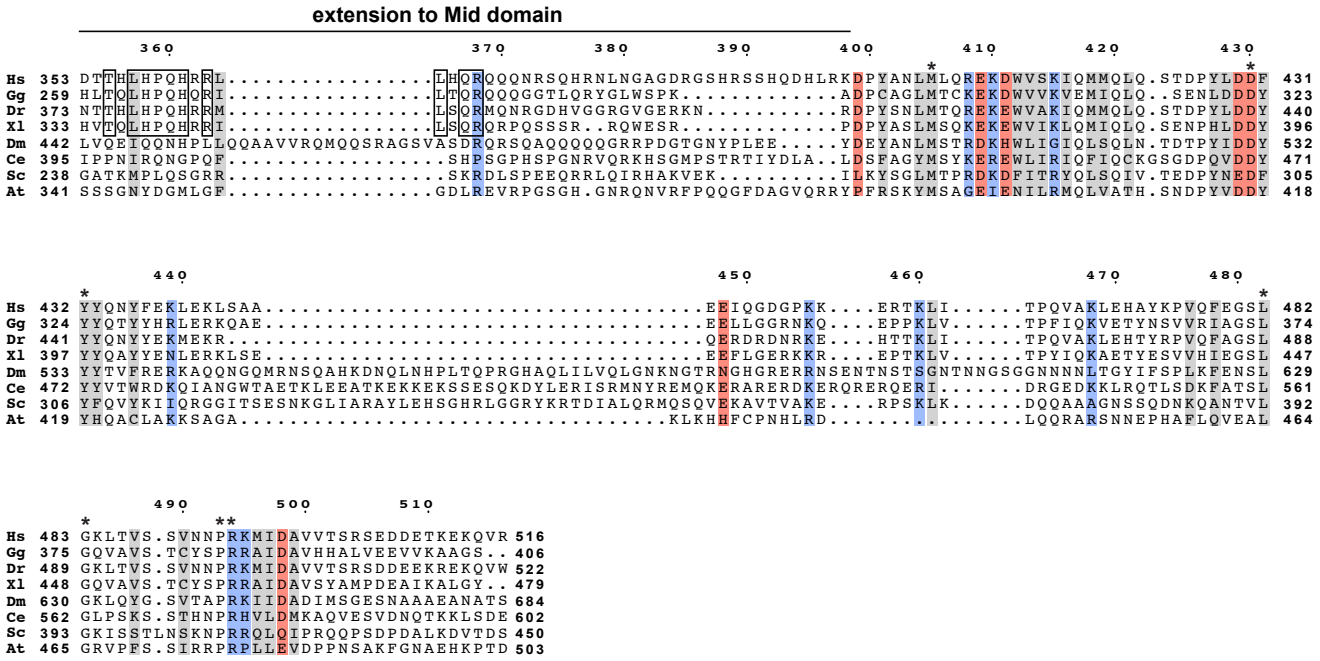

B Pat-C

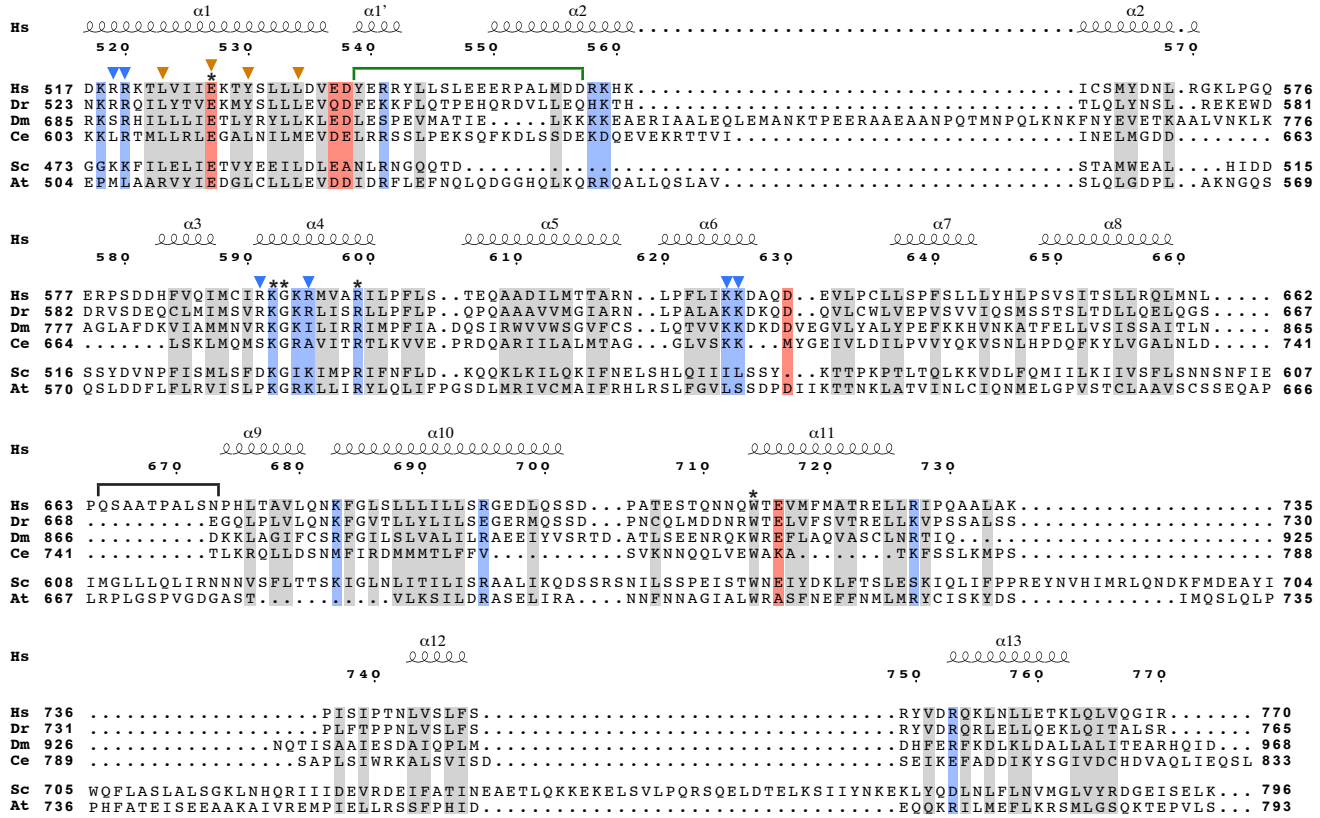

Figure S2. Braun et al.

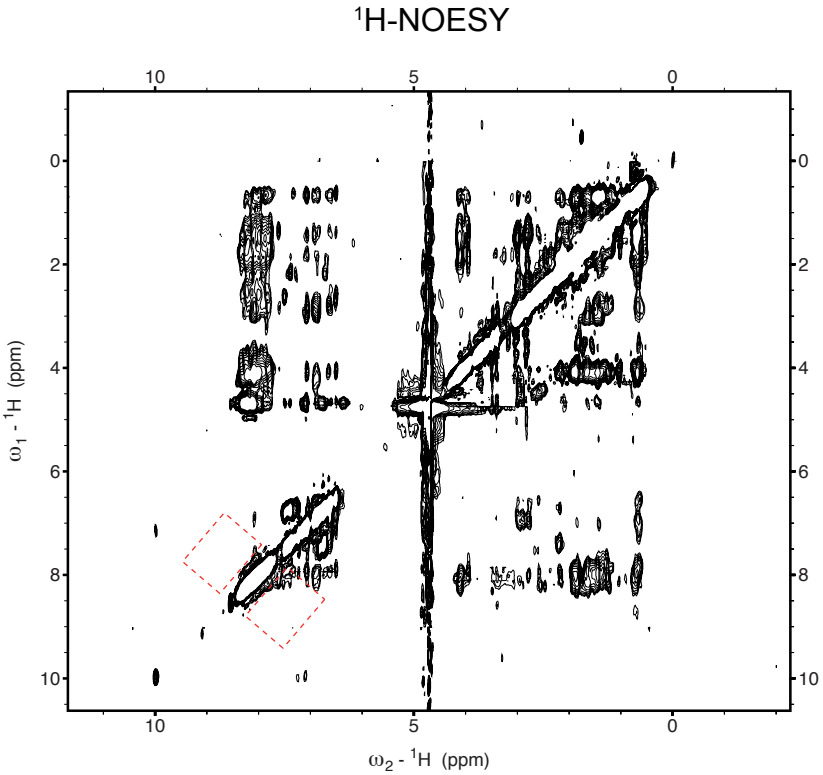

Figure S3. Braun et al

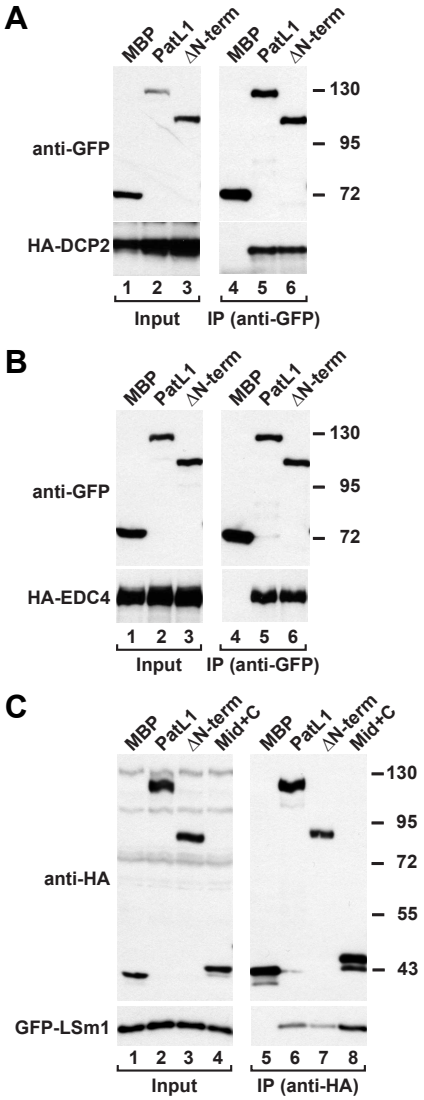

Figure S4. Braun et al.

A Superposition of Pat-C wild-type and Pat-C-Δloop

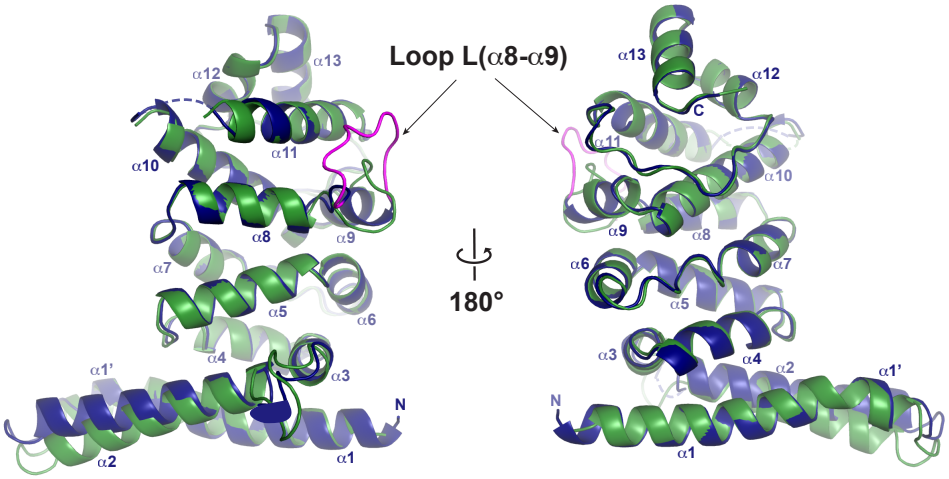

Back view Front view

B Crystal form III: bound sulfate

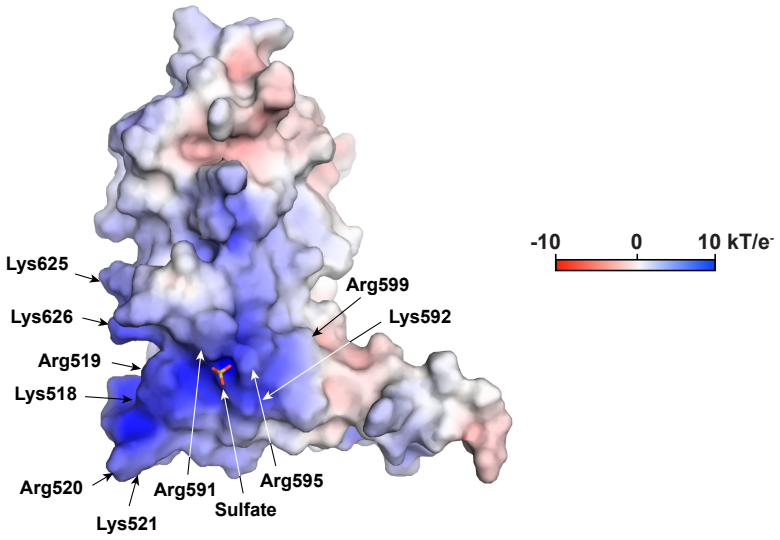

Front view

Figure S5. Braun et al.

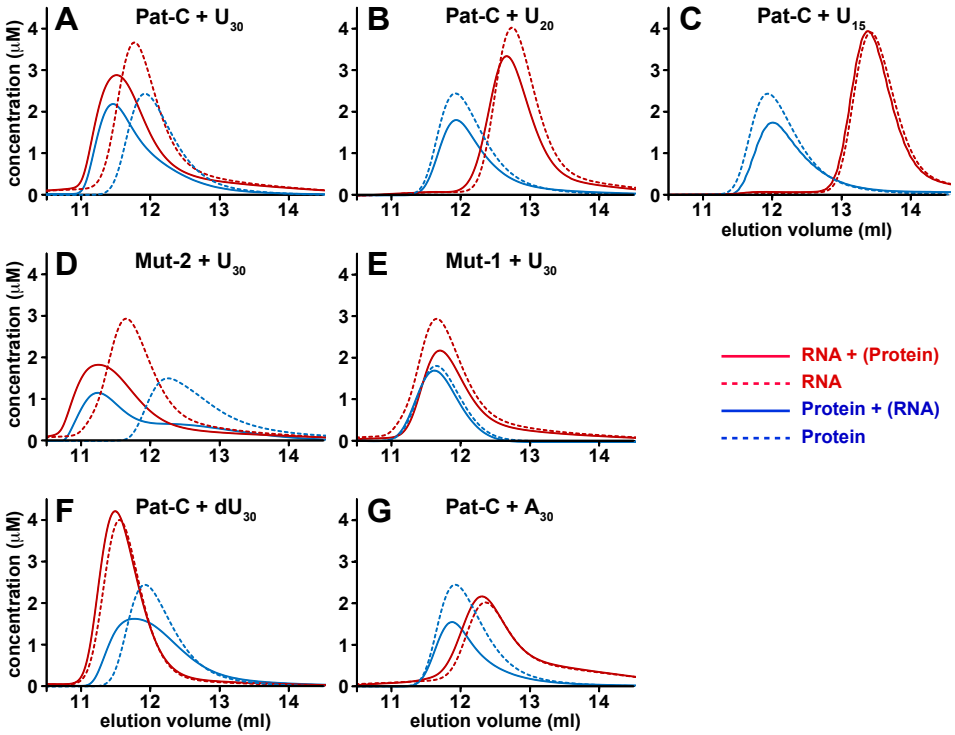

Table S1. Elution volumes and molecular weights of wild-type human Pat-C and corresponding mutants as determined by analytical gel filtration and MALS.

	Gel filtration		**MALS**	**Expected MW for monomer**
	Elution volume [ml]	**Apparent MW[kDa]**	**MW [kDa]**	**[kDa]**
Pat-C	11.92	33	30	29.5
Pat-C Δloop	11.83	35	31	28.0
Pat-C Mut-1	11.75	36	30	29.0
Pat-C Mut-2	12.09	31	32	29.2
Pat-C Mut-3	12.40	26	31	27.6
Mid-Pat-C	10.38	73	47	43.2

Table S2. Data collection, phasing and refinement statistics

Crystallographic statistics	**Form I (Δ loop)**			**Form II**	**Form III (Δ loop)**
Construct	SeMeth 517-767 Δ664-673			SeMeth 517 – 767	Native 517 – 767 Δ664-673
Structure determination	MAD			MR	MR
Data set		peak	infl. point		
Data Statistics					
Space group	$P2_12_12_1$			$P2_12_12_1$	$P2_12_12$
Unit cell (a / b / c), (Å)	56.7, 70.8, 134.0			102.2, 108.6, 108.8	61.0, 100.1, 141.6
Unit cell (α / β / γ), (°)	90.0, 90.0, 90.0			90.0, 90.0, 90.0	90.0, 90.0, 90.0
Wavelength (Å)	0.97880	0.97880	0.97922	0.97940	1.00000
R_{sym}, (%) [a]	9.9 (66.4)	9.3 (62.2) [c]	10.0 (70.1) [c]	13.1 (88.0)	11.9 (59.4)
Completeness, (%) [a]	99.3 (99.6)	100.0 (100.0) [c]	100.0 (100.0) [c]	99.4 (99.9)	98.8 (98.1)
I/σ(I) [a]	9.1 (2.2)	16.8 (3.7) [c]	10.8 (2.3) [c]	9.1 (1.9)	11.1 (2.2)
Unique reflections	32006	52824 [c]	51658 [c]	22432	18701
Multiplicity [a]	4.0 (4.0)	7.7 (7.7) [c]	4.2 (4.1) [c]	4.7 (4.8)	3.3 (3.1)
Resolution range, (Å) [a]	67.0 - 2.1 (2.15 - 2.1)	67.0 - 2.2 (2.26 - 2.2)	67.0 - 2.2 (2.26 -2.2)	43.9 - 3.1 (3.18 – 3.1)	47.2 - 2.95 (3.03 - 2.95)
Phasing Statistics					
Phasing power (anom.)		1.738	0.871		
R_{cullis} (anom.)		0.661	0.871		
Mean FOM		0.515			
Refinement Statistics					
R_{cryst}/ R_{free} (%)	19.9 / 23.2			24.8 / 28.1	24.8 / 29.2
Molecules per ASU					
HsPat-C	2			4	3
K/SCN/sulfate	2/4/0			0/0/0	0/0/4
Prot. atoms/ H_2O /lig.s	3840/521/14			7682/8/0	5523/44/20
B factor prot./H_2O/lig.s (Å^2)	32.8/35.0/37.7			77.9/50.2/-	51.0/26.0/75.1
Ramachandran plot [b] (favored/allowed/outlier %)	99.4/0.6/0			96.0/4.0/0	96.8/3.2/0
R.m.s. deviations					
bond lengths, (Å)	0.008			0.005	0.007
bond angles, (°)	0.921			0.675	0.763

[a] Numbers in parentheses are for the highest-resolution shell
[b] Calculated using Molprobity
[c] Values relate to unmerged Friedel pairs

Published April 19, 2010

HPat provides a link between deadenylation and decapping in metazoa

Gabrielle Haas, Joerg E. Braun, Cátia Igreja, Felix Tritschler, Tadashi Nishihara, and Elisa Izaurralde

Max Planck Institute for Developmental Biology, D-72076 Tübingen, Germany

Decapping of eukaryotic messenger RNAs (mRNAs) occurs after they have undergone deadenylation, but how these processes are coordinated is poorly understood. In this study, we report that *Drosophila melanogaster* HPat (homologue of Pat1), a conserved decapping activator, interacts with additional decapping factors (e.g., Me31B, the LSm1–7 complex, and the decapping enzyme DCP2) and with components of the CCR4–NOT deadenylase complex. Accordingly, HPat triggers deadenylation and decapping when artificially tethered to an mRNA reporter. These activities reside, unexpectedly, in a proline-rich region. However, this region alone cannot restore decapping in cells depleted of endogenous HPat but also requires the middle (Mid) and the very C-terminal domains of HPat. We further show that the Mid and C-terminal domains mediate HPat recruitment to target mRNAs. Our results reveal an unprecedented role for the proline-rich region and the C-terminal domain of metazoan HPat in mRNA decapping and suggest that HPat is a component of the cellular mechanism that couples decapping to deadenylation in vivo.

Introduction

Eukaryotic mRNAs are degraded by two alternative pathways, both of which are initiated by a gradual shortening of the poly(A) tail by deadenylation. In one, the 3′ to 5′ decay pathway, the poly(A) tail is first removed, and then the exosome and cofactors digest the mRNA exonucleolytically from the 3′ end (Houseley et al., 2006). In the other, the 5′ to 3′ decay pathway, deadenylation is followed by the removal of the 5′ cap structure by the decapping enzyme DCP2; decapped mRNA is then susceptible to 5′ to 3′ exonucleolytic degradation by XRN1 (Bail and Kiledjian, 2006; Simon et al., 2006).

The decapping enzyme DCP2 requires additional proteins for full activity and/or stability (Bail and Kiledjian, 2006; Simon et al., 2006). Proteins that enhance decapping in *Saccharomyces cerevisiae* include DCP1, EDC1–3 (enhancer of decapping 1, 2, and 3), the heptameric LSm1–7 complex, Dhh1 (DExH/D-box RNA helicase 1; Me31B in *Drosophila melanogaster*), and Pat1 (HPat in *D. melanogaster*). With the exception of EDC1 and -2, these proteins are conserved, yet most are not functionally characterized in multicellular eukaryotes.

In *S. cerevisiae*, Pat1 interacts with the Lsm1–7 complex and Dhh1 (Bonnerot et al., 2000; Bouveret et al., 2000; Fromont-Racine et al., 2000; Tharun et al., 2000; Coller et al., 2001; Tharun and Parker, 2001; Fischer and Weis, 2002). The Pat1–LSm1–7 complex preferentially binds to the 3′ ends of oligoadenylated mRNAs that have undergone deadenylation, thereby protecting them from 3′ trimming and further degradation (He and Parker, 2001; Tharun and Parker, 2001; Chowdhury et al., 2007; Chowdhury and Tharun, 2008, 2009). This complex then activates decapping, most likely by recruiting additional decapping activators and the decapping enzyme DCP2 (Hatfield et al., 1996; Bouveret et al., 2000; He and Parker, 2001; Chowdhury et al., 2007; Decker et al., 2007; Chowdhury and Tharun, 2008, 2009; Pilkington and Parker, 2008; Tharun, 2009). Pat1 also associates with DCP1, DCP2, and EDC3 in yeast, which is consistent with a role in decapping (Fromont-Racine et al., 2000; Tharun et al., 2000; Tharun and Parker, 2001; Pilkington and Parker, 2008). Additionally, Pat1 and the LSm1–7 complex copurify with Xrn1 (Bouveret et al., 2000), suggesting a possible role for Pat in coupling decapping to 5′ to 3′ mRNA degradation.

Like many components of the 5′ to 3′ mRNA decay pathway, Pat1 localizes to P bodies and, moreover, is required

Correspondence to Elisa Izaurralde: elisa.izaurralde@tuebingen.mpg.de

Abbreviations used in this paper: dsRNA, double-stranded RNA; F-Luc, firefly luciferase; IP, immunoprecipitation; MBP, maltose-binding protein; Mid, middle; R-Luc, *Renilla* luciferase; RT-qPCR, quantitative RT-PCR; Tral, trailer hitch.

Supplemental Material can be found at:
http://jcb.rupress.org/content/suppl/2010/04/18/jcb.200910141.DC1.html

The Rockefeller University Press $30.00
J. Cell Biol. Vol. 189 No. 2 289–302
www.jcb.org/cgi/doi/10.1083/jcb.200910141

Published April 19, 2010

for P-body integrity (Pilkington and Parker, 2008). A fraction of Pat1 is also found in polysomes (Bonnerot et al., 2000; Wyers et al., 2000), suggesting that it associates with actively translated mRNAs and may commit them to degradation in response to a triggering signal (Bonnerot et al., 2000). Intriguingly, Pat1 was reported to play dual roles in translation: it stimulates translation initiation (Wyers et al., 2000) but is also required for general translational repression during glucose deprivation (Coller and Parker, 2005). Furthermore, Pat1 overexpression can repress translation and cause mRNAs to accumulate in P bodies (Coller and Parker, 2005). These and additional studies suggest that Pat1 is a key regulator in the transition of mRNAs from a translationally active state associated with polysomes to a ribosome-free translationally repressed state that commits the mRNA to degradation (Coller and Parker, 2005; Pilkington and Parker, 2008). In this repressed state, mRNAs may aggregate into P bodies (Coller and Parker, 2005).

Pat1 is conserved in eukaryotes, and Pat1 orthologues in *D. melanogaster* and human cells (HPat and PatL1, respectively) localize to P bodies (Eulalio et al., 2007a; Scheller et al., 2007). The role of metazoan Pat1 orthologues in decapping is also conserved, as suggested by the observation that codepletion of HPat and Me31B strongly inhibits decapping triggered by microRNAs or by tethered GW182 in *D. melanogaster* cells (Eulalio et al., 2007c). Nonetheless, the interactions of Pat1 orthologues with additional decapping activators and the role of Pat1 orthologues in decapping remain largely unknown in multicellular eukaryotes.

Pat1 proteins are characterized by a conserved N-terminal sequence, a proline-rich region, a middle (Mid) domain, and a C-terminal domain (termed Pat-C). A study in *S. cerevisiae* showed that the Pat1 Mid domain interacts with the LSm1–7 ring and is essential for decapping in vivo (Pilkington and Parker, 2008). Sequences located N- or C-terminally to the Mid domain stimulate but are not required for decapping. Furthermore, Pat-C is required for Pat1 to localize to P bodies and confers the interaction with DCP1, EDC3, and RNA (Pilkington and Parker, 2008).

In this study, we analyzed HPat interactions and function in *D. melanogaster* using coimmunoprecipitation (co-IP) and complementation assays. In addition to the interaction between HPat and Me31B, DCP2 or the LSm1–7 complex, which are conserved in yeast, our study revealed that HPat interacts with the CCR4–NOT deadenylase complex. These findings suggest that HPat plays a role in coupling decapping to deadenylation. Accordingly, we observed that HPat promotes deadenylation and decapping of mRNAs in tethering assays. Unexpectedly, these activities are mediated by a proline-rich region, which we show is also required for P-body integrity. However, in contrast to results in yeast, we show that in addition to the Mid domain, both the proline-rich region and Pat-C are required to restore decapping in cells depleted of endogenous HPat. Our findings reveal that yeast and *D. melanogaster* differ significantly as to which HPat domains are required for decapping, highlighting the importance of characterizing decapping complexes in metazoa.

Results

HPat coimmunoprecipitates Me31B, DCP2, and the LSm1–7 complex

To systematically investigate the network of interactions between HPat and decapping activators in metazoa, we coexpressed HA-, V5-, or GFP-tagged versions of these proteins in *D. melanogaster* S2 cells and used anti-HA antibodies to coimmunoprecipitate V5- or GFP-tagged proteins from cell lysates. We used this method to detect interactions with DCP1, DCP2, EDC3, EDC4, Me31B, Tral (trailer hitch), XRN1, and components of the LSm1–7 complex.

HPat coimmunoprecipitated with Me31B but not with DCP1, EDC3, or Tral (Fig. 1 A, lanes 7–10). Both EDC3 and Tral interact directly with Me31B (Tritschler et al., 2009), suggesting that the interaction of HPat with Me31B mutually excludes an interaction with Me31B–EDC3 or Me31B–Tral (see Figs. 3 and 4). When coexpressed in *Escherichia coli*, recombinant protein fragments of HPat and Me31B interact, showing the proteins bind each other directly (unpublished data).

In yeast, Pat1 associates with the LSm1–7 complex (Bonnerot et al., 2000; Bouveret et al., 2000; Fromont-Racine et al., 2000; Tharun et al., 2000; Tharun and Parker, 2001). Accordingly, we observed that HPat coimmunoprecipitated LSm1, -3, and -7 (Fig. 1 B). HPat interaction with LSm1 was insensitive to RNase A treatment (Fig. S1 A), suggesting that it is not mediated by RNA. LSm1 and -7 also coimmunoprecipitated with Me31B but not with any of the other proteins tested (Fig. 1 C; Tritschler et al., 2007, 2008). Finally, we observed that HPat coimmunoprecipitated DCP2 in an RNA-independent manner but not XRN1 or EDC4 (Fig. 1 D; Fig. S1, B and C; and not depicted). Thus, in addition to the interactions with Me31B and the LSm1–7 ring, which are conserved in *S. cerevisiae*, we detected an RNase A–insensitive interaction between HPat and DCP2. In contrast to our findings in this study, this interaction is sensitive to RNase A treatment in yeast (Tharun and Parker, 2001).

Me31B binds to the conserved N-terminal sequence of HPat

The interaction of HPat with Me31B is conserved in *S. cerevisiae* (Coller et al., 2001; Fischer and Weis, 2002). Despite conservation, the protein domains involved in this interaction were not defined. To identify them, we performed co-IP assays using different HPat and Me31B deletion mutants. Pat1 orthologues are characterized by a conserved N-terminal sequence of ∼50 residues, a proline-rich region, a Mid domain, and a C-terminal domain termed Pat-C (Fig. 2, A and B). The boundary between the Mid domain and Pat-C was chosen on the basis of sequence alignments between Pat1 orthologues from various species.

We observed that Me31B interacted only with an N-terminal fragment of HPat (residues 1–499) but not with a construct comprising the Mid domain and Pat-C (Fig. 2 C, lanes 8 and 9). The N-terminal fragment contains the conserved N-terminal sequence (residues 1–56; Fig. 2 B) and the proline-rich region (13.6%), which is particularly long in the *D. melanogaster* protein and also rich in glutamine residues (16%; Fig. 2 A,

Published April 19, 2010

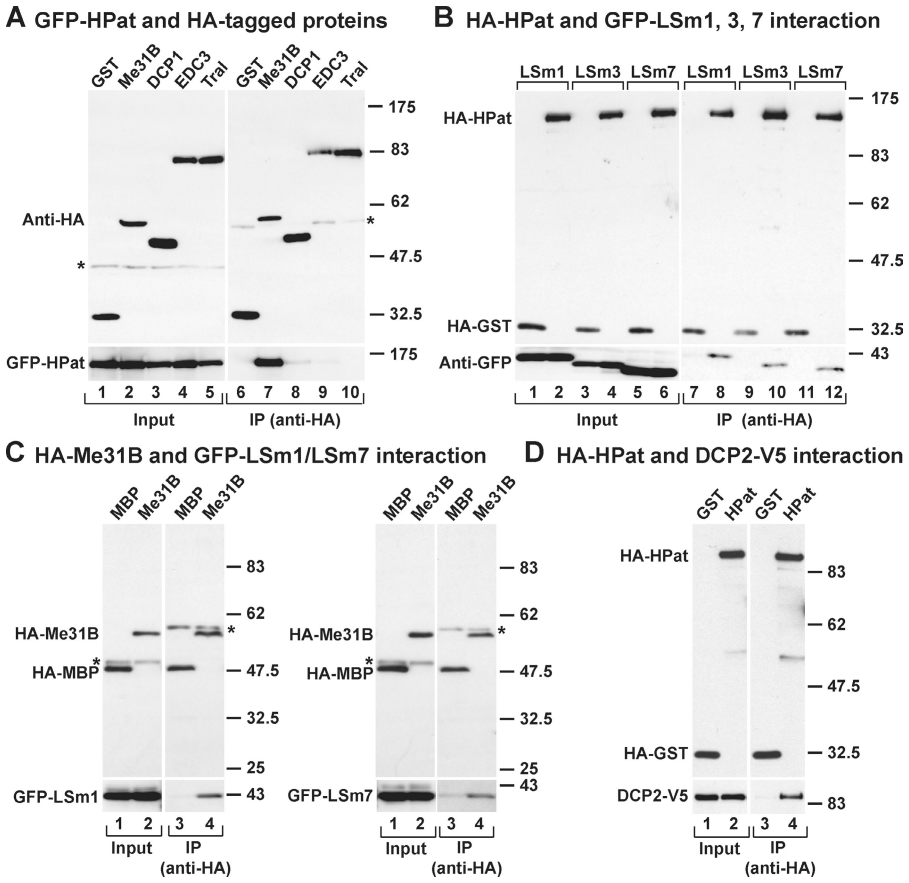

Figure 1. **HPat coimmunoprecipitates DCP2, Me31B, and the LSm1–7 complex.** (A–D) GFP-, V5-, and HA-tagged proteins were coexpressed in S2 cells as indicated. Cell lysates were immunoprecipitated using a monoclonal anti-HA antibody. HA-tagged versions of GST or MBP served as negative controls. Inputs (1%) and immunoprecipitates (10%) were analyzed by Western blotting. In D, 30% of the IP fraction was loaded. Asterisks indicate cross-reactivity of the primary antibodies with an endogenous protein (input panels) or of the secondary antibody with the immunoglobulin heavy chain (IP panels). Molecular mass is indicated in kilodaltons.

P-rich region). Because the interaction of HPat with Me31B is conserved, we hypothesized it could be mediated by the conserved N-terminal sequence. Indeed, we observed that an HPat protein lacking the N-terminal sequence did not interact with Me31B (Fig. 2 C, lane 10). Conversely, a protein fragment comprising only the conserved N-terminal sequence was sufficient for the interaction with Me31B (Fig. 2 D, lane 9). Thus, the conserved N-terminal sequence represents the Me31B-binding site in HPat.

HPat, EDC3, or Tral assembles with Me31B into distinct protein complexes

Me31B is a DEAD-box helicase and, like all members of this protein family, consists of two RecA-like domains (Fig. 3 A). Previously, we showed that the C-terminal RecA-like domain interacts in a mutually exclusive manner with the FDF motifs of EDC3 and Tral (Tritschler et al., 2008, 2009). Surprisingly, in this study, we could also detect an interaction between the Me31B C-terminal RecA-like domain and full-length HPat (Fig. 3 B, lane 8) or with the HPat conserved N-terminal sequence (Fig. 2 D, lane 12). However, HPat did not interact with EDC3 or Tral (Fig. 1 A), suggesting that HPat, EDC3, and Tral may form mutually exclusive interactions with Me31B.

To investigate this possibility further, we cotransfected S2 cells with mixtures of plasmids encoding three proteins: EDC3 (or Tral), HPat, and Me31B. We used three different mixtures, each containing a plasmid expressing one HA-tagged and two GFP-tagged proteins. We then assayed whether the proteins fused to GFP could be coimmunoprecipitated from cell lysates using anti-HA antibodies. We observed that HA-Me31B coimmunoprecipitated GFP-HPat and -EDC3, showing that Me31B does indeed interact with both proteins (Fig. 3 C, lanes 8–10). In contrast, HA-HPat coimmunoprecipitated GFP-Me31B but not GFP-EDC3 (Fig. 3 D, lanes 8–10), whereas HA-EDC3 coimmunoprecipitated GFP-Me31B but not GFP-HPat (Fig. 3 E, lanes 8–10). Similar results were obtained when EDC3 was substituted by Tral in the co-IP assays (Fig. S2), suggesting that Me31B associates with HPat, Tral, and EDC3 to form distinct protein complexes.

EDC3 competes with HPat for binding to Me31B

The crystal structure of RCK (human Me31B orthologue) in complex with the FDF motif of EDC3 revealed surface residues on RCK (or Me31B) that are critical for the interaction with EDC3 and Tral (Tritschler et al., 2009). To determine whether HPat competes with EDC3 and Tral for this same binding surface, we tested whether an Me31B mutant that does not interact with EDC3 (or Tral) could still bind HPat. Specifically, we took advantage of an Me31B (Mut1) mutated at four surface residues involved in the interaction with the FDF motifs of EDC3 and Tral. We also tested an Me31B mutant (Mut2) that interacts with Tral but not with EDC3 (Tritschler et al., 2009). In IP assays, the two Me31B mutants interacted with HPat (Fig. 4 A, lanes 8–10), whereas Me31B-Mut1 did not interact with EDC3 as expected (Fig. 4 A, lane 12).

Published April 19, 2010

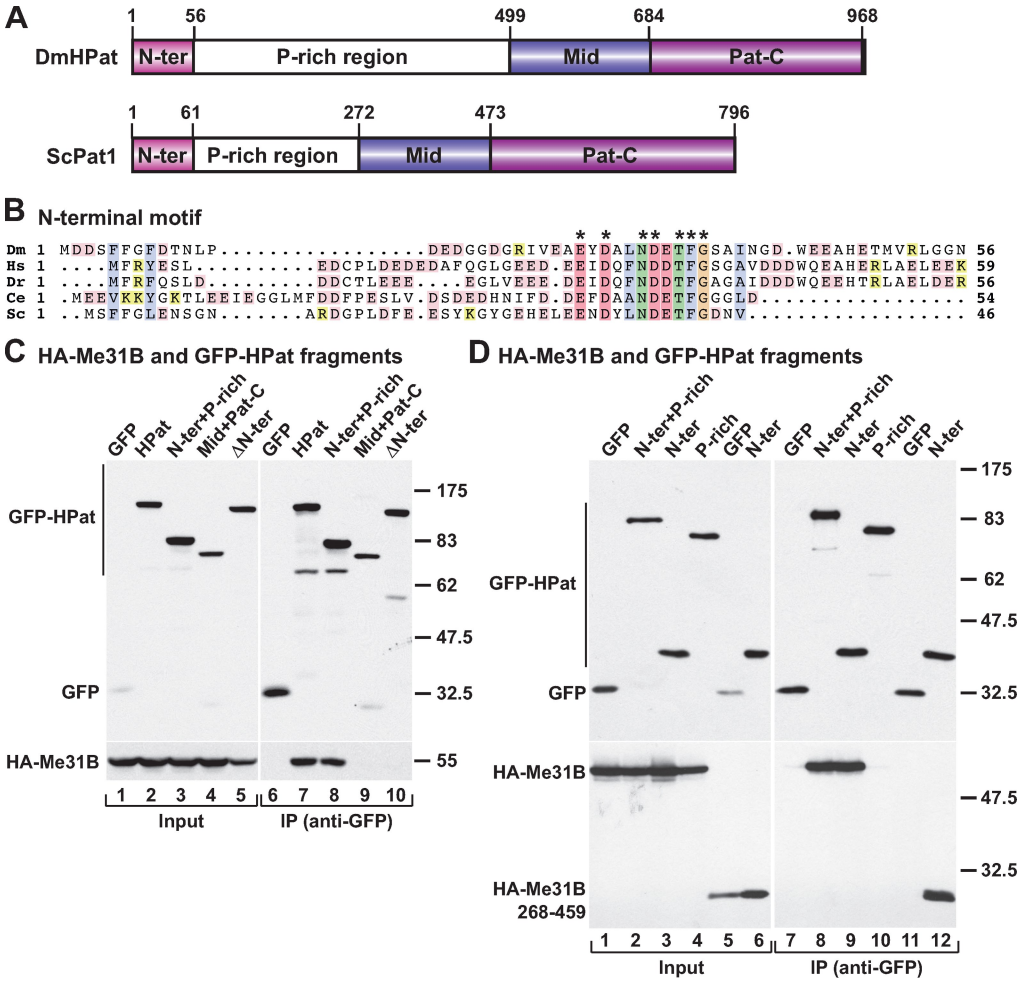

Figure 2. **The N-terminal conserved sequence mediates HPat interaction with Me31B.** (A) Domain organization of HPat. HPat proteins contain a conserved N-terminal (N-ter) sequence, a glutamine/proline-rich region (P-rich), a Mid domain, and Pat-C. Numbers above the protein outline represent amino acid positions at fragment boundaries for the *D. melanogaster* protein. *S. cerevisiae* Pat1 is shown for comparison. (B) Sequence alignment of the N-terminal conserved sequence of Pat1 orthologues from *Homo sapiens* (Hs), *Danio rerio* (Dr), *D. melanogaster* (Dm), *Caenorhabditis elegans* (Ce), and *S. cerevisiae* (Sc). Asterisks indicate invariant residues. Hydrophobic, polar, and acidic residues are shaded in blue, green and magenta, respectively. Glycines are shaded orange. Unconserved acidic and basic residues are shaded light magenta and yellow, respectively. (C and D) Interaction between full-length GFP-HPat or HPat fragments with full-length Me31B or its C-terminal RecA-like domain. Cell lysates were immunoprecipitated and analyzed as described in Fig. 1. Molecular mass is indicated in kilodaltons.

Our results indicate that HPat binds to Me31B via surface residues different than those contacting EDC3 (or Tral); yet, the Me31B interaction with HPat and EDC3 (or Tral) appears to be mutually exclusive, suggesting that the binding surfaces partially overlap. Alternatively, EDC3 (or Tral) may interfere with HPat binding as the result of steric hindrance.

To further investigate whether EDC3, Tral, and HPat form mutually exclusive interactions with Me31B, we performed competition assays. In these assays, we tested whether a peptide containing the Me31B-binding domain of EDC3 (i.e., the FDF motif) competed with HPat for binding to Me31B when added to cell lysates before IP. Indeed, the peptide did interfere with HPat binding to Me31B, as expected for a mutually exclusive interaction (Fig. 4 B, lanes 9 and 10). As a control, we tested the corresponding peptide carrying alanine substitutions of the phenylalanine residues in the EDC3-FDF motif (ADA peptide); this peptide no longer binds Me31B and had no effect (Fig. 4 B, lanes 11 and 12; Tritschler et al., 2009). Because the EDC3-FDF peptide also competes with Tral for binding to Me31B (Tritschler et al., 2009), we conclude that HPat, EDC3, and Tral interact with Me31B in a mutually exclusive manner.

The Mid domain of HPat confers interaction with the LSm1–7 complex

Next, we tested which HPat domains can interact with LSm1 and DCP2. We observed that a fragment of HPat containing the Mid domain plus Pat-C (residues 500–968) was necessary and sufficient to interact with both LSm1 and DCP2 (Fig. 5, A–D). When the Mid domain and Pat-C were tested individually, we observed that both LSm1 and DCP2 interacted with the Mid domain but not with Pat-C (Fig. 5, B and D). However, the interaction of DCP2 with the Mid domain was less efficient than with the fragment also containing Pat-C, suggesting that Pat-C contributes to DCP2 binding. These results, together with the observation that DCP2 does not interact with LSm1 (Fig. S1 D), suggest that DCP2 binds HPat independently of the LSm1–7 ring.

Published April 19, 2010

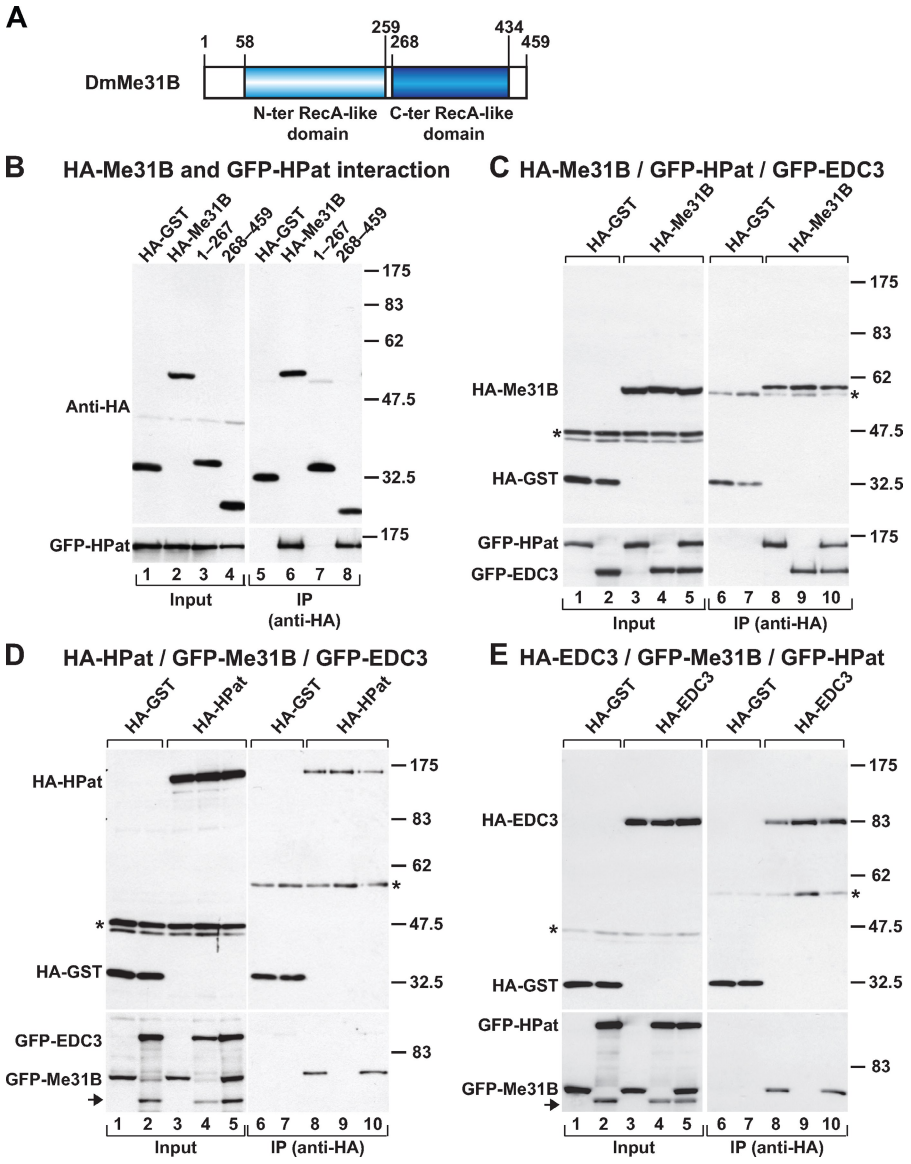

Figure 3. **HPat interacts with the C-terminal RecA-like domain of Me31B.** (A) Me31B consists of two RecA-like domains. Numbers above the protein outline represent amino acid positions at fragment boundaries for the *D. melanogaster* protein. N-ter, N-terminal; C-ter, C-terminal. (B) HA-tagged Me31B or the indicated Me31B protein fragments were coexpressed in S2 cells with GFP-HPat. Cell lysates were immunoprecipitated and analyzed as described in Fig. 1. (C–E) S2 cells were cotransfected with mixtures of three plasmids. In C, the plasmids encoded HA-Me31B, GFP-HPat, and GFP-EDC3; in D, the plasmids encoded HA-HPat, GFP-Me31B, and GFP-EDC3; in E, the mixture consisted of HA-EDC3, GFP-Me31B, and GFP-HPat. In all panels, HA-GST served as a negative control. Cell lysates were immunoprecipitated and analyzed as described in Fig. 1. Arrows indicate EDC3 or HPat protein degradation fragments. Asterisks indicate cross-reactivity of the primary antibodies with an endogenous protein (input panels) or of the secondary antibody with the immunoglobulin heavy chain (IP panels). (B–E) Molecular mass is indicated in kilodaltons.

The proline-rich region is required for P-body localization

HPat localizes to P bodies both in *S. cerevisiae* and in metazoa and is required for P-body integrity (Eulalio et al., 2007a,b; Parker and Sheth, 2007). This localization does not appear to be affected by a GFP tag (Fig. 6 A). Therefore, we sought to define which interactions are critical for HPat accumulation in P bodies by examining where HPat fragments localize. A fragment of HPat comprising the N-terminal conserved sequence and the proline-rich region localized to P bodies in 37% of the cell population (Fig. 6 B), whereas a fragment comprising the Mid domain and Pat-C, which interacts with DCP2 and the LSm1–7 ring, dispersed throughout the cytoplasm (Fig. 6 C). This suggests that the N-terminal fragment retains the ability to localize to P bodies, although not as efficiently as full-length HPat, which localized to P bodies in 87% of the cell population (Fig. 6 A).

We next investigated whether the N-terminal conserved sequence or the proline-rich region were sufficient for P-body localization. A GFP fusion of the HPat N-terminal sequence, which interacts with Me31B, spread throughout the cell (Fig. 6 D). Moreover, when overexpressed, this protein fusion affected the integrity of endogenous P bodies, significantly reducing them in number and size (Fig. 6 D). In contrast, the proline-rich region accumulated in P bodies in 47% of the cells (Fig. 6 E), suggesting that the proline-rich region is sufficient for P-body localization. In line with this interpretation, we found that an HPat mutant lacking the proline-rich region was evenly distributed throughout the cell (Fig. 6 F). Furthermore, the overexpression of this mutant affected the integrity of endogenous P bodies in a dominant-negative manner. We conclude that the proline-rich region of HPat plays a critical role in maintaining P-body integrity and promoting HPat accumulation in P bodies.

HPat promotes degradation of bound mRNAs

To better understand the function of HPat in decapping, we investigated whether binding of HPat to an mRNA was sufficient to promote degradation. To this end, we made use of the tethering

Published April 19, 2010

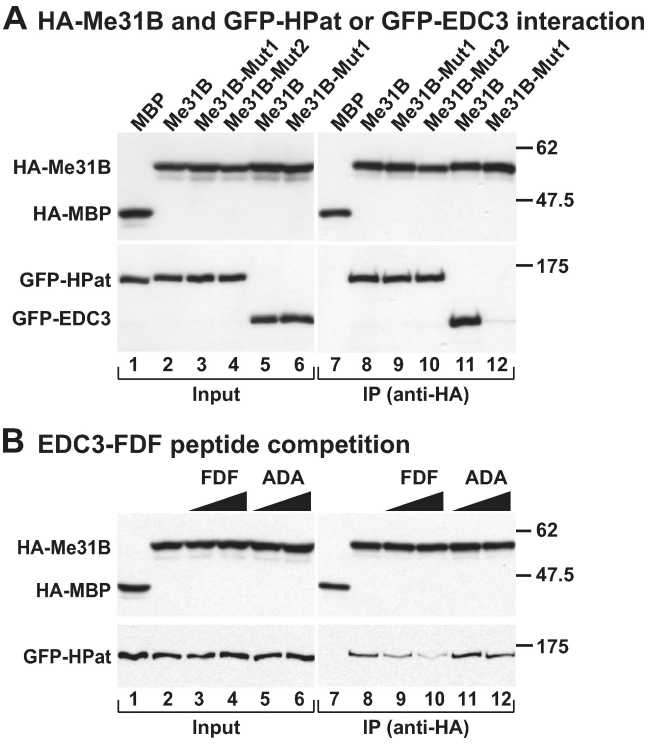

Figure 4. **Me31B establishes mutually exclusive interactions with HPat, EDC3, and Tral.** (A) HA-tagged Me31B or the indicated Me31B mutants were coexpressed in S2 cells with GFP-HPat or -EDC3. Cell lysates were immunoprecipitated and analyzed as described in Fig. 1. Me31B mutants carry alanine substitutions of the following residues: Gln281, His284, Tyr288, and Lys292 (Mut1) or Phe405, His408, Glu411, and Lys412 (Mut2). (B) HA-MBP or -Me31B was coexpressed with GFP-HPat in S2 cells. Cell lysates were immunoprecipitated using a monoclonal anti-HA antibody. In lanes 3–6 and 9–12, increasing amounts (5 and 20 µg) of purified recombinant EDC3-FDF peptide or of the corresponding ADA mutant were added to the cell lysates before IP as indicated. (A and B) Molecular mass is indicated in kilodaltons.

assay previously described (Gehring et al., 2005). This assay involves the expression of λN fusion proteins that bind with high affinity to five BoxB hairpins (5BoxB) in the 3′ untranslated region of a firefly luciferase (F-Luc) reporter mRNA (F-Luc–5BoxB reporter).

S2 cells were transiently transfected with the F-Luc–5BoxB reporter, a plasmid expressing HPat fused to the λN-HA peptide, and a plasmid encoding *Renilla* luciferase (R-Luc). As negative control, we used an inactive mutant of the Argonaute-1 protein (AGO1-F2V2) because this protein is comparable in size with HPat. Relative to cells expressing the AGO1-F2V2 mutant, tethered λN-HA–HPat reduced F-Luc activity 2.5-fold (Fig. 7 A). A stronger inhibitory effect was observed for GW182, which served as a positive control (Fig. 7 A; Behm-Ansmant et al., 2006).

To determine whether HPat inhibits F-Luc activity by repressing translation directly or indirectly by reducing mRNA levels, we analyzed by Northern blot the steady-state levels of the F-Luc–5BoxB mRNA. We found that λN-HA–HPat partially reduced reporter mRNA (Fig. 7, A and B [lane 3]) at a level that fully accounted for the decrease of F-Luc activity (Fig. 7 A, black vs. gray bars). HPat did not affect the expression of an F-Luc reporter lacking the BoxB elements (Fig. S1 E). Together, these results indicate that HPat directs bound mRNAs to degradation.

The proline-rich region is required for HPat to degrade bound mRNAs

We next performed tethering assays using the aforementioned HPat deletion mutants. We observed that deleting the conserved N-terminal sequence, which interacts with Me31B, reduced HPat activity in the tethering assay (Fig. 7 A, ΔN-ter). In contrast, HPat mutants lacking either the Mid domain or Pat-C individually or simultaneously (Fig. 7, A and B, N-ter+P-rich) were fully active.

Unexpectedly, deleting the proline-rich region abolished HPat activity (Fig. 7, A and B, ΔP-rich). Conversely, the proline-rich region alone was more active than full-length HPat (Fig. 7, A and B, P-rich). All proteins were expressed at comparable levels (Fig. 7 C). We conclude that the proline-rich region is both necessary and sufficient to trigger degradation of bound mRNAs.

HPat triggers deadenylation and decapping

Given the role of HPat and orthologues in mRNA decapping, we next tested whether HPat-mediated mRNA degradation required the activity of decapping activators. To this end, we performed the tethering assay in cells codepleted of two decapping activators, DCP1 and EDC4. In such cells, decapping was efficiently inhibited, blocking mRNA degradation caused by tethered GW182 (Fig. 7, D and E [lane 2 vs. lane 1]). The accumulated transcripts were shorter, which is consistent with the observation that GW182 triggers mRNA deadenylation (Behm-Ansmant et al., 2006). We confirmed that these transcripts lack a poly(A) tail by oligo (dT)–targeted RNase H cleavage (Fig. 7 F). Specifically, in cells expressing λN-HA–AGO1-F2V2, both the F-Luc reporter and the endogenous rp49 mRNA (encoding ribosomal protein L32) migrated faster after oligo (dT)–directed RNase H cleavage had removed the poly(A) tail (Fig. 7 F, lane 2 vs. lane 1). In contrast, in cells expressing λN-HA–GW182, RNase H treatment did not affect F-Luc reporter mobility, indicating that it was already deadenylated (Fig. 7 F, lane 4 vs. lane 3).

Codepletion of DCP1 and EDC4 also prevented HPat-mediated degradation of the reporter, which accumulated both in the poly- and deadenylated form (Fig. 7, E [lane 3] and F [lane 6 vs. lane 5]). The polyadenylated form corresponded to the fraction of the mRNA that was not degraded by HPat (Fig. 7 B, lane 3). The accumulation of the deadenylated form indicates that HPat promotes deadenylation. This finding might explain why luciferase activity is not restored despite restoration of mRNA levels (Fig. 7 D) because deadenylated transcripts are translated less efficiently. Similar results were obtained for all HPat fragments containing the proline-rich region (Fig. 7, D and E).

We could not analyze the effect of codepleting DCP1 and EDC4 in cells expressing two HPat fragments (N-ter+P-rich and P-rich) because overexpressing these fragments had cytotoxic effects (i.e., low recovery of transfected cells). This was not observed in control cells, suggesting that in the background

Published April 19, 2010

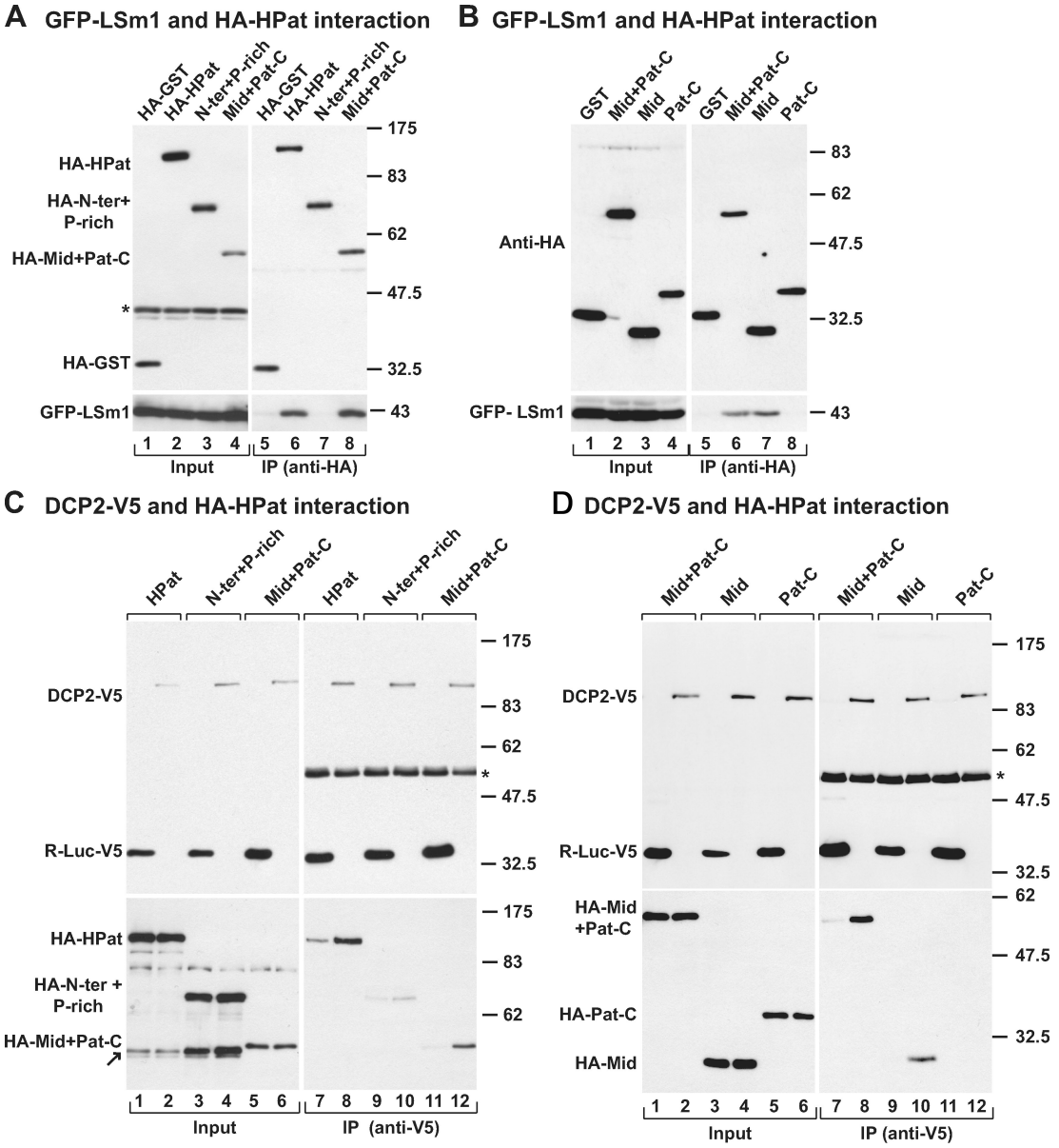

Figure 5. **The Mid domain and Pat-C interact with DCP2 and the LSm1–7 complex.** (A–D) Interaction between full-length HPat or HPat fragments with GFP-LSm1 or DCP2-V5. Protein interactions were analyzed as described in Fig. 1. Asterisks indicate cross-reactivity of the anti-HA antibody with an endogenous protein (input panels) or of the V5 antibody with the immunoglobulin heavy chain (IP panels). Note that in C, a degradation product arising from full-length HPat, an HPat fragment containing the N-terminal (N-ter) and proline-rich (P-rich) regions (in lanes 1–4), and the fragment containing the Mid domain and Pat-C (lanes 5 and 6) have a similar mobility (arrow). Molecular mass is indicated in kilodaltons.

of the double DCP1–EDC4 knockdown, these protein fragments are toxic.

To further demonstrate that HPat triggers deadenylation followed by decapping, we performed two independent experiments. First, we examined the F-Luc–5BoxB mRNA in cells expressing a dominant-negative mutant of DCP2 that strongly inhibits decapping in S2 cells partially depleted of endogenous DCP2. Again, in the presence of GW182 or HPat, the reporter accumulated in the deadenylated form, co-migrating with an F-Luc–5BoxB transcript lacking the poly(A) tail (Fig. 7 H).

In the second experiment, we exposed transfected cells to actinomycin D to inhibit transcription and then analyzed the levels of F-Luc–5BoxB mRNA over time (as compared with the long-lived rp49 mRNA, which has a half-life >8 h). In cells expressing the AGO1-F2V2 mutant, the half-life of F-Luc–5BoxB mRNA was ∼2 h, whereas in cells expressing λN-HPat or the proline-rich region, the half-life of this mRNA was ∼40 min or 10 min, respectively (Fig. 7 I). Importantly, in cells expressing HPat or the proline-rich region, the F-Luc–5BoxB transcripts accumulating 15–90 min after adding actinomycin D were deadenylated (Fig. 7 I). These results further demonstrate that HPat-mediated decay is initiated by deadenylation. Collectively, our results indicate that HPat triggers deadenylation followed by decapping of bound mRNAs and that these activities reside in the proline-rich region.

Published April 19, 2010

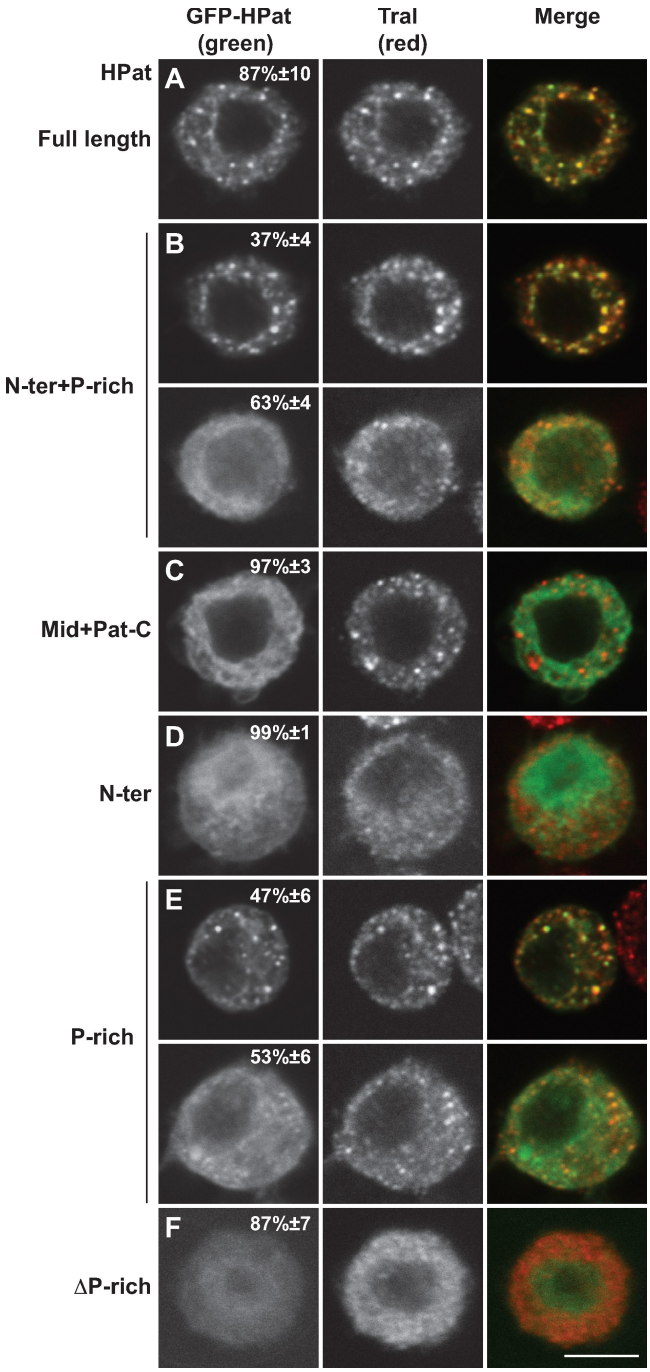

Figure 6. **The proline-rich region is required for HPat accumulation in P bodies.** (A–F) Confocal fluorescent micrographs of fixed S2 cells expressing GFP-tagged fusions of full-length HPat or the protein fragments indicated on the left. Cells were stained with affinity-purified anti-Tral antibodies. The merged images show the GFP signal in green and the Tral signal in red. The fraction of cells exhibiting a staining identical to that shown in the representative panel was determined by scoring at least 100 cells per transfection in three independent transfections performed per protein. Mean values ± standard deviations are shown. N-ter, N-terminal; P-rich, proline-rich. Bar, 5 µm.

HPat interacts with components of the CCR4–NOT deadenylase complex

The finding that HPat triggers deadenylation followed by decapping of bound mRNA suggests that HPat interacts with components of the deadenylase complex. Accordingly, we observed that HPat coimmunoprecipitated components of the CCR4–NOT complex (including POP2, CCR4, NOT2, NOT3/5, and NOT4) in an RNA-independent manner (Fig. 8 A). These results suggest that HPat acts as an adaptor molecule, bridging the interaction between the deadenylation and decapping machineries. However, it is important to note that HPat is not required for deadenylation per se because depleting HPat causes deadenylated mRNAs to accumulate. Thus, in the absence of HPat, only decapping but not deadenylation is inhibited (Fig. 9; Eulalio et al., 2007c), which is in agreement with the results reported previously in yeast (Bouveret et al., 2000; He and Parker, 2001; Tharun and Parker, 2001).

To define the domains of HPat required for the interaction with CCR4–NOT deadenylase complex components, we performed co-IP assays with the aforementioned protein fragments. We observed that the Mid domain was both necessary and sufficient for HPat to interact with CCR4 (Fig. 8, B and C).

The Mid domain and Pat-C are required for decapping in vivo

The tethering assay allows functional domains to be identified once HPat is artificially tethered to an mRNA, but additional domains may also be essential for HPat function because they mediate target binding. To further investigate the requirement for HPat domains in decapping, we established a complementation assay in which endogenous HPat was depleted using a double-stranded RNA (dsRNA) targeting HPat ORF. HPat fragments were then tested for their ability to restore decapping in HPat-depleted cells. Transcripts encoding the recombinant proteins were made resistant to the dsRNA by introducing mutations that disrupt base pair interactions with the dsRNA without altering the protein sequence.

To monitor decapping, we used the F-Luc–5BoxB reporter tethered to GW182. The GW182 triggers deadenylation of the F-Luc–5BoxB reporter, which is then decapped, and subsequently, the mRNA body is digested exonucleolytically (Fig. 7; Behm-Ansmant et al., 2006). Inhibiting decapping prevents mRNA degradation by GW182, and so deadenylated decay intermediates accumulate (Fig. 7 E, lane 2 vs. lane 1). Therefore, the accumulation of the deadenylated F-Luc–5BoxB mRNA reflects a block in decapping.

As shown in Fig. 9 A, tethered λN-HA–GW182 reduces mRNA levels threefold relative to that measured in cells expressing the λN-HA peptide alone. Depleting HPat did not significantly restore reporter mRNA levels (unpublished data). This result was expected because we previously showed that at least two decapping activators must be codepleted in S2 cells to inhibit decapping (Eulalio et al., 2007c).

We then tested whether we could inhibit decapping of the F-Luc–5BoxB reporter in cells depleted of HPat plus EDC4, DCP1, or Me31B and whether decapping could be restored by expressing a dsRNA-resistant form of HPat. To our surprise, although all combinations inhibited decapping, the dsRNA-resistant form of HPat restored decapping only in cells co-depleted of HPat and Me31B (Fig. 9 B, lane 4 vs. lane 2). These observations indicate that, in this context and/or for this reporter, the HPat–Me31B interaction is dispensable for decapping.

Published April 19, 2010

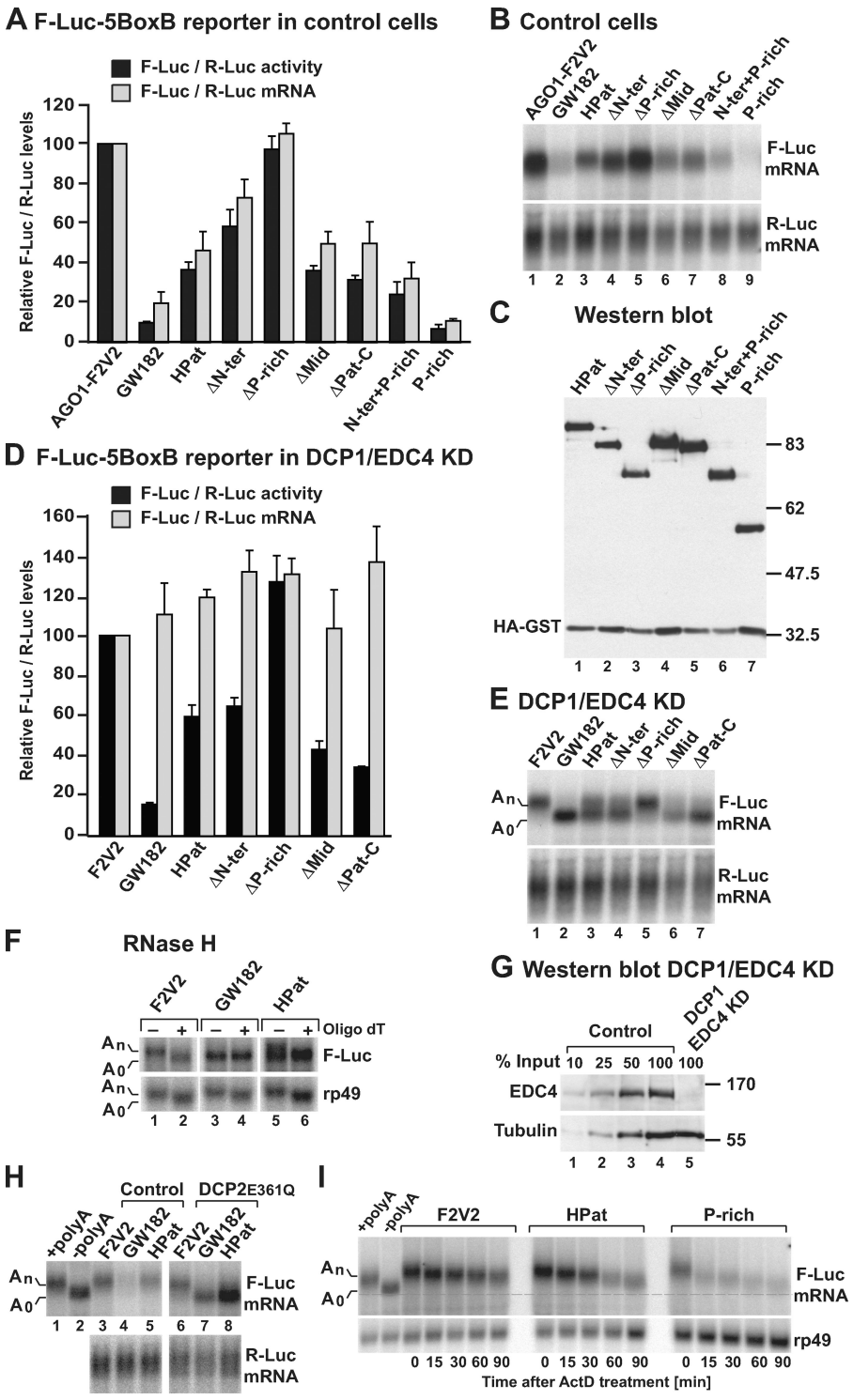

Figure 7. **HPat triggers deadenylation and decapping of bound mRNAs.** (A–F) Control S2 cells (treated with GFP dsRNA) or cells codepleted of DCP1 and EDC4 were transfected with a mixture of three plasmids, one expressing the F-Luc–5BoxB reporter, another expressing R-Luc, and a third expressing λN-HA–AGO1-F2V2 (negative control) or λN-HA fusions of wild-type HPat or fragments, as indicated. F-Luc activity and mRNA levels were normalized to those of the *Renilla* and set to 100 in cells expressing λN-HA–AGO1-F2V2. Mean values ± standard deviations from three independent experiments are shown. B and E show Northern blot analysis of representative RNA samples shown in A and D, respectively. (C) Full-length HPat and fragments were expressed at comparable levels. (F) RNA samples shown in E (lanes 1–3) were treated with RNase H in the absence or presence of oligo (dT) and analyzed by Northern blot. rp49 mRNA served as a positive control for the RNase H treatment. (G) Western blot analysis of control and DCP1–EDC4-depleted cell lysates. α-Tubulin served as a loading control. KD, knockdown. (C and G) Molecular mass is indicated in kilodaltons. (H) Tethering assay in cells expressing a dominant-negative mutant of DCP2 (E361Q). In lanes 1 and 2, samples isolated from cells expressing poly- and unadenylated F-Luc–5BoxB mRNA served as size markers. (I) S2 cells were transfected as described in A. 3 d after transfection, cells were treated with 5 µg/ml actinomycin D (ActD) and harvested at the indicated time points. The dashed line indicates the position of the deadenylated decay intermediate. N-ter, N-terminal; P-rich, proline-rich.

We next tested whether HPat mutants could restore reporter mRNA degradation in the background of the double Me31B–HPat knockdown. Here, the HPat mutant lacking the Me31B-binding sequence restored mRNA degradation (Fig. 9 B, lane 6), which is consistent with a study in *S. cerevisiae* showing that deleting the N-terminal sequence of Pat1 only modestly affects decapping (Pilkington and Parker, 2008).

Unlike results obtained in yeast (Pilkington and Parker, 2008), in our experiments, mRNA degradation was not restored by HPat mutants lacking Pat-C alone or in combination with the Mid domain, indicating that Pat-C is also required for decapping in vivo (Fig. 9, B [lanes 12 and 14] and C). Moreover, deleting the proline-rich region or the Mid domain also impaired decapping (Fig. 9, B [lanes 8 and 10] and C). Finally, expressing the proline-rich region alone was not sufficient to restore decapping (Fig. 9, B [lane 16] and C). All proteins were expressed at comparable levels and had no dominant-negative effects when expressed in control cells (Fig. 9, A and E). Thus, with the

Published April 19, 2010

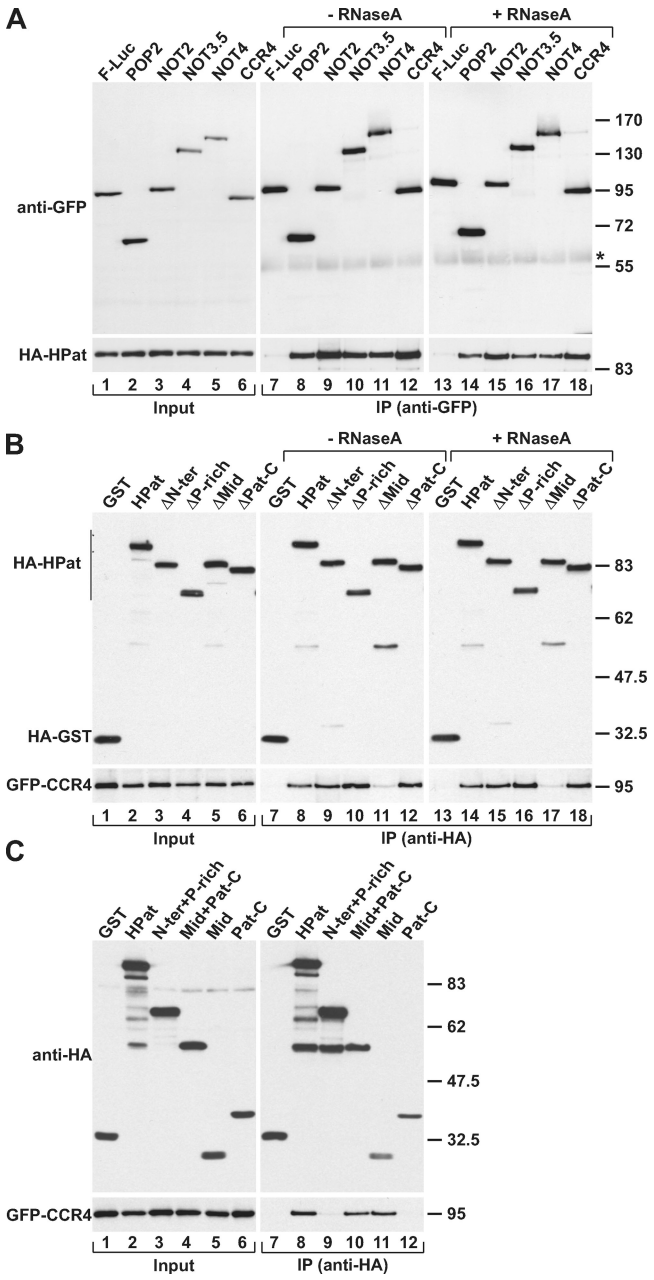

Figure 8. **HPat interacts with components of the CCR4–NOT complex.** (A–C) Interaction between HA-HPat wild type or mutants and GFP-tagged components of the CCR4–NOT complex. In lanes 13–18 of A and B, cell lysates were treated with RNase A before IP. F-Luc–GFP (A) or HA-GST (B and C) served as negative controls. The asterisk indicates cross-reactivity of the secondary antibody with the immunoglobin heavy chain. Molecular mass is indicated in kilodaltons. N-ter, N-terminal; P-rich, proline-rich.

exception of the N-terminal sequence, all domains of HPat contribute to decapping in vivo.

HPat recruitment to mRNAs is mediated by the Mid domain and Pat-C

The Mid domain and Pat-C were not required for HPat to promote mRNA degradation in tethering assays but were required for decapping in complementation assays, so we speculate that these domains contribute to target mRNA binding. To investigate this possibility, we confirmed and extended, for HPat, previous studies showing that wild-type Pat1 coimmunoprecipitates a variety of yeast mRNAs (Tharun et al., 2000; Tharun and Parker, 2001). We used real-time quantitative RT-PCR (RT-qPCR) to analyze the levels of an F-Luc mRNA reporter coimmunoprecipitating with HPat and observed that HA-HPat coimmunoprecipitated the F-Luc reporter 10-fold more efficiently than did HA-GST, which served as a background control for the IPs (Fig. 10 A). Furthermore, an HPat mutant lacking Pat-C was partially impaired in the association with the reporter mRNA, whereas deleting the Mid domain abolished association with the F-Luc mRNA (Fig. 10 A). All proteins were present in the immunoprecipitates at comparable levels (Fig. 10 B). Thus, the Mid domain, which interacts with the LSm1–7 ring, CCR4, and DCP2, is required for HPat recruitment to mRNAs. This activity is likely stimulated by the contribution of Pat-C.

In yeast, Pat1 has been reported to associate with mRNAs via LSm1-dependent and -independent mechanisms and to exhibit RNA-binding activity (Tharun and Parker, 2001; Pilkington and Parker, 2008). Accordingly, we observed that HPat association with the F-Luc reporter was not affected in cells depleted of LSm1 (Fig. 10, A and B). These results suggest that HPat could be recruited to mRNA targets via a redundant mechanism, including the interaction with the deadenylase complex, the interaction with the LSm1–7 ring, or direct RNA binding.

Discussion

Decapping of eukaryotic mRNAs depends on prior deadenylation, which ensures that functional, polyadenylated mRNAs are not decapped prematurely. However, little is known regarding the mechanisms that promote decapping of deadenylated mRNAs in vivo. In this study, we show that the protein HPat coimmunoprecipitates with decapping factors, including DCP2, Me31B, and the LSm1–7 ring as well as components of the CCR4–NOT deadenylase complex. These findings suggest that HPat acts as a bridging factor between the deadenylation and decapping machineries. Furthermore, the HPat proline-rich region is necessary and sufficient to trigger deadenylation and decapping of bound mRNAs. However, in addition to the proline-rich region, both the Mid domain and Pat-C are required to restore decapping in cells depleted of endogenous HPat. Finally, we show that the Mid domain and Pat-C are required for HPat recruitment to mRNAs. Therefore, our work suggests a model whereby HPat associates with mRNAs undergoing deadenylation via interactions with the deadenylase complex or the LSm1–7 ring; subsequently, HPat recruits decapping factors, thereby committing deadenylated mRNAs to degradation through the 5′ to 3′ mRNA decay pathway.

HPat interacts with decapping activators and the CCR4–NOT deadenylase complex

In this study, we show that in *D. melanogaster* cells, HPat coimmunoprecipitates Me31B, DCP2, the LSm1–7 ring, and components of the CCR4–NOT deadenylase complex (Fig. 10 C). We mapped the domains on HPat that mediate these interactions

Published April 19, 2010

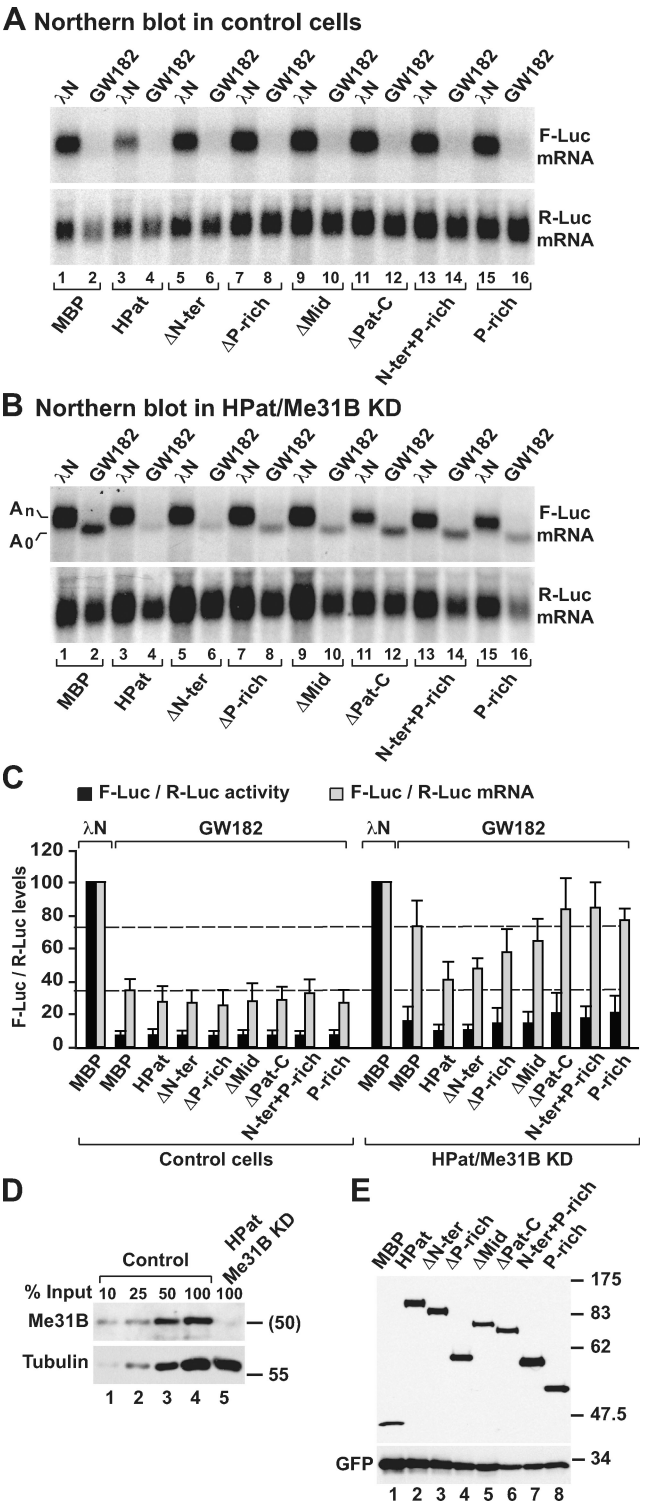

Figure 9. **Complementation assay.** (A–E) Control S2 cells (treated with GFP dsRNA) or cells codepleted of HPat and Me31B were cotransfected with a mixture of three plasmids, one expressing the F-Luc–5BoxB reporter, another expressing λN-HA–GW182 or the λN-HA peptide, and a third expressing R-Luc. Plasmids (5 ng) expressing HA-MBP, wild-type HA-HPat, or fragments (lacking the λN tag) were included in the transfection mixtures, as indicated. RNA samples were analyzed by Northern blot. (C) F-Luc activity and mRNA levels were normalized to that of the R-Luc. For each condition, the normalized values of F-Luc activity and mRNA levels were set to 100 in control cells expressing the λN-HA peptide and HA-MBP. Mean values ± standard deviations from three independent experiments are shown. Dashed lines indicate F-Luc–5BoxB mRNA levels in cells expressing MBP and GW182. (D) Western blot analysis of control and HPat–Me31B-depleted cell lysates. α-Tubulin served as a loading control. (E) Full-length HPat and fragments were expressed at comparable levels. (D and E) Molecular mass is indicated in kilodaltons. KD, knockdown; N-ter, N-terminal; P-rich, proline-rich.

and showed that the Mid domain is required for HPat to interact with CCR4 and the LSm1–7 ring. Similarly, in *S. cerevisiae*, the corresponding region of Pat1 confers binding to the LSm1–7 ring (Pilkington and Parker, 2008). Moreover, the Mid domain cooperates with Pat-C to mediate DCP2 binding, suggesting that DCP2 binds HPat independently of the LSm1–7 ring. Future experiments will unravel whether HPat binds decapping and deadenylation factors simultaneously or consecutively and whether these interactions are direct.

We also show that a conserved N-terminal sequence of HPat interacts with the C-terminal RecA-like domain of Me31B. Surprisingly, this conserved sequence is dispensable for HPat activity in complementation assays, suggesting that mRNAs targeted for GW182-dependent degradation are efficiently decapped even when HPat and Me31B do not interact directly. However, the HPat–Me31B interaction may play a role in decapping mRNAs degraded by pathways distinct from the microRNA pathway.

An important observation is that HPat also interacted with components of the CCR4–NOT deadenylase complex. Because HPat is not required for deadenylation per se (Eulalio et al., 2007c; this study), an interaction with the CCR4–NOT complex most likely plays a role in recruiting HPat to mRNAs undergoing deadenylation, providing a mechanism to couple decapping to the removal of the mRNA poly(A) tail.

Me31B is part of at least three distinct protein complexes

Previously, we showed that Me31B interacts with EDC3 and Tral to form distinct protein complexes (Tritschler et al., 2009). This study shows that a third complex exists, consisting minimally of Me31B, HPat, and the LSm1–7 ring. The interaction between Me31B and HPat is also detected in yeast (Coller et al., 2001; Fischer and Weis, 2002); however, our study revealed that EDC3, Tral, and HPat compete for binding to Me31B. Thus, Me31B establishes mutually exclusive interactions with EDC3, Tral, and HPat. The ability of Me31B and orthologues to establish mutually exclusive interactions with multiple partners provides a mechanistic explanation for the myriad functions performed by this protein and further supports the idea that Me31B and its orthologues act as remodeling subunits in diverse protein complexes (Tritschler et al., 2009). The role of these complexes in posttranscriptional mRNA regulation (e.g., decapping or translational repression) is specified by the additional components.

The proline-rich region is required for P-body assembly and mRNA decapping

In this study, we show that the proline-rich region of HPat promotes deadenylation and decapping of bound RNAs and is required for P-body localization, indicating that this region

Published April 19, 2010

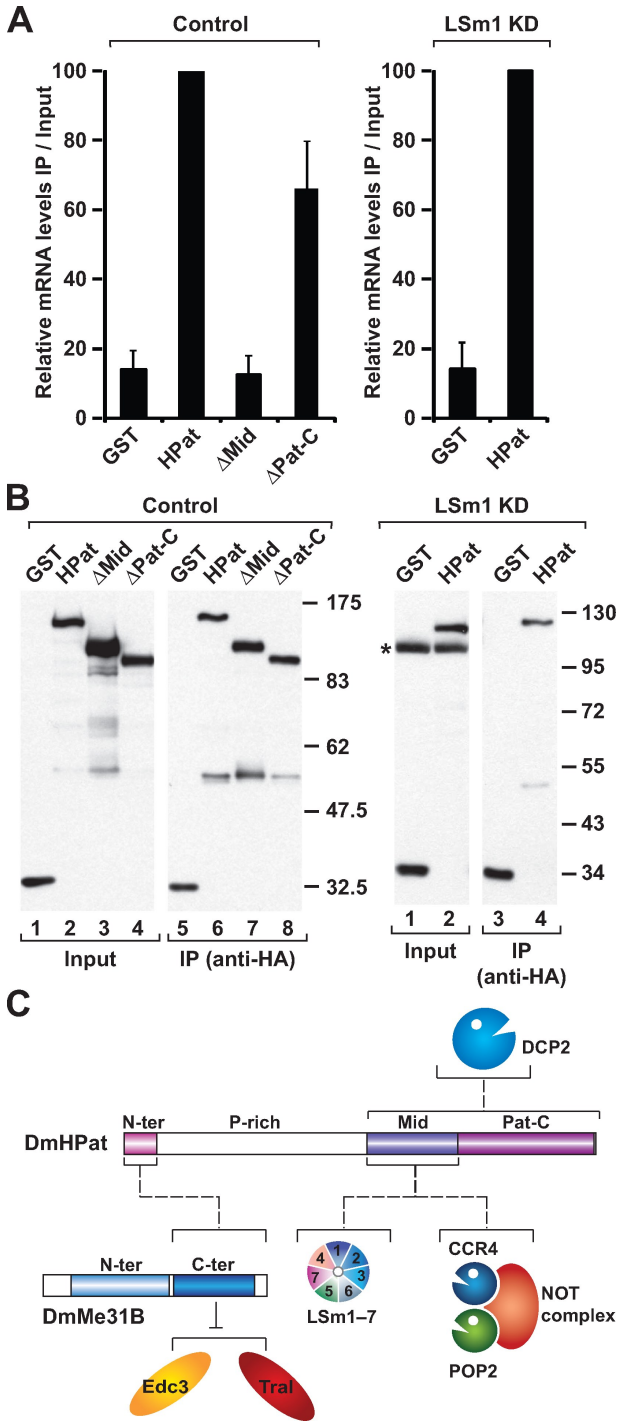

Figure 10. **The Mid domain is required for HPat recruitment to mRNA targets.** (A) Control or LSm1-depleted S2 cells were transfected with a mixture of three plasmids, one expressing an F-Luc reporter, another expressing HA-GST, wild-type HA-HPat, or mutants, and a third plasmid expressing R-Luc. Cell lysates were immunoprecipitated using an anti-HA antibody. The levels of the F-Luc reporter in the immunoprecipitates (IP) were analyzed by RT-qPCR and normalized to the corresponding input sample. Mean values ± standard deviations from four independent experiments are shown. (B) The efficacy of the IPs was examined by Western blotting. Molecular mass is indicated in kilodaltons. (C) Schematic model summarizing the protein interactions described in this study. KD, knockdown; N-ter, N-terminal; P-rich, proline-rich.

interacts with additional components of the mRNA decay pathway. However, in IP assays, the proline-rich region was dispensable for HPat interaction with decapping factors or deadenylase complex components, suggesting that the binding partners of this region remain to be identified.

How can a proline-rich region mediate such diverse activities? Proline residues could play a structural role by keeping this region in an extended conformation, rendering short sequence motifs accessible for interaction with protein partners. In addition, proline-rich regions can also provide multiple, nonspecific binding sites for protein–protein interactions, thereby contributing to the assembly of multiprotein complexes (Williamson, 1994).

P-body components often contain low-complexity Q/N-rich regions proposed to facilitate P-body formation via self-association or association with Q/N-rich domains on other proteins (Decker et al., 2007; Mazzoni et al., 2007; Reijns et al., 2008). These regions are often rich in proline in addition to or instead of glutamine. The region of *D. melanogaster* HPat required for P-body localization is rich in proline and glutamine; however, the length and composition of this region varies among Pat1 orthologues from different species, suggesting that the physical interactions between decapping activators that are critical for P-body localization may not be conserved. This view is supported by evidence from *S. cerevisiae* in which Pat-C but not the proline-rich region is required for Pat1 to accumulate in P bodies (Pilkington and Parker, 2008).

The Mid domain is required for HPat binding to mRNAs

In addition to the proline-rich region, we show that the Mid domain and Pat-C are required to restore decapping in cells depleted of endogenous HPat. However, the Mid domain and Pat-C are dispensable for mRNA degradation when HPat is artificially tethered to an mRNA. One possible explanation for this difference is that the reporters used in these assays are decapped through distinct mechanisms. An alternative but not mutually exclusive explanation is that the Mid domain and Pat-C play a role in target binding and therefore are no longer required once HPat is tethered to an mRNA. Consistent with this second possibility, we show that the Mid domain is essential for HPat to associate with mRNAs. The Mid domain may interact with mRNAs indirectly, via the LSm1–7 ring, as shown in yeast (Tharun and Parker, 2001; Chowdhury and Tharun, 2008, 2009). However, our results indicate that HPat can associate with mRNAs in LSm1-depleted cells, suggesting that HPat binds RNA either directly or through other interacting partners (e.g., the CCR4–NOT complex). In agreement with this, in *S. cerevisiae*, both the Mid domain and Pat-C exhibit RNA-binding activity (Pilkington and Parker, 2008).

What role might the Pat-C domain play in decapping? In *S. cerevisiae*, it exhibits RNA-binding activity. Accordingly, in *D. melanogaster* S2 cells, this domain contributes to target mRNA binding. However, the absolute requirement for this domain in complementation assays suggests that it may have additional functions in mRNA decapping.

Published April 19, 2010

A role for HPat in mediating the deadenylation dependence of decapping

Our findings suggest that in vivo HPat facilitates the deadenylation dependence of decapping. Several lines of evidence support this assertion. First, HPat may be preferentially recruited to deadenylated mRNAs because it associates with the LSm1–7 ring, a protein complex which binds oligoadenylated mRNAs preferentially (Tharun and Parker, 2001; Chowdhury and Tharun, 2008, 2009). In addition, we found that components of the deadenylase complex interact with HPat, suggesting that HPat is recruited to mRNAs actively undergoing deadenylation. Once recruited, the association between HPat and decapping factors will promote the assembly of decapping complexes in cis, committing deadenylated mRNAs to degradation via the 5′ to 3′ mRNA decay pathway.

Materials and methods

DNA constructs

Luciferase reporters and plasmids for the expression of GFP- or λN-HA–tagged cDNAs encoding full-length AGO1-F2V2, DCP1, DCP2, EDC3, EDC4, GW182, LSm1, LSm3, LSm7, Me31B, and Tral were described previously (Eulalio et al., 2007b; Tritschler et al., 2007, 2008, 2009). A plasmid for the expression of HA-XRN1 was obtained by inserting the XRN1 ORF into the Not1 and Xba1 sites of pAc5.1–λN-HA vector. A plasmid for the expression of DCP2-V5 was obtained by inserting the DCP2 ORF into the EcoRV and Xho1 sites of pAc5.1A, in frame with the V5 epitope. Plasmids for the expression of HA- or GFP-tagged HPat were obtained by inserting the HPat ORF into the EcoRV and Not1 sites of pAc5.1–λN-HA and pAc5.1-EGFP vectors. HPat fragments were cloned into the pAc5.1–λN-HA and pAc5.1-EGFP vectors. For the complementation assay shown in Fig. 9, the λN tag was deleted, and cDNAs were made resistant to HPat dsRNA, which targets mRNA sequences encoding aa 743–968 of HPat. Plasmids for the expression of deadenylase complex components were obtained by inserting the corresponding cDNAs in the pAc5.1–λN-EGFP vector using the restriction sites EcoRV–Not1 (POP2, which is related to CAF1), EcoR1–Not1 (CCR4), HindIII–XbaI (NOT2), HindIII–Not1 (NOT3/5), and XhoI–BstBI (NOT4).

Co-IP assays, Western blotting, and fluorescence microscopy

Transfections were performed in 6-well dishes using Effectene transfection reagent (QIAGEN). Protein co-IPs, Western blotting, and immunofluorescence were performed as described previously (Tritschler et al., 2007, 2008, 2009). For co-IPs, cells were collected 3 d after transfection, washed with PBS, and lysed for 15 min on ice in NET buffer (50 mM Tris, pH 7.4, 150 mM NaCl, 1 mM EDTA, and 0.1% Triton X-100) supplemented with protease inhibitors. Cells were spun at 16,000 *g* for 15 min at 4°C. Anti-HA (Covance) or anti-GFP antibodies were added to the supernatants (2.5 µl/2 × 10^6 cells). After 1 h at 4°C, 25 µl of protein G–agarose (Roche) was added, and the mixtures were rotated for 1 h at 4°C. Beads were washed three times with NET buffer and once with NET buffer without Triton X-100. Bound proteins were eluted with sample buffer. Proteins were separated by SDS-PAGE and transferred to nitrocellulose membranes. Membranes were blocked in PBS containing 5% fat-free milk powder and 0.3% Tween 20. Western blotting was performed with polyclonal anti-HA antibodies (1:1,000; Sigma-Aldrich) or anti-GFP antibodies (1:2,000), using the CDP-Star chemiluminescent immunoblot system (Western-Star kit; Tropix), as recommended by the manufacturer.

For immunofluorescence, S2 cells were allowed 15 min to adhere to poly-D-lysine–coated coverslips and fixed with 2% paraformaldehyde for 10 min. Cells were then permeabilized with 0.1% Triton X-100 in PBS (10 min) and stained with an affinity-purified anti-Tral antibody diluted 1:250 in PBS containing 1% BSA (1 h). Alexa Fluor 594–labeled goat anti–mouse antibody (Invitrogen) was used at a dilution of 1:1,000. Cells were mounted using Fluoromount-G (SouthernBiotech). Images were acquired at room temperature using a confocal microscope (TCS SP2; Leica) fitted with a Plan-Apochromat 100× NA 1.40 oil immersion objective and a series of three photomultipliers (Hamamatsu Photonics) controlled with the Leica confocal software (version 2.61). Images were prepared using Photoshop (Adobe).

Tethering and complementation assays

RNA interference was performed as described previously (Eulalio et al., 2007c). For the λN-tethering assay, the following plasmids were cotransfected: 0.1 µg reporter plasmid (F-Luc–5BoxB or F-Luc), 0.4 µg pAc5.1–R-Luc as transfection control, and 0.025 µg of plasmids expressing λN-HA–protein fusions. For the complementation assay, cells were depleted on days 0 and 4, transfected on day 6, and collected on day 9. The transfection mixtures contained 0.1 µg reporter plasmid (F-Luc–5BoxB), 0.4 µg pAc5.1–R-Luc as transfection control, and 0.1 µg of plasmids expressing the λN-HA peptide or λN-HA–GW182. When indicated, 0.005 µg of plasmids expressing wild-type HPat or HPat fragments was cotransfected. HA–maltose-binding protein (MBP) served as a negative control. In all experiments, cells were collected 3 d after transfection. F-Luc and R-Luc activities were measured using the Dual-Luciferase reporter assay system (Promega). Northern blotting was performed as described previously (Behm-Ansmant et al., 2006). RNase H (USB) digestion using a $(dT)_{15}$ oligonucleotide was performed according to the manufacturer's instructions.

Reverse transcription and RT-qPCR

The interaction of HPat with mRNAs was tested as described by Zekri et al. (2009). In these experiments, the transfection mixtures contained 0.3 µg of an F-Luc reporter plasmid, 0.2 µg of the *Renilla* transfection control, and 0.5 µg of plasmid expressing full-length HPat or fragments or HA-GST. S2 cells (10–12 × 10^6 cells) were collected 3 d after transfection, washed with PBS, and lysed in 0.5 ml of NET buffer (50 mM Tris, pH 7.4, 150 mM NaCl, 1 mM EDTA, and 0.1% NP-40) supplemented with protease inhibitors. Cells were lysed by three 30-s sonications, followed by a 15-min incubation on ice. Cells were spun at 16,000 *g* for 15 min at 4°C. Anti-HA antibodies were added to the cleared lysates (2.5 µl/2 × 10^6 cells). After 1 h at 4°C, aliquots (1/10) of the cleared lysates (input) were kept aside for both RNA extraction and Western blotting analysis, and 20 µl of protein G–agarose was added to the remaining lysate. Before addition to the lysates, protein G–agarose beads were preincubated with 0.5 mg of yeast RNA and 30 µg BSA for 1 h at 4°C. Lysates were rotated with protein G–agarose beads for 1 h at 4°C. Beads were washed four times with NET buffer and once with NET buffer and eluted with 60 µl of 2× SDS-PAGE protein sample buffer. 40 µl of the eluate was used for RNA analysis. RNA was prepared from input and immunoprecipitates using TRIZOL-LS reagent (Invitrogen) according to the manufacturer's protocol. DNase treatment was performed using the TURBO DNA-free kit (Applied Biosystems) for 30 min at 37°C. RNAs were detected via cDNA synthesis and real-time quantitative PCR. cDNAs were synthesized with M-MuLV reverse transcription (Fermentas) and the F-Luc reporter–specific primer 5′-TGTTTACATAACCGGACATAATCA-3′, according to the manufacturer's protocols. Quantitative PCR analysis was performed using gene-specific primer pairs (as indicated below) and SYBR green PCR master mix (Applied Biosystems). Each sample was analyzed in triplicate. mRNA levels in the immunoprecipitates were normalized to the respective input levels. Primer sequences for F-Luc reporter are 5′-GGCCGAAGACGCCAAAAACATAAAG-3′ (forward) and 5′-AATAACGCGCCCAACACCGGCA-3′ (reverse).

Online supplemental material

Fig. S1 shows that HPat interacts with LSm1 and DCP2 in an RNA-independent manner. Fig. S2 shows that HPat and Tral interact with Me31B in a mutually exclusive manner. Online supplemental material is available at http://www.jcb.org/cgi/content/full/jcb.200910141/DC1.

We are grateful to M. Fauser and S. Helms for technical assistance. We thank S.F. Newbury for the gift of *D. melanogaster* XRN1 cDNA.

This study was supported by the Max Planck Society, by grants from the Deutsche Forschungsgemeinschaft (FOR855 and the Gottfried Wilhelm Leibniz Program awarded to E. Izaurralde), and by the Sixth Framework Programme of the European Commission through the SIROCCO (Silencing RNAs: organisers and coordinators of complexity in eukaryotic organisms) Integrated Project LSHG-CT-2006-037900. T. Nishihara is the recipient of a fellowship from the Toyobo Biotechnology Foundation.

Submitted: 26 October 2009
Accepted: 24 March 2010

References

Bail, S., and M. Kiledjian. 2006. More than 1 + 2 in mRNA decapping. *Nat. Struct. Mol. Biol.* 13:7–9. doi:10.1038/nsmb0106-7

Behm-Ansmant, I., J. Rehwinkel, T. Doerks, A. Stark, P. Bork, and E. Izaurralde. 2006. mRNA degradation by miRNAs and GW182 requires both CCR4:NOT deadenylase and DCP1:DCP2 decapping complexes. *Genes Dev.* 20:1885–1898. doi:10.1101/gad.1424106

Bonnerot, C., R. Boeck, and B. Lapeyre. 2000. The two proteins Pat1p (Mrt1p) and Spb8p interact in vivo, are required for mRNA decay, and are functionally linked to Pab1p. *Mol. Cell. Biol.* 20:5939–5946. doi:10.1128/MCB.20.16.5939-5946.2000

Bouveret, E., G. Rigaut, A. Shevchenko, M. Wilm, and B. Séraphin. 2000. A Sm-like protein complex that participates in mRNA degradation. *EMBO J.* 19:1661–1671. doi:10.1093/emboj/19.7.1661

Chowdhury, A., and S. Tharun. 2008. lsm1 mutations impairing the ability of the Lsm1p-7p-Pat1p complex to preferentially bind to oligoadenylated RNA affect mRNA decay in vivo. *RNA*. 14:2149–2158. doi:10.1261/rna.1094208

Chowdhury, A., and S. Tharun. 2009. Activation of decapping involves binding of the mRNA and facilitation of the post-binding steps by the Lsm1-7-Pat1 complex. *RNA*. 15:1837–1848. doi:10.1261/rna.1650109

Chowdhury, A., J. Mukhopadhyay, and S. Tharun. 2007. The decapping activator Lsm1p-7p-Pat1p complex has the intrinsic ability to distinguish between oligoadenylated and polyadenylated RNAs. *RNA*. 13:998–1016. doi:10.1261/rna.502507

Coller, J., and R. Parker. 2005. General translational repression by activators of mRNA decapping. *Cell*. 122:875–886. doi:10.1016/j.cell.2005.07.012

Coller, J.M., M. Tucker, U. Sheth, M.A. Valencia-Sanchez, and R. Parker. 2001. The DEAD box helicase, Dhh1p, functions in mRNA decapping and interacts with both the decapping and deadenylase complexes. *RNA*. 7:1717–1727. doi:10.1017/S135583820101994X

Decker, C.J., D. Teixeira, and R. Parker. 2007. Edc3p and a glutamine/asparagine-rich domain of Lsm4p function in processing body assembly in *Saccharomyces cerevisiae*. *J. Cell Biol.* 179:437–449. doi:10.1083/jcb.200704147

Eulalio, A., I. Behm-Ansmant, and E. Izaurralde. 2007a. P bodies: at the crossroads of post-transcriptional pathways. *Nat. Rev. Mol. Cell Biol.* 8:9–22. doi:10.1038/nrm2080

Eulalio, A., I. Behm-Ansmant, D. Schweizer, and E. Izaurralde. 2007b. P-body formation is a consequence, not the cause, of RNA-mediated gene silencing. *Mol. Cell. Biol.* 27:3970–3981. doi:10.1128/MCB.00128-07

Eulalio, A., J. Rehwinkel, M. Stricker, E. Huntzinger, S.-F. Yang, T. Doerks, S. Dorner, P. Bork, M. Boutros, and E. Izaurralde. 2007c. Target-specific requirements for enhancers of decapping in miRNA-mediated gene silencing. *Genes Dev.* 21:2558–2570. doi:10.1101/gad.443107

Fischer, N., and K. Weis. 2002. The DEAD box protein Dhh1 stimulates the decapping enzyme Dcp1. *EMBO J.* 21:2788–2797. doi:10.1093/emboj/21.11.2788

Fromont-Racine, M., A.E. Mayes, A. Brunet-Simon, J.C. Rain, A. Colley, I. Dix, L. Decourty, N. Joly, F. Ricard, J.D. Beggs, and P. Legrain. 2000. Genome-wide protein interaction screens reveal functional networks involving Sm-like proteins. *Yeast*. 17:95–110. doi:10.1002/1097-0061(20000630)17:2<95::AID-YEA16>3.0.CO;2-H

Gehring, N.H., J.B. Kunz, G. Neu-Yilik, S. Breit, M.H. Viegas, M.W. Hentze, and A.E. Kulozik. 2005. Exon-junction complex components specify distinct routes of nonsense-mediated mRNA decay with differential cofactor requirements. *Mol. Cell*. 20:65–75. doi:10.1016/j.molcel.2005.08.012

Hatfield, L., C.A. Beelman, A. Stevens, and R. Parker. 1996. Mutations in trans-acting factors affecting mRNA decapping in *Saccharomyces cerevisiae*. *Mol. Cell. Biol.* 16:5830–5838.

He, W., and R. Parker. 2001. The yeast cytoplasmic LsmI/Pat1p complex protects mRNA 3′ termini from partial degradation. *Genetics*. 158:1445–1455.

Houseley, J., J. LaCava, and D. Tollervey. 2006. RNA-quality control by the exosome. *Nat. Rev. Mol. Cell Biol.* 7:529–539. doi:10.1038/nrm1964

Mazzoni, C., I. D'Addario, and C. Falcone. 2007. The C-terminus of the yeast Lsm4p is required for the association to P-bodies. *FEBS Lett.* 581:4836–4840. doi:10.1016/j.febslet.2007.09.009

Parker, R., and U. Sheth. 2007. P bodies and the control of mRNA translation and degradation. *Mol. Cell*. 25:635–646. doi:10.1016/j.molcel.2007.02.011

Pilkington, G.R., and R. Parker. 2008. Pat1 contains distinct functional domains that promote P-body assembly and activation of decapping. *Mol. Cell. Biol.* 28:1298–1312. doi:10.1128/MCB.00936-07

Reijns, M.A., R.D. Alexander, M.P. Spiller, and J.D. Beggs. 2008. A role for Q/N-rich aggregation-prone regions in P-body localization. *J. Cell Sci.* 121:2463–2472. doi:10.1242/jcs.024976

Scheller, N., P. Resa-Infante, S. de la Luna, R.P. Galao, M. Albrecht, L. Kaestner, P. Lipp, T. Lengauer, A. Meyerhans, and J. Díez. 2007. Identification of PatL1, a human homolog to yeast P body component Pat1. *Biochim. Biophys. Acta*. 1773:1786–1792. doi:10.1016/j.bbamcr.2007.08.009

Simon, E., S. Camier, and B. Séraphin. 2006. New insights into the control of mRNA decapping. *Trends Biochem. Sci.* 31:241–243. doi:10.1016/j.tibs.2006.03.001

Tharun, S. 2009. Lsm1-7-Pat1 complex: a link between 3′ and 5′-ends in mRNA decay? *RNA Biol.* 6:228–232. doi:10.4161/rna.6.3.8282

Tharun, S., and R. Parker. 2001. Targeting an mRNA for decapping: displacement of translation factors and association of the Lsm1p-7p complex on deadenylated yeast mRNAs. *Mol. Cell*. 8:1075–1083. doi:10.1016/S1097-2765(01)00395-1

Tharun, S., W. He, A.E. Mayes, P. Lennertz, J.D. Beggs, and R. Parker. 2000. Yeast Sm-like proteins function in mRNA decapping and decay. *Nature*. 404:515–518. doi:10.1038/35006676

Tritschler, F., A. Eulalio, V. Truffault, M.D. Hartmann, S. Helms, S. Schmidt, M. Coles, E. Izaurralde, and O. Weichenrieder. 2007. A divergent Sm fold in EDC3 proteins mediates DCP1 binding and P-body targeting. *Mol. Cell. Biol.* 27:8600–8611. doi:10.1128/MCB.01506-07

Tritschler, F., A. Eulalio, S. Helms, S. Schmidt, M. Coles, O. Weichenrieder, E. Izaurralde, and V. Truffault. 2008. Similar modes of interaction enable Trailer Hitch and EDC3 to associate with DCP1 and Me31B in distinct protein complexes. *Mol. Cell. Biol.* 28:6695–6708. doi:10.1128/MCB.00759-08

Tritschler, F., J.E. Braun, A. Eulalio, V. Truffault, E. Izaurralde, and O. Weichenrieder. 2009. Structural basis for the mutually exclusive anchoring of P body components EDC3 and Tral to the DEAD box protein DDX6/Me31B. *Mol. Cell*. 33:661–668. doi:10.1016/j.molcel.2009.02.014

Williamson, M.P. 1994. The structure and function of proline-rich regions in proteins. *Biochem. J.* 297:249–260.

Wyers, F., M. Minet, M.E. Dufour, L.T. Vo, and F. Lacroute. 2000. Deletion of the PAT1 gene affects translation initiation and suppresses a PAB1 gene deletion in yeast. *Mol. Cell. Biol.* 20:3538–3549. doi:10.1128/MCB.20.10.3538-3549.2000

Zekri, L., E. Huntzinger, S. Heimstädt, and E. Izaurralde. 2009. The silencing domain of GW182 interacts with PABPC1 to promote translational repression and degradation of microRNA targets and is required for target release. *Mol. Cell. Biol.* 29:6220–6231. doi:10.1128/MCB.01081-09

Haas et al., http://www.jcb.org/cgi/content/full/jcb.200910141/DC1

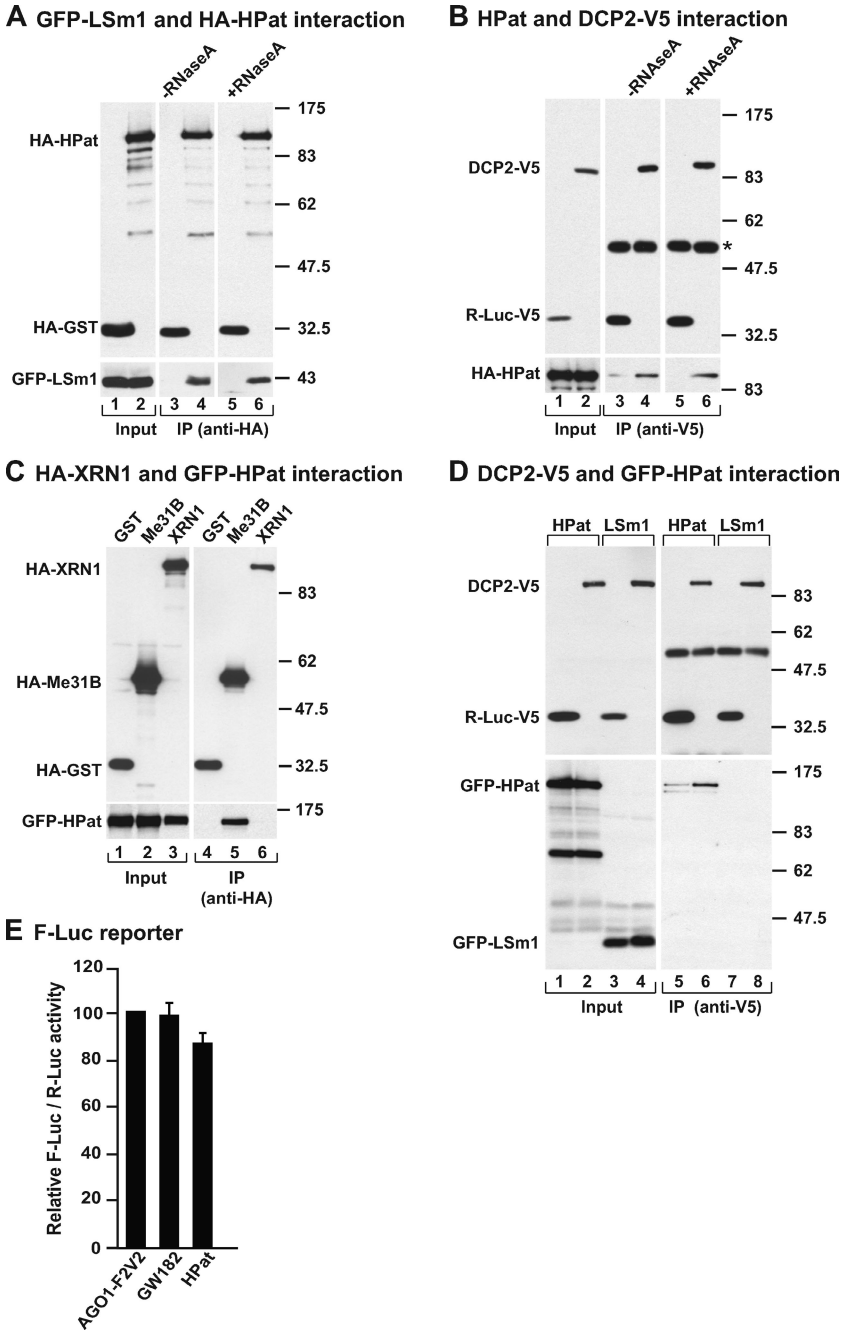

Figure S1. **HPat interacts with LSm1 and DCP2 in an RNA-independent manner.** (A–D) Lysates from S2 cells coexpressing the indicated HA-, V5-, or GFP-tagged proteins were immunoprecipitated using a monoclonal anti-HA or -V5 antibodies. In lanes 5 and 6 of panels A and B, cell lysates were treated with RNase A before IP. Inputs (1%) and immunoprecipitates (10%) were analyzed by Western blotting using anti-GFP, -V5, and -HA antibodies. In B and D, 30% of the immunoprecipitate was loaded. HA-GST, R-Luc–V5, or HA-MBP served as negative controls. The asterisk indicates cross-reactivity of the secondary antibody with the immunoglobin heavy chain. Molecular mass is indicated in kilodaltons. (E) S2 cells were transfected with a mixture of three plasmids, one expressing the F-Luc reporter without 5BoxB, another expressing R-Luc, and a third expressing λN-HA–AGO1-F2V2 (negative control) or λN-HA fusions of GW182 or wild-type HPat, as indicated. F-Luc activity was normalized to that of the *Renilla* and set to 100 in cells expressing λN-HA–AGO1-F2V2. Mean values ± standard deviations from three independent experiments are shown.

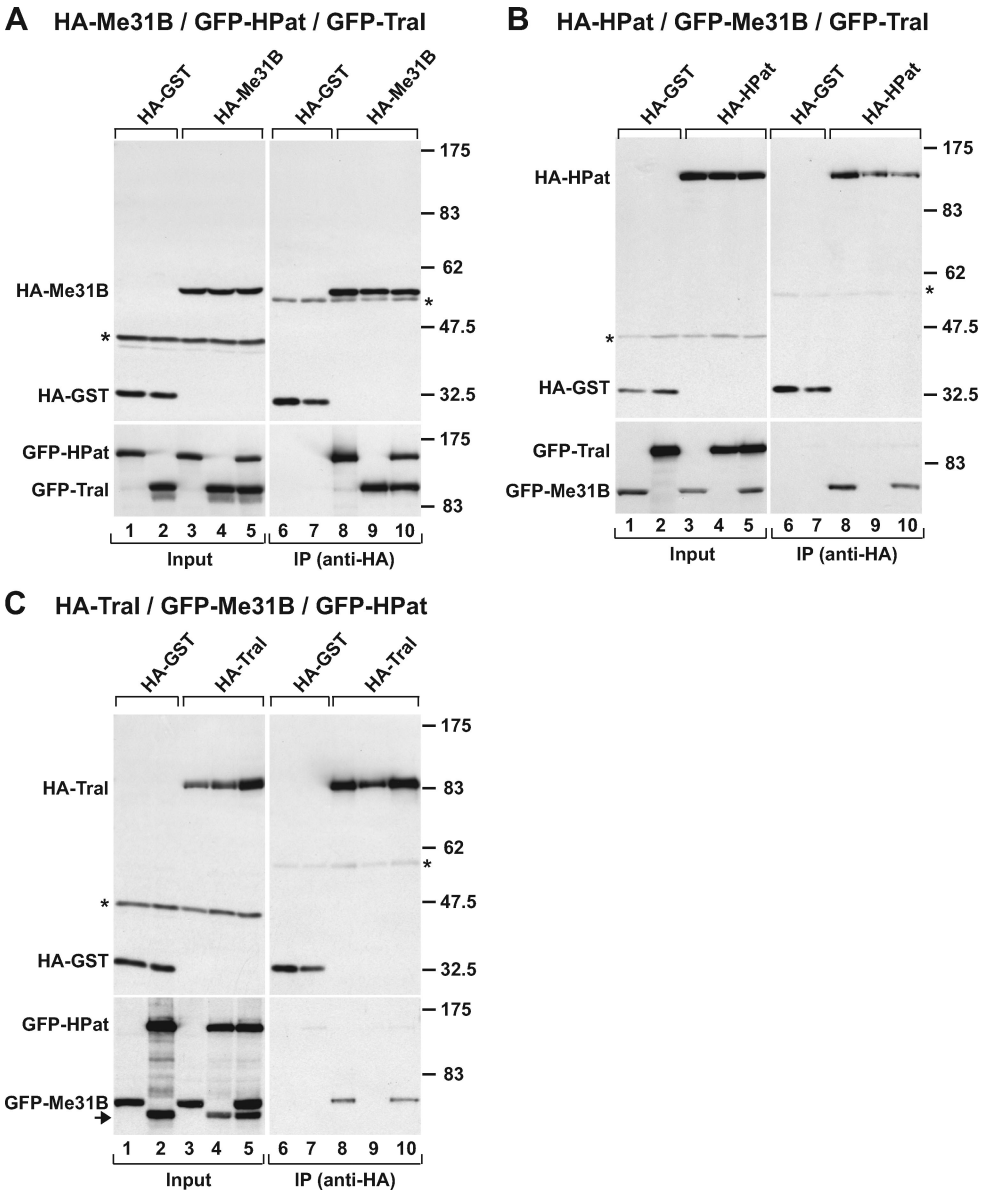

Figure S2. **HPat and Tral interact with Me31B in a mutually exclusive manner.** (A–C) S2 cells were cotransfected with mixtures of three plasmids. In A, the plasmids encoded HA-Me31B, GFP-HPat, and GFP-Tral; in B, the plasmids encoded HA-HPat, GFP-Me31B, and GFP-Tral; in C, the mixture consisted of HA-Tral, GFP-Me31B, and GFP-HPat. Cell lysates were immunoprecipitated using a monoclonal anti-HA antibody. In all panels, HA-GST served as a negative control. Inputs and immunoprecipitates were analyzed as described in Fig. 1. Asterisks indicate cross-reactivity of the primary antibodies with an endogenous protein (input panels) or of the secondary antibody with the immunoglobulin heavy chain (IP panels). The arrow indicates an HPat protein degradation fragment. Molecular mass is indicated in kilodaltons.

DCP1 forms asymmetric trimers to assemble into active mRNA decapping complexes in metazoa

Felix Tritschler[1], Joerg E. Braun[1], Carina Motz, Catia Igreja, Gabrielle Haas, Vincent Truffault, Elisa Izaurralde[2], and Oliver Weichenrieder[2]

Department of Biochemistry, Max Planck Institute for Developmental Biology, Spemannstrasse 35, D-72076 Tübingen, Germany

Edited by James E. Dahlberg, University of Wisconsin Medical School, Madison, WI, and approved October 29, 2009 (received for review August 28, 2009)

DCP1 stimulates the decapping enzyme DCP2, which removes the mRNA 5′ cap structure committing mRNAs to degradation. In multicellular eukaryotes, DCP1-DCP2 interaction is stabilized by additional proteins, including EDC4. However, most information on DCP2 activation stems from studies in *S. cerevisiae*, which lacks EDC4. Furthermore, DCP1 orthologs from multicellular eukaryotes have a C-terminal extension, absent in fungi. Here, we show that in metazoa, a conserved DCP1 C-terminal domain drives DCP1 trimerization. Crystal structures of the DCP1-trimerization domain reveal an antiparallel assembly comprised of three kinked α-helices. Trimerization is required for DCP1 to be incorporated into active decapping complexes and for efficient mRNA decapping in vivo. Our results reveal an unexpected connectivity and complexity of the mRNA decapping network in multicellular eukaryotes, which likely enhances opportunities for regulating mRNA degradation.

DCP2 | miRNAs | P-bodies | EDC4 | Ge-1

In eukaryotes, removal of the mRNA 5′ cap structure is catalyzed by the decapping enzyme DCP2 (1, 2); to be fully active and/or stable, DCP2 requires additional proteins (1, 2). Yeast DCP2 interacts directly with DCP1 and this interaction is required for decapping in vivo and in vitro (3–7). In humans, the DCP2-DCP1 interaction requires additional proteins, which together assemble into multimeric decapping complexes that also include the enhancers of decapping 3 and 4 (EDC3 and ECD4), and the DEAD-box protein DDX6/RCK (8, 9).

DCP2 is highly conserved and most information on DCP2 activation stems mainly from studies in *S. cerevisiae* and *S. pombe* (3–7). Fungi, however, lack EDC4 as well as many extensions and additional domains present in decapping activators of metazoan orthologs (8–10). For example, all eukaryotic DCP1 proteins contain an N-terminal EVH1 domain (3, 5, 6); however, DCP1 orthologs from metazoa and plants also have a proline-rich C-terminal extension (9, 10). The sequence of this extension is not conserved except for a 14-residue short motif (motif I, MI) conserved in metazoa with the exception of *C. elegans* (Fig. 1*A* and Fig. S1) and a C-terminal domain conserved in plants and metazoa (Fig. 1*A*, referred to as TD).

The DCP1 C-terminal domain is predicted to adopt an α-helical conformation. In this work, we show that this domain trimerizes in an asymmetric fashion. We solved the crystal structure of the trimerized domain for both human and *D. melanogaster* DCP1 and show that the trimer adopts an unprecedented fold, with no current similarities in the protein database. We further show that DCP1 trimerization is required for the assembly of active decapping complexes and for mRNA decapping in vivo. The conservation of structurally critical residues indicates that this domain adopts a similar fold in DCP1 orthologs of other multicellular eukaryotes. Consequently, within mRNA decapping complexes in these organisms, the stoichiometry of the protein components is likely more complex than previously thought.

Results and Discussion

Crystal Structure of the Human DCP1a Trimerization Domain. To investigate the role of the conserved C-terminal domain of human DCP1a in mRNA decapping we expressed the domain in *E. coli* (DCP1a residues S539 to L582). Using static light scattering measurements coupled with size exclusion chromatography, we found unexpectedly that the purified domain forms stable trimers in solution (Table S1). We have termed this domain the DCP1-trimerization domain (DCP1-TD). Furthermore, although the recombinant polypeptide contains 51 residues per monomer (i.e., 44 from DCP1a-TD and seven from the expression vector), NMR spectroscopy yields >115 peaks in the ^{15}N-HSQC spectrum (Fig. S2), suggesting that in solution the trimers are asymmetric (assuming a single trimeric assembly).

We determined the crystal structure of this unusual assembly to a resolution of 2.3 Å (R_{work} = 20.8, R_{free} = 25.2, Table S2). The structure reveals an unprecedented, antiparallel bundle of three kinked α-helices (two up, one down), in which the structural environment for a given side-chain differs for each of the three molecules (Fig. 1 *B–F*). The central sequence (K544-L571) of each molecule is α-helical, with a strong kink at D558 that separates helix α1 from helix α2 with an elbow angle of ≈90° (Fig. 1*F*). At the kink, residue L554 from helix α1 makes van der Waals contacts with F561 from helix α2, while D558 caps the N terminus of helix α-2 by hydrogen-bonding with the peptide NH-groups of residues S560 and F561 (Fig. 1*F*). Alignment of DCP1 sequences from various species shows only these three residues are invariant (Fig. 2*A*, asterisks), indicating the elbow is a conserved structural feature of DCP1 trimerization domains from multicellular eukaryotes.

The three polypeptide chains (termed A, B, and C in Fig. 1 *B–F*) superimpose over the central sequence, with a maximal C_α r.m.s.d. of 1.15 Å (chain A and B, residues 544–571). To assemble the trimer, chain B interacts with chains A and C in an antiparallel fashion, causing helices α1 of chain A and α2 of chain C to interact in parallel. Chains A and B are thus related by a pseudotwofold axis close to F561 (Fig. 1*D*), while chains C and B are related by a pseudotwofold axis close to I552 (Fig. 1*E*). This arrangement places most hydrophobic side chains into a densely packed core (Figs. 1*B* and 2*A*, residues shaded in blue), explaining the stability of the trimer. The resulting DCP1a trimerization domain could be characterized as a novel fold if the chains were connected *in cis*.

Using the structural information, we constructed three mu-

Author contributions: E.I. designed research; F.T., J.E.B., C.M., C.I., G.H., V.T., and O.W. performed research; F.T., J.E.B., C.M., C.I., G.H., V.T., E.I., and O.W. analyzed data; and F.T., J.E.B., E.I., and O.W. wrote the paper.

The authors declare no conflict of interest.

This article is a PNAS Direct Submission.

Freely available online through the PNAS open access option.

Data deposition: Coordinates of the human DCP1a and the *D. melanogaster* DCP1 trimerization domains have been deposited in the Protein Data Bank, www.pdb.org (PDB ID code 2WX3 and 2WX4).

[1]F.T. and J.E.B. contributed equally to this work.

[2]To whom correspondence may be addressed. E-mail: elisa.izaurralde@tuebingen.mpg.de or oliver.weichenrieder@tuebingen.mpg.de.

This article contains supporting information online at www.pnas.org/cgi/content/full/0909871106/DCSupplemental.

BIOCHEMISTRY

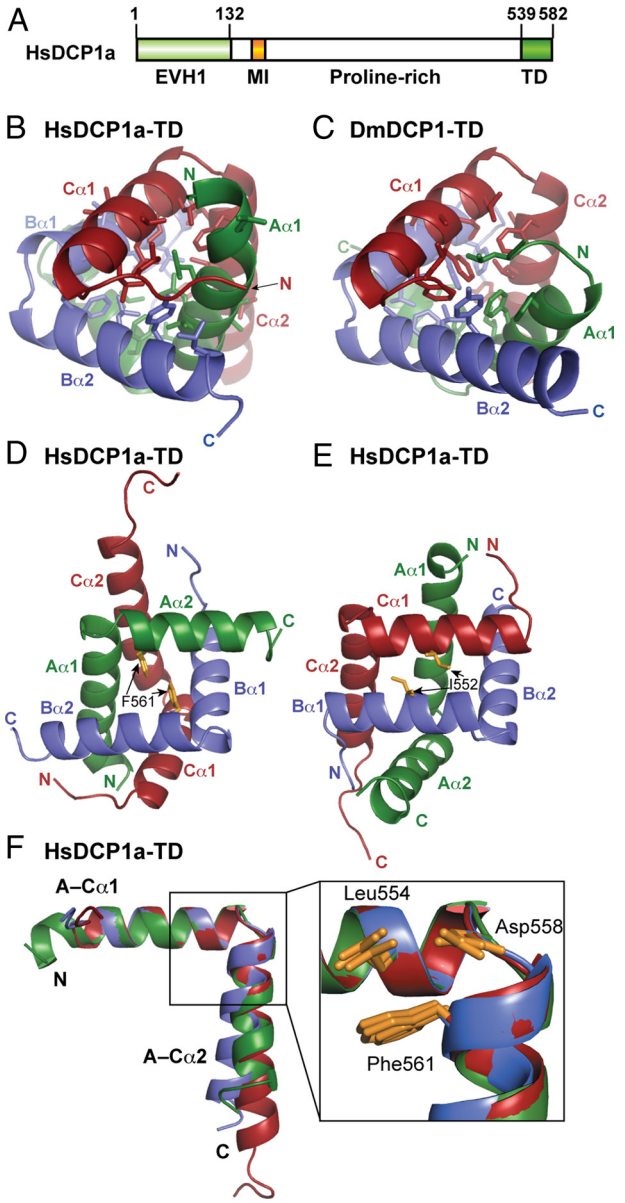

Fig. 1. Structure of the DCP1-trimerization domain. (*A*) Domain organization of human DCP1a (HsDCP1a), indicating the EVH1 domain, motif I (MI), and the trimerization domain (TD). (*B* and *C*) Crystal structures of human DCP1a-TD and of the *D. melanogaster* orthologue, respectively. Chains A, B, and C are shown in green, blue, and red, respectively, with the N-termini of chains A and C in the front and the N terminus of chain B in the back. Residues from the hydrophobic core are shown as sticks. A total of 4,700 Å^2 is buried by the interfaces of the three chains in HsDCP1a-TD. (*D* and *E*) Asymmetric arrangement of the chains. Views down the two pseudodyads of HsDCP1a-TD, relating chains A and B or chains C and B, respectively. (*F*) Superposition and comparison of the three chains of HsDCP1a-TD with a close-up of the helix elbow. Interhelical angles are 86°, 95°, 86°, for chains A, B, and C, respectively. Strictly conserved side chains are shown as sticks.

tants designed to either disrupt the interface with chain A (Mutant-1, L554S, F561R, L565S; Fig. 2*A*, green triangles), or chain C (Mutant-2, I552S, I555R, L562E; Fig. 2*A*, red triangles) or to completely prevent oligomerization (Mutant-3, L551R, I555S, F561R, L565S; Fig. 2*A*, blue triangles). Static light scattering shows all mutants remain monomeric (Table S1). Notably, we did not detect dimeric assemblies suggesting that the DCP1 C-terminal domain oligomerizes as trimer exclusively.

Crystal Structure of the *Drosophila melanogaster* DCP1 Trimerization Domain. Despite the apparent stability of this unusual asymmetric homotrimeric assembly, we could not formally rule out the possibility that this particular protein sequence causes a unique artifact. Therefore, we crystallized the trimerization domain of *D. melanogaster* DCP1 (residues L328 to D366), which is only 36% identical to the human DCP1a trimerization domain (identity calculated over the central sequence of the TDs: HsDCP1a 544–571, DmDCP1 331–358; Fig. 2*A*). We found it also trimerizes with the same topology but in a different crystal packing environment and with two independent copies in the asymmetric unit (Fig. 1*C*, Fig. S3, and Table S2). Moreover, when *D. melanogaster* DCP1 is mutated at structural positions equivalent to those in human DCP1a mutants (Mut-1, Mut-2, and Mut-3), trimerization is again disrupted (Table S1). We therefore conclude that the C terminus of DCP1 contains a trimerization domain, which is conserved in metazoa but absent in fungi.

Functional Analysis of the Human and *D. melanogaster* DCP1 Trimerization Domain. Further analysis showed DCP1 also oligomerizes in vivo. In human HEK293 cells, we coexpressed hemagglutinin (HA)-tagged DCP1a with green fluorescent protein (GFP)-tagged wild-type or mutant DCP1a, and then performed coimmunoprecipitations with anti-GFP antibodies. HA-DCP1a coimmunoprecipitated with GFP-DCP1a, but not with the negative control protein GFP-MBP (Fig. 2*B*, lane 9 vs. 8). As expected, the trimerization domain (GFP-DCP1a-TD) is sufficient for oligomerization (Fig. 2*C*, lane 6); while for DCP1a mutants 1, 2 and 3 oligomerization is strongly impaired (Fig. 2*B*, lanes 10–12). Accordingly, deleting the trimerization domain prevents DCP1a oligomerization (Fig. 2*B*, lane 13). Similarly, we confirmed that the trimerization domain of *D. melanogaster* DCP1 is also sufficient for oligomerization in vivo (Fig. 2*D*).

Because we were able to disrupt oligomerization in vivo using information from the crystal structure, we infer DCP1 in human and *D. melanogaster* cells exist as asymmetric trimers. Accordingly, the possibility that the observed DCP1a self-association is indirect and results from the incorporation of several monomeric DCP1a copies into larger decapping complexes can be ruled out, as it is inconsistent with the crystal structures and with the findings described below.

We next showed human DCP1a trimerization is required for assembly of active decapping complexes. We immunopurified GFP-DCP1a (wild-type and mutants) from HEK293 cells and, using an m^{7}G-capped RNA substrate, tested for decapping activity in vitro. Decapping activity coimmunopurified with GFP-DCP1a as reported before (8, 10) (Fig. 2*E*, lane 3). This activity likely comes from the associated DCP2 (as a positive control, compare an immunoprecipitation of GFP-DCP2, Fig. 2*E*, lane 9) since adding nucleotide diphosphate kinase converts the m^{7}GDP product to m^{7}GTP (8, 10) (Fig. 2*E*, lanes 10 and 11). Strikingly, trimerization-defective mutants of DCP1a or DCP1a-ΔTD did not copurify with decapping activity (Fig. 2*E*, lanes 4–7), although the amounts of these proteins in the decapping assay were comparable to those of wild-type DCP1a (Fig. 2*F*).

Trimerization Is Required for DCP1a to Interact with DCP2 and EDC4. Two scenarios can explain why DCP1a trimerization-defective mutants fail to copurify with decapping activity: either these mutants are not incorporated into DCP2-containing complexes, or they fail to stimulate DCP2 decapping activity. To discriminate between these possibilities, we examined the association of DCP1a with additional components of the decapping complex (i.e., EDC4, DCP2, EDC3, and DDX6/RCK). These all coimmunoprecipitated with DCP1a, as reported before (8, 11–14) (Fig. 3*A–D*, lanes 9). DCP1-DCP2 association is likely stabilized by endogeneous EDC4 or other components (8, 9, 12, 14). We found DCP1a trimerization-defective mutants 1, 2, and 3 and

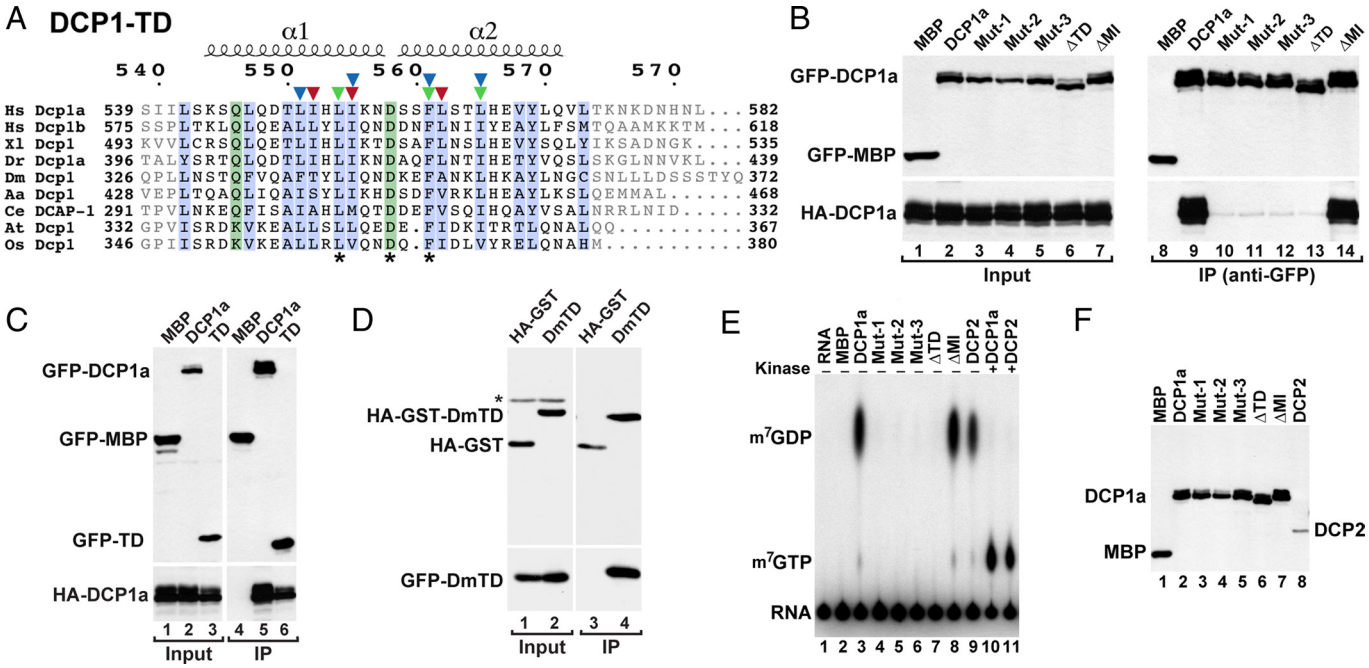

Fig. 2. DCP1 trimerization occurs in vivo and is required for the assembly of active decapping complexes. (*A*) Structure-based alignment of the trimerization domain (TD) of DCP1 orthologs from *Homo sapiens* (Hs), *Xenopus laevis* (Xl), *Danio rerio* (Dr); *Drosophila melanogaster* (Dm), *Aedes aegypti* (Aa), *Caenorhabditis elegans* (Ce), *Arabidopsis thaliana* (At), and *Oryza sativa* (Os). Residues from the hydrophobic core of the trimerization domain are shaded blue, residues mediating conserved intrachain hydrogen bonds are shaded green. The portion of the sequence that is α-helical in all three chains of HsDCP1a-TD is indicated. Triangles mark mutated residues in mutant-1 (green), mutant-2 (red) and mutant-3 (blue). Gray letters indicate residues with variable conformation, likely to be affected by crystal packing. (*B* and *C*) DCP1 trimerization in vivo. GFP- and HA-tagged proteins were coexpressed in human cells as indicated. Cell lysates were immunoprecipitated using anti-GFP antibodies. GFP-tagged maltose binding protein (GFP-MBP) served as a negative control. Protein samples were analyzed by Western blotting using anti-HA and anti-GFP antibodies. (*D*) Lysates from *D. melanogaster* (Dm) S2 cells expressing HA-GST or HA-GST-DmTD together with GFP-tagged DmTD, were immunoprecipitated using anti-HA antibodies. Inputs and immunoprecipitates were analyzed as described above. The asterisk indicates cross-reactivity of the anti-HA antibody with an endogenous protein. (*E*) GFP-tagged proteins were expressed in human cells, as indicated. Cell lysates were immunoprecipitated using anti-GFP antibodies. The immunoprecipitates were tested for decapping activity using in vitro synthesized ^{32}P-labeled capped mRNA. (*F*) Samples corresponding to panel (*E*) were analyzed by Western blot to ensure that equivalent amounts of DCP1a wild-type and mutants were used for the decapping assay.

DCP1a-ΔTD were strongly impaired in the interaction with EDC4 and DCP2 (Fig. 3 *A* and *B*, lanes 10–13). Therefore, the fact that DCP1a mutants that cannot trimerize also lack decapping activity can be explained by the failure to associate with DCP2 and EDC4. Notably, the trimerization domain itself is not sufficient to coimmunoprecipitate EDC4 or DCP2 (Fig. 3 *E* and *F*, lane 6). These results show that the oligomerization of DCP1-TD in vivo does not require an association with EDC4 or DCP2 and that additional sequences in DCP1 are necessary for binding EDC4 and DCP2.

EDC3 and DDX6/RCK assemble with DCP1a independently of DCP2 and EDC4. Indeed, loss of trimerization does not affect the interaction of DCP1a with EDC3 and DDX6/RCK (Fig. 3 *C* and *D*, lanes 10–13). However, EDC3 and DDX6 do not interact with a DCP1a mutant that lacks the conserved motif MI (Fig. 3 *C* and *D*, lane 14), while DCP2 and EDC4 still do (Fig. 3 *A* and *B*, lane 14). Despite the lack of interaction with EDC3 and DDX6, DCP1a-ΔMI still oligomerizes (Fig. 2*B*, lane 14), demonstrating once again that the observed self-association of DCP1 is independent of other decapping factors and occurs by an asymmetric trimerization. Furthermore, immunopurified DCP1a-ΔMI complexes retain decapping activity in vitro, while immunopurified DCP1a-ΔTD complexes do not (Fig. 2*E*, lanes 8 vs. 7). Consequently, a minimal decapping complex consisting of DCP1, DCP2 and EDC4 may be sufficient for decapping activity.

Specificity of DCP1 Trimerization In Vivo. Human cells express two DCP1 orthologs, DCP1a and DCP1b, whose trimerization domains exhibit 50% identity over the central sequence (HsDCP1a 544–571, HsDCP1b 580–607; Fig. 2*A*). It was therefore of interest to investigate whether human DCP1a and DCP1b heteromerize. We observed that HA-DCP1b coimmunoprecipitated with GFP-DCP1a, indicating that DCP1a and DCP1b can indeed heteromerize (Fig. 4*A*, lane 6). Consistently, we found heteromerization required the trimerization domain (Fig. 4*A*, lane 7).

To investigate the specificity of this interaction further, we substituted the trimerization domain of human DCP1a with the equivalent domain from *D. melanogaster* DCP1 and examined whether the chimeric protein (DCP1a-DmTD) oligomerized and interacted with wild-type DCP1a and DCP1b. As expected, the chimeric protein homomerized, indicating that *D. melanogaster* DCP1-TD trimerizes independently of the additional flanking sequences (Fig. 4*B*, lane 8). In contrast, we observed no interaction between the chimeric DCP1a-DmTD and DCP1a or DCP1b (Fig. 4 *A* and *C*, lane 8, and *B*, lane 6). Thus, heteromerization is observed only between highly related sequences. Furthermore, BLAST searches using the trimerization domains of DCP1a and DCP1b failed to identify any significantly similar sequence in the human genome. Thus, we conclude that DCP1a and DCP1b are unlikely to heteromerize with alternative, unrelated proteins.

Trimerization Enhances DCP1a Accumulation in P-Bodies. DCP1a and partners localize to P-bodies (8, 9, 15–17). We therefore tested the localization of DCP1a mutants, to define what interactions

BIOCHEMISTRY

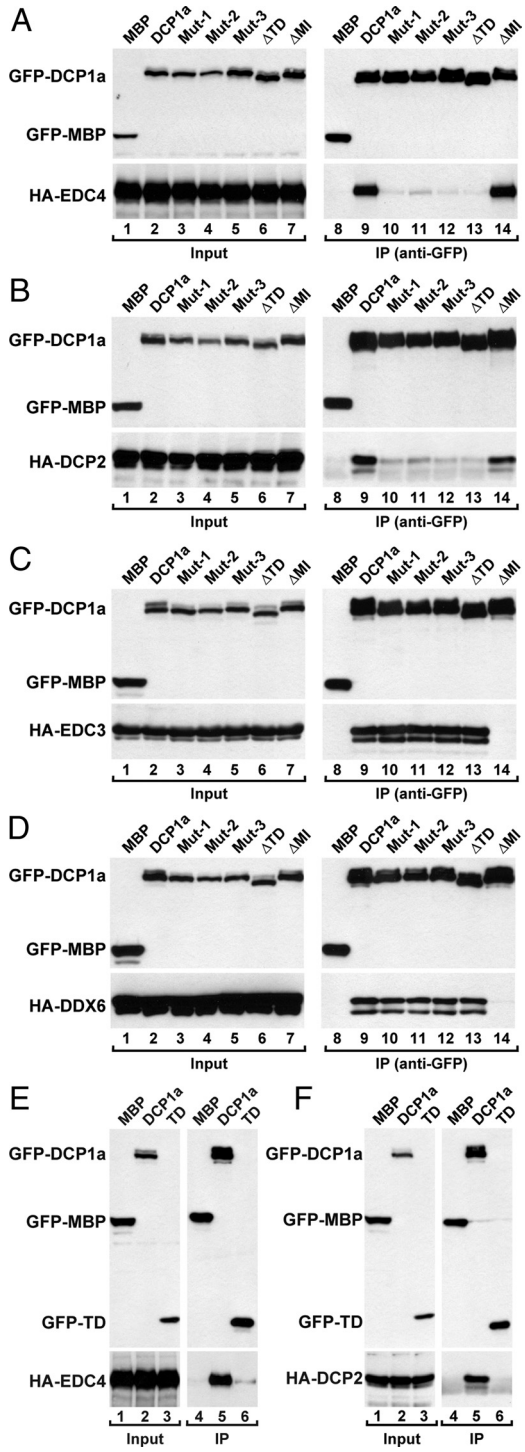

Fig. 3. Role of trimerization in the interactions of DCP1 with partner proteins. (*A–F*) GFP- and HA-tagged proteins were expressed in human cells as indicated above the panels. Cell lysates were immunoprecipitated using anti-GFP antibodies. GFP-MBP served as a negative control. Protein samples were analyzed by Western blotting using anti-GFP and anti-HA antibodies. DCP1a interaction with EDC4 (*A*). DCP1a interaction with DCP2 (*B*). DCP1a interaction with EDC3 (*C*). DCP1a interaction with DDX6/RCK (*D*). Interaction of DCP1a and DCP1a-TD with EDC4 (*E*) or DCP2 (*F*).

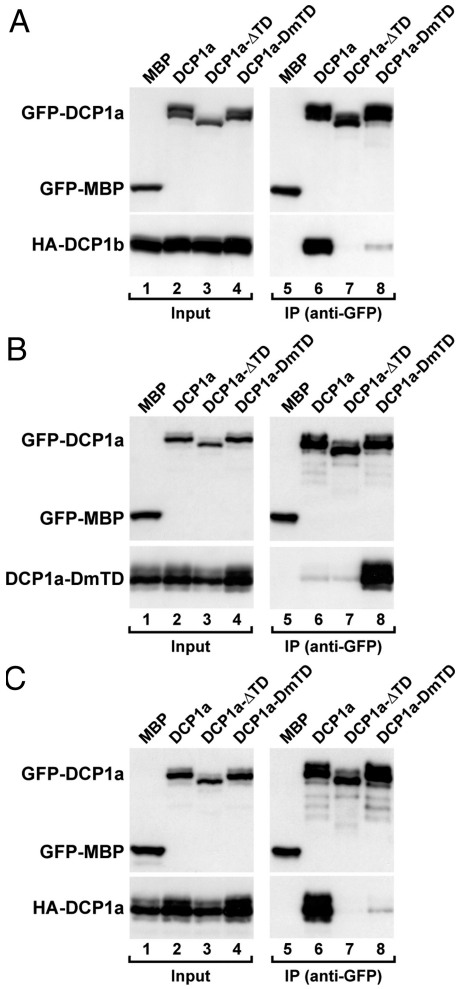

Fig. 4. Specificity of DCP1 trimerization. (*A–C*) GFP- and HA-tagged proteins were expressed in human cells as indicated above the panels. Cell lysates were immunoprecipitated using anti-GFP antibodies. GFP-MBP served as a negative control. Protein samples were analyzed by Western blotting using anti-GFP and anti-HA antibodies.

are critical for P-body accumulation. As reported (8, 9), GFP-DCP1a accumulates in cytoplasmic foci corresponding to endogenous P-bodies (Fig. 5*A*). Deleting the conserved motif MI did not affect this pattern (Fig. 5*B*). In contrast, the trimerization-deficient mutants and DCP1a-ΔTD dispersed throughout the cytoplasm, although some signal was still detectable in P-bodies (Fig. 5 *C* and *D* and Fig. S4). The isolated trimerization domain did not localize to P-bodies (Fig. 5*E*). Importantly, the chimeric DCP1a protein containing the *D. melanogaster* trimerization domain did localize to P-bodies in human cells (Fig. 5*F*). We conclude that trimerization per se, independently of the sequence of the trimerization domain, is required for DCP1a to efficiently accumulate in P-bodies.

DCP1 Trimerization Is Important for Efficient Decapping in Vivo. To test the biological significance of the identified DCP1 trimerization domain and its functional relevance in mRNA decapping we established a complementation assay in *D. melanogaster* cells, which express a single DCP1 paralog. In the complementation assay, endogenous DCP1 was depleted using a dsRNA targeting the DCP1 ORF. A dsRNA targeting GFP was used as a negative control. Wild-type DCP1 and a DCP1 mutant lacking the trimerization domain were then tested for the ability to restore decapping in DCP1-depleted cells. Transcripts encoding the proteins were made resistant to the dsRNA by introducing mutations that disrupt base pair interactions with the dsRNA without altering the protein sequence.

To assay mRNA decapping we monitored miRNA-mediated

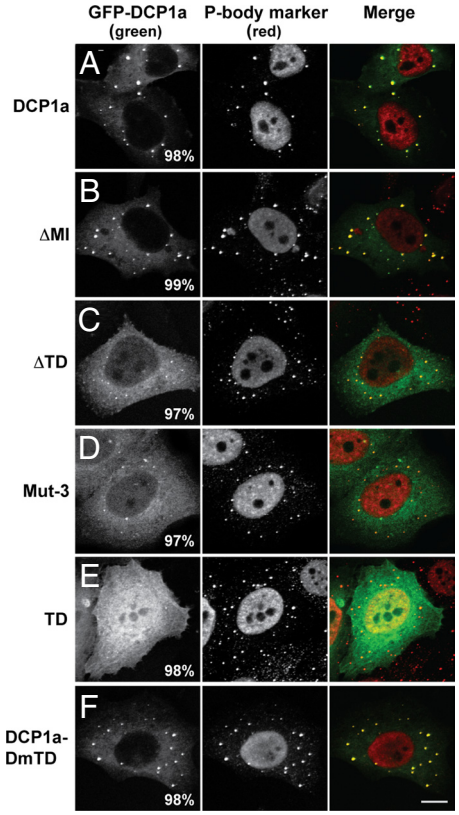

Fig. 5. Trimerization enhances accumulation of DCP1a in P-bodies. (*A–F*) Representative confocal fluorescent micrographs of fixed human HeLa cells expressing wild-type GFP-DCP1a or the mutants indicated on the left. Cells were stained with antibodies cross-reacting with EDC4 and a nuclear human antigen (23). The merged images show the GFP signal in green and the EDC4 signal in red. The fraction of cells exhibiting a staining identical to that shown in the representative panel was determined by scoring at least 100 cells in three independent transfections performed per protein. (Scale bar, 10 μm.)

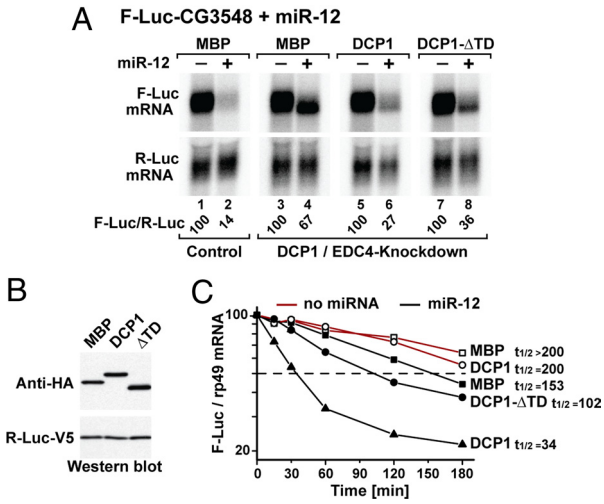

Fig. 6. Trimerization is required for efficient decapping in vivo (*A–C*) *D. melanogaster* S2 cells were treated with dsRNA targeting the ORF of *DCP1* and *EDC4* mRNAs. Control cells were treated with GFP dsRNA. These cells were subsequently transfected with a mixture of three plasmids: one expressing the F-Luc-CG3548 reporter; another expressing miR-12 primary transcripts (+miR-12) or the corresponding empty vector (-); and a third expressing *Renilla* luciferase (R-Luc). Plasmids (5 ng) encoding wild-type HA-DCP1, HA-DCP1ΔTD or HA-MBP were included in the transfection mixtures, as indicated. RNA samples were analyzed by Northern blot. Firefly luciferase mRNA levels were normalized to those of the *Renilla* luciferase. For each condition, the normalized values of F-Luc mRNA were set to 100 in the absence of miR-12. (*B*) Shows that HA-DCP1, HA-DCP1ΔTD and HA-MBP are expressed at comparable levels. (*C*) The decay of F-Luc-CG3548 mRNA was monitored in the presence (black lines) or absence (red lines) of miR-12 in depleted cells following inhibition of transcription by actinomycin D. The levels of the F-Luc-CG3548 mRNA were normalized to rp49 mRNA and plotted against time. mRNA half-lives ($t_{1/2}$) calculated from the decay curves are indicated in minutes.

mRNA degradation. We previously showed that miRNA targets are degraded by exonucleolytic digestion of the mRNA body only after they are first deadenylated and then decapped (18, 19). Therefore, we could prevent miRNA targets from being degraded by inhibiting decapping (18, 19). In our assay, we used the F-Luc-CG3548 reporter consisting of the firefly luciferase (F-Luc) ORF fused to the 3′ UTR of the *D. melanogaster* gene CG3548, which is silenced by miR-12 (19). Each transfection mixture included either a plasmid encoding the primary miR-12 transcript or the corresponding control vector without an insert, plus a transfection control plasmid expressing *Renilla* luciferase (R-Luc).

Our results showed the F-Luc-CG3548 mRNA is degraded in a miR-12-dependent manner (Fig. 6*A*, lane 2 vs. 1). Depleting DCP1 did not restore reporter mRNA levels. This result is expected since we previously showed that, in S2 cells, at least two decapping activators must be codepleted to restore the levels of miRNA reporters (19). Accordingly, codepletion of endogenous DCP1 plus EDC4 from S2 cells strongly inhibited decapping of the F-Luc-CG3548 reporter, leading to the accumulation of F-Luc-CG3548 mRNA as a fast migrating deadenylated form (Fig. 6*A*, lane 4). We therefore performed the complementation assay in this sensitized background.

We thus tested whether in cells codepleted of DCP1 and EDC4, we could restore mRNA degradation by expressing wild-type DCP1 or the DCP1 mutant lacking the trimerization domain. We restored target mRNA degradation in cells depleted of the endogenous DCP1 by expressing the dsRNA-resistant version of wild-type DCP1 (Fig. 6*A*, lane 6). In contrast, the DCP1-ΔTD mutant was impaired in restoring mRNA degradation indicating that decapping is still inhibited in these cells (Fig. 6*A*, lane 8). DCP1 and DCP1-ΔTD were expressed at comparable levels (Fig. 6*B*). Notably, in control cells, neither DCP1 nor DCP1-ΔTD inhibited mRNA degradation in a dominant negative manner (Fig. S4). Finally, the changes in steady state levels of F-Luc-CG3548 mRNA in cells depleted of DCP1 and EDC4 were accompanied by corresponding changes in the half-life of the mRNA (Fig. 6*C*). We conclude that DCP1 trimerization is required for efficient mRNA decapping in vivo.

Concluding Remarks. In this study, we identified a protein trimerization domain in the DCP1 protein. In metazoa, this domain is physiologically important for DCP1 to be incorporated into active mRNA decapping complexes and for mRNA decapping in vivo. This is remarkable, not only because trimers are rare among homomeric protein assemblies, but particularly because such an entirely asymmetric arrangement has not been described before in a physiological context (20).

Trimerization of DCP1 reveals an unexpected connectivity and complexity of the decapping network in multicellular eukaryotes, as both EDC3 and EDC4 are known or presumed to form homodimers (11, 13, 15, 21). We find that DCP1a can interact with DCP2 and EDC4 independently of the interaction with EDC3 and DDX6/RCK. Therefore, we can now conceive of multimeric assemblies consisting of (*i*) DCP1, EDC4, and DCP2, (*ii*) DCP1, EDC3, and DDX6 or (*iii*) combinations of both. Presently, we do not know precisely how DCP1 trimers associate with EDC3 and EDC4 dimers and why DCP1 oligomerizes in a

BIOCHEMISTRY

nonsymmetric fashion. It shall be challenging to determine the structural details of such assemblies and their possible significance for regulating mRNA decapping or for promoting P-body formation.

Methods

Detailed experimental procedures are given in the *SI Text*. Briefly, the trimerization domains of human DCP1a (residues 539–582) and *D. melanogaster* DCP1 (residues 328–366), N-terminally tagged with GST, were expressed in the *E. coli* strain BL21 Gold (DE3) (Stratagene) at 25 °C overnight. The proteins were purified by glutathione affinity step (GSTrap HP column; GE Healthcare). After cleaving the GST with PreScission protease, the complexes were further purified by gel filtration (HiLoad 26/60 Superdex 75 columns; GE Healthcare). The structure of the human protein was solved using single-wavelength anomalous dispersion data, collected from a crystal with selenomethionine-substituted protein. The structure of the *D. melanogaster* protein was solved by molecular replacement using the structure of the human protein as search model. Coimmunoprecipitation assays and immunofluorescence were performed as described in ref. 22. Decapping assays were performed as described in ref. 10, with the modifications indicated in the *SI Text*.

ACKNOWLEDGMENTS. We thank R. Büttner, M. Fauser, and S. Helms for technical assistance and the staff at the PX beamlines of the Swiss Light Source for assistance with data collection. This work was funded by the Max Planck Society and by grants from the Deutsche Forschungsgemeinschaft (FOR855) and the Gottfried Wilhelm Leibniz Program awarded to E.I., and by the Sixth Framework Program of the European Commission through the Silencing RNAs: organisers and coordinators of complexity in eukaryotic organisms (SIROCCO) Integrated Project LSHG-CT-2006–037900. O.W. holds a personal VIDI fellowship from the Dutch National Science Organization (CW 700.54.427).

1. Bail S, Kiledjian M (2006) More than 1 + 2 in mRNA decapping. *Nat Struct Mol Biol* 13:7–9.
2. Simon E, Camier S, Séraphin B (2006) New insights into the control of mRNA decapping. *Trends Biochem Sci* 31:241–243.
3. Deshmukh MV, et al. (2008) mRNA decapping is promoted by an RNA-binding channel in Dcp2. *Mol Cell* 29:324–336.
4. Sakuno T, et al. (2004) Decapping reaction of mRNA requires Dcp1 in fission yeast: Its characterization in different species from yeast to human. *J Biochem* 136:805–812.
5. She M, et al. (2004) Crystal structure of Dcp1p and its functional implications in mRNA decapping. *Nat Struct Mol Biol* 11:249–256.
6. She M, et al. (2008) Structural basis of dcp2 recognition and activation by dcp1. *Mol Cell* 29:337–349.
7. Steiger M, Carr-Schmid A, Schwartz DC, Kiledjian M, Parker R (2003) Analysis of recombinant yeast decapping enzyme. *RNA* 9:231–238.
8. Fenger-Grøn M, Fillman C, Norrild B, Lykke-Andersen J (2005) Multiple processing body factors and the ARE binding protein TTP activate mRNA decapping. *Mol Cell* 20:905–915.
9. van Dijk E, et al. (2002) Human Dcp2: A catalytically active mRNA decapping enzyme located in specific cytoplasmic structures. *EMBO J* 21:6915–6924.
10. Lykke-Andersen J (2002) Identification of a human decapping complex associated with hUpf proteins in nonsense-mediated decay. *Mol Cell Biol* 22:8114–8121.
11. Jínek M, et al. (2008) The C-terminal region of Ge-1 presents conserved structural features required for P-body localization. *RNA* 14:1991–1998.
12. Tritschler F, et al. (2007) A divergent Sm-fold in EDC3 proteins mediates DCP1-binding and P-body targeting. *Mol Cell Biol* 27:8600–8611.
13. Tritschler F, et al. (2009) Structural basis for the mutually exclusive anchoring of P-body components EDC3 and Tral to the DEAD-box protein DDX6/Me31B. *Mol Cell* 13:661–668.
14. Xu J, Yang JY, Niu QW, Chua NH (2006) Arabidopsis DCP2, DCP1, and VARICOSE form a decapping complex required for postembryonic development. *Plant Cell* 18:3386–3398.
15. Decker CJ, Teixeira D, Parker R (2007) Edc3p and a glutamine/asparagine-rich domain of Lsm4p function in processing body assembly in *Saccharomyces cerevisiae*. *J Cell Biol* 179:437–449.
16. Eulalio A, Behm-Ansmant I, Izaurralde E (2007) P bodies: At the crossroads of post-transcriptional pathways. *Nat Rev Mol Cell Biol* 8:9–22.
17. Parker R, Sheth U (2007) P bodies and the control of mRNA translation and degradation. *Mol Cell* 25:635–646.
18. Behm-Ansmant I, et al. (2006) mRNA degradation by miRNAs and GW182 requires both CCR4:NOT deadenylase and DCP1:DCP2 decapping complexes. *Genes Dev* 20:1885–1898.
19. Eulalio A, et al. (2007) Target-specific requirements for enhancers of decapping in miRNA-mediated gene silencing. *Genes Dev* 21:2558–2570.
20. Levy ED, Pereira-Leal JB, Chothia C, Teichmann SA (2006) 3D complex: A structural classification of protein complexes. *PLoS Comput Biol* 2:e155.
21. Ling SH, et al. (2008) Crystal structure of human Edc3 and its functional implications. *Mol Cell Biol* 28:5965–5976.
22. Lazzaretti D, Tournier I, Izaurralde E (2009) The C-terminal domains of human TNRC6A, B and C silence bound transcripts independently of the Argonaute proteins. *RNA* 15:1059–1066.
23. Kedersha N, Anderson P (2007) Mammalian stress granules and processing bodies. *Methods Enzymol* 431:61–81.

Supporting Information

Tritschler et al. 10.1073/pnas.0909871106

SI Text

Protein Expression, Purification, and Crystallization. cDNA sequences encoding the trimerization domains of *H. sapiens* DCP1a (Q9NPI6; Ser-539 to Leu-582) and *D. melanogaster* DCP1 (Q9W1H5; Leu-328 to Asp-366) were amplified from oligo$(dT)_{15}$-primed cDNA libraries obtained from human HeLa cells or *D. melanogaster* S2 cells, respectively. The amplified cDNA fragments were inserted into a modified pRSFDuet-1 vector (Novagen) downstream of the GST ORF. The GST-tagged proteins were expressed in the *E. coli* strain BL21 Gold (DE3) (Stratagene) at 25 °C overnight. The proteins were purified from cleared cell lysates by a glutathione affinity step (GSTrap HP column; GE Healthcare). After cleavage of the GST with PreScission protease, the proteins were further purified by gel filtration (HiLoad 26/60 Superdex 75 pg; GE Healthcare).

Diffraction quality crystals were grown by hanging drop vapor diffusion. Drops containing 1 μL of protein solution [16 mg/mL (human protein) or 7 mg/mL (*D. melanogaster* protein) in 10 mM Na-Hepes, pH 8.0, 50 mM NaCl, and 1 mM DTT] plus 1 μL of reservoir solution were equilibrated at 19 °C over 500 μL of reservoir [50 mM Mes, pH 6.0, and 1.2 M Na-Malonate (human protein) or 100 mM Mes, pH 6.5, 1.2 M ammonium sulfate, and 5% 1,4-Dioxane (*D. melanogaster* protein)]. Crystals of the human protein grew to a size of at least $200 \times 50 \times 30$ μm^3 within 1 day. Crystals were flash-frozen in liquid nitrogen after cryoprotection in 50 mM Mes, pH 6.0, and 2.3 M Na-Malonate.

Crystals of the *D. melanogaster* protein grew to a size of approximately $150 \times 40 \times 20$ μm^3 within ≈12 h and were cryoprotected in 100 mM Mes, pH 6.5, 1.2 M ammonium sulfate, 5% 1,4-dioxane, and 25% glycerol.

Structure Determination and Refinement. Diffraction data were collected on beamline X10SA of the Swiss Light Source (SLS). Diffraction images of selenomethionine-substituted human protein (one methionine per molecule, resulting from the 5′-cloning site) were processed with XDS (1) to 2.4 Å resolution. According to XTRIAGE (2) the crystal was merohedrally (-h,-k, l) twinned (twinning fraction 24%). The structure was solved using single-wavelength anomalous dispersion. We used AutoSHARP (3) to identify (SHELX D) and refine (SHARP) selenium sites, followed by automatic density modification (SOLOMON). Assuming one molecule per asymmetric unit (67% solvent) and searching for three selenium sites (resolution cutoffs 30–2.8 Å) resulted in an electron density map that displayed distinct protein and solvent regions. After phase extension and further statistical phase improvement with PIRATE as part of the CCP4 Suite (4) the density was good enough to directly place six α-helical fragments using COOT (5). After rigid body refinement (REFMAC) using native data (2.3-Å resolution, twinning fraction 18%), this model was good enough to prime autobuilding (121 out of 132 final residues) with flex-wARP (6). The model was completed manually using COOT and REFMAC (7) for refinement. A twin-specific target function did not improve the map any further. At least one of the three selenium sites refined by SHARP seems to have been an artifact of the twinning. Crystals of the *D. melanogaster* protein were untwinned and diffracted to 2.8 Å resolution. The structure was solved by molecular replacement using PHASER (8) and a polyalanine model of a truncated version of the human protein as search model. The model for the two monomers in the asymmetric unit (74% solvent) was (re-)built manually using COOT and REFMAC for refinement. Stereochemical properties were analyzed with MOLPROBITY (9) and WHATCHECK (10).

Analytical Size Exclusion Chromatography and Static Light Scattering. Proteins were prepared as described for crystallization, except that the preparative gel filtrations were done in chromatography buffer (10 mM Hepes, pH 8.0, 150 mM NaCl, and 1 mM DTT). Approximately 250 μg of each protein in a volume of 500 μL was injected onto a Superdex 75 10/300 GL analytical gel filtration column (15 °C equilibrated in chromatography buffer) at a flow rate of 0.4 mL/min. Multiangle static laser light-scattering was done online with analytical gel filtration chromatography using miniDAWN TREOS and Optilab rEX instruments (Wyatt Technologies) and the associated software (AstraV) for molecular weight determination.

NMR Measurements. The 2D ^{1}H-^{15}N HSQC spectrum of human DCP1a was measured at 291 K on a Bruker AV III-800 spectrometer, processed and analyzed using the Topspin (Topspin V. 2.1.1, Bruker) software. The spectrum was recorded with 1,024 (t1) × 128 (t2) complex points using 128 scans per increment and a relaxation delay of 0.8 s.

Coimmunoprecipitation Assays and Western Blotting. Plasmids allowing the expression of DCP1a, DCP2, DDX6/RCK, EDC3, and EDC4 in human cells were generated by cloning the corresponding cDNAs into the pEGFP-C1 vector (Clontech) or the pCI-neo-λN-HA vector (11). Human DCP1b was cloned between the *Xho*I and *Eco*R1 sites of the pλN-HA-C1 vector. DCP1 mutants were generated by site-directed mutagenesis using the QuikChange mutagenesis kit from Stratagene and the appropriate oligonucleotide sequences. In DCP1-ΔMI residues 155 to 168 are deleted. In DCP1-ΔTD, residues 539–582 are deleted. In the chimeric DCP1a-DmTD protein, residues 539–582 of human DCP1a are substituted with residues 329–372 of *D. melanogaster* DCP1.

For coimmunoprecipitation assays, HEK293 cells were grown in 10-cm plates and transfected using Lipofectamine 2000 (Invitrogen). The transfection mixtures contained 7 μg of the GFP- and HA-constructs. Two days after transfection, cells were washed with PBS and lysed for 15 min on ice in NET buffer (50 mM Tris at pH 7.5, 150 mM NaCl, 1 mM EDTA, 0.1% Triton X-100, and 10% glycerol) supplemented with protease inhibitors (1 mL NET buffer/plate). Cell lysates were spun at 18,000 × *g* for 15 min at 4 °C. Polyclonal anti-GFP antibodies were added to the supernatants (dilution 1:100). Samples were incubated for 1h at 4 °C, 25 μL Protein G-agarose (Roche) were added and the mixtures were rotated for an additional hour at 4 °C. Beads were washed three times with NET buffer and once with NET buffer without Triton X-100. Bound proteins were eluted with 100 μL protein sample buffer and analyzed by Western blotting. For the GFP-tagged proteins we analyzed 2% of the inputs and 10% of the immunoprecipitates. For HA-tagged EDC3, EDC4, RCK, and DCP1 we analyzed 1.5% of the input and 20% of the immunoprecipitates. For HA-DCP2 we analyzed 1% of the input and 40% of the immunoprecipitates. HA-tagged proteins were detected by Western blot analysis using horseradish peroxidase linked anti-HA high affinity (3F10) antibodies (Roche, Catalog no. 12013819001 dilution 1:5,000). GFP-tagged proteins were detected using a mixture of two monoclonal anti-GFP antibodies (Roche, catalog number 11814460001, dilution 1:2,000) and a secondary horseradish peroxidase linked anti-mouse IgG anti-

body (GE Healthcare, NA931V). Western blots were developed using ECL Plus Western Blotting Detection System (GE Healthcare).

Decapping Assays. Decapping assays were performed as described before (12), using an in vitro synthesized RNA (127-nucleotides). The RNA probe was labeled with [α-^{32}P]GTP using the ScriptCap m^{7}G Capping System and the ScriptCap 2′-O-Methyltransferase kit (EPICENTRE Biotechnologies). Human HEK293 cells were transfected with plasmids expressing GFP-tagged proteins (10 μg plasmid/10-cm dish). Two days after transfection, cells were washed with PBS and lysed as described above for the immunoprecipitation assays. Samples were processed as described for the immunoprecipitation assays, with the exception that the last washing step was performed with NET-2 buffer (50 mM Tris·HCl, pH 7.5, 150 mM NaCl, 0.05% Triton X-100, and 0.1 mg/mL BSA). Aliquots of the beads (5 μL of a 1:2 slurry in NET-2 buffer) were incubated for 30 min at 30 °C in a thermomixer (at 700 rpm) with approximately 50 ng RNA substrate in a final volume of 10 μL in decapping buffer [50 mM Tris·HCl, pH 7.9, 30 mM ammonium sulfate, 1 mM $MgCl_2$, and 0.1 mM cap structure analog (NEB)]. When indicated 1 U of nucleoside 5′-diphosphate kinase (Sigma) and ATP (0.5 mM final concentration) were added, and samples were incubated for an additional 30 min. Reactions were stopped by adding up to 50 mM EDTA and analyzed on PEI cellulose TLC plates (Merck) in 0.75 M LiCl (1 μL/sample). Unlabeled GDP, m^{7}GMP, m^{7}GDP, and m^{7}GTP were used as markers.

Fluorescence Microscopy. For fluorescence microscopy, human HeLa cells were grown on coverslips in 24-well plates and transfected using Lipofectamine 2000 (Invitrogen). The transfection mixtures contained either 0.3 μg (for DCP1 wild-type) or 0.5 μg (for DCP1 mutants) of plasmids expressing GFP-protein fusions.

Two days after transfection, cells were fixed with 4% paraformaldehyde in PBS for 10 min, and permeabilized for 10 min with PBS containing 0.5% Triton X-100. Endogenous P-bodies were detected using a monoclonal antibody (sc-8418, Santa Cruz Biotechnology), which cross-reacts with EDC4 (13) at a 1:1,000 dilution in PBS containing 0.1% Tween-20, and 10% FBS (FBS). Alexa Fluor 594-coupled goat-anti-mouse secondary antibody (Molecular Probes) was used at a 1:1,000 dilution. Cells were mounted using Fluoromount-G (Southern Biotechnology Associates, Inc.). Images were acquired using a Leica TCS SP2 confocal.

Immunoprecipitations, RNA Interference, and Complementation Assay in *D. melanogaster* S2 Cells. Protein coimmunoprecipitations in S2 cells were performed as described before (14, 15). Luciferase reporters and plasmids for expression of miRNAs and HA-tagged proteins were described before (14, 15). Mutants of *D. melanogaster* DCP1 were generated by site-directed mutagenesis using the plasmid pAc5.1B-λN-HA-DCP1 (dsRNA resistant) as template, using the QuikChange mutagenesis kit from Stratagene. Plasmid pAc5.1B-λNHA-DCP1 (dsRNA resistant) carries mutations that prevent the interaction with DCP1-dsRNA without changing the protein sequence. RNA interference was performed as described before (14) with the exception that cells were depleted on days 0 and 4, transfected on day 7 and collected on day 10. Transfections of S2 cells were performed in six-well plates, using Effectene transfection reagent (Qiagen). For miRNA-mediated silencing assays, the transfection mixtures contained 0.1 μg of firefly luciferase reporter plasmid, 0.4 μg the *Renilla* transfection control, and 0.4 μg plasmids expressing miRNA primary transcripts or the corresponding vector without insert. When indicated, 0.025–1 μg of plasmids expressing recombinant proteins were cotransfected. Firefly and *Renilla* luciferase activities were measured 3 days after transfection using the Dual-Luciferase Reporter Assay System (Promega). Total RNA was isolated using TriFast (Peqlab Biotechnologies) and analyzed as described before (14).

1. Kabsch W (1993) Automatic processing of rotation diffraction data from crystals of initially unknown symmetry and cell constants. *J Appl Crystallogr* 26:795–800.
2. Zwart PH, Grosse-Kunstleve RW, Lebedev AA, Murshudov GN, Adams PD (2008) Surprises and pitfalls arising from (pseudo)symmetry. *Acta Crystallogr D Biol Crystallogr* 64:99–107.
3. Vonrhein C, Blanc E, Roversi P, Bricogne G (2007) Automated structure solution with autoSHARP. *Methods Mol Biol* 364:215–230.
4. Cowtan K (2002) General quadratic functions in real and reciprocal space and their application to likelihood phasing. *Acta Crystallogr D Biol Crystallogr* 56:1612–1621.
5. Emsley P, Cowtan K (2004) Coot: Model-building tools for molecular graphics. *Acta Crystallogr D Biol Crystallogr* 60:2126–2132.
6. Cohen SX, et al. (2008) ARP/wARP and molecular replacement: The next generation. *Acta Crystallogr D Biol Crystallogr* 64:49–60.
7. Murshudov GN, Vagin AA, Dodson EJ (1997) Refinement of macromolecular structures by the maximum-likelihood method. *Acta Crystallogr D Biol Crystallogr* 53:240–255.
8. McCoy AJ, et al. (2007) Phaser crystallographic software. *J Appl Cryst* 40:658–674.
9. Davis IW, et al. (2007) MolProbity: All-atom contacts and structure validation for proteins and nucleic acids. *Nucleic Acids Res* 35:W375–W383.
10. Hooft RW, Vriend G, Sander C, Abola EE (1996) Errors in protein structures. *Nature* 381:272.
11. Lazzaretti D, Tournier I, Izaurralde E (2009) The C-terminal domains of human TNRC6A, B, and C silence bound transcripts independently of the Argonaute proteins. *RNA* 15:1059–1066.
12. Lykke-Andersen J (2002) Identification of a human decapping complex associated with hUpf proteins in nonsense-mediated decay. *Mol Cell Biol* 22:8114–8121.
13. Kedersha N, Anderson P (2007) Mammalian stress granules and processing bodies. *Methods Enzymol* 431:61–81.
14. Eulalio A, et al. (2007) Target-specific requirements for enhancers of decapping in miRNA-mediated gene silencing. *Genes Dev* 21:2558–2570.
15. Eulalio A, Huntzinger E, Izaurralde E (2008) GW182 interaction with Argonaute is essential for miRNA-mediated translational repression and mRNA decay. *Nat Struct Mol Biol* 15:346–353.

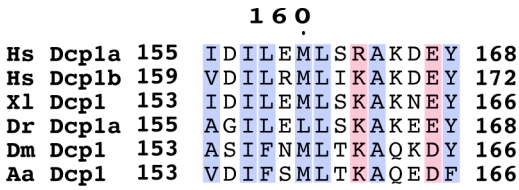

Fig. S1. Sequence alignment of conserved motif MI of DCP1 orthologs from *Homo sapiens* (Hs), *Xenopus laevis* (Xl), *Danio rerio* (Dr), *Drosophila melanogaster* (Dm), and *Aedes aegypti* (Aa). This motif is not conserved in DCP1 orthologs from *Caenorhabditis elegans* and plants. Conserved residues are shaded blue (hydrophobic) or red (charged).

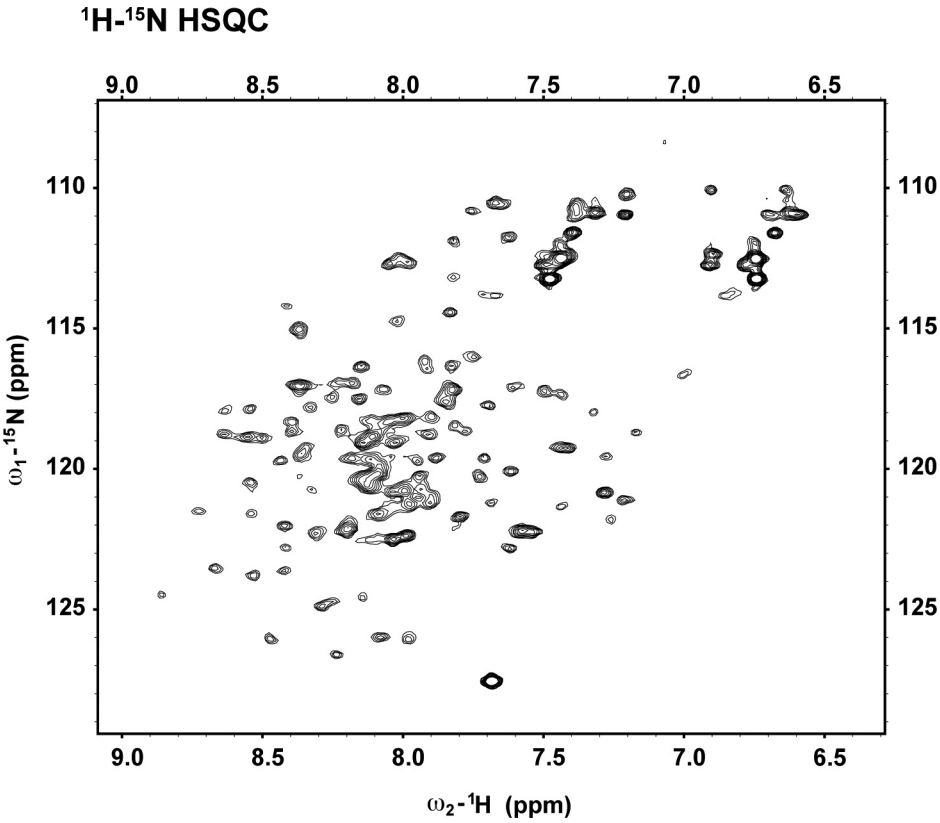

Fig. S2. 2D-^{1}H-^{15}N HSQC spectrum of human DCP1a-TD measured at 291 K. The spectrum shows at least 115 well-resolved NH-peaks. A pure and symmetric homotrimer, however, would yield only a single set of backbone resonances (51 peaks). The molecular diffusion coefficient of the protein [0.74 ($\pm$ 0.02) $\times 10^{-10}$ m^2/s] is in perfect agreement with the molecular mass of the homotrimer at 291 K and excludes significant exchange between higher or lower oligomeric forms.

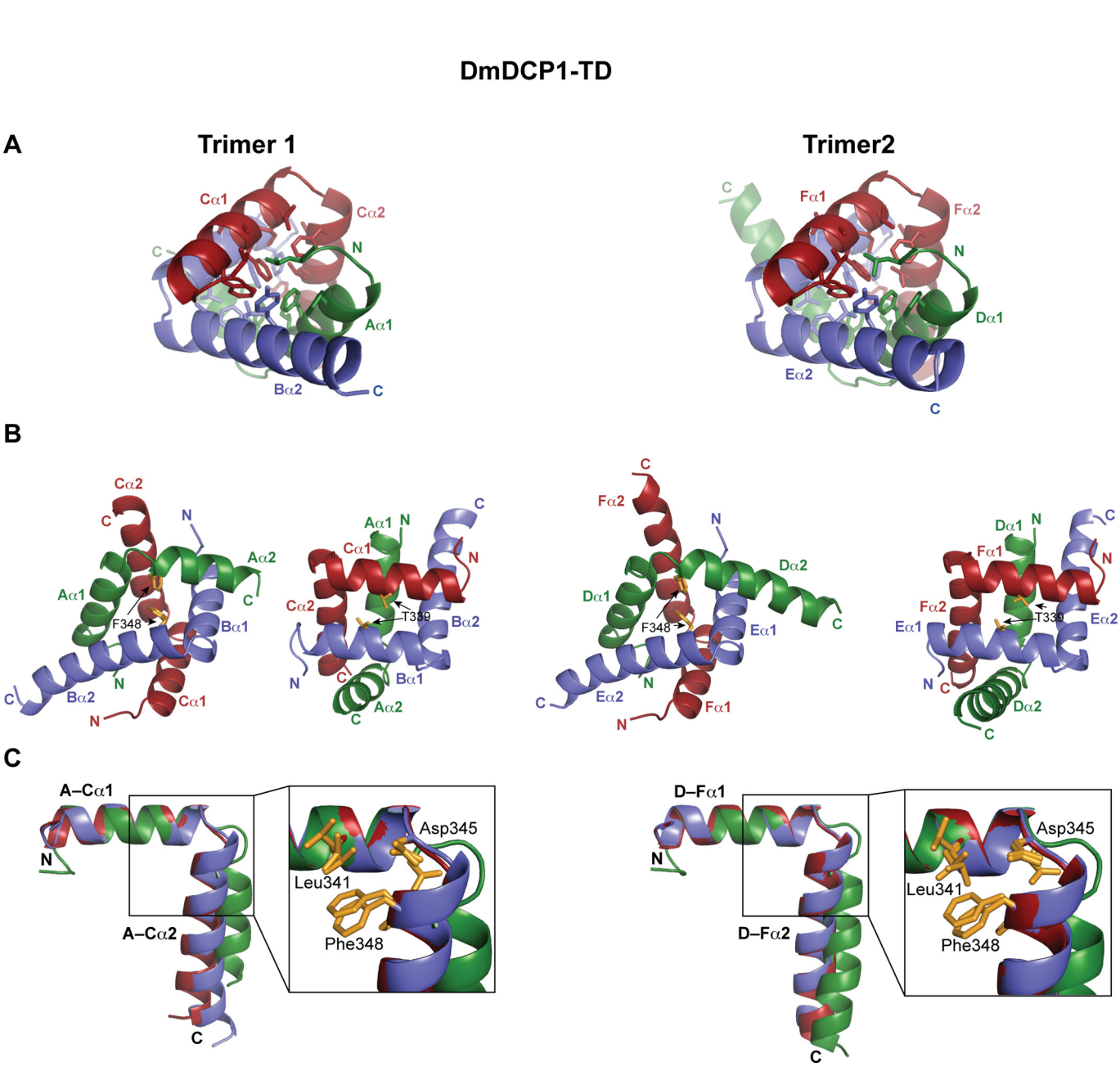

Fig. S3. Crystal structure of the DCP1-trimerization domain from *D. melanogaster* (DmDCP1-TD). The two crystallographically independent trimers are shown side by side. Left side: Trimer 1 with chains A (green), B (blue), and C (red). Right side: Trimer 2 with chains D (green), E (blue), and F (red). (*A*) Top view with the N-termini of chains A and C (D and F in trimer 2) in the front and the N terminus of chain B (E in trimer 2) in the back. Residues from the hydrophobic core are shown as sticks. A total of 4,200 Å^2 (4,000 Å^2 in trimer 2) is buried by the interfaces of the three chains. (*B*) Asymmetric arrangement of the chains, oriented like in Fig. 1 *D* and *E*, with corresponding residues labeled. The pseudodyad relating chains A and B in the human protein is absent in DmDCP1-TD due to a partial unwinding of the N-terminal turn in helix Aα2 (Dα2 in trimer 2). (*C*) Superposition of helix α1 and comparison of the three chains of DmDCP1-TD with a close-up on the helix elbow. Strictly conserved side-chains are shown as sticks. Note that helix Aα2 (Dα2 in trimer 2) is shifted in its relative position when compared to the other two chains of the DmDCP1 trimer or to the human ortholog (Fig. 1*F*).

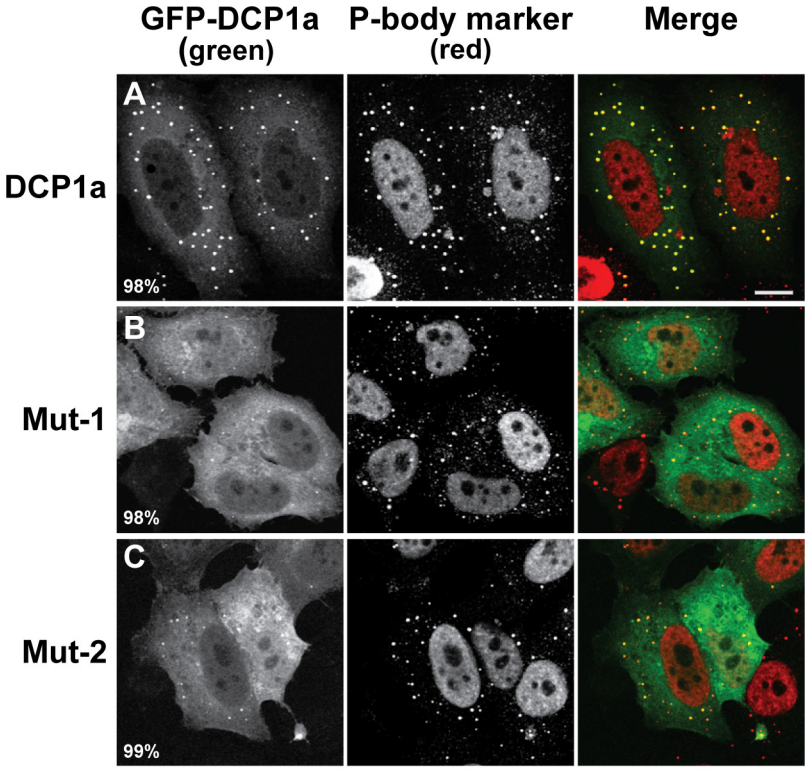

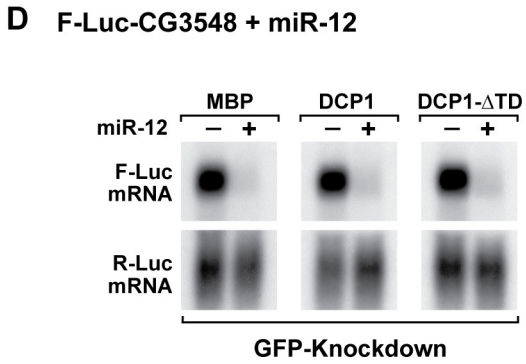

Fig. S4. Trimerization enhances accumulation of DCP1a in P-bodies and is required for decapping in vivo. (*A*–*C*) Representative confocal fluorescent micrographs of fixed human HeLa cells expressing GFP-DCP1a wild-type or the mutants indicated on the left. Cells were stained with an antibody that cross-reacts with EDC4 and a human nuclear antigen. The merged images show the GFP signal in green and the EDC4 signal in red. The fraction of cells exhibiting a staining identical to that shown in the representative panel was determined by scoring at least 100 cells in three independent transfections performed per protein. (Scale bar, 10 μm.) (*D*) *D. melanogaster* S2 cells were treated with dsRNA targeting the ORF of DCP1 and EDC4 mRNAs. Control cells were treated with GFP dsRNA. These cells were subsequently transfected with a mixture of three plasmids: one expressing the F Luc-CG3548 reporter; another expressing miR-12 primary transcripts (+miR-12) or the corresponding empty vector (−); and a third expressing *Renilla* luciferase (R Luc). Plasmids (5 ng) encoding wild-type HA-DCP1, HA-DCP1ΔTD, or HA-MBP were included in the transfection mixtures, as indicated. The panel shows RNA samples isolated from control cells.

Table S1. Molecular weight of wild-type human or *D. melanogaster* DCP1 trimerization domains and corresponding mutants as determined by static light scattering

	Human DCP1a-TD	*D. melanogaster* DCP1-TD
	MW[kDa]	MW[kDa]
Wild-type	16.3	15.1
Theoretical trimer	*17.4*	*15.6*
Mut-1	7.4	3.8
Mut-2	7.1	5.6
Mut-3	5.3	5.6
Theoretical monomer	*5.8*	*5.2*

Table S2. Data collection, phasing and refinement statistics

	HsDCP1a-TD	HsDCP1a-TD	DmDCP1-TD
	Se-Met	Native	Native
Data collection			
Space group	$P3_221$	$P3_221$	$P6_122$
Cell dimensions			
(a/b/c), Å	64.2, 64.2, 103.3	64.7, 64.7, 103.0	120.9, 120.9, 134.5
($\alpha/\beta/\gamma$) °	90.0, 90.0, 120.0	90.0, 90.0, 120.0	90.0, 90.0, 120.0
Wavelength, Å	0.9792	1.0688	1.0643
Resolution, Å	38–2.8 (2.87–2.80)	80–2.3 (2.37–2.31)	50–2.8 (2.87–2.80)
R_{merge}, %	6.6 (25.5)	8.0 (55.7)	10.7 (80.0)
I/σ (I)	22.0 (7.3)	11.9 (2.5)	13.0 (2.0)
Completeness, %	99.8 (100.0)	98.9 (95.7)	98.2 (96.0)
Completeness, anomalous, %	99.6 (96.9)	—	—
Redundancy	8.3 (6.3)	3.5 (3.5)	4.8 (4.4)
Redundancy, anomalous	4.6 (3.5)	—	—
Phasing			
R_{cullis}	0.929	—	—
Phasing power	0.552	—	—
Mean figure of merit	0.192	—	—
Refinement			
Resolution, Å	—	2.3	2.8
No. reflections	—	10708	13830
R_{work}/R_{free}, %	—	20.8/25.2	21.5/26.7
No. atoms			
Protein	—	1050	2053
Ligand/ion	—	0	25
Water	—	54	54
B-factors			
Protein, Å^2	—	33.1	42.5
Ligand/ion, Å^2	—	—	101.7
Water, Å^2	—	40.0	41.1
Ramachandran plot			
Most favoured regions, %		98.4	96.7
Disallowed regions, %		0.0	0.0
R.m.s. deviations			
Bond lengths, Å	—	0.0183	0.0113
Bond angles, °	—	1.648	1.272

*Values in parentheses are for the highest-resolution shell.

Molecular Cell
Short Article

Structural Basis for the Mutually Exclusive Anchoring of P Body Components EDC3 and Tral to the DEAD Box Protein DDX6/Me31B

Felix Tritschler,[1] Joerg E. Braun,[1] Ana Eulalio,[1] Vincent Truffault,[1] Elisa Izaurralde,[1,*] and Oliver Weichenrieder[1,*]
[1]Max Planck Institute for Developmental Biology, Spemannstrasse 35, D-72076 Tübingen, Germany
*Correspondence: elisa.izaurralde@tuebingen.mpg.de (E.I.), oliver.weichenrieder@tuebingen.mpg.de (O.W.)
DOI 10.1016/j.molcel.2009.02.014

SUMMARY

The DEAD box helicase DDX6/Me31B functions in translational repression and mRNA decapping. How particular RNA helicases are recruited specifically to distinct functional complexes is poorly understood. We present the crystal structure of the DDX6 C-terminal RecA-like domain bound to a highly conserved FDF sequence motif in the decapping activator EDC3. The FDF peptide adopts an α-helical conformation upon binding to DDX6, occupying a shallow groove opposite to the DDX6 surface involved in RNA binding and ATP hydrolysis. Mutagenesis of Me31B shows the relevance of the FDF interaction surface both for Me31B's accumulation in P bodies and for its ability to repress the expression of bound mRNAs. The translational repressor Tral contains a similar FDF motif. Together with mutational and competition studies, the structure reveals why the interactions of Me31B with EDC3 and Tral are mutually exclusive and how the respective decapping and translational repressor complexes might hook onto an mRNA substrate.

INTRODUCTION

DEAD box proteins are RNA-dependent ATPases that participate in most, if not all, steps of cellular RNA metabolism (Linder and Lasko, 2006). They are thought to unwind short RNA duplexes in a nonprocessive manner and/or disrupt RNA-protein interactions (Jankowsky and Bowers, 2006). DEAD box proteins are characterized by 11 evolutionarily conserved motifs (Q, I, Ia, GG, Ib, II, III, IV, QxxR, V, and VI), including the signature sequence DEAD (motif II), from which the name of the family is derived. The 11 motifs define the conserved core of the protein family, which consists of two globular RecA-like domains connected by a flexible hinge (Caruthers et al., 2000).

The human DEAD box protein DDX6 (also known as RCK/p54) and its orthologs in *X. laevis* (Xp54), *D. melanogaster* (Me31B), *C. elegans* (CGH-1), and *S. cerevisiae* (Dhh1p) play a critical role in posttranscriptional gene regulation by mediating both translational repression and mRNA decapping (reviewed by Weston and Sommerville, 2006). DDX6 and Me31B in human and *D. melanogaster* cells, respectively, are also implicated in the miRNA pathway (Chu and Rana, 2006; Eulalio et al., 2007).

DDX6 and its orthologs associate with multiple partners to form distinct protein complexes that may repress translation and/or enhance decapping, depending on which other proteins are in these complexes. In *S. cerevisiae*, Dhh1p interacts with Pat1, the LSm1–7 complex, and EDC3 (Coller et al., 2001; Coller and Parker, 2005; Decker et al., 2007); in human cells, DDX6 coimmunoprecipitates with the decapping enzyme DCP2 and the decapping activators DCP1, EDC3, and Ge-1 (also known as EDC4; Fenger-Grøn et al., 2005). These interactions are conserved. Indeed, we recently showed that *D. melanogaster* Me31B coimmunoprecipitates with EDC3, the related protein Trailer hitch (Tral), and the *S. cerevisiae* Pat1 ortholog (HPat; Eulalio et al., 2007; Tritschler et al., 2007, 2008).

EDC3 and Tral (also known as vertebrate RAP55 or *S. cerevisiae* Scd6p) share a domain organization consisting of a divergent N-terminal LSm domain and a central FDF motif (Albrecht and Lengauer, 2004; Anantharaman and Aravind, 2004; Tritschler et al., 2007, 2008). They are thought to act as molecular scaffolds, using their modular domain organization to bridge multiple protein interactions. Indeed, Tral coimmunoprecipitates with DCP1 and the translational regulator CUP, whereas EDC3 coimmunoprecipitates with DCP1 and DCP2 (Decker et al., 2007; Fenger-Grøn et al., 2005; Tritschler et al., 2007, 2008). Moreover, both EDC3 and Tral interact with the C-terminal RecA-like domain of Me31B, via regions encompassing the FDF motifs (Decker et al., 2007; Tritschler et al., 2008).

We aimed to gain insight into how the FDF motifs of EDC3 and Tral interact with DDX6 and its orthologs to form complexes with functions in translational repression and/or mRNA decapping. To this end, we determined the crystal structure, at 2.3 Å resolution, of the C-terminal domain of human DDX6 in complex with an EDC3-FDF peptide. The structure reveals a tight heterodimer, with the EDC3-FDF peptide adopting a helical conformation upon binding to DDX6. In orthologous proteins from different species, residues critical for heterodimerization are conserved. We show that these residues are involved in the interaction between the *D. melanogaster* proteins Me31B and DmEDC3. We further show that Me31B uses the same surface to interact with the FDF motif of Tral. Thus, DDX6/Me31B interacts with EDC3 and Tral in a mutually exclusive manner to form distinct protein complexes, thereby providing a mechanistic explanation for the functional diversity of the DDX6/Me31B helicase.

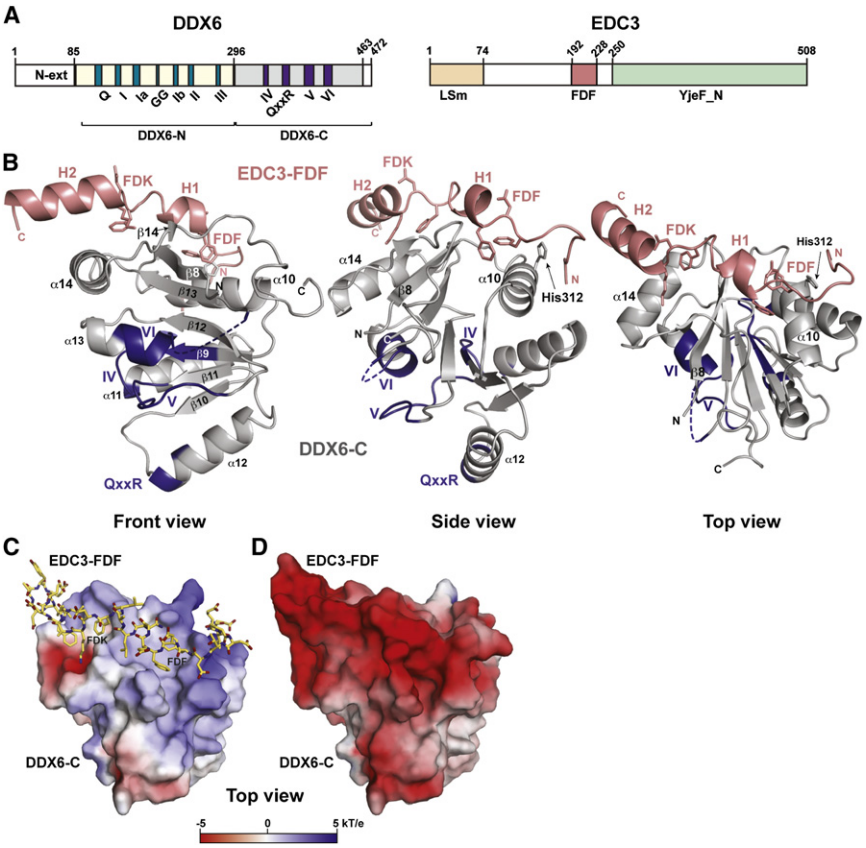

Figure 1. Structure of the DDX6-C/EDC3-FDF Heterodimer

(A) Domain organization of DDX6 and EDC3. The structured part of the DDX6 C-terminal domain is shown in gray, with the conserved helicase motifs in purple. The EDC3-FDF peptide is highlighted in salmon. Numbers correspond to the human proteins.

(B) Ribbon diagrams of the complex colored as in (A). Side chains for the EDC3-FDF and EDC3-FDK motifs and for DDX6-His312 are shown as sticks.

(C and D) Electrostatic potentials were mapped onto the respective molecular surface and contoured from −5 kT/e (red) to +5 kT/e (blue). In (C), EDC3-FDF is represented as sticks (carbons in yellow, oxygens in red, nitrogens in blue) on the molecular surface of DDX6-C. (D) shows the molecular surface of the complex and changes in charge distribution.

RESULTS

Structure of the DDX6 C-Terminal Domain in Complex with an EDC3-FDF Peptide

The C-terminal RecA-like domain of Me31B coimmunoprecipitates with EDC3 and Tral protein fragments encompassing the FDF motifs (Tritschler et al., 2008). Hence, we looked for direct interactions between the bacterially expressed proteins. We found that a small fragment of human EDC3 that contains the FDF motif (residues Phe192–Arg228, referred to as EDC3-FDF; Figure 1A) was sufficient to efficiently copurify with the C-terminal RecA-like domain of DDX6 (residues Lys296–Pro472, referred to as DDX6-C; Figure 1A and data not shown). We purified the heterodimeric complex and obtained two unrelated crystal forms, each containing two heterodimers per asymmetric unit (Table 1). The four refined DDX6-C–EDC3-FDF complexes superpose well, with a maximum pairwise root-mean-square deviation (rmsd) of 0.77 Å (see Figure S1 available online).

The EDC3-FDF Peptide Binds DDX6-C Opposite to the Catalytically Important Interface

DDX6-C adopts a typical RecA-like α/β fold, characterized by a central six-stranded parallel β sheet (β8–β13, in Dhh1p numbering) sandwiched between α helices (α10–α14) that alternate with strands in the protein sequence (Figures 1B and 2A). When compared to yeast Dhh1p (Cheng et al., 2005), DDX6-C superimposes with an rmsd of 0.80 Å.

The EDC3-FDF peptide binds across the β8-edge of the β sheet in a shallow groove between α helices α10 and α14 (Figure 1B; for difference electron density, see Figure S2). As inferred from the structures of Dhh1p and the DEAD box helicase Vasa in complex with RNA and an ATP analog, the peptide binds opposite to the helicase motifs IV, QxxR, V, and VI and thus opposite to the catalytically important interface that is formed between DDX6-C and the DDX6 N-terminal RecA-like domain (Figures 1B and 2B; Cheng et al., 2005; Sengoku et al., 2006). We could not, however, test whether EDC3 binding affects DDX6 catalytic activity, because purified recombinant DDX6 does not exhibit detectable ATPase activity in vitro (data not shown).

The EDC3-FDF Peptide in Complex with DDX6-C Adopts a Helical Conformation

When the EDC3-FDF peptide is bound to DDX6-C, it folds into two consecutive α helices (H1 and H2; Figures 1B and 2C). The helices are preceded and connected by the FDF motif and a related FDK sequence, respectively, motifs that share a strikingly similar structure (Figure 1B). The N-terminal residues of the EDC3-FDF peptide (residues Glu197–Asp203) form a structured loop that wraps around His312, which protrudes from α helix α10 of DDX6-C (Figure 1B, side view).

The FDF motif adopts a particularly interesting conformation that represents an unusual recognition element: the aromatic rings of phenylalanines Phe204 and Phe206 stack perpendicularly to each other in an edge-to-face orientation and are accommodated by DDX6-C in a complementary hydrophobic pocket (Figures 1B, 3A, and 3B). Consequently, the aspartate Asp205 bulges out from between them and caps α helix H1 (Figures 3A and 3B), both neutralizing the positive helix dipole and forming a stabilizing hydrogen bond with the main-chain nitrogen of Gly208 (in H1). Similarly, α helix H2 is capped by Asp214 of the

Table 1. Crystallographic Statistics

	Form I	Form II
Space group	C2	$P2_12_12_1$
Unit cell dimensions (a/b/c) (Å)	172.6, 47.9, 65.8	46.9, 80.0, 110.3
Unit cell angles (α/β/γ), (°)	90.0, 96.4, 90.0	90.0, 90.0, 90.0
Wavelength (Å)	0.978	0.978
R_{merge} (%)[a]	10.1 (55.5)	6.6 (36.1)
Completeness (%)[a]	98.4 (99.7)	95.5 (98.2)
I/σ(I)[a]	10.8 (2.6)	16.5 (4.2)
Number of unique reflections	22482	17392
Multiplicity[a]	2.9 (2.8)	4.6 (4.5)
Resolution range (Å)[a]	46.1–2.3 (2.36–2.3)	45.5–2.3 (2.36–2.3)
R_{cryst}/R_{free} (%)	19.0/26.0	21.0/27.5
Molecules per asymmetric unit		
DDX6-C/EDC3-FDF	2/2	2/2
CAPS/glycerol/phosphate	6/0/4	0/4/0
Number of protein atoms/waters	3144/235	2952/111
Average B factor for protein atoms (Å^2)	26.1	33.3
Ramachandran plot (favored/allowed/outlier %)	97.1/2.9/0	98/2/0
Rmsd from ideal geometry		
Bond lengths, (Å)	0.019	0.019
Bond angles, (°)	1.73	1.78

[a] Numbers in parentheses are for the highest-resolution shell.

FDK motif. Like Asp205 in the FDF motif, Asp214 in the FDK motif bulges out from between the two flanking residues, probably due to their intimate interaction with DDX6-C (Figure 3C).

An Intertwined Network of Interactions Anchors the EDC3-FDF Peptide to DDX6

Approximately 31% (~1000 Å^2) of the total EDC3-FDF surface area is buried in the complex. Much of this is due to hydrophobic contacts, which exploit complementary shapes; but the interface also contains a buried water molecule and numerous direct hydrogen bonds (Figures 3A–3C and Figure S3).

Among the specific hydrogen bonds, most contacts come from α helix α10 of DDX6-C, contacts which constrain the structure of the FDF motif and fix its orientation. On DDX6-C, the side chains of His312 and Thr316 fix the backbone (the carbonyl oxygen of Thr202 and the nitrogen of Asp203, respectively) of the EDC3 N-terminal loop that precedes the FDF motif. Furthermore, the side chain of the conserved EDC3 Asp203 is fixed by a salt bridge to DDX6-C Arg320, and the conserved EDC3 Asn209 (in α helix H1) is contacted by DDX6-C Gln309 (Figures 3A and 3B and Figure S3).

The structure of the FDK motif is similarly stabilized by a water-mediated contact of DDX6-C Tyr302, which fixes the main-chain carbonyls of EDC3 Phe213 and Leu210 (Figure 3B). Additionally, Lys215 from the FDK motif is fixed in a specific pocket on DDX6-C and provides one hydrogen bond to Glu439 on α helix α14 and another hydrogen bond to the carbonyl oxygen of Ile446 in the DDX6-C C-terminal extension (Figure 3C). Finally, the C-terminal end of α helix H2 is fixed by EDC3-Asp223, which accepts a hydrogen bond from DDX6-Lys436 (Figure 3C).

Specificity of the DDX6-EDC3-FDF Interaction

To understand how EDC3-FDF discriminates between DDX6 and other RNA helicases that are structurally closely related, we aligned and superimposed (core rmsd in brackets) the structures of DDX6-C, human UAP56 (1.2 Å; Shi et al., 2004; Zhao et al., 2004), *D. melanogaster* Vasa (1.5 Å; Sengoku et al., 2006), *S. cerevisiae* eIF4A (1.6 Å; Caruthers et al., 2000), human eIF4AIII (1.7 Å; Andersen et al., 2006; Bono et al., 2006), and human DDX3X (1.6 Å; Högbom et al., 2007). We found that the critical side chains of Tyr302, Gln309, His312, and Thr316 are conserved as a group only among DDX6 orthologs (Figure 2A; red boxes). Furthermore, in Vasa and DDX3X, the C-terminal extension would clash with the EDC3-FDF peptide. Consequently, other RNA helicases should not interact with EDC3-FDF. In agreement with this, we observed that EDC3 and Tral interact with Me31B (the *D. melanogaster* DDX6 ortholog), but not with the related DEAD box proteins UAP56, eIF4A, Belle (DDX3), or p68 (Figure S4A).

A Coupled Binding-Folding Mechanism for FDF Peptide-DDX6 Recognition

The binding surface of DDX6-C in complex with the EDC3-FDF peptide is very similar to that of yeast Dhh1p in the absence of binding partners. In contrast, the EDC3-FDF peptide is unlikely to be structured in the unbound form, because the N-terminal loop as well as the FDF and FDK motifs would lose their stabilizing interactions. Consequently, the short α helices H1 and H2 would also be significantly destabilized in the unbound conformation, since the capping aspartates from the FDF and FDK motifs would not be kept in a fixed position without DDX6-C.

To determine experimentally whether the structure of the EDC3-FDF peptide is induced by the rigid conformation of the DDX6-C binding surface, we took NMR measurements of the isolated peptide in solution. In the absence of DDX6, we found no significant α-helical content (Figure S5). Consistent with this, the crystal structure of the C-terminal domain of human EDC3 (residues 203–508) shows that the region encompassing the FDF motif is disordered (Ling et al., 2008). Together, these observations suggest that a coupled binding-folding mechanism operates when the EDC3-FDF peptide interacts with DDX6 (Dyson and Wright, 2005).

The resulting complex is significantly different from the free DDX6 helicase and shows a markedly more negative surface potential (Figures 1C versus Figure 1D). Indeed, in the α-helical conformation adopted by the EDC3-FDF peptide bound to DDX6, a whole series of acidic EDC3-FDF side chains becomes clustered and oriented toward the solvent, creating a large negatively charged patch, which may exclude or favor the recruitment of additional factors (Figures 1C, 1D, and 2C; Asp205, Glu207, Asp214, Glu220, Glu221).

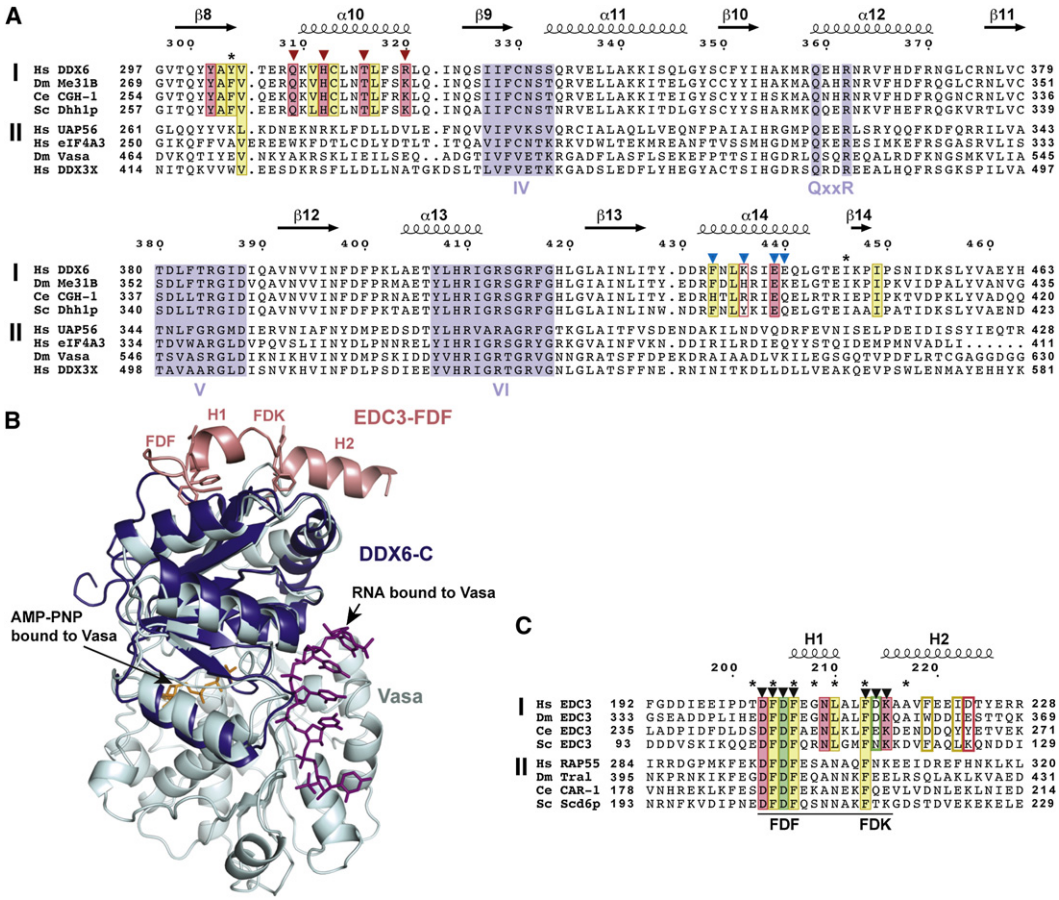

Figure 2. Structure-Based Alignments of DDX6 and EDC3

(A) Sequence alignment of DDX6 orthologs (group I) from *H. sapiens* (DDX6), *D. melanogaster* (Me31B), *C. elegans* (CGH-1), and *S. cerevisiae* (Dhh1) with functionally distinct helicases (group II), UAP56 (*H. sapiens*), eIF4AIII (*H. sapiens*), Vasa (*D. melanogaster*), and DDX3X (*H. sapiens*). Positions involving side-chain interactions between DDX6 and EDC3 are boxed red (specific hydrogen bonds) or yellow (hydrophobic contacts). Boxes are filled if the residues are highly conserved. Boxes are extended to group II if the residues are conserved in both groups. Positions involving specific main-chain contacts are marked with an asterisk. Triangles indicate residues mutated in this study (red triangles indicate residues mutated in DDX6-C^{Mut-1} or Me31B^{Mut-1}, blue triangles indicate residues mutated in Me31B^{Mut-2}). Conserved helicase motifs are shaded in purple. Secondary structure assignment and numbering correspond to DDX6.

(B) Structural superposition of DDX6-C (purple) bound to EDC3-FDF (salmon) with Vasa (pale cyan; Sengoku et al., 2006) bound to RNA (magenta) and an ATP analog (orange).

(C) Sequence alignment of EDC3 orthologs (group I) with orthologs of Tral (group II) from *H. sapiens* (Rap55), *D. melanogaster* (Tral), *C. elegans* (CAR-1), and *S. cerevisiae* (Scd6p). The region that aligns best between EDC3 and Tral is underlined. Helix-capping residues are boxed in green. For the remaining symbols, see (A).

The FDF Motif Is Essential for DDX6-EDC3 Heterodimerization

To identify contacts that are essential for the DDX6-EDC3 interaction, we performed binding assays in vitro using recombinant DDX6-C and minimal, synthetic EDC3-FDF peptides with an N-terminal fluorescein label (EDC3 residues 197–224). We tested both a wild-type peptide (EDC3-FDF^{Fluo}) and a peptide in which the two phenylalanines of the FDF motif were replaced with alanines (EDC3-ADA^{Fluo}).

When mixed with an excess of wild-type EDC3-FDF^{Fluo}, the bulk of DDX6-C shifts to a lower elution volume, consistent with the formation of a well-behaved globular complex (Figure S6A). In contrast, the EDC3-ADA^{Fluo} peptide does not detectably interact with DDX6-C (Figure S6B), demonstrating that, in vitro, the FDF motif is essential for heterodimerization.

To identify similarly important residues on the side of DDX6-C, we substituted Gln309, His312, Thr316, and Arg320 with alanines (DDX6-C^{Mut-1}). In the crystal structure, these residues interact with residues surrounding the FDF motif and represent specificity determinants, as suggested by a phylogenetic comparison (Figures 2A and 3A; boxed residues). As expected, DDX6-C^{Mut-1} no longer interacted with EDC3-FDF^{Fluo} in the gel filtration assay (Figure S6C). It eluted at the same position as the isolated protein (wild-type or mutant) in the absence of peptide, also indicating that the mutations do not affect the protein fold.

The DDX6-EDC3 Heterodimerization Interface Is Conserved

The human and *D. melanogaster* (Dm) proteins are highly conserved (83% and 50% sequence identity for the structured

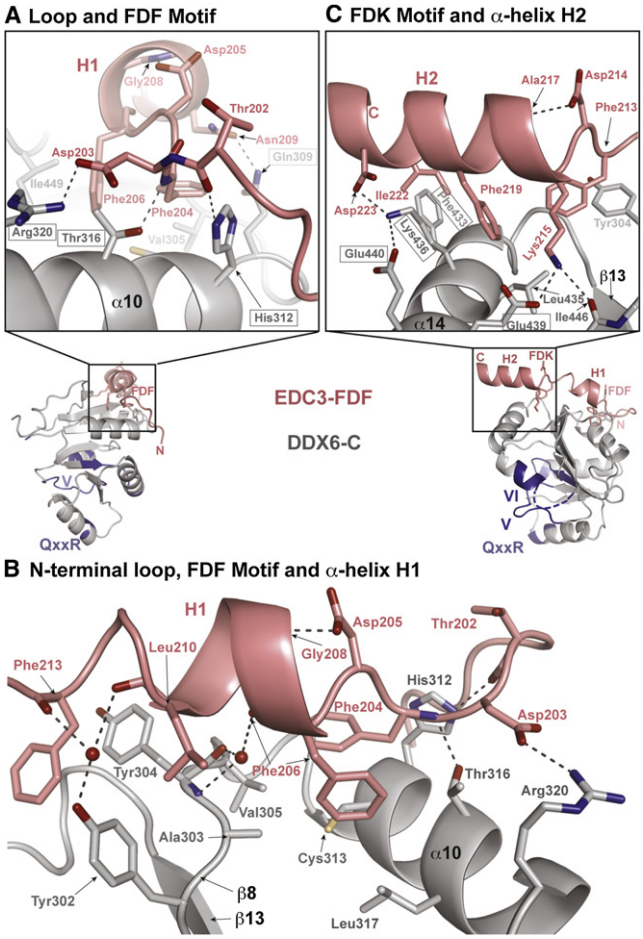

Figure 3. Molecular Interface between DDX6-C and EDC3-FDF

DDX6-C (gray) and EDC3-FDF (salmon) are shown as ribbons with selected side-chain and main-chain atoms as sticks (oxygens in red, nitrogens in blue, sulfurs in yellow). Fixed water molecules are shown as red spheres and hydrogen bonds and salt bridges as dotted lines.

(A) Interactions of the N-terminal loop, the FDF motif, and α helix H1. The four residues mutated in DDX6-C^{Mut-1} have boxed labels.

(B) Interactions of the N-terminal loop, the FDF motif, and α helix H1. β strand β8 is drawn as a loop for clarity.

(C) Interactions of the FDK motif and α helix H2. Equivalent residues mutated in Me31B^{Mut-2} have boxed labels.

parts of DDX6-C and EDC3-FDF, respectively); thus, mutations based on the structure of the human DDX6-EDC3 complex can be easily mapped onto the *D. melanogaster* Me31B-DmEDC3 proteins (Figures 2A and 2C). This enabled us to investigate the effect of such mutations in the context of the full-length proteins in *D. melanogaster* Schneider cells (S2 cells), where these interactions were previously characterized (Tritschler et al., 2007, 2008).

To examine how DmEDC3 mutations affect Me31B binding, HA-tagged wild-type or mutant DmEDC3 was expressed in S2 cells, together with a green fluorescent protein (GFP) fusion of Me31B. We then tested whether anti-HA antibodies could coimmunoprecipitate GFP-Me31B from cell lysates. We found that alanine substitution of Phe345 in the FDF motif of DmEDC3 (corresponding to Phe204 in human EDC3, Figure 2C) strongly impaired the interaction with Me31B (Figure 4A, lane 10). Surprisingly, alanine substitution of Phe347 had only a modest effect (Figure 4A, lane 11). Consistently, when the two phenylalanines in the FDF motif were substituted with alanines, it did not exacerbate the effect of the single Phe345Ala substitution (Figure 4A, lane 12 versus lane 10); this indicates that the first phenylalanine of the FDF motif, which reorients the peptide backbone, is critical for the interaction with Me31B. Similarly, substituting the phenylalanine of the FDK motif with alanine strongly reduced the interaction with Me31B (Figure S4B, lane 9), indicating that both the FDF and FDK motifs play a crucial role in this interaction.

Interestingly, substituting the bulged aspartate (DmEDC3 Asp346) in the FDF motif with either alanine or lysine strongly impaired binding to Me31B (Figure 4A, lanes 13 and 14, respectively), yet this residue does not contribute directly to the heterodimerization interface. Because Asp346 caps and stabilizes helix H1, this result suggests that the absence of Asp346 prevents the EDC3-FDF peptide from adopting the conformation required for binding to Me31B.

On the Me31B heterodimerization surface, double or quadruple substitutions of conserved residues strongly reduced binding to DmEDC3. In particular, an HA-tagged Me31B carrying alanine substitutions of residues surrounding the FDF motif (Gln281, His284, Tyr288, and Lys292; referred to as Me31B^{Mut-1}, and corresponding to DDX6-C^{Mut-1}; Figure 2A, red triangles) abolished binding to DmEDC3 (Figure 4B, lane 13). These results agree with those obtained for the interaction between human DDX6 and EDC3 in vitro (Figure S6). Furthermore, HA-Me31B carrying alanine substitutions of residues interacting with EDC3 helix H2 (Phe405, His408, Glu411, and Lys412; referred to as Me31B^{Mut-2}; Figure 2A, blue triangles) failed to interact with DmEDC3 (Figure 4B, lanes 14–16), indicating that in addition to the FDF and FDK motifs, helix H2 strongly contributes to the affinity of the interaction.

Tral and EDC3 Use a Similar Mode to Interact with Me31B

Previously, we showed that a Tral fragment comprising the FDF motif coimmunoprecipitates with the C-terminal RecA-like domain of Me31B, suggesting that Tral and EDC3 use a similar mode to interact with Me31B (Tritschler et al., 2008). If this were the case, the Tral-Me31B interaction should be abolished by mutating Tral residues located at positions similar to EDC3 residues mediating the interaction with Me31B.

Using the coimmunoprecipitation assays described above, we found that alanine substitutions of any residue in the FDF motif of Tral, or of the phenylalanine in the FEE motif, prevented Tral from binding to Me31B (Figure 4A and Figure S4B). As for EDC3-FDF, the substitution of the bulged aspartate in the FDF motif of Tral abolished Me31B binding, suggesting that the Tral-FDF peptide adopts a similar helical conformation upon binding to Me31B (Figure 4A, lane 27). Consistently, and as expected for a mutually exclusive interaction, a DmEDC3-FDF peptide, but not the corresponding ADA mutant, competed with Tral for binding to Me31B when added to cell lysates before immunoprecipitation (Figure 4C).

Nevertheless, the exact mode of interaction of Tral and EDC3 with Me31B likely differs. Indeed, for Me31B mutations at

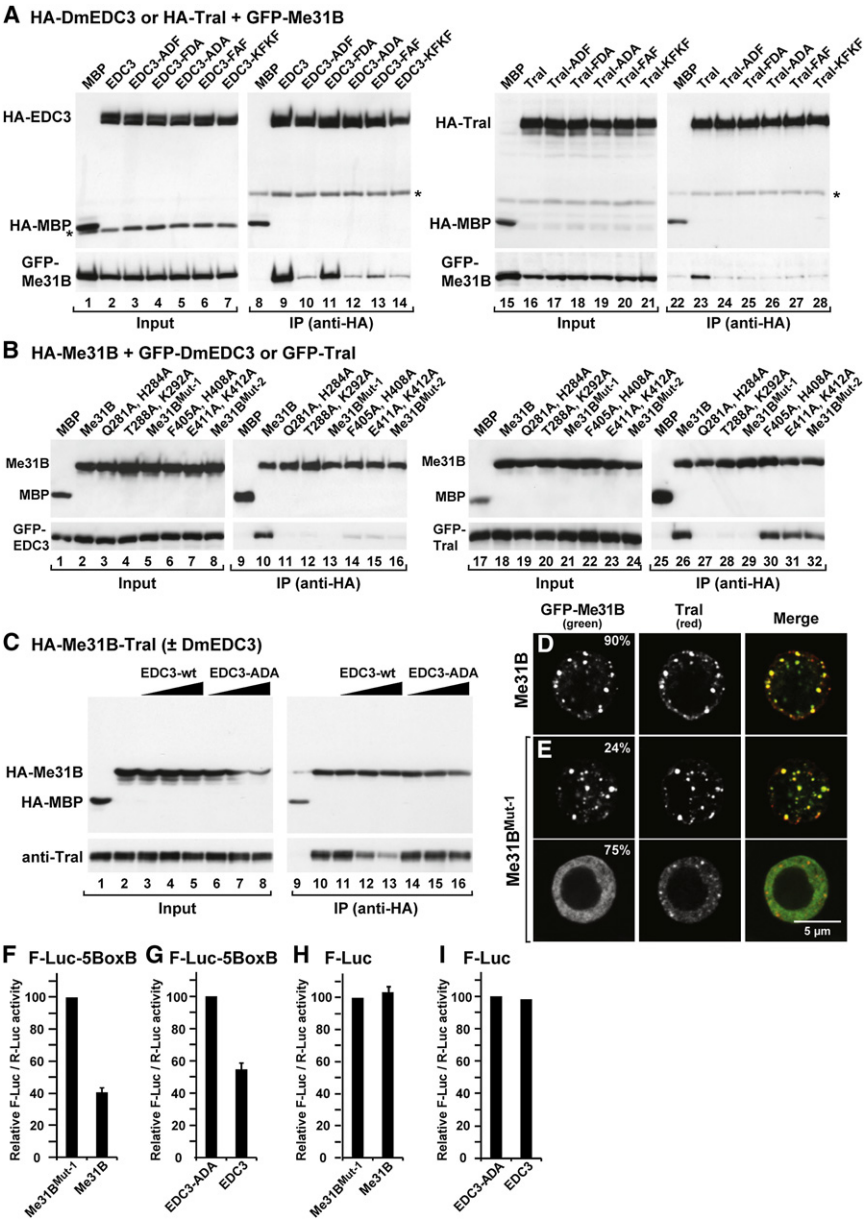

Figure 4. Functional Analysis of Conserved Residues

(A) HA-tagged maltose-binding protein (MBP), wild-type EDC3 or Tral, and the indicated EDC3 or Tral mutants were coexpressed in S2 cells with GFP-Me31B, as indicated. Cell lysates were immunoprecipitated using an anti-HA antibody. The KFKF mutants carry lysine substitutions of aspartate residues preceeding and within the FDF motifs of EDC3 and Tral. Inputs (1%) and immunoprecipitates (10%) were analyzed by western blotting using anti-HA and anti-GFP antibodies. Asterisks indicate crossreactivity of the anti-HA antibody.

(B) HA-tagged MBP, wild-type Me31B, or Me31B mutants were coexpressed in S2 cells with GFP-EDC3 or GFP-Tral, as indicated. Cell lysates were immunoprecipitated and analyzed as described in (A).

(C) HA-MBP or wild-type HA-Me31B was expressed in S2 cells. Cell lysates were immunoprecipitated by using anti-HA antibodies. The presence of endogenous Tral in the immunoprecipitates was analyzed by western blot using anti-Tral antibodies. In lanes 3–8 and 11–16, increasing amounts (0.5, 5, and 10 μg) of purified recombinant EDC3-FDF peptide or of the corresponding ADA mutant were added to the cell lysates prior to immunoprecipitation. Samples were analyzed as described in (A).

(D and E) Confocal fluorescent micrographs of fixed S2 cells expressing GFP-Me31B wild-type or mutant. Cells were stained with anti-Tral antibodies. The fraction of cells exhibiting a staining similar to that shown in the representative panel was determined by scoring at least 100 cells in two independent transfections performed per protein. The merged images show the GFP signal in green and the Tral signal in red.

(F–I) S2 cells were transfected with the F-Luc–5BoxB or F-Luc reporters, a plasmid expressing *Renilla* luciferase, and vectors expressing λN-HA fusions of wild-type or mutant Me31B and EDC3, as indicated. Firefly luciferase activity was normalized to that of the *Renilla* and set to 100 in cells expressing the mutant proteins. Mean values and standard deviations from three independent experiments are shown. Mutant proteins have a comparable effect as the λN-HA peptide alone (data not shown).

residues surrounding the FDF motif (Me31B^{Mut-1}), we observed that if a mutation impaired the interaction with EDC3, then it also impaired the interaction with Tral (Figure 4B, lanes 27–29). In contrast, mutating Me31B residues that interact with helix H2 (Me31B^{Mut-2}) abolished binding to EDC3, but not to Tral (Figure 4B, lanes 14–16 versus 30–32). These results suggest that the highly conserved FDF and FDK motifs of Tral and EDC3 probably compete for the same binding pocket on the helicase; in contrast, the sequences corresponding to the less conserved helix H2 may play a different role in RAP55/Tral (Figure 2C).

Me31B Interaction with EDC3 or Tral Is Required for P Body Localization

To test whether disrupting EDC3 binding would also affect the accumulation of Me31B in P bodies, we visualized the localization of Me31B^{Mut-1}. We observed that 90% of cells expressing wild-type GFP-Me31B displayed GFP foci (Figure 4D and Figure S7A). These foci correspond to endogenous P bodies, as judged by the staining with anti-Tral antibodies or by the accumulation of HA-Ge-1. In contrast, only 24% of cells expressing GFP-Me31B^{Mut-1} displayed foci comparable to those observed with the wild-type protein (Figure 4E), whereas ~75% of cells expressing the mutant protein had no detectable GFP foci (Figure 4E).

In cells in which GFP-Me31B^{Mut-1} was dispersed throughout the cytoplasm, the number of endogenous P bodies was reduced (Figure 4E and Figure S7B). Because Tral (and Ge-1) accumulate in P bodies independently of Me31B (Tritschler et al., 2008), these results suggest that overexpressing GFP-Me31B^{Mut-1} inhibits P body formation in a dominant-negative manner.

We previously showed that DmEDC3 and Tral localize to P bodies independently of Me31B (Tritschler et al., 2007, 2008). Consistently, the DmEDC3^{ADA} and Tral^{ADA} mutants (which do not interact with Me31B) accumulated in endogenous P bodies as efficiently as the wild-type proteins (Figures S7C–S7F).

Me31B Interaction with EDC3 or Tral Is Required to Repress the Expression of Bound mRNAs

Previous studies in *Xenopus* oocytes showed that DDX6 represses the expression of bound mRNAs (Minshall et al., 2001; Minshall and Standart, 2004). To determine whether repression required the interaction with EDC3, we adopted the tethering assay used in these studies (Minshall et al., 2001; Minshall and Standart, 2004). This assay involves the expression of a λN-HA fusion of Me31B that binds with high affinity to five BoxB sites (5BoxB) in the 3′UTR of a firefly luciferase reporter mRNA. *Renilla* luciferase served as transfection control. We observed that Me31B repressed firefly luciferase expression, as reported before for *Xenopus* RCK (Figure 4F; Minshall et al., 2001; Minshall and Standart, 2004). In contrast, the Me31B mutant that no longer interacts with Tral and EDC3 did not have a significant effect on firefly luciferase levels (Figure 4F). Similarly, when EDC3 is tethered to the firefly luciferase mRNA, luciferase expression is inhibited relative to the activity measured in cells expressing the λN-HA peptide alone or the EDC3 mutant that does not interact with Me31B (Figure 4G). None of the proteins affected the expression of an F-Luc reporter lacking BoxB elements (F-Luc; Figures 4H and 4I). These results indicate that Me31B and EDC3 must interact to repress the expression of bound mRNAs.

DISCUSSION

The crystallographic analysis of DDX6-C in complex with the EDC3-FDF peptide reveals that these proteins interact via a highly conserved interface. In DDX6, the surface required for heterodimerization is preformed; in contrast, the EDC3-FDF peptide is unstructured in solution and adopts an α-helical conformation only upon binding to DDX6.

The association of EDC3 with DDX6 may represent an important step in the assembly of a multimeric complex dedicated to mRNA decapping. Indeed, EDC3 also interacts with the decapping enzyme DCP2 and the decapping activator DCP1 (Decker et al., 2007; Tritschler et al., 2007, 2008) and may enhance decapping by positioning the catalytic subunit of the decapping complex (DCP2) in proximity to DCP1. The interaction with the FDF peptide thus anchors the decapping activity onto DDX6, which, as a helicase, could bind the mRNA substrate in an ATP-dependent manner.

DDX6 and its orthologs also play a fundamental role in regulating translation of maternal mRNAs during oogenesis and early embryogenesis (reviewed by Weston and Sommerville, 2006). In agreement with this, *Xenopus* DDX6 represses the expression of bound mRNAs (Minshall et al., 2001; Minshall and Standart, 2004). We show that this repressive activity requires the interaction with EDC3 or Tral. Nevertheless, the precise molecular mechanism by which DDX6 orthologs exert their repressive functions remains to be established.

DEAD box proteins are highly specific despite having a conserved helicase core, and they cannot be mutually interchanged. Their specificity is governed by interactions with other protein partners and/or RNPs (Linder and Lasko, 2006). We show here that DDX6/Me31B achieves specificity, at least in part, through mutually exclusive interactions with partners such as EDC3 and Tral; these partners associate with the helicase to form distinct protein complexes (Tritschler et al., 2008). In these alternative complexes, when RNA stimulates the ATP hydrolysis activity of DDX6 orthologs, the RNP substrate may be remodeled to facilitate the action of other components in these complexes (e.g., DCP2). In this scenario, DDX6 orthologs would function as "blind" remodeling subunits in diverse protein complexes. The final outcome of their action would thus be specified by both the additional proteins they associate with and the composition of the mRNP target. Therefore, to understand the precise molecular function of DDX6 orthologs, the biochemical, functional, and structural properties of the complexes in which they are assembled should be characterized further.

EXPERIMENTAL PROCEDURES

Protein Expression, Purification, and Crystallization

N-terminally tagged His_6-RCK-C and GST-EDC3-FDF were coexpressed in the *E. coli* strain Rosetta 2(DE3) (Novagen) at 25°C overnight. Complexes were purified by consecutive Ni^{2+} and glutathione affinity steps. After cleaving the tags with 3C protease, complexes were further purified by ion exchange chromatography and gel filtration (Mono Q 5/50 GL and HiLoad 26/60 Superdex 75 columns (GE Healthcare)). A detailed description of crystallization conditions is provided in the Supplemental Data.

Structure Determination and Refinement

Diffraction data were collected on beamline PXII of the Swiss Light Source (SLS), Villigen, Switzerland. For both crystal forms, the structure was solved independently by molecular replacement using the C-terminal domain (K256-A420) of Dhh1p (PDB-ID 1s2m) as a search model. Additional information is provided in the Supplemental Data.

Coimmunoprecipitation Assays, Western Blotting, and Fluorescence Microscopy

Plasmids expressing GFP- or λN-HA-tagged EDC3, Tral, and Me31B in S2 cells have been described (Tritschler et al., 2007, 2008). Mutants were generated by site-directed mutagenesis using the QuikChange Site-Directed Mutagenesis Kit from Stratagene and the appropriate oligonucleotide sequences. Transfections, coimmunoprecipitations, western blotting, and immunofluorescence were performed as described before (Tritschler et al., 2007, 2008).

Tethering Assays

Plasmids for performing the tethering assay in S2 cells were described before (Rehwinkel et al., 2005). Transfections of S2 cells were performed in 6-well plates, using Effectene transfection reagent (QIAGEN). The transfection mixtures contained 0.1 μg reporter plasmid (F-Luc-5BoxB or F-Luc), 0.4 μg pAc5.1-R-Luc as transfection control, and 0.01 μg (Me31B) or 0.1 μg (EDC3) of plasmids expressing λN-HA-protein fusions. Firefly and *Renilla* luciferase activities were measured 3 days after transfection using the Dual-Luciferase Reporter Assay System (Promega).

ACCESSION NUMBERS

Atomic coordinates and structure factors for crystal form I and form II have been deposited with the Protein Data Bank under ID codes 2wax and 2way, respectively.

SUPPLEMENTAL DATA

The Supplemental Data include supplemental text, Supplemental References, and seven figures and can be found with this article online at http://www.cell.com/molecular-cell/supplemental/S1097-2765(09)00130-0.

ACKNOWLEDGMENTS

We are grateful to R. Büttner and S. Helms for excellent technical assistance and to K. Kinkelin for generating some of the DNA constructs used in this study. We thank Dr. K. Zeth and the staff at the PX beamlines of the Swiss Light Source for assistance with data collection. This study was supported by the Max Planck Society, by a grant from the Deutsche Forschungsgemeinschaft (DFG, FOR855), and by the Sixth Framework Programme of the European Commission through the SIROCCO Integrated Project LSHG-CT-2006-037900. O.W. holds a personal VIDI fellowship from the Dutch National Science Organization (NWO-VIDI, CW 700.54.427).

Received: September 29, 2008
Revised: December 24, 2008
Accepted: February 18, 2009
Published: March 12, 2009

REFERENCES

Albrecht, M., and Lengauer, T. (2004). Novel Sm-like proteins with long C-terminal tails and associated methyltransferases. FEBS Lett. *569*, 18–26.

Anantharaman, V., and Aravind, L. (2004). Novel conserved domains in proteins with predicted roles in eukaryotic cell-cycle regulation, decapping and RNA stability. BMC Genomics *5*, 45.

Andersen, C.B., Ballut, L., Johansen, J.S., Chamieh, H., Nielsen, K.H., Oliveira, C.L., Pedersen, J.S., Séraphin, B., Le Hir, H., and Andersen, G.R. (2006). Structure of the exon junction core complex with a trapped DEAD-box ATPase bound to RNA. Science *313*, 1968–1972.

Bono, F., Ebert, J., Lorentzen, E., and Conti, E. (2006). The crystal structure of the exon junction complex reveals how it maintains a stable grip on mRNA. Cell *126*, 713–725.

Caruthers, J.M., Johnson, E.R., and McKay, D.B. (2000). Crystal structure of yeast initiation factor 4A, a DEAD-box RNA helicase. Proc. Natl. Acad. Sci. USA *97*, 13080–13085.

Cheng, Z., Coller, J., Parker, R., and Song, H. (2005). Crystal structure and functional analysis of DEAD-box protein Dhh1p. RNA *11*, 1258–1270.

Chu, C.Y., and Rana, T.M. (2006). Translation repression in human cells by microRNA-induced gene silencing requires RCK/p54. PLoS Biol. *4*, e210. 10.1371/journal.pbio.0040210.

Coller, J., and Parker, R. (2005). General translational repression by activators of mRNA decapping. Cell *122*, 875–886.

Coller, J.M., Tucker, M., Sheth, U., Valencia-Sanchez, M.A., and Parker, R. (2001). The DEAD box helicase, Dhh1p, functions in mRNA decapping and interacts with both the decapping and deadenylase complexes. RNA *7*, 1717–1727.

Decker, C.J., Teixeira, D., and Parker, R. (2007). Edc3p and a glutamine/asparagine-rich domain of Lsm4p function in processing body assembly in Saccharomyces cerevisiae. J. Cell Biol. *179*, 437–449.

Dyson, H.J., and Wright, P.E. (2005). Intrinsically unstructured proteins and their functions. Nat. Rev. Mol. Cell Biol. *6*, 197–208.

Eulalio, A., Rehwinkel, J., Stricker, M., Huntzinger, E., Yang, S.-F., Doerks, T., Dorner, S., Bork, P., Boutros, M., and Izaurralde, E. (2007). A target-specific requirement for enhancers of decapping in miRNA-mediated gene silencing. Genes Dev. *21*, 2558–2570.

Fenger-Grøn, M., Fillman, C., Norrild, B., and Lykke-Andersen, J. (2005). Multiple processing body factors and the ARE binding protein TTP activate mRNA decapping. Mol. Cell *20*, 905–915.

Högbom, M., Collins, R., van den Berg, S., Jenvert, R.M., Karlberg, T., Kotenyova, T., Flores, A., Karlsson Hedestam, G.B., and Schiavone, L.H. (2007). Crystal structure of conserved domains 1 and 2 of the human DEAD-box helicase DDX3X in complex with the mononucleotide AMP. J. Mol. Biol. *372*, 150–159.

Jankowsky, E., and Bowers, H. (2006). Remodeling of ribonucleoprotein complexes with DExH/D RNA helicases. Nucleic Acids Res. *34*, 4181–4188.

Linder, P., and Lasko, P. (2006). Bent out of shape: RNA unwinding by the DEAD-box helicase Vasa. Cell *125*, 219–221.

Ling, S.H., Decker, C.J., Walsh, M.A., She, M., Parker, R., and Song, H. (2008). Crystal structure of human Edc3 and its functional implications. Mol. Cell. Biol. *28*, 5965–5976.

Minshall, N., and Standart, N. (2004). The active form of Xp54 RNA helicase in translational repression is an RNA-mediated oligomer. Nucleic Acids Res. *32*, 1325–1334.

Minshall, N., Thom, G., and Standart, N. (2001). A conserved role of a DEAD box helicase in mRNA masking. RNA *7*, 1728–1742.

Rehwinkel, J., Behm-Ansmant, I., Gatfield, D., and Izaurralde, E. (2005). A crucial role for GW182 and the DCP1:DCP2 decapping complex in miRNA-mediated gene silencing. RNA *11*, 1640–1647.

Sengoku, T., Nureki, O., Nakamura, A., Kobayashi, S., and Yokoyama, S. (2006). Structural basis for RNA unwinding by the DEAD-box protein Drosophila Vasa. Cell *125*, 287–300.

Shi, H., Cordin, O., Minder, C.M., Linder, P., and Xu, R.M. (2004). Crystal structure of the human ATP-dependent splicing and export factor UAP56. Proc. Natl. Acad. Sci. USA *101*, 17628–17633.

Tritschler, F., Eulalio, A., Truffault, V., Hartmann, M.D., Helms, S., Schmidt, S., Coles, M., Izaurralde, E., and Weichenrieder, O. (2007). A divergent Sm-fold in EDC3 proteins mediates DCP1-binding and P-body targeting. Mol. Cell. Biol. *27*, 8600–8611.

Tritschler, F., Eulalio, A., Helms, S., Schmidt, S., Coles, M., Weichenrieder, O., Izaurralde, E., and Truffault, V. (2008). A similar mode of interaction enables Trailer Hitch and EDC3 to associate with DCP1 and Me31B in distinct protein complexes. Mol. Cell. Biol. *28*, 6695–6708.

Weston, A., and Sommerville, J. (2006). Xp54 and related (DDX6-like) RNA helicases: roles in messenger RNP assembly, translation regulation and RNA degradation. Nucleic Acids Res. *34*, 3082–3094.

Zhao, R., Shen, J., Green, M.R., MacMorris, M., and Blumenthal, T. (2004). Crystal structure of UAP56, a DExD/H-box protein involved in pre-mRNA splicing and mRNA export. Structure *12*, 1373–1381.

Molecular Cell, Volume *33*

Supplemental Data

Structural Basis for the Mutually Exclusive Anchoring of P Body Components EDC3 and Tral to the DEAD Box Protein DDX6/Me31B

Felix Tritschler, Joerg E. Braun, Ana Eulalio, Vincent Truffault, Elisa Izaurralde, and Oliver Weichenrieder

DNA constructs

cDNA sequences encoding the FDF peptide of *H. sapiens* EDC3 (gi:18204641; Phe192 to Arg228) and *H. sapiens* DDX6-C (gi:458727; Lys296 to Pro472) were amplified from an oligo $(dT)_{15}$-primed human cDNA library, and cloned into a modified pRSFDuet-1 (Novagen) vector.

Crystallization

Diffraction quality crystals were grown by sitting drop vapor diffusion. Drops containing 0.4 µl protein solution (at 12 mg/ml in 10 mM Na-HEPES pH 7.5, 5 mM DTT and 100 mM NaCl) plus 0.4 µl reservoir solution were equilibrated at 19°C over 75 µl of reservoir. After two weeks crystal form I (clustered plates of 80 x 80 x 10 μm^3) was obtained over 100 mM N-cyclohexyl-3-aminopropanesulfonic acid pH 10.5, 1.2 M NaH_2PO_4, 0.8 M K_2HPO_4 and 200 mM Li-SO_4. Crystal form II (a single rod of 50 x 10 x 10 μm^3) was obtained over 40 mM KH_2PO_4, 16% PEG8000 and 20% glycerol. For crystal form II, the single rod was directly flash-frozen in liquid nitrogen. For crystal form I, single fragments were broken from the clusters and cryoprotected in 1.8 M NaH_2PO_4, 1.2 M K_2HPO_4 and 200 mM Li-SO_4 before flash-freezing.

Structure determination and refinement

Diffraction images were processed with XDS (Kabsch 1993). Due to poor diffraction quality of crystal form II in one particular orientation, data were cut at 2.3 Å resolution and are only 95.5 % complete. The structure was solved for both crystal forms independently by molecular replacement using PHASER (McCoy, 2007). As a search model, we took the C-terminal domain (K256-A420) of Dhh1p (PDB-ID 1s2m). For each crystal form two copies of the search model were placed per asymmetric unit. After an initial NCS-restrained refinement (REFMAC, Murshudov et al., 1997) of the adjusted DDX6-C model, the EDC3-FDF peptide could be built unambiguously in COOT (Emsley and Cowtan, 2004), guided for the sequence register by the well-defined aromatic side-chains. Further refinement without NCS restraints was done in REFMAC and COOT iteratively. Data collection and structure refinement statistics are shown in Table S1. According to MolProbity (Davis et al., 2007) the geometry of the structures is excellent. All three-dimensional representations are done with PyMOL (http://www.pymol.org). Electrostatic potentials were calculated using the Adaptive Poisson-Boltzmann Solver software (Baker et al., 2000).

Analytical size exclusion chromatography

Components were mixed in chromatography buffer (10 mM HEPES, pH 7.5, 300 mM NaCl, 1 mM DTT) using a protein concentration of 30 μM, and a peptide concentration of approximately 60 μM. After 30 min at 15 °C, 100 μl were injected onto the column (15 °C) at a flow rate of 0.4 ml/min. UV absorption was monitored simultaneously at 280 nm (E280) and 490 nm (E490). Protein concentrations of DDX6-C and DDX6-C^{Mut-1} were estimated from the theoretical molar extinction coefficient ε_{280} at 280 nm. Synthetic peptides (EDC3-FDF^{Fluo}: Fluorescein-

EEIPDTDFDFEGNLALFDKAAVFEEIDT; EDC3-ADA^{Fluo}: Fluorescein-EEIPDTDADAEGNLALFDKAAVFEEIDT; EMC Microcollections, Tübingen, Germany) were monitored at 490 nm, via N-terminal fluorescein groups. Due to the lack of an exact molar extinction coefficient (ε_{490}) for the labeled peptide we chose to normalize peptide absorption based on a pilot experiment, where we assumed a saturated 1:1 complex of DDX6-C and EDC3-FDF. For calculating protein concentrations in the presence of labeled peptide the contribution of the peptide to the value of E280 was first subtracted.

NMR measurements

^{1}H-NOESY and ^{1}H -TOCSY spectra of EDC3-FDF were acquired at 291K on a Bruker AV III-600 spectrometer, processed and analyzed using the Topspin (Topspin V. 2.1.1, Bruker, Karlsruhe) software. Both spectra were recorded with 1024 (t_2) × 512 (t_1) complex points using 128 scans per increment and a relaxation delay of 1 s. The ^{1}H -NOESY spectrum was recorded with an NOE mixing time of 120 ms and the ^{1}H -TOCSY spectrum was recorded with a spin lock mixing time of 70 ms.

SUPPLEMENTAL REFERENCES

Baker, N., Holst, M., and Wang, F. (2000). Adaptive Multilevel Finite Element Solution of the Poisson- Boltzmann Equation; II: Refinement at Solvent Accessible Surfaces in Biomolecular Systems. J. Comput. Chem. *21*, 1343–1352.

Davis, I.W., Leaver-Fay, A., Chen, V.B., Block, J.N., Kapral, G.J., Wang, X., Murray, L.W., Arendall III, W.B., Snoeyink, J., Richardson, J.S. and Richardson, D.C. (2007). MolProbity: all-atom contacts and structure

validation for proteins and nucleic acids. Nucleic Acids. Res. *35*, W375-W383.

Emsley, P., and Cowtan, K. (2004.) Coot: model-building tools for molecular graphics. Acta Crystallogr. D Biol. Crystallogr. *60,* 2126–2132.

Kabsch, W. (1993). Automatic processing of rotation diffraction data from crystals of initially unknown symmetry and cell constants. Journal of Applied Crystallography *26*, 795-800.

McCoy, A.J., Grosse-Kunstleve, R.W., Adams, P.D., Winn, M.D., Storoni, L.C., and Read, R.J. (2007). Phaser crystallographic software J. Appl. Cryst. *40*, 658–674.

Murshudov, G.N., Vagin, A.A., and Dodson, E.J. (1997). Refinement of Macromolecular Structures by the Maximum-Likelihood Method. Acta Crystallogr. D Biol. Crystallogr. *53*, 240–255.

Tritschler et al.
Supplemental Figure S1

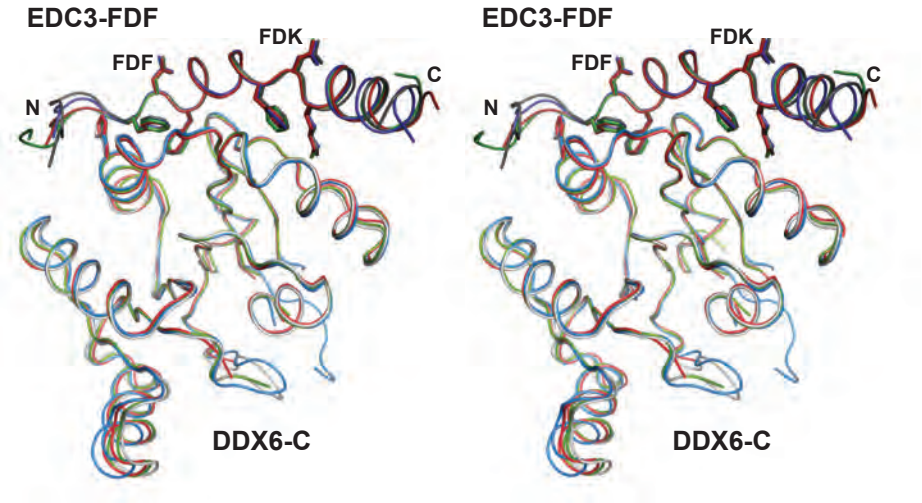

Figure S1. Superposition of the four crystallographically independent DDX6-C / EDC3-FDF complexes (stereo).
The structures of the four complexes, IA (gray), IB (blue), IIA (red) and IIB (green), were superimposed by secondary-structure matching (SSM) and are shown as tubes. Selected side-chains are drawn as sticks.

Tritschler et al.
Supplemental Figure S2

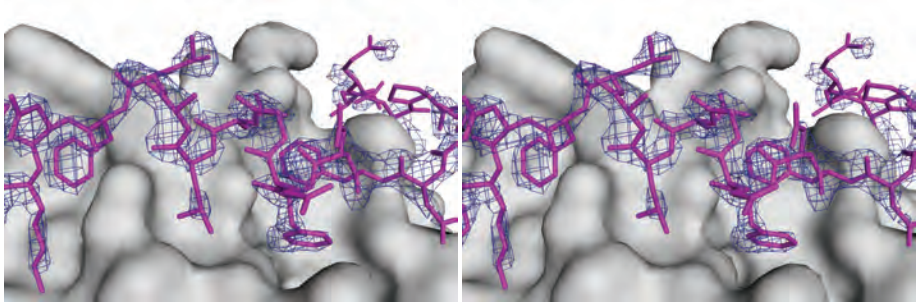

Figure S2. Difference density for the EDC3-FDF peptide (stereo).
Difference electron density ($(|Fo|-|Fc|)e^{i\alpha(c)}$) is contoured around the EDC3-FDF peptide at 2.0 sigmas over the mean, where |Fo| are the observed structure factor amplitudes and |Fc| and α(c) are structure factor amplitudes and phases calculated from a model lacking this EDC3-FDF peptide. EDC3-FDF is shown as sticks (magenta) over the surface of DDX6-C (gray).

Tritschler et al.
Supplemental Figure S3

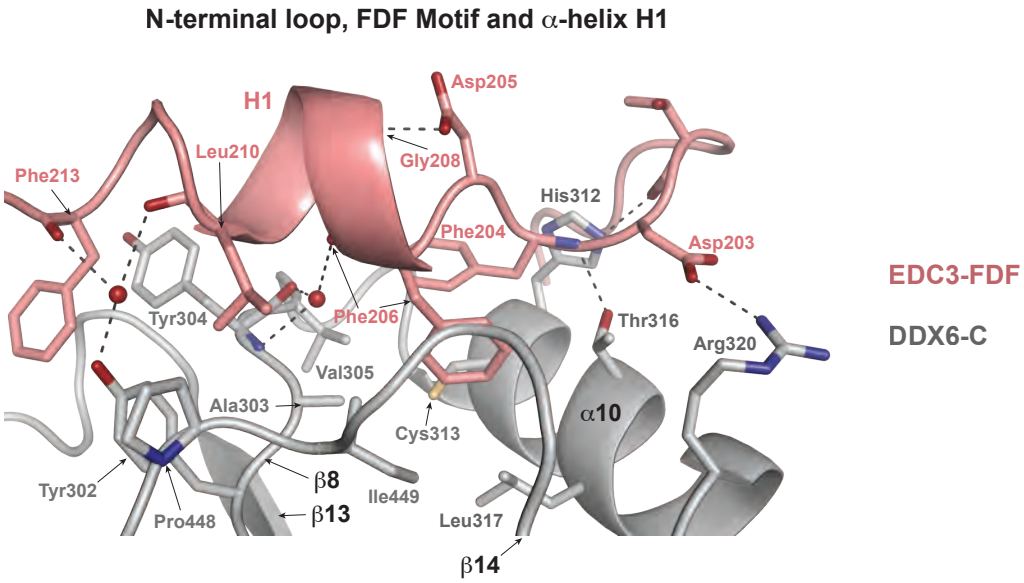

Figure S3. Molecular interface between DDX6-C and the EDC3-FDF peptide including the EDC3 N-terminal loop, the FDF motif and α-helix H1. DDX6-C (gray) and EDC3-FDF (salmon) are shown as ribbons with selected side-chain and main-chain atoms as sticks (oxygens in red, nitrogens in blue, sulfurs in yellow). Fixed water molecules are shown as red spheres, hydrogen bonds and salt bridges as dotted lines. β-strands β8 and β14 are drawn as loops for clarity. This view is identical to that shown in Figure 3B, but includes the DDX6-C C-terminal extension, which contributes to the interface with residues Pro448 and Ile449.

Tritschler et al.
Supplemental Figure S4

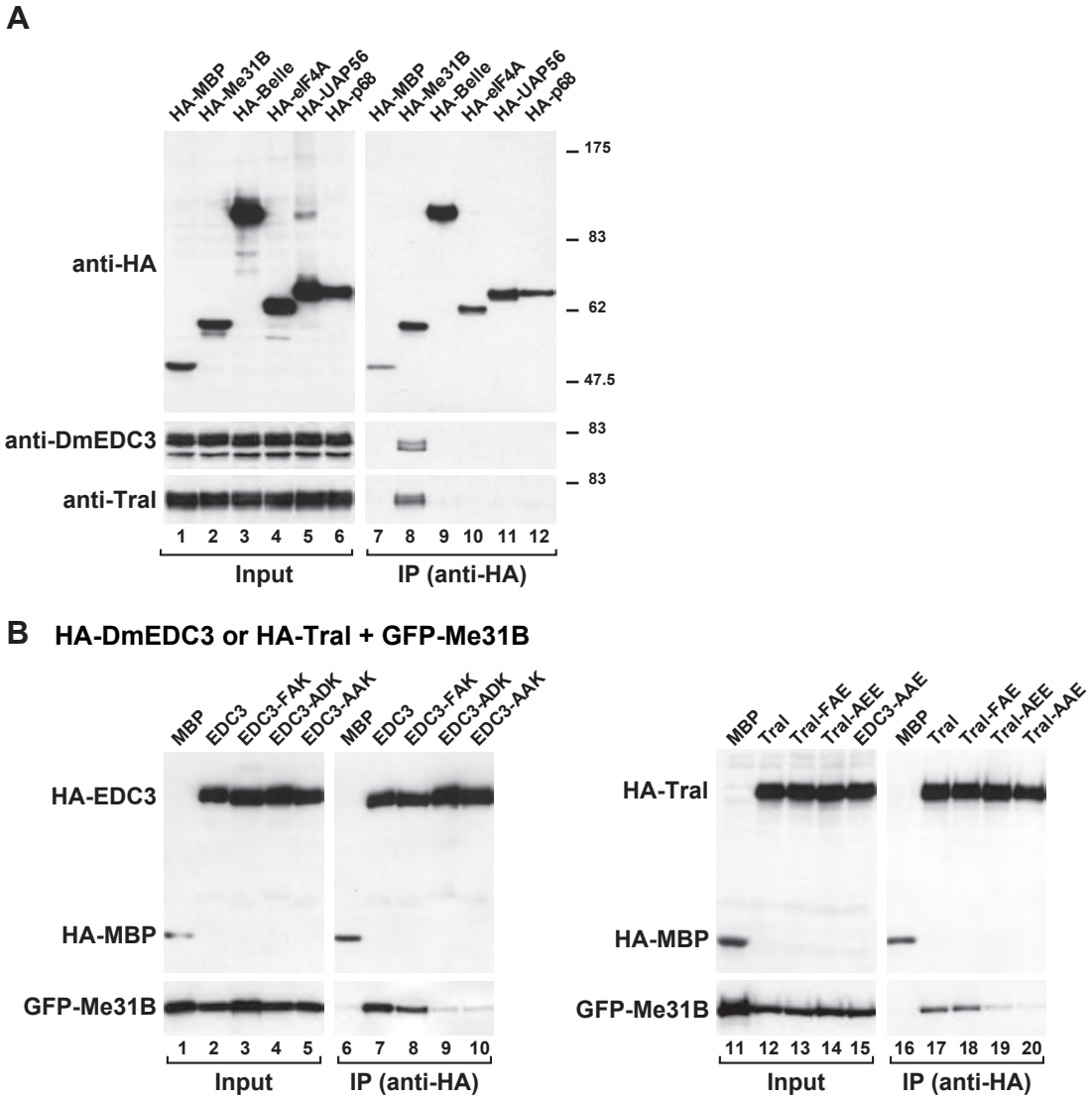

Figure S4.
(**A**) Interaction between EDC3 and Tral with various DEAD-box proteins. HA-tagged fusions of maltose binding protein (MBP), wild-type Me31B or the indicated DEAD-box proteins were expressed in S2 cells. Cell lysates were immunoprecipitated using a monoclonal anti-HA antibody. Inputs (1%) and immunoprecipitates (10%) were analyzed by Western blotting using polyclonal anti-HA antibodies. The presence of endogenous EDC3 or Tral in the immunoprecipitates was detected using anti-EDC3 or anti-Tral antibodies.

(**B**) Functional analysis of residues in the FDK and FEE motifs of EDC3 and Tral, respectively. HA-tagged MBP, wild-type EDC3 or Tral, and the indicated EDC3 or Tral mutants were coexpressed in S2 cells with GFP-Me31B, as indicated. Cell lysates were immunoprecipitated using anti-HA antibodies. Inputs (1%) and immunoprecipitates (10%) were analyzed by Western blotting using anti-HA and anti-GFP antibodies.

Tritschler et al.
Supplemental Figure S5

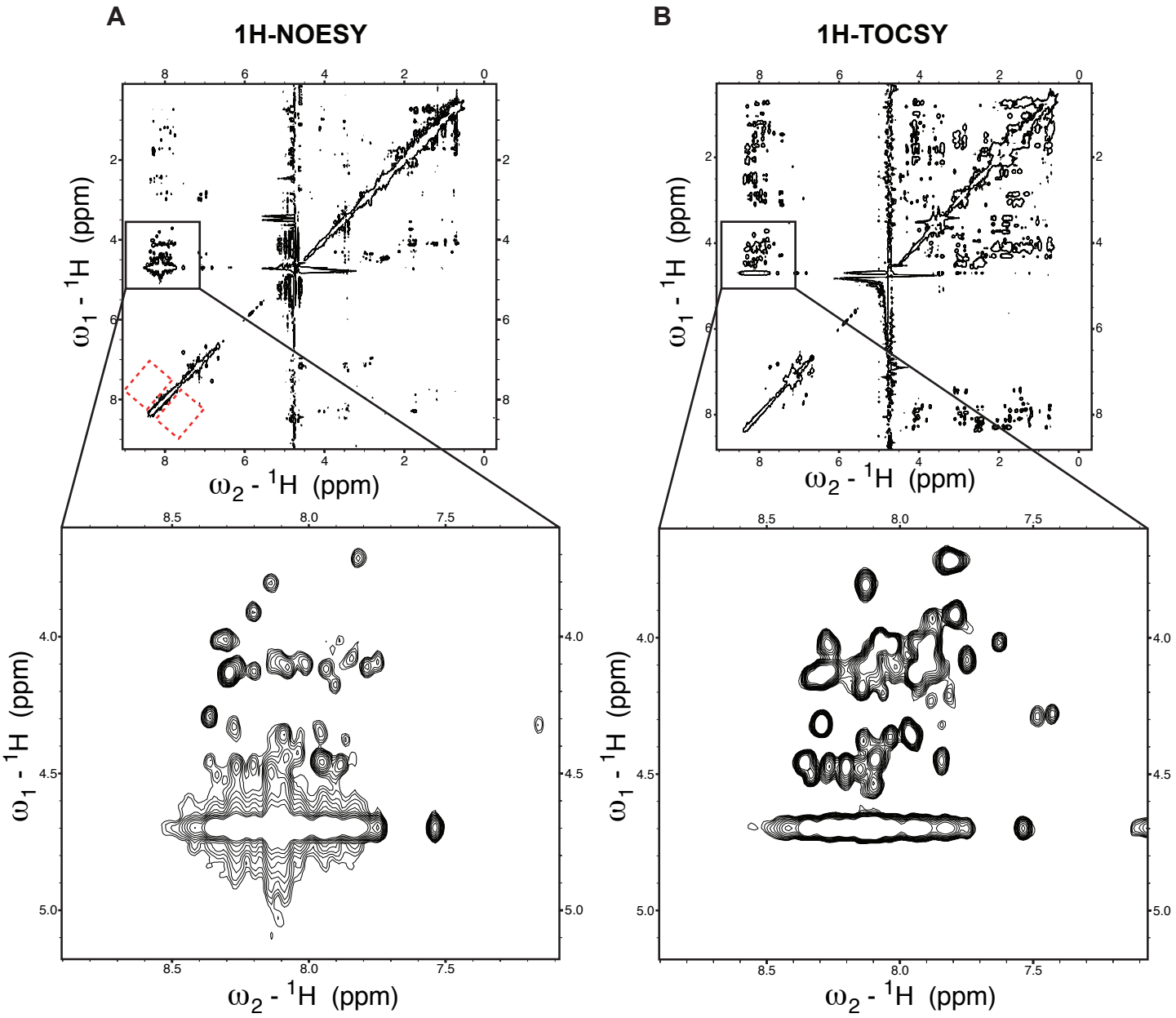

Figure S5. NOESY and TOCSY spectra of free EDC3-FDF.
NOESY (A) and TOCSY (B) spectra of unlabeled EDC3-FDF are shown. As expected for an unfolded peptide, a very low chemical shift dispersion is observed in the region of the amide protons (dispersion from 7.75 to 8.35 ppm), thus excluding the possibility for the peptide to adopt a β-stranded structure. Closer examination of the spectra also shows that the peptide does not adopt a helical structure due to the lack of strong sequential H^N – H^N contacts (red, dashed box) as well as strong intraresidue H^N – H^α contacts. Comparison of the H^N – H^α peak positions of the TOCSY- to those of the NOESY-spectrum (see zoomed region) shows that most of the larger NOESY crosspeaks are not similarly located, meaning they are sequential. (For a helical peptide, each TOCSY H^N – H^α peak would be expected to have a strong NOESY equivalent). Finally the lack of structural information in the NOESY spectra such as methyl-methyl and methyl-aromatic contacts further shows that the EDC3-FDF is unfolded in solution. For additional information see Supplemental Experimental Procedures.

Tritschler et al.
Supplemental Figure S6

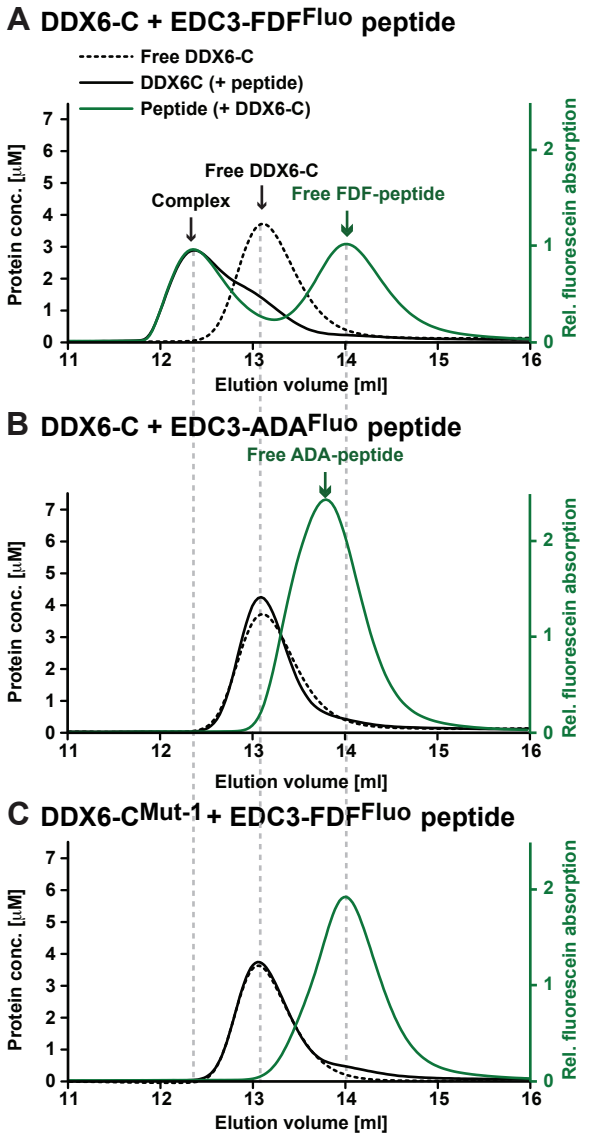

Figure S6. Heterodimerization of DDX6-C and EDC3-FDF^{Fluo} *in vitro*.
Analytical gel filtration experiments were done with variants of DDX6-C, either in the absence of EDC3 peptides (black dashed lines), or with an excess of fluorescein-labeled EDC3 peptides (black solid lines). DDX6-C concentrations are shown in black (left axis). Relative EDC3-peptide absorption is shown in green (right axis), normalized to the amount in the complex. Elution volumes of the free components and of the complex are indicated by arrows and dashed gray lines. For additional information see Supplemental Experimental Procedures.
(**A**) Complex formation between DDX6-C and the EDC3-FDF^{Fluo} peptide.

(**B**) Mutation of the EDC3-FDF^{Fluo} peptide and disruption of the complex. The free EDC3-ADA^{Fluo} peptide elutes earlier than the free EDC3-FDF^{Fluo} peptide.

(**C**) Mutation of the DDX6-C domain and disruption of the complex. The elution of the free DDX6-C^{Mut-1} quadruple mutant is unaffected, compared to the wild-type.

Tritschler et al.
Supplemental Figure S7

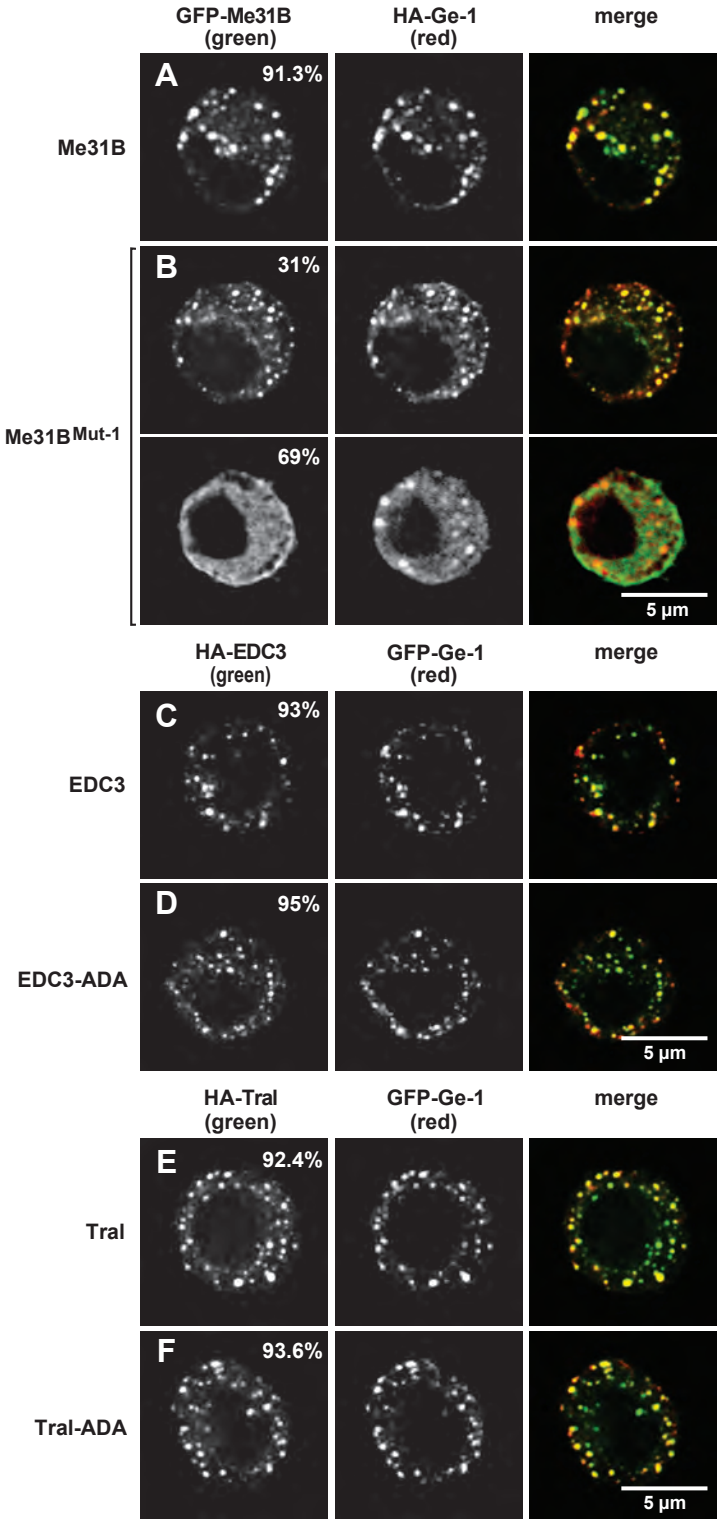

Figure S7. Me31B interaction with EDC3 (or Tral) is required for P-body localization. Confocal fluorescent micrographs of fixed S2 cells expressing the indicated HA and GFP protein fusions. Cells were stained with anti-HA antibodies. The fraction of cells exhibiting a staining similar to that shown in the representative panel was determined by scoring at least 100 cells in three independent transfections performed per protein. The merged images show the GFP signal in green and the HA signal in red.

(**A,B**) S2 cells expressing HA-tagged Ge-1 and GFP-fusions of full length Me31B (wild-type, A) or mutant (B).

(**C,D**) S2 cells expressing GFP-Ge-1 and HA-fusions of full length EDC3 wild-type or the ADA mutant.

(**E,F**) S2 cells expressing GFP-Ge-1 and HA-fusions of full length Tral wild-type or the ADA mutant.